The Fate of Polyacrylamide as a Slick-Water Hydraulic Fracturing Additive, and the analysis of the associated Flow-Back Fluids

CHRISTOPHER JAMES WARD

Dedication

This PhD is dedicated to my mum, who never got the chance to see the final result of all this nonsense.

"Do you know what is interesting about caves, Leonard?"

"What?"

"Nothing"

Sheldon Cooper, 2007

Christopher James Ward

Abstract

In the UK, the first well to be fracked onshore used a fracking fluid containing only two additives; an undisclosed salt and polyacrylamide (PAM). This type of simple, predominantly water-based fluid is known as a 'slick-water'. PAM is used in nearly 100 % of slick-water fluids in the USA, and so it is likely to be a major constituent of UK fluids. The potential for extensive use means the interaction between the PAM and shale must be investigated. Therefore, the aim of this thesis was to investigate the interactions between a PAM slick-water fluid and relevant UK shale gas lithologies, alongside the analysis of associated flow-back fluids from these experiments.

Batch reaction experiments were setup to quantify; 1) the sorption of PAM; and, 2) the composition of associated flow-back fluids. Experiments were conducted at both room temperature (RT) and subsurface conditions (HPHT).

Maximum coverages showed shales to adsorb up to 15,365 mg/kg of PAM, increasing up to 22,972 mg/kg when subjected to increased pressures and temperatures indicative of the UK subsurface. Up to 98 % of the PAM in solution could be removed from solution by adsorption. Of the adsorbed PAM, a maximum of 1.4 % of will desorb during a freshwater flush (typical of the latter stages of a frack). Therefore, PAM is likely to remain downhole, open to degradation.

The addition of PAM to water-based fluid increases the sodium content to ~500 mg/L, producing a slightly saline fluid. Analysis of flow-back fluids from experiments showed that concentrations of the majority of metals analysed, both in RT and HPHT conditions, increased relative to the fracking fluid. Under HPHT conditions, larger concentrations of most contaminants, including Al, Cu, Fe, Mg, Mn and Si, were observed compared to the RT fluids, suggesting subsurface conditions will aid the return of larger amounts of contaminants to the surface.

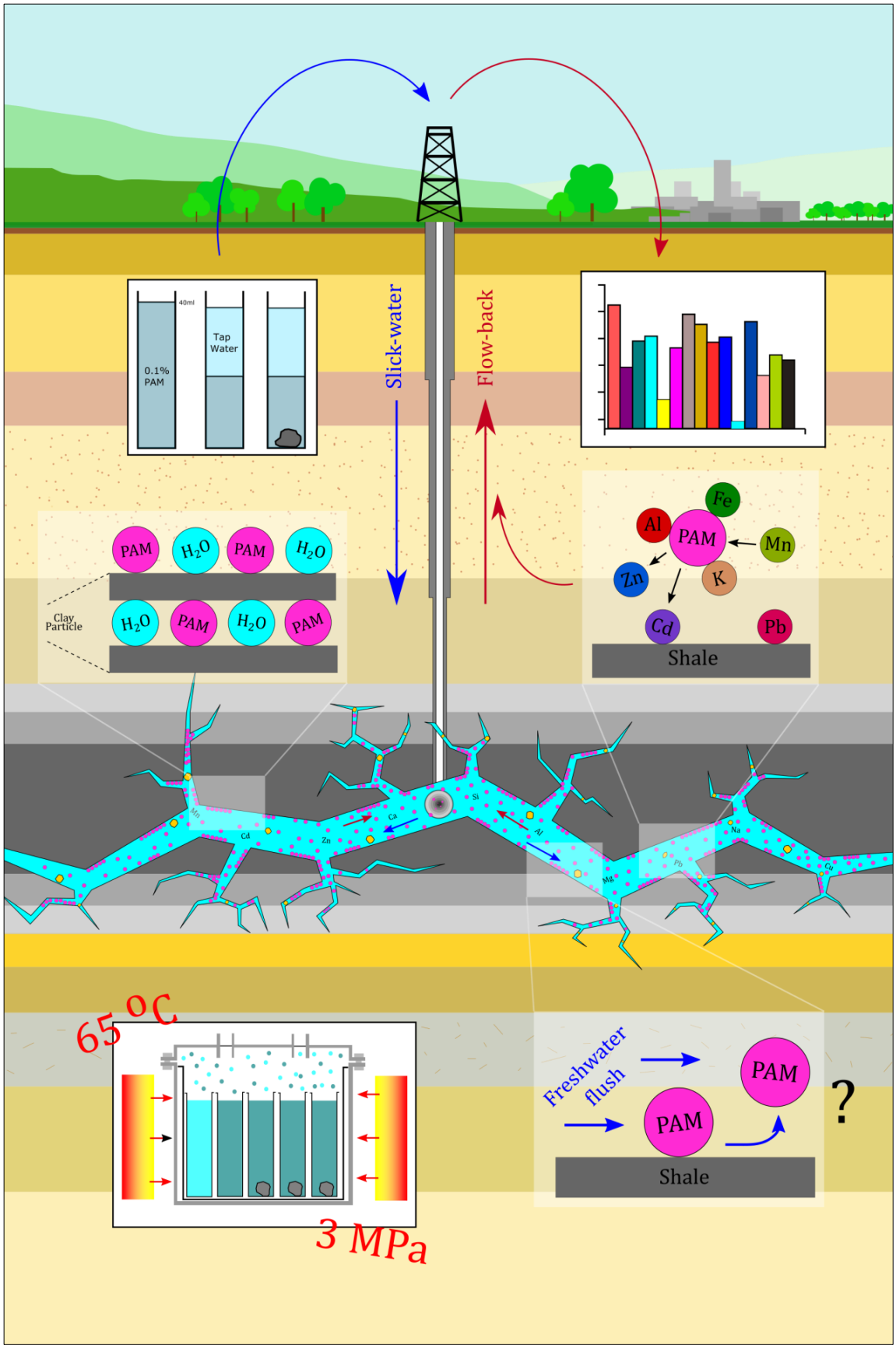
40ml
0.1% PAM
Tap Water
Slick-water
Flow-back
PAM
H_2O
Clay Particle
Fe
Al
PAM
Mn
Zn
K
Cd
Pb
Shale
65 °C
3 MPa
Freshwater flush
PAM
PAM
Shale
?

Declaration

No part of this thesis has been previously submitted for a degree at this or any other institution. The work described here is entirely that of the author, except where reference is made to previously published or unpublished work.

Copyright

Acknowledgments

Supervisory Team

I would like to start by thanking my supervisory team, primarily Prof Fred Worrall. He has taught me a lot over the last three years, providing me with the support and guidance both in the office and the laboratory. Thank you for keeping me on track, particularly with something we initially both didn't know much about and thank you for constantly reading thesis chapter, paper drafts, presentations and posters….and eventually coming round to my slightly different way of presenting things. I would like to thank Andy Aplin for being the second supervisor and for particular help on the XRD and mineralogy side of things. I would like to thank Ian Davey and Sally Gallagher of the Environment Agency for their very useful input and overall enthusiasm of the project and my work, and for the hugely helpful email responses when there were questions.

I would also like to thank my internal progress reviewers Chris Greenwell and Martin Smith for the constructive review process and the help and advice when needed.

Family and Friends

Firstly, I would like to thank my parents for supporting me in any way possible throughout my PhD, especially to my mother who pushed me to apply and start, but who sadly didn't make it through to see the end.

Thanks to all my friends in the department of earth sciences who have ultimately made it the best fun in the world. Thanks to Olly Sanford for sitting next to me and providing nonsense and distraction. Thanks to Sarah Clancy, Jack Lee, Sean O'Neill, Matt Funnell, Erin Scott, Tim Armitage, Chris Harbord, Kit Hardman, Katharine Groves, Emma Ownsworth, Katy Burrows, Miles Wilson, Kate Horan, Tom Utley, Madeleine Stow, Jamie Schofield, Pavlos Farangitakis, Liz Atar, Kate Heerema, Jordan Phethean, Nico Schliffke, Emma Gregory, Dimitris Michelioudakis, Adam Robinson, Mathieu Dellinger and Natalia Wasielka for all the coffee breaks, ski trips, fantasy football, fieldtrips, pub trips and adventures (and even helping me off a mountain with a broken leg). With special thanks again to Tom Utley, Kit Hardman and Katharine Groves for all the fun and company on all the fieldtrips; the driving, cooking, conversation, radio chat, pranks and makeshift 'ambulancing'.

Regarding fieldtrips I would also like to thank Dr David Selby, Dr Chris Saville and Janice Oakes for most importantly how much I have learnt alongside them about teaching and

supporting students in the field, both in the Lake District and Assynt in some of the most miserable weather…..and also the fun and games.

Finally external of the department, my best friend Dr Alex Peach who has been an annoyance since day 1 of undergraduate and here we both still are! He has provided me with entertainment for the last ten years and even managed to get me to go to America for his wedding. Also, in no particular order my friends Kate Goodridge, Adam Abo Saiz Henriksen, Jenna Saiz Henriksen, Jack Tuxford, Thomas Moat, Clement Myers and Caroline Rider-Dobson for all the trips and support when we could all get together.

Scientific Community and Industry

Outside of the department I would like to thank Dr Tom Knott of Leicester University for undertaking XRF analysis of my samples and for providing excellent answers to many of my probably very basic questions. To Gary Oswald for providing excellent tuition on the X-Ray diffractometer, meaning I could analyse all my own samples. To Ian Boothroyd for helping me hugely with the carbon analysis on the elemental analyser. To Laurence Evans and Bart McTigue of Tarmac Ltd for providing me with Congleton Sand samples and an excellent tour of the workings of the Congleton Hall sandstone quarry.

Environment Agency and Supporting Companies

I would like to thank the Environment Agency for providing the funding for this PhD project meaning that I never had to worry about a penny. I would also like to thank them, in particular Ian Davey and Sally Gallagher for the fantastic support they gave to me and this project. I would also like to thank ReFINE and Fred Worrall for providing some of the funding towards this project also.

Technical and Admin staff at Department of Earth Sciences

Without them, this project would have not come together. To Ian Chaplin and Sophie Edwards for helping with rock cutting and preparation. Thanks to Paula Elliot and Karen Atkinson for helping with all travel and car hire and Jo Banner for all the demonstrating and other admin I needed.

Contents

List of Figures

List of Tables

Nomenclature

Ads-Des – Adsorb-Desorption

BGS – British Geological Survey

CHN – Carbon-Hydrogen-Nitrogen Analysis

EA – Elemental Analysis

HPHT – High Pressure High Temperature

ICP-OES – Inductively Coupled Plasma Optical Emission Spectroscopy

LBS – Lower Bowland Shale

PAM – Polyacrylamide

RT – Room Temperature

TC – Total Carbon

TGA – Thermogravimetric Analysis

TIC – Total Inorganic Carbon

TOC – Total Organic Carbon

UBS – Upper Bowland Shale

XRD – X-Ray Diffraction

XRF – X-Ray Fluorescence

1. Introduction

1.1. Project Context and Motivation

Shale gas, in the UK, is proposed as a promising energy strategy in a context of steadily declining global natural gas reserves (Gibbons et al., 2016; Broderick et al., 2011). In theory, UK shale gas would offer energy security; a means to provide some support to the transition to a lower carbon economy; and also help public finances both in terms of investment and broader economic stimulus (Gibbons et al., 2016). The primary sponsors of this project, the Environment Agency, observed the potential future of a hydraulic fracturing industry within the UK and launched multiple projects to investigate the various implications that fracking may have upon the environment. This study, assessing the interactions between shales and fracking fluids, was one of them. Ultimately, the aim of this project for the Environment Agency was to assess the results and see how they could potentially influence the regulation of such activities, which may or may not start in earnest soon within the UK.

As is relatively well known, the USA is a major market in terms of hydraulic fracturing with the industry surging in the mid-nineties (Montgomery and Smith, 2010). Rapid growth led to the very quick advancement of technologies associated with hydraulic fracturing (King, 2010) and this led to a situation where no real environmental monitoring baseline was able to be established prior to the development of the industry. At the beginning of this PhD project in 2016, only two wells in the UK onshore sector had been fracked for shale gas (Andrews, 2013): Elswick-1 (exploratory single production gas well which stimulated sandstones) and Preese Hall 1A. Cuadrilla's Preese Hall 1A, was spudded on August 16th 2010 (De Pater and Baisch, 2011), and fracked in 2011. The drilling of these wells went ahead after a long period of shale gas exploration and proprietary drilling that started with the 2008 release of the 13th Onshore Oil and Gas Licensing round, the first round to specifically mention shale gas exploration (Gibbons et al., 2016). Preese Hall 1A was subsequently halted in June 2011 after 2 seismic events (magnitude 2.3 and magnitude 1.5 (Green et al., 2012) were induced from hydraulic fracturing operations (Andrews, 2013) on the 1st April and 27th May, 2011 respectively. As a result the UK government brought in a moratorium on all fracking activities and no fracking occurred until 2018. At the time of writing, Cuadrilla had recently hydraulically fracked the Preston New Road site. Using the Cuadrilla ePortal (https://www.cuadrillaresourceseportal.com) operations are thought to have caused 3 + seismic events, the most notable being; ML 0.4 (23/10/2018), ML 0.3 (25/10/2018) and ML 0.76 (26/10/2018) (Cuadrilla ePortal; BGS, 2018). Seismic data for the Preese Hall seismic events shown in Figure 1.1.

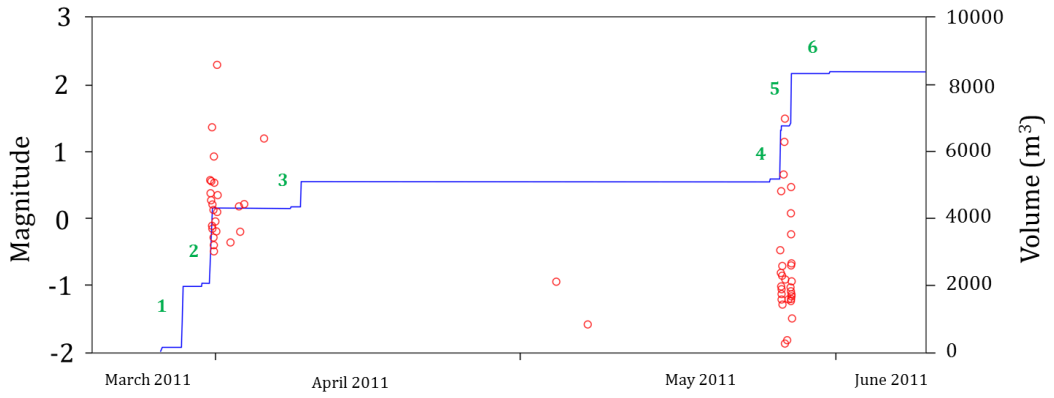

Figure 1.1: *Image of the seismic activity following the Preese Hall 2011 hydraulic fracture operations through March to June 2011.The blue line represents the volume of injected fluid alongside the seismic activity (red circles) for the 6 stages of hydraulic fracturing that occurred (green numbers). Operations were ceased on the 27th May 2011 after the second earthquake of magnitude 1.5. Image adapted from "The Blackpool Earthquakes, 2011" (BGS, 2011).*

The hydraulic fracture of Cuadrillas Preston New Road site in Lancashire brought the moratorium on fracking activities to an end. It was this hiatus in operations between 2011 and 2018 that gave the UK the perfect environmental baseline to measure the pre and post effects of any such operations. Cuadrilla resources have also recently set up a live update system called the ePortal (https://www.cuadrillaresourceseportal.com/), displaying monthly data on seismicity, traffic, noise, air quality, surface water and groundwater for the recently active Preston New Road site in Lancashire, UK (2018 to early 2019). This project stems from multiple projects offered at similar times to understand the effects of fracking in UK-based scenarios. Specifically, this project focuses on the additive Polyacrylamide (PAM) and how this interacts with the shales, adsorbing, and desorbing, degrading and influencing flow-back fluid compositions.

There have been multiple reports, documentaries and films in the mainstream media regarding fracking and its environmental consequences. Arguably the greatest impact was achieved by a film called 'Gasland' by Josh Fox in 2010. The most important impacts that have been attributed to shale gas activities are generally accepted to be groundwater contamination, fugitive emissions and seismicity (Montcoudiol et al., 2017). One of the most notable studies into all aspects of the footprint of hydraulic fracturing was the SHeeR project (www.sheerproject.eu), focussing on the "*understanding, preventing and mitigating the potential environmental impacts and risks of Shale Gas Exploration and Exploitation*". This study has published multiple articles and conference proceedings on all aspects including but not exclusively; induced seismicity (Bommer et al., 2016), impacts on groundwater (Montcoudiol et al., 2017), the modelling of hydraulic fractures (López-Comino et al., 2017) and air quality (Jarosławski and Pawlak, 2018). Outside of the SHeeR project, multiple studies have also been

conducted on other potential environmental impacts from fracking operations that include as examples: emissions from increased traffic can increase NO_x on operational days by up to 30 % (Goodman et al., 2016; Reap, 2015); landscape disturbance assessing the placement of well pads (Clancy et al., 2017); air pollution (Cesur et al., 2017; Weinhold, 2012); as well as some that took a more general summarising approach to encompass a review of all toxicological matters relating to pollutants including water contamination, outdoor air pollutants and ground pollutants (Kovats et al., 2014).

1.2. Principles of hydraulic fracturing

Shale gas is classed as an 'unconventional' resource. Unconventional fossil fuels are classed as fuels or formations that are difficult to extract, usually requiring complex production and exploitation methods to do so (Chew., 2014). Hydraulic fracturing is an unconventional well stimulation technique whereby, in its simplest form, fluid and proppant (sand particles) are forced down a wellbore under high pressure to create fractures in the rock. The fracturing of the rock is achieved by making sure the fluid pressure exceeds the least principle and tensile stresses of the host rock (Davies et al., 2012). Fractures grow perpendicular to the direction of least principle stress (Fisher and Warpinski, 2012) and release adsorbed gases (Broderick et al., 2011; Zoback et al., 2010) from the low permeability source rock (Keshavarzi et al., 2012) into the fracturing fluid. Micro seismicity can be used to estimate fracture growth length (Maxwell et al., 2002) with fractures extending up to several hundred metres above or below the borehole (Fisher and Warpinski, 2012). The fracking fluid is then returned to surface during fluid flow-back events after the initial frack stages and can carry back with it new components from interaction with the shale at depth (Almond et al., 2014; Anderson et al., 2010; Gregory et al., 2011). Produced waters, or flow-back fluids, are termed as waters that will return to the surface over the lifespan of a well (Mullins and Daugulis, 2018). Essentially, hydraulic fracturing makes use of a liquid to fracture reservoir rocks (Gandossi and Von Estorff, 2015) to obtain adsorbed content of economic interest. This process is summarised in Figure 1.2, a simplified cross section of how a fracking well operates.

The recovery of the injected fluids is highly variable, with anything from 15 % to 80 % recovered in the flow-back fluids (Broderick et al., 2011). Recently and most notably, hydraulic fracturing has been in the spotlight due to its potential hazardous environmental effects, where the public are increasingly interested in understanding fluid compositions (EPA, 2015) of both the fracking fluids, and the flow-back fluids. Fracking's drive of an economic boom, especially in the United States, the consequences of which are described as both "revolutionary" and "disastrous" (Jackson et al., 2014).

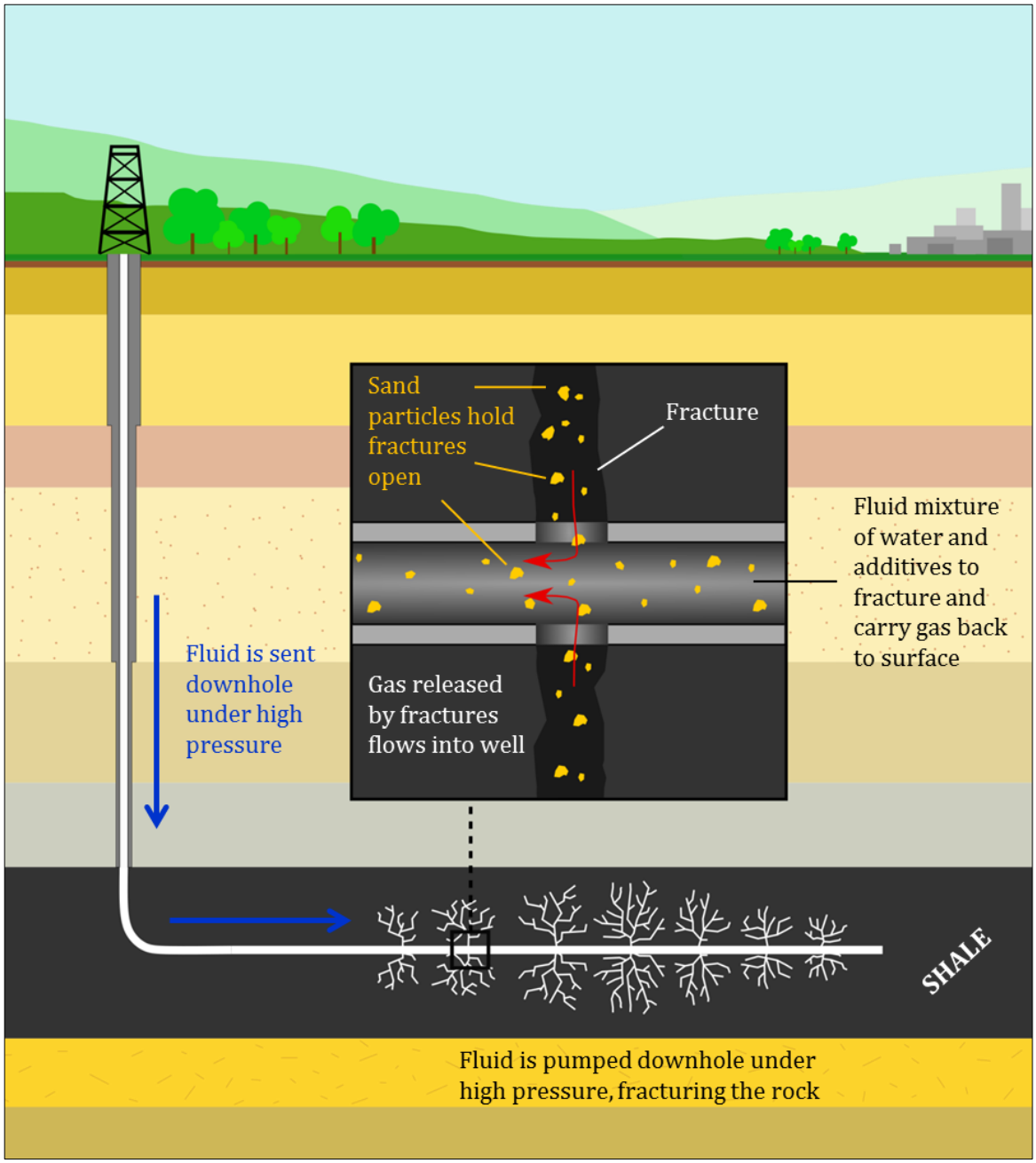

Figure 1.2: *Basic schematic of how a hydraulic fracturing well works. Stage 1) A well is drilled, cased and cemented as normal into either a horizontal or vertical shale; stage 2) Perforations of the casing in the shale are made with explosives so the shale is exposed through the casing; stage 3) high pressure fluid is pumped in stages downhole to fracture the shale at the exposed points. Sand particles called proppant are carried within the fluid to hold open the fractures to allow the gas to flow; stage 4) fluid flows back into the wellbore containing gas and proppant, this is called flow-back fluid; stage 5) Fresh water is pumped downhole as a flush stage to flush out any excess particles, additives and proppant. Diagram is created from multiple sources (BBC, 2018; Broderick et al., 2011; Gandossi and Von Estorff, 2015; Gregory et al., 2011; ReFINE, 2018; Zoback et al., 2010)*

1.3. A Short History of Hydraulic Fracturing

Hydraulic fracturing is by no means a new tool in the oil and gas industry (King, 2012). Hydraulic fracturing is known as far back as 1821 when shale gas was produced from a natural seepage in the Appalachian Mountains (Selley, 2012). In 1857 when gunpowder was used to fracture rock at a well in Canadaway Creek, New York State (Morton, 2013). Canadaway Creek used a technique of lowering gunpowder downhole and creating an explosion with a red hot iron which resulted in the fracture of the rock and the increase in gas flow (Morton, 2013). Although the technique described above was rudimentary, in 1865 when Col. Robert Edwards and brother developed a method whereby water was used to dampen these explosions (Morton, 2013). Col. Edwards' use of water is the first example of anything related to a "hydraulic" based fracturing operation. Hydraulic fracturing technology then developed largely over the next century to the more familiar method known today. The first fracturing experiment was successful in 1947 resulting in enhanced commercial production (Gandossi and Von Estorff, 2015; King, 2012). From the 1940's until 2010, ~2.5 million operations have been performed worldwide with at least 1 million of these in the USA (EPA, 2015; King, 2012; Montgomery and Smith, 2010). The use of hydraulic fracturing rapidly increased in the USA in the mid 1990's and was driven by the extraction of unconventional resources from tight resources such as sands, shales and other low permeability formations (Jackson et al., 2014).

1.4. Hydraulic Fracturing Globally

The USA is seen as the major player within the fracking industry, with fracking reasserting its mark on the global oil and gas production markets. Annual gas production in the US increased from 5.6×10^9 m^3 in 1998 to approximately 1.39×10^{11} m^3 in 2010, and is expected to grow threefold in the next decade (Gregory et al., 2011). Whilst there is an established industry, predominantly in the USA, hydraulic fracturing is also used in China, Australia (some states), Argentina, Denmark, Poland, South Africa. Unconventional gas is still in the early exploration phase in most of Europe (Lang, 2014). Some countries, including, France, Ireland, Germany, Bulgaria, New Zealand, Scotland, and alongside some American, Canadian and Australian states have banned the practice of hydraulic fracking. Moratoriums on fracking are in place in such countries as the Netherlands and Tunisia (Sher and Wu, 2018; Thompson, 2019).

1.5. Hydraulic Fracturing in the United Kingdom

More than 2000 wells have been drilled onshore in the UK for oil and gas purposes, and about 200 of these have been hydraulically fractured to enhance production of oil and gas, (Mair et al., 2012). Many of these were drilled onshore vertically and then horizontally out to sea (Mair et al., 2012). The first UK well to encounter shale gas was drilled in 1875 (Mair et al., 2012), however, it was not exploited for the purposes of shale gas but for the conventional resources that were present in far higher abundance (Figure 1.3). Within the UK, most of the exploration for what we now know as shale gas began in the 1980's.

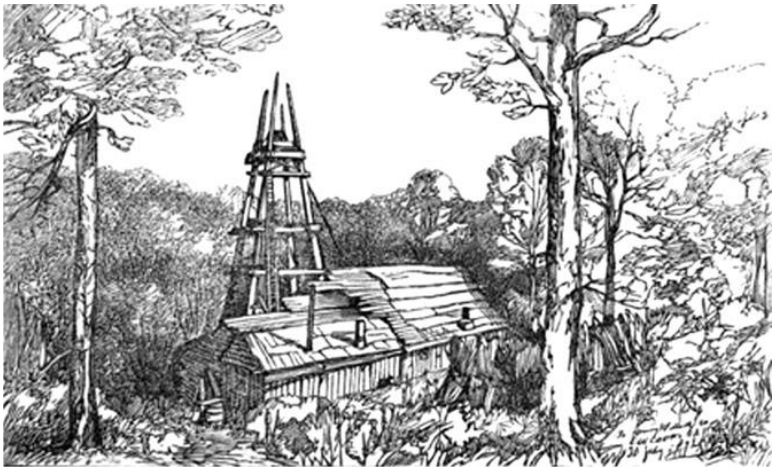

Figure 1.3: *Drawing of the 1875 Netherfield No.1 Well in Sussex. Drawing by E Cooke, Esq. Image taken from (Selley, 2012).*

The next major catalyst for the fracking industry in the UK was in 2003 when the Petroleum Revenue Act was repealed, allowing companies' production assets to not be counted under corporation tax (Selley, 2012). Technologies for extraction advanced and, in 2008, the UK government funded projects to review the UK's shale gas potential (Harvey and Gray, 2010). In the UK, large areas of onshore acreage were licensed to companies in 2006 for the purposes of shale gas exploration, and most notably, in 2010, Cuadrilla Resources embarked on a three well exploratory programme (Selley, 2012) that culminated in the drilling of the wells Elswick, Grange Hill and Preese Hall. Elswick and Grange Hill were exploratory wells whilst Preese Hall was an exploratory well with the specific purpose of testing a vertical hydraulic fracture at the same lateral formation as the aforementioned wells. After the 2011 hiatus emplaced upon fracking in the UK due to the Blackpool Earthquakes, a further well was drilled, Preston New Road. Preston New Road was intended to exploit the same formations, but this time with a horizontal frack. At the time of writing, Preston New Road has completed the drilling phase and was actively hydraulically fracturing the rock (late 2018, early 2019).

Hydraulic fracturing at this site was paused numerous times due to seismic activity greater than magnitude 0.5.

1.6. Hydraulic Fracturing Fluid Additives

The additives used in the hydraulic fracturing fluids themselves are one of the key reasons fracking is highlighted as an environmental concern, particularly in terms of water contamination and safety (Vengosh et al., 2013). In theory, the additives must be safe to handle, environmentally friendly, non-damaging to fractures, inexpensive and able to control fluid loss (Montgomery, 2013). The additives used in fracking fluids can be of all manner of chemicals (Gregory et al., 2011) or natural ingredients and serve multiple purposes (Broderick et al., 2011; Gregory et al., 2011; King, 2012). Globally, many different chemicals have been used as additives in hydraulic fracturing fluids. One of the most comprehensive lists compiled of all fracking fluids is from the United States Environmental Protection Agency (USEPA). In March 2015 the USEPA complied 39000 fluid disclosures from operators between 1st January 2011 and 28th February 2013 (EPA, 2015). All of this data was compiled using the FracFocus Chemical Disclosure Registry (www.fracfocus.org). Some of the typical constituents of a fracking fluid are detailed in Table 1.1.

ADDITIVE	PURPOSE
Acid	Dissolve minerals and initiate cracks
Corrosion Inhibitor	Protect casing from corrosion
Biocide	Eliminate bacteria that can cause corrosion
Base Carrier Fluid	Create fracture geometry and suspend proppant
Breaker	Delays the breakdown of gels
Clay Control	Lock down clays in the shale structure (temporary or permanent)
Crosslinker	Maintains viscosity with temperature increase
Friction Reducer	Reduces friction effects of water in the pipe
Gel	Thickens water to suspend the proppant
Iron Control	Helps prevent precipitation of metal oxides
Non-Emulsifier	Used to break/separate oil-water mixtures
pH Adjuster	Maintains effectiveness of additives like crosslinkers
Proppant	Keep fractures open allowing flow
Scale Inhibitor	Prevent scale in pipe and formation
Surfactant	Reduce surface tension of the treatment fluid and improve fluid recovery

Table 1.1: *Typical frack fluid additive types and their functions. Which types are required are totally dependent on numerous factors to do with the frack. Data adapted from (Broderick et al., 2011; EPA, 2015; Gregory et al., 2011)*

Typically fracking fluids consist of 90-99 % water, 0.4-9.99 % sand proppant and 0-2 % additives (EPA, 2015; Gregory et al., 2011; Hammond et al., 2015; Mair et al., 2012). Figure 1.4 shows a representation of the volume difference between carrier fluid and additives.

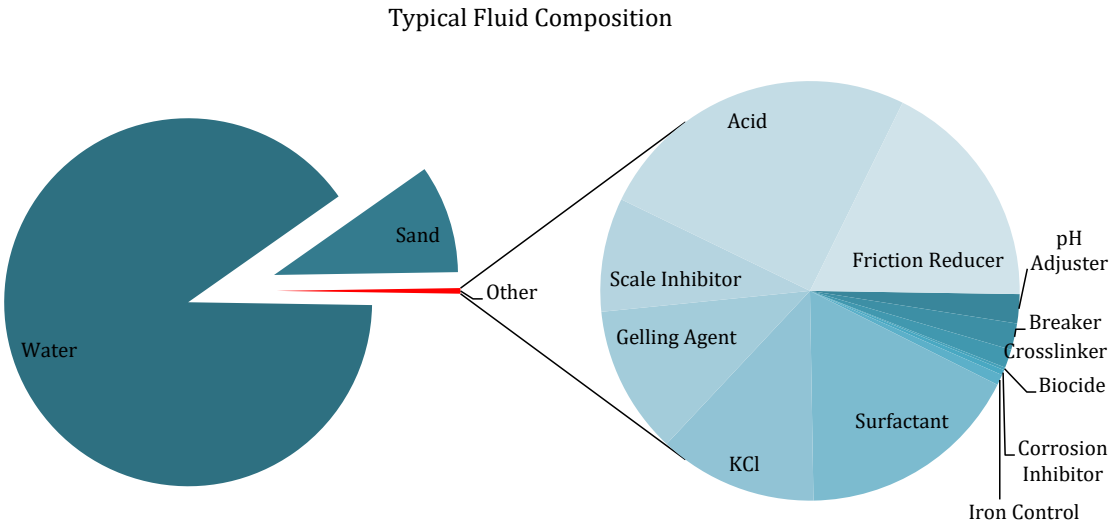

Figure 1.4: *Typical fracking fluid composition based on the use of typical multiple additives. Diagram adapted from (Broderick et al., 2011; Burton et al., 2014; Cox et al., 2013; Ferrer and Thurman, 2015; Gregory et al., 2011)*

In recent years, more research has been undertaken into the effects and compositions of fracking fluids (Ferrer and Thurman, 2015; King, 2012; Xiong et al., 2018a, 2018b). Some studies have researched the effects of certain additives by producing their own synthetic fracking fluids (Drollette, 2014a, 2014b; Heybob and Mouser, 2015; Kekacs et al., 2015). Most of these studies have focussed on the risks to water, be it groundwater or flow-back waters. Some have concluded that fracking operations do not necessarily interfere with aquifers and it is more likely the topography and groundwater geochemistry that affects methane levels (Molofsky et al., 2018). By characterising brines Vengosh et al., (2013) assesses if there is an impact from such operations concluding that naturally occurring pathways have always been the source of high concentration brines or methane (Warner et al., 2012). Others cite that activities could provide levels of totals dissolved solids (TDS) that vary by orders of magnitude: TDS of 344 µg/L and selenium of 329 µg/L (Fontenot et al., 2013) and up to 12,000 mg/L of barium (Phan et al., 2015). Flow-back fluids have elevated concentrations of multiple minerals; studies show that Cl, Br, Ca, Na and Sr can be up to 6700 times higher than natural samples (Warner et al., 2013) and that U and As could be mobilized under certain conditions (Phan et al., 2015).

1.6.1. Additives used in the UK

So far, there are very few additives that have been used in the UK, either for conventionals or unconventionals, and both onshore and offshore. Of additives that have been confirmed as used for the fracking of unconventionals in the UK, only two have been formally published, both for sites operated by Cuadrilla Resources. Two additives, a friction reducer and a chemical tracer (Broderick et al., 2011) were used at the Preese Hall and Preston New Road (Cuadrilla Resources, 2018a, 2018b) sites.

ADDITIVE	TYPE	QUANTITY	% BY VOLUME
Water	United Utilities Mains Water	8399 m^3	97.93
Proppant	Congleton Sand	108.1 tonnes	0.473
Proppant	Chelford Sand	354.6 tonnes	1.55
Friction Reducer	Polyacrylamide Emulsion	3.7 m^3	0.043
Chemical Tracer	Sodium Salt	0.425 kg	0.00043

Table 1.2: *Composition of hydraulic fracturing fluid for the Preese Hall 1A well in Lancashire, UK. Table adapted from (Broderick et al., 2011).*

ADDITIVE	TYPE	QUANTITY	% BY VOLUME
Water	United Utilities Mains Water	<= 765 m^3	unknown
Proppant	Congleton Sand	<= 75 tonnes	unknown
Proppant	Chelford Sand	<= 75 tonnes	unknown
Friction Reducer	Polyacrylamide	unknown	max 0.05 %
Chemical Tracer	HCl	<= 3 m^3	< 10%

Table 1.3: *Composition of hydraulic fracturing fluid for the Preston New Road site in Lancashire, UK. Table adapted from Preston New Road 1Z hydraulic Fracture Plan (Cuadrilla Resources, 2018a).*

These types of very simple fluid outlined in Table 1.2 and Table 1.3 are known as slick-water fluids (Kaufman et al., 2008), fluids that are predominantly composed of water and 1-2 additives, usually a friction reducer and a chemical tracer (Palisch et al., 2010).

In terms of hydraulic fracturing additives that have been deemed non-hazardous for UK operations, the Environment Agency, with the Joint Agencies Groundwater Directive Advisory Group (JAGDAG) and Amec Foster Wheeler have conducted assessments into

numerous potential additives (JAGDAG and UK Technical Advisory Group on the Water Framework Directive, 2018). In total, 462 chemicals were analysed for public consultation, and of these 462, 158 were classed as 'non-hazardous pollutants'. Within this data, polyacrylamide was found to be a 'non-hazardous pollutant'.

1.6.2. Polyacrylamide

Polyacrylamide, or PAM as it is referred to throughout this study, is a water soluble synthetic polymer (Smith et al., 1997; Yang et al., 2010) formed from the monomer acrylamide (Caulfield et al., 2002): it has the chemical formula $(C_3H_5NO)_n$. (Figure 1.5). The PAM is generally prepared from free radical polymerisation of acrylamide using a variety of methods (Caulfield et al., 2002). Sometimes also referred to as 2-propenamide or homopolymer (Acros Organics, 2009), PAM has a multitude of uses including clarification of drinking water, oil recovery, soil conditioning and biomedical applications (Caulfield et al., 2002; Xiong et al., 2018b).

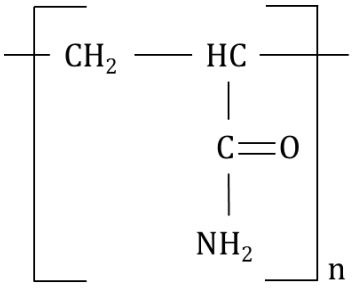

Figure 1.5: *General structure of Polyacrylamide. Diagram adapted from (Caulfield et al., 2002; Smith et al., 1997; SNF FLOEGER, n.d.; Xiong et al., 2018b).*

PAM is classed as 'non-volatile' and is above GHS (Globally Harmonised System of Classification and Labelling of Chemicals) category 5 (Stringfellow et al., 2014). This GHS categorisation means it may be harmful if swallowed, inhaled or via dermal exposure. It is also a category 5 hazardous chemical based upon the EU/Swiss poison classification (Montgomery, 2013) meaning that between 2000-5000 mg/kg may form a lethal dose. PAM's have no reported herbicidal properties and are considered non-toxic due to their inability to pass biological membranes (Smith et al., 1997).

1.6.2.1. Polyacrylamide as an additive

Traditionally, PAM has been largely used as a flocculant in the wastewater and agricultural industries (Smith et al., 1997; Xiong et al., 2018a). More recently it has been used as a viscosity modifier and a friction reducer in both enhanced oil recovery and hydraulic fracturing operations (Xiong et al., 2018a). Polyacrylamide is currently one of the most commonly used fracking additives in the United States (FracFocus, 2017). The PAM is added to fluids as a 'friction reducer' (Xiong et al., 2018b), minimising the friction between the fluid and the pipe allowing higher pump rates (Ferrer and Thurman, 2015). The PAM is commonly used in the three forms, non-ionic, cationic and anionic and generally are thermally stable up to 400 °F (204 °C) (Kaufman et al., 2008).

PAM is a very common friction reducer; data and literature suggest that it is now used in nearly 100 % of hydraulic fracturing operations (King, 2010). Of 100 randomly selected Pennsylvania wells from 2015 to present, 100 % of slick-water jobs used PAM as a friction reducer (Xiong et al., 2018b). However, as part of the study of Xiong et al. (2018b), 100 wells from the Bakken field (Montana and North Dakota) and 100 randomly selected wells from the Marcellus province (Pennsylvania, Washington and West Virginia) showed that PAM was not actually the most popular friction reducer. In these 200 wells, the most popular friction reducer was actually light petroleum distillates (Figure 1.6). Petroleum distillates took up 23 % and 37 % respectively of the friction reducing agents found within the random wells in the Bakken and Marcellus shales. PAM was used in lots of wells, but only stated as a friction reducer in 13 %. The remaining PAM was classed as an 'other ingredient'. The USEPA reports that 61 % of all 39,000 wells analysed used light petroleum distillates in some capacity (EPA, 2015). PAM, in any of its forms was used in 1.45 % of all wells analysed (EPA, 2015), however, some may have been missed in a general review due to the multiple naming conventions of PAM (2-propenamide, acrylamide polymer, polymerised friction reducer) (FracFocus, 2018). A full list of the 200 wells analysed for this study can be found in Digital Appendix A.1.

a)

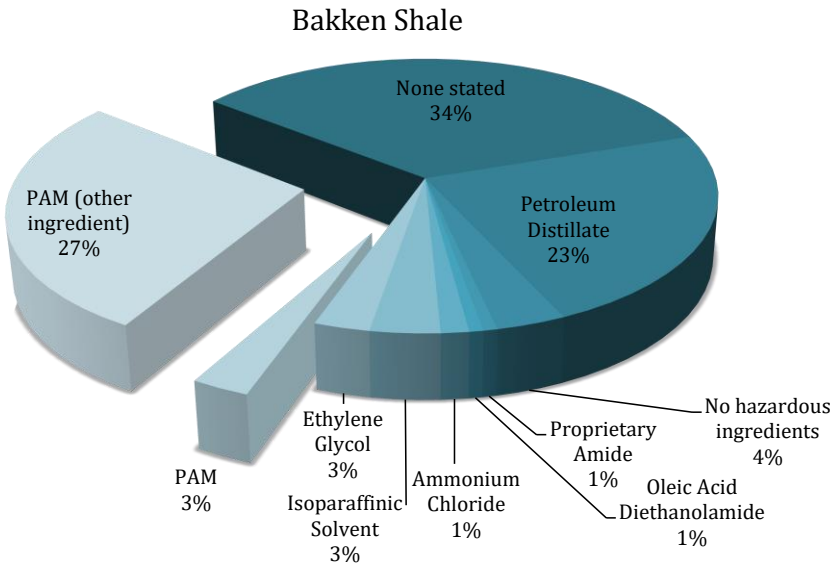

b)

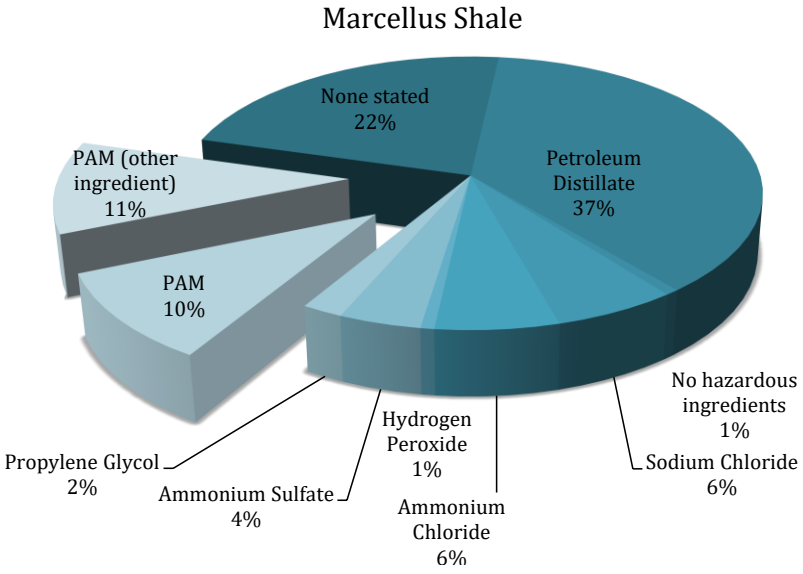

c)

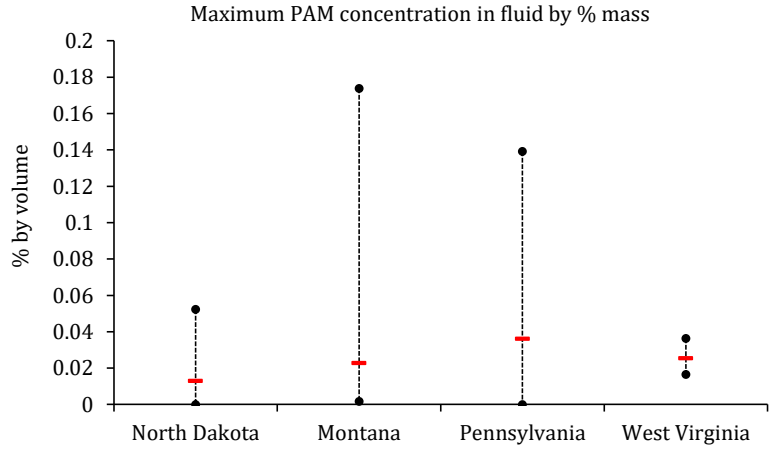

Figure 1.6: *Literature summary of 200 randomly selected wells in the Bakken (a) and Marcellus Shale (b) areas. Analysis sought the friction reducer used, and where not stated, if PAM was used as a non-specified 'other ingredient'. Collated results on the concentration of PAM used where present (c).*

In terms of the adsorption of PAM in the context of the fracking industry, there is very minimal literature assessing specifically the adsorption properties of PAM to shales or relevant lithologies. One of the closest studies mentioning adsorption is that of Xiong et al., 2018b who suggests polymer loss due to adsorption at ~35 % of the total 85 % polymer loss. Result of ~35 % polymer loss are similar to some of the results obtained within this study, from Chapter 3 onwards. The majority of PAM adsorption studies refer to interactions with either soils specifically. Examples of the interaction of PAM and soil can be found in Malik and Letey (1991) and Sojka and Entry (2000), concluding that high molecular weight PAMs can remve clay size sediment particles in flowing water and, effectively immobilising microorganisms – something which may prove useful in the subsurface in terms of solubised metals in redox conditions (discussed in Section 6.7). Another study by Sojka et al (2007) discusses PAMs more general use in agromany. The interactions between polymers, particularly PAM, are investigated in such studies, referring to interactions with clays or organic matter. Aside from PAM's popular use in agriculture, some studies have investigated the use of PAM in the drilling industries, both conventional and unconventional. The polymer PAM mainly reacts with the clay minerals (Deng et al., 2006a) within the borehole or rock formations. Tekin et al, (2005) investigates the adsorption potential of positively charged PAM onto kaolinite, citing that with a decrease in pH the adsorption decreases, alongside increasing kaolinite surface areas, in temperatures up to 600 °C (Tekin et al., 2005), temperatures and pH states that could be indicative of a deep, subsurface hydraulic fracturing environment. Volpert et al (1998) investigates the adsorption interactions between hydrophobically associating PAM's on clays and silicates, citing affinity is much greater on the silicate surface (Volpert et al., 1998) making the lithology type and mineralogy to which fracking occurs (more often than not shale type lithologies) an important factor in terms of PAM adosbancy. In terms of drilling, a few studies have looked at the interactions of PAM. Examples of this include: Bailey et al, (1994) stating that the adsorption of such polymers on particular clays, such as montmorillonite, is strongly dependent on electrolyte concentration and that high adsorption levels of the polymer aid the stabilisation of weakened and eroding materials in the wellbore and Li et al., (2018) investigating how the adsorption of PAM into the wellbore can decrease reservoir permeability by up to ~ 72 %, but the use of urea can breakdown the hydrogen bonding holding the adsorption, to aid recovery (Li et al., 2018).

1.7. Adsorption

In the context of this study, adsorption is predominantly investigated in terms of much aqueous PAM, used as a slick-water additive, is removed from the solution by means of adsorption. In this study, the PAM is classed as the adsorbent and shale (or rock type) classed

as the adsorbate. Adsorption is classed as a surface phenomenon occurring at the interface of two phases (Srivastava and Eames, 1998), where a gas or a liquid mixture is attracted to a solid, forming attachments (Foo and Hameed, 2010). It is defined as the enrichment of material or increase in the density of the fluid in the vicinity of an interface (Rouquerol et al., 1999). In its simplest form, molecules of a substance are stuck to the surface of another substance by either physical or chemical means. In this study, this would refer to PAM molecules sticking (adsorbing) to the surface of the rock. In the wider world, adsorption is becoming increasingly popular in the water treatment industry because of its simplicity, cost effectiveness and regeneration capacity (Ahmaruzzaman, 2008; Kundu and Gupta, 2006). The adsorption of polymers can also be exploited in the drilling industries, where high adsorption levels can help stabilise materials against erosion and increase lifetime (Bailey et al., 1994).

Primarily there are two types of adsorption, physical and chemical, otherwise known as physisorption and chemisorption, respectively. Physisorption is caused by Van der Waals forces and electrostatic interactions (Ruthven, 1984) whereas chemisorption primarily involves valency forces between adsorbate and adsorbent (Srivastava and Eames, 1998). Physisorption is classified as a general phenomenon with a low degree of specificity. It can occur as multilayer, especially at higher pressures (Rouquerol et al., 1999) and is always exothermic although the heat loss is low. This type of adsorption is reversible, as no chemical bonds have formed, and so desorption is possible where the molecule keeps its identity at returns to the fluid phase in an unaltered form (Rouquerol et al., 1999). Chemisorption, on the other hand, is where the molecules are linked to the reactive parts of the surface, confined to monolayer type adsorption (Rouquerol et al., 1999). Chemisorption is often irreversible in normal or similar conditions to adsorption.

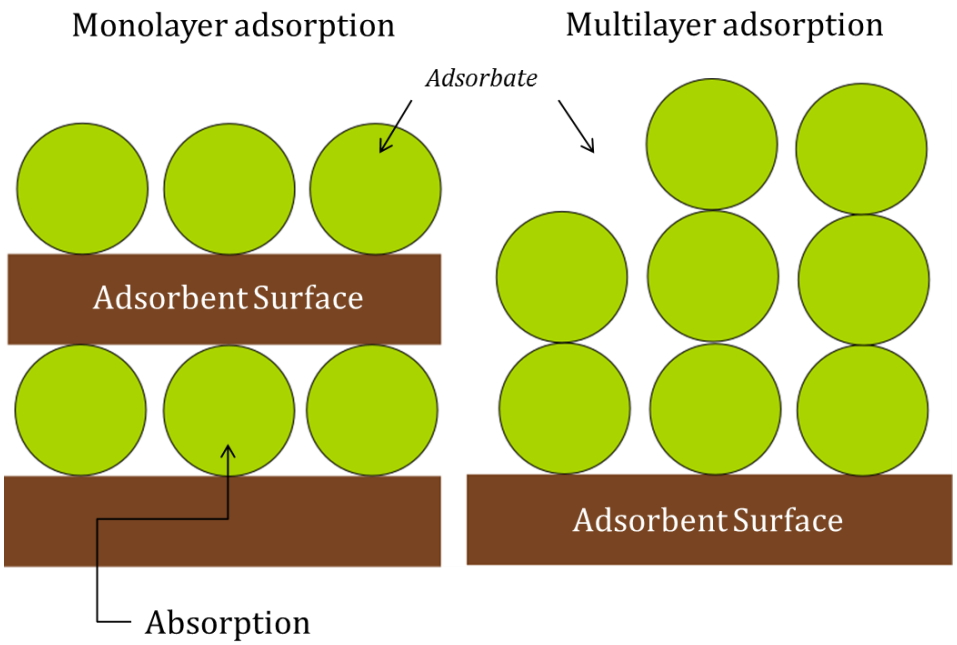

Figure 1.7: *A graphical summary of how adsorption works compared to absorption, showing both monolayer and multilayer adsorption. In the context of this study, the adsorbent surface is clay/shale and the adsorbate is PAM.*

Isotherms are a way of expressing the amount adsorbed by an adsorbent under pressure and a constant temperature; they describe, in the case of this study, how pollutants interact with the adsorbent and are critical for the expression of surface properties and adsorbent capacities (Foo and Hameed, 2010). There are multiple types of isotherm that can be fitted to multiple types of experimental data, from the heavily favoured and simplistic linear, Freundlich and Langmuir isotherms to the far more complex Temkin, Polanyi-Manis and BET isotherms. There are multiple sources of literature that explain these types very well (Ahmaruzzaman, 2008; Foo and Hameed, 2010; Freundlich, 1906; Kinniburgh, 1986; Kundu and Gupta, 2006; Langmuir, 1917; Rouquerol et al., 1999). Within this study, the linear, Freundlich and Langmuir isotherms are used, predominantly because of their simplicity and their ability to fit a variety of adsorption data well (Kinniburgh, 1986). These three isotherms, linear, Freundlich and Langmuir, are described in more detail in Section 3.4. The Freundlich and Langmuir isotherms are two-parameter isotherms (Foo and Hameed, 2010). The Freundlich isotherm (Freundlich, 1906) is an empirical model and an exponential equation that can be applied to multilayer adsorption (Foo and Hameed, 2010), assuming that the adsorbate concentration increases, so too does the adsorbate on the adsorbent surface (Allen et al., 2003). On the other hand, the Langmuir Isotherm (Langmuir, 1917) assumes that adsorption takes place at specific homogenous sites (Kundu and Gupta, 2006), i.e. once a sorbate molecule occupies a site, no further adsorption can take place, also known as monolayer adsorption (Allen et al., 2003). Langmuir isotherms are characterised, graphically, as plateauing out at a 'maximum coverage', a saturation point at which no further adsorption

can take place as all sites are occupied and multilayer adsorption cannot occur (Allen et al., 2003). At lower concentrations Langmuir theory follows Henrys Law (Linear isotherm) (Foo and Hameed, 2010; Kundu and Gupta, 2006; Rouquerol et al., 1999).

Adsorption is principally controlled by temperature, time, concentration, pH and pressure (Guo et al., 2018), but this is dependent on whether the adsorption is physical or chemical. In terms of pH, if the system the polymer is in, in this case non-ionic PAM, is too alkali or acidic then the molecular structure of the polymer will be destroyed or altered (Guo et al., 2018). For this study, slick-water systems are generally neutral to weak alkali. Adsorption of adsorbates (in this study both non-ionic PAM and some metals discussed in Chapter 6) onto surfaces tends to decrease with an increase in pH (towards more alkali solutions) (McGuire et al., 2006). Under neutral conditions, adsorption quantity is unaffected. The rise of pH causes an increase in negative charges and thus stronger electrostatic repulsions between disassociated carboxyl groups located within macromolecules that make up the surface (Wiśniewska et al., 2016). Temperature effects on adsorption can be variable, and are fairly infrequently reported upon in the worldwide literature (Wiśniewska, 2012). Initially, a temperature increase from 0 – 45 °C would increase the adsorption rate, due to the increase in the diffusion speed of polymer molecules, thus collisions at the interface of the adsorbate and adsorbent increase. At certain temperatures, varying depending on adsorbent and adsorbate, the desorption rate will increase as polymers will separate from the surfaces and literally melt back into solution, dependent on a critical temperature (Guo et al., 2018).

For the purposes of this study, slick-water fluids produced are pH neutral and non-ionic. Tests are conducted in both room temperature (Chapter 3) and elevated temperature environments (Chapter 4), indicative of the onshore UK shale gas basins (Andrews, 2014, 2013; Broderick et al., 2011). The pressures required for hydraulic fracturing at 2.5-3 km depth onshore cannot be met by the capability of available laboratory equipment.

1.8. The Bowland Shale

Within the UK, there are three major prospects for the exploration and exploitation of shale gas; the carboniferous potential of the Midland Valley in Scotland (Monaghan, 2014); the Jurassic Kimmeridge shales of the Weald Basin (Andrews, 2014; Mair et al., 2012); and the Bowland Shales of the North of England (Andrews, 2013; Gross et al., 2015). The Bowland Shale is quite possibly the most well-known shale gas resource in the UK and identified as the main potential resource (Newport et al., 2016) for UK onshore carboniferous deposits (Waters and Davies, 2006). Deposited during the late Visean and early Namurian periods of the Carboniferous (Andrews, 2013), approximately 347-318 Ma, the Bowland shale is a hemi-pelagic mudstone located mostly in the NW of Lancashire (Waters et al., 2013). The deposition

of the shale occurred alongside deposition of limestones, during the syn- and post-rift stages of a back-arc basin (Gross et al., 2015).

It is estimated that the Bowland Shale Group, inclusive of both the Upper and Lower Bowland shales, contains between 822 and 2281 trillion cubic feet (tcf) (2.33×10^{13} to 6.46×10^{13} m^3) of gas-in-place (Andrews, 2013; Mair et al., 2012; U.S. Energy Information Administration, 2015). The Bowland shale is a carbon rich shale of interest with multiple analyses undertaken on it over the last 40 years. Total organic carbon (TOC) values range from just above 0 % to ~ 14 % (Andrews, 2013; Armstrong et al., 1997; Gross et al., 2015; Kenomore et al., 2017; Konitzer et al., 2015; Maynard et al., 1991; Newport et al., 2016; Smith et al., 2010; Spears and Amin, 1981; U.S. Energy Information Administration, 2015) with the majority of data greater than the 2 % TOC viability cut off for UK Namurian black shales (Andrews, 2013; Charpentier and Cook, 2011) with the majority of data above the 2 % TOC cut-off for UK Namurian black shales, discussed in Chapter 2 (Figure 1.8).

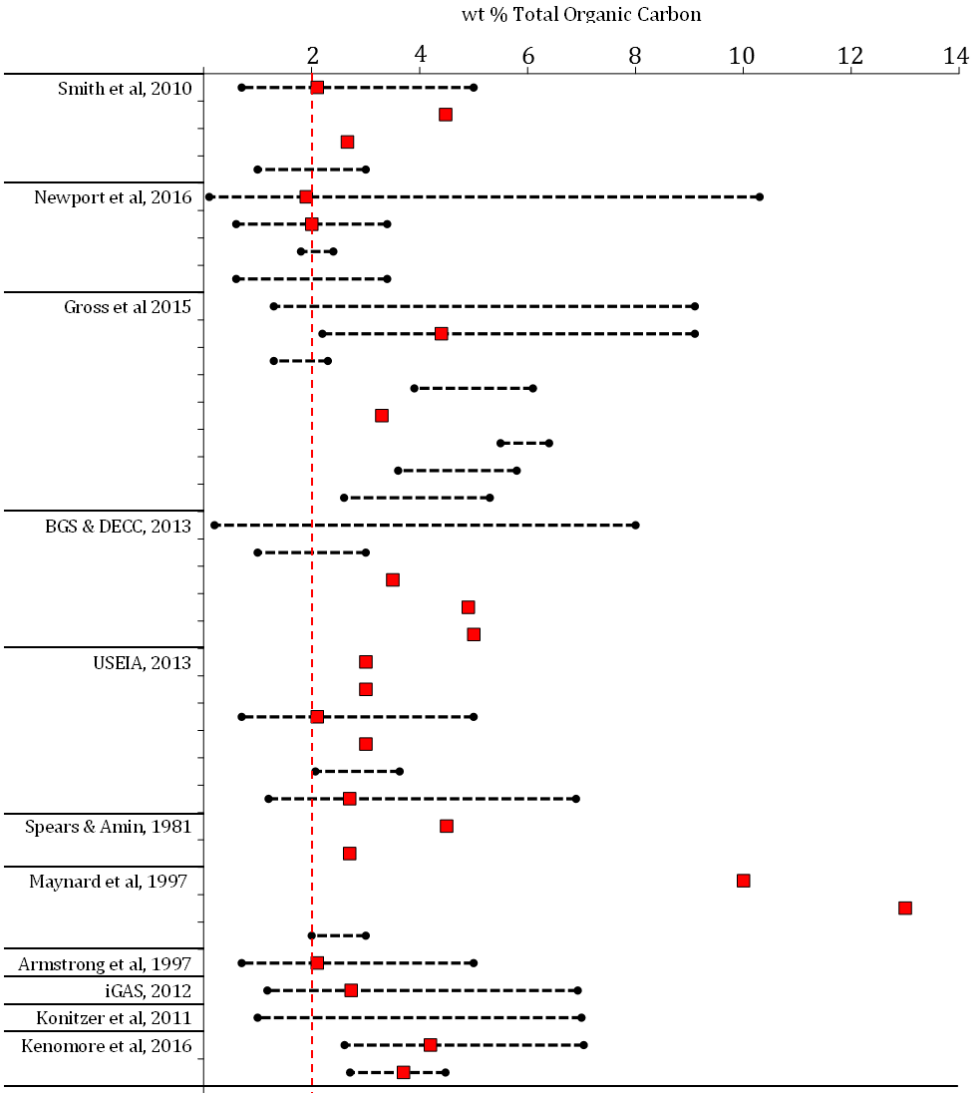

Figure 1.8: *All TOC values for the Bowland Shale from various locations and depths from a number of sources (Andrews, 2013; Armstrong et al., 1997; Gross et al., 2015; Kenomore et al., 2017; Konitzer et al., 2015; Maynard et al., 1991; Newport et al., 2016; Smith et al., 2010; Spears and Amin, 1981; U.S. Energy Information Administration, 2015). Black dashed lines represent the range of TOC measurements observed on the relevant dataset, and red squares denote the average value, where presented. Red line denotes the > 2 % cut off for UK Namurian Black shales.*

It has been discussed that the Bowland shale contains anomalously high levels of trace elements inclusive of selenium (Se), molybdenum (Mo) and arsenic (As) (Parnell et al., 2016). The concentrations can range from 20.5 ppm to 41.1 ppm (Parnell et al., 2016) which may have an effect on flow-back fluid composition.

Only three wells have fracked for unconventionals to date in this country, Elswck-1, Preese Hall 1A and Preston New Road 1Z. Preese Hall 1A and Preston New Road 1Z both targeted the Lower Bowland Shale at subsurface depths of 8220 ft and 7500 ft, respectively. Preston New Road drilled a further 800 m for a horizontal fracking procedure (Cuadrilla Resources, 2018a; Hird et al., 2011).

1.9. Flow-back Fluids

Flow-back fluids, and metals concentrations are one of the biggest areas of interest within the hydraulic fracturing research. One of the most important, and largest, sources of information regarding flow-back fluid is the USGS Produced Waters database (Blondes et al., 2017). The USGS Produced Waters database stores data for 114,943 wells that have been hydraulically fractured and have disclosed data of flow-back fluids (data ranges that are analysed in this study are shown in Figure 1.9). One of the limitations of the USGS Produced Waters study is that not all wells disclose all components and data can be sparse, amongst the multiple parameters.

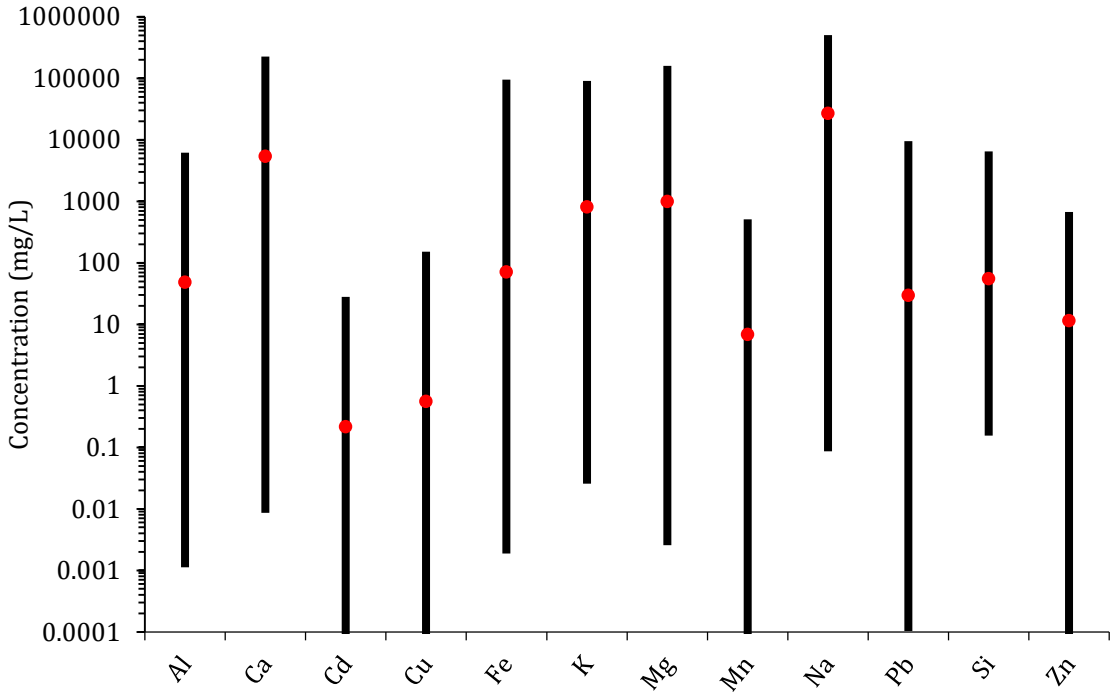

Figure 1.9: *Data summary from the USGS produced waters database (Blondes et al., 2017) showing reported data for metals analysed ONLY in this study, as seen in Chapter 6. High and low ranges are denoted by the black line, and average values are denoted by the red square. Data is sourced from 114,943 wells.*

Another limitation of the database is the fact that with a database so large and sometimes sparse, numerical errors are highly likely, especially in terms of units in mg/L or µg/L. The database is, however, still useful, especially in terms of the size (number of wells) and the variability of data. On a smaller scale, within the UK, there is almost no flow-back data to call upon. One of the key flow-back data sources used in this study is summarised by Broderick et al., (2011) for the flow-back composition of Preese Hall 1A. A summary of data by

Broderick et al., (2011) (Table 1.4) may give pointers as to what to expect in future fracking operations using a relatively simple slick-water fluid, particularly from the Lower Bowland Shale.

	EU Regulatory (mg/L)	Flowback 1 (mg/L)	Flowback 2 (mg/L)	Flowback 3 (mg/L)	Flowback 4 (mg/L)	Flowback 5 (mg/L)
Arsenic (As)	0.01	0.0062	0.001	0.001	0.0012	0.0026
Cadmium (Cd)	0.005	0.00129	0.0005	0.0005	0.002	0.001
Chromium (Cr)	0.05	0.025	0.00403	0.003	0.0205	0.0539
Copper (Cu)	0.002	0.936	0.00804	0.005	0.0376	0.0344
Lead (Pb)	0.01	0.6	0.01	0.01	0.04	0.0449
Mercury Hg)	0.001	0.000024	0.00001	0.00001	0.00001	0.000012
Nickel (Ni)	0.02	0.0203	0.005	0.005	0.02	0.02

Table 1.4: *Concentration of metals regulated by the EU in flowback fluids from Preese Hall 1A over five flowback events (Broderick et al., 2011).*

There have been multiple studies in the USA looking at the composition of flow-back waters. Studies into the shale geochemistry and trace data are summed up well by Chermak and Schreiber (2014) which links to most other studies of flow-back fluids, and is designed to be used as a "first step in using compiled datasets to examine large scale patterns". Enomoto et al., 2015 is a more targeted look into the geochemistry and mineralogy of Devonian shales in the Appalachian Basin, suggesting rock types are more quartz and carbonate rich rather than clay rich. Lavergren et al (2009) analyses the same subject but with a broader 'black shale' perspective, assessing the mobility of certain metals stating that the shales are rich in hazardous metals such as cadmium (0.005-15.9 mg/kg), uranium (2.11-227 mg/kg) and Molybdenum (3-240 mg/kg), as examples. Metal concentrations within shales analysed across all literature, can vary substantially between, shales, basins, environments and sample type. In terms of flow-back fluids specifically, most studies show that the largest concentrations come in the form of sodium (49,400 mg/L) and calcium (20,800 mg/L) (Chapman et al., 2012; Shih et al., 2015) and occasionally potassium (17,043 mg/L) (Maguire et al 2014) but this is largely dependent on shale type, as these studies analyse predominantly the Marcellus shale, with Maguire-Boyle and Barron, (2014) also accounting for the Eagle Ford and the Barnett shale formations. As mentioned previously, flow-back fluids do have elevated concentrations of multiple minerals. Few major studies have been conducted relating to the UK. The most notable UK studies focus around the impact in groundwater that Se could have (Parnell et al., 2016) and general groundwater impacts to the UK (Broderick et al., 2011; Stuart, 2012). In terms of a more general European summary of groundwater impact, M4 Shale Gas consortium have conducted assessments into the wider impact of groundwater quality (Jacobsen et al., 2015),

alongside smaller sub projects focussing on the impact of water and soil, the impact on air quality, public perceptions and program management and popular science contributions. More details on these sub-projects can be found on their website: www.m4shalegas.eu.

In terms of how metals are mobilised or adsorbed in soils (and the subsurface), thus determining what may or may not be present in flow-back fluids, the principle governing factors are pH, organic matter, clay content and redox potential, alongside other miscellaneous factors (Rieuwerts et al., 1998). Metals solubility generally increases at lower pH's, and vice versa (Chuan et al., 1996; EPA, 2007; Rieuwerts et al., 1998). Overall, more acidic and reducing concentrations are more ideal for metal solubilisation, with Chuan et al, (1996) suggesting that pH has a more significant effect than reducing conditions. Organic matter is another key component, either within soils or clay content. Organic matter is typically greater within shales than soils, due to clay content, but the general principles remain the same. Some soils may contain no clay and only organic matter Adsorption of metals by organic material is predominantly through ion exchange (Rieuwerts et al., 1998), through negatively charged functional groups such as phenol, carboxylate and amino groups (Eriksson, 1989; Rieuwerts et al., 1998). Typically, in deep groundwaters and moderate to high TOC shales, Eh (or redox potential) is low (Evans, 1989) and promotes metal solubility. The metal solubility is highly dependent on the metal type and the temperature, however, and some low Eh conditions do not favour metal solubility (Rieuwerts et al., 1998). In reducing environments, sulphates are typically reduced by bacteria to sulphides that are insoluble, however if the pH is <5, this does not occur (Bloomfield, 1981). From here, sulphides minerals are usually oxidised to sulphates at higher Eh levels (Evans, 1989). Throughout this study, the above can be speculated upon, however redox factors were not specifically measured for regarding the simulated flow-back fluids observed in Chapter 6.

1.10. Thesis aims and objectives

The aim of this thesis was to assess the interaction between certain samples of shale and the friction reducer polyacrylamide (PAM). Assessing the interactions focusses predominantly on both the adsorption and desorption properties of adsorbent and adsorbate. These interactions will be tested both at room temperature and in higher temperature and higher pressure (HPHT) environments. Fluids from all experiments will be analysed as 'flow-back' fluids. The general aims and objectives of this study can by summarised as the following:

- Characterise the Bowland Shale and other lithologies relevant to this study through XRD, XRF and carbon analyses. Results of these analyses can firstly be used to investigate potential factors in the adsorption, desorption and flow-back results

and secondly, be used in and compared to wider literature for the Bowland Shale and associated lithologies.

- Quantify any PAM that is removed from the slick-water solution by means of adsorption, firstly at room temperature and pressure conditions. PAM is likely to adsorb to the shale lithologies when slick-water fluid and rock interact. Exact amounts of adsorption have not been well studied in the context of fracking.
- In addition to room conditions, quantify any PAM removed from solution by adsorption under higher pressures and temperature conditions that are indicative of UK basins, in particular the Bowland Basin.
- Quantify how much of any adsorbed PAM can be desorbed back into solution, stimulated by the 'freshwater-flushing' phase of hydraulic fracturing operations. Based upon literature, it is unlikely that any adsorbed PAM will desorb easily, or in quantities matching adsorption, thus leaving it open to depolymerisation or degradation downhole over longer time periods.
- Assess the composition of all simulated flow-back fluids associated with the adsorption and desorption experiments. Fluids will be analysed for a specific set of contaminants to aid understanding of what flow-back fluids may result in the context of UK geology.
- Investigate how the addition of 1 g of PAM to 1 L of mains tap water, creating a 1000 mg/L solution of PAM slick-water fluid can alter the composition of a tap water solution, alongside creating a more viscous fluid. It will also particularly increase the salinity greatly, providing potential environmental issues at the point of flow-back and disposal.
- Investigate how the addition of PAM is likely to influence other metals within the fluid, not just salinity.

Ultimately, the results of this study will be used by the principle project funders, the Environment Agency, and other governing bodies to provide informed information about the regulation of fracking additives and such activities. Such data and results may have the potential to be incorporated into policy for the future safeguarding of the industry and the environment.

1.11. Thesis Outline

The thesis is divided into the following:

- **Chapter 2**: Sample Collection and Characterisation. This chapter explains how samples for use in this project were selected because of their relevance to a UK shale gas industry. Sample locations and type are outlined. Selected samples are characterised using various quantitative and qualitative methods so that data from these can be cross-referenced to any adsorption, desorption and metals data further on in the study.
- **Chapter 3:** The Adsorption of Polyacrylamide at Room Temperature. This chapter compiles the results of the room temperature adsorption experiments. The purpose was to assess how much polyacrylamide could be removed from a synthetic lab produced slick-water fluid (PAM and water) of various concentrations. The results were then plotted on three main isotherms, Linear, Freundlich and Langmuir, to obtain adsorption capacities. The qualitative and quantitative data from Chapter 2 is statistically analysed against any adsorption data to understand what is controlling the adsorption capacity
- **Chapter 4:** The Adsorption of Polyacrylamide in High Pressure High Temperature Environments. Similar to Chapter 3, this chapter assesses the adsorption on a smaller subset of samples at higher pressures and temperatures. Results are plotted onto isotherms and the same statistical analyses are undertaken on the results against sample characterisation data. This chapter addresses whether increases in pressure or temperature (to near subsurface conditions) will have other effects upon the adsorption of PAM.
- **Chapter 5:** The Desorption Properties of Adsorbed Polyacrylamide. This chapter assesses the desorption properties of any PAM that has adsorbed to the rock surface. It is key to know the desorption properties of PAM, as much as the adsorption properties, as this is one key indicator of how PAM may degrade or mobilise in the subsurface.
- **Chapter 6:** The Colloidal Behaviour of Polyacrylamide as a Hydraulic Fracturing Fluid Additive. To understand how PAM may alter the release of potential contaminants from fracking fluids, we need to test its behaviour as a colloid. This chapter will assess how the colloidal properties of PAM interactions with shale and Cadmium and how the two systems promote or inhibit movement across a dialysis membrane. All of these experiments are conducted at room temperature and further reveal how PAM may behave in the environment.

- **Chapter 7:** Metals Analysis of Flow-back Fluids. A large-scale composition analysis of all of the fluids from the room temperature and high-pressure high temperature adsorption experiments. Fluids are analysed for certain metals/analytes to establish the likely concentrations of flow-back fluids and how they may be affected by environment, lithology type and additive concentration.
- **Chapter 8:** Conclusions. A synthesis of all results, discussions and findings for all chapters in this study. Further research onward from the project is explored.

2. Sample Collection and Characterisation

2.1. Introduction

For this project to fit into the context of the UK fracking industry, shales of interest needed to be sourced from the UK. Across the United Kingdom, there are 3 major areas of interest: Carboniferous shales across the north of England (Andrews, 2013); the Jurassic shales of the Weald Basin in southern England (Andrews, 2014); and the Carboniferous shales of the Midland Valley in central Scotland (Monaghan, 2014). As the Carboniferous Bowland shale is the only one of these shales to have received licenses for the development of commercial fracking, it is this shale that is focussed on for this study. The Bowland Shale unit is the largest shale gas unit in the UK (Andrews, 2013) and is also the main hydrocarbon source of UK onshore Carboniferous deposits (Waters and Davies, 2006).

Deposited during the late Visean and early Namurian, the Bowland Shale unit is a hemi-pelagic mudstone, approximately 2700 m at its thickest in the NW of Lancashire (Waters et al., 2013). The Upper and Lower Bowland Shales sit at the top of the 'Bowland-Hodder Group' which incorporates the Hodderense and Pendleside limestone formations. Overlying the Bowland-Hodder Unit is the Millstone Grit group, of which the lowermost member is the Pendle Grit formation. The Pendle Grit was the first of a major set of deposits of medium to coarse grained siliclastic sediments into the post rift Craven Basin in the early Namurian (Kane et al., 2009). A summary of the aforementioned stratigraphy is shown in Figure 2.1. Outcrops of the Bowland Shales can be seen in various locations in the Forest of Bowland and the Ribble Valley, detailed in Figure 2.2, and including, but not exclusive to, the areas of Hazelhurst Fell, Wolf Fell, Sykes Quarry and Langden Brook (Figure 2.2 and Table 2.3).

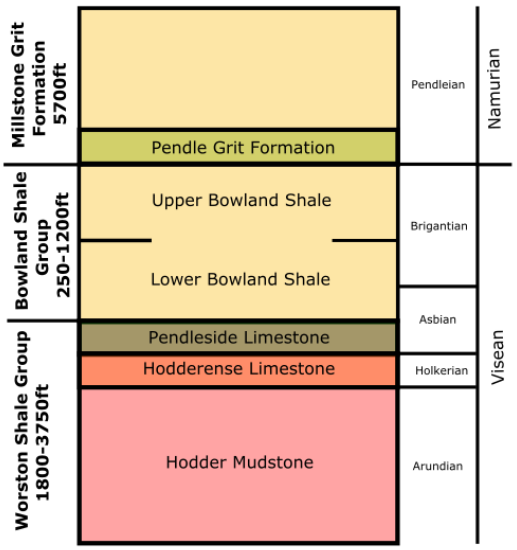

Figure 2.1: *A simplified stratigraphic section, edited from the BGS and Earp et al., 1961, showing the major units observed in the field.*

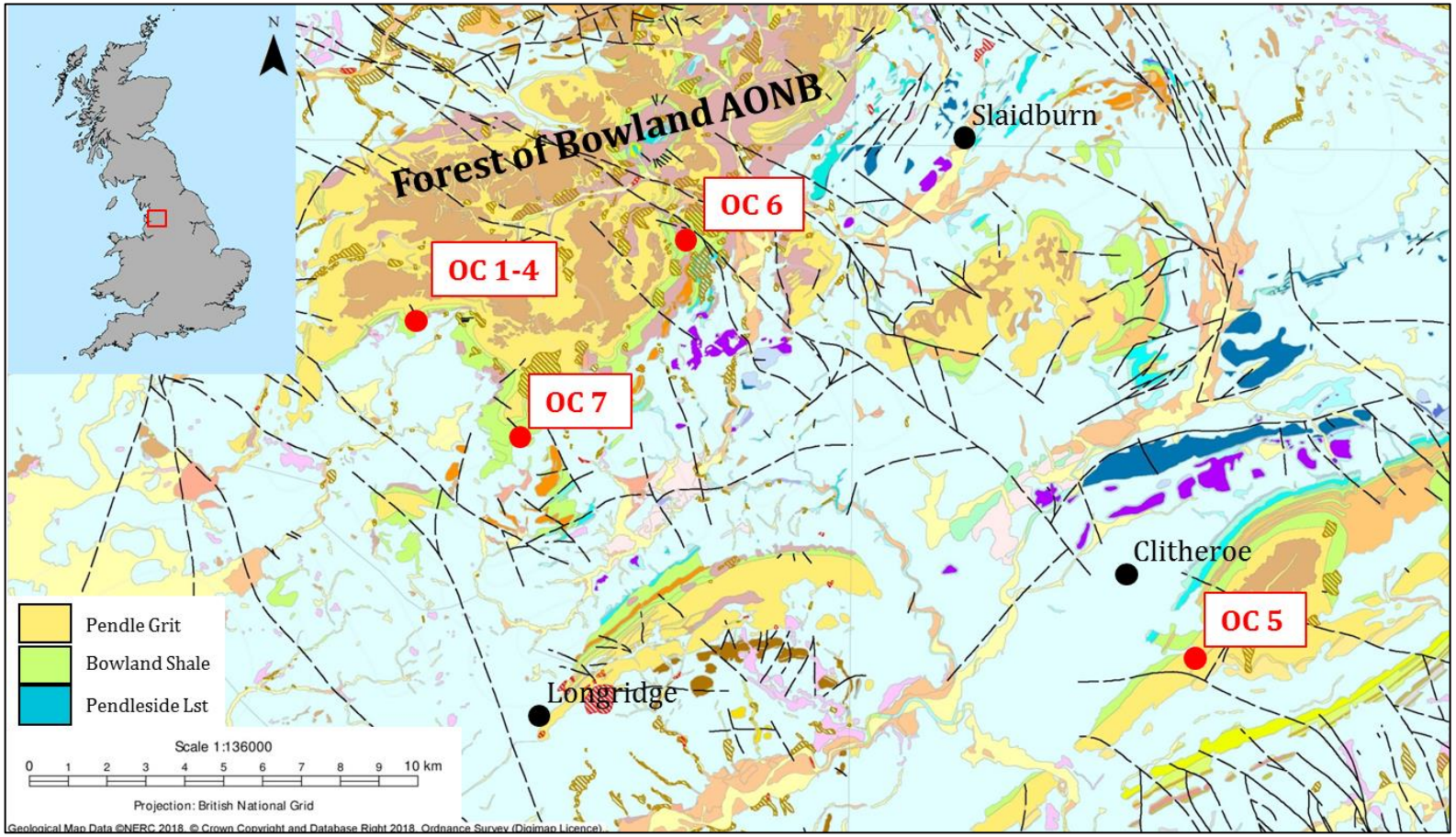

Figure 2.2: *Map showing the major outcrop areas for the Pendle Grit, Bowland Shale and Pendleside Limestone in the Forest of Bowland and Clitheroe area. Samples detailed in Table 2.1 are shown as red dots; OC 1-4 (Hazelhurst Fell); OC 5 (Nick O'Pendle); OC 6 (Sykes Quarry) and; OC 7 (Wolf Fell).*

2.2. Sample Collection and Preparation

It was decided that samples for this study should come from: both borehole and outcrop; and, from lithologies both stratigraphically above and below the Carboniferous shales of interest, the Pendle Grit and Hodderense Limestone (Figure 2.1). This use of 'non-shale' samples (Pendle Grit and Hodderense Limestone) would account for either; any interbedded units near boundaries and; if any fractures and/or fluids were to migrate beyond exploited shales during fracking operations. The main reason for using samples from both outcrop and borehole was availability. Outcrop samples are essentially unlimited, purely depending on how much is sampled at any one time. Borehole samples on the other hand are strictly limited, however having actual samples of subsurface rock types that are likely to be frack, or have been fracked, is invaluable to the project. It should be noted that all samples adhere to the naming convention detailed in Table 2.1.

In total, 13 samples were obtained for analysis. These 13 were a combination of both borehole and outcrop, and a mix of all relevant lithologies, not exclusively shales. The spread of all samples used is shown in Figure 2.3 and a summary table of all samples is given in Table 2.1.

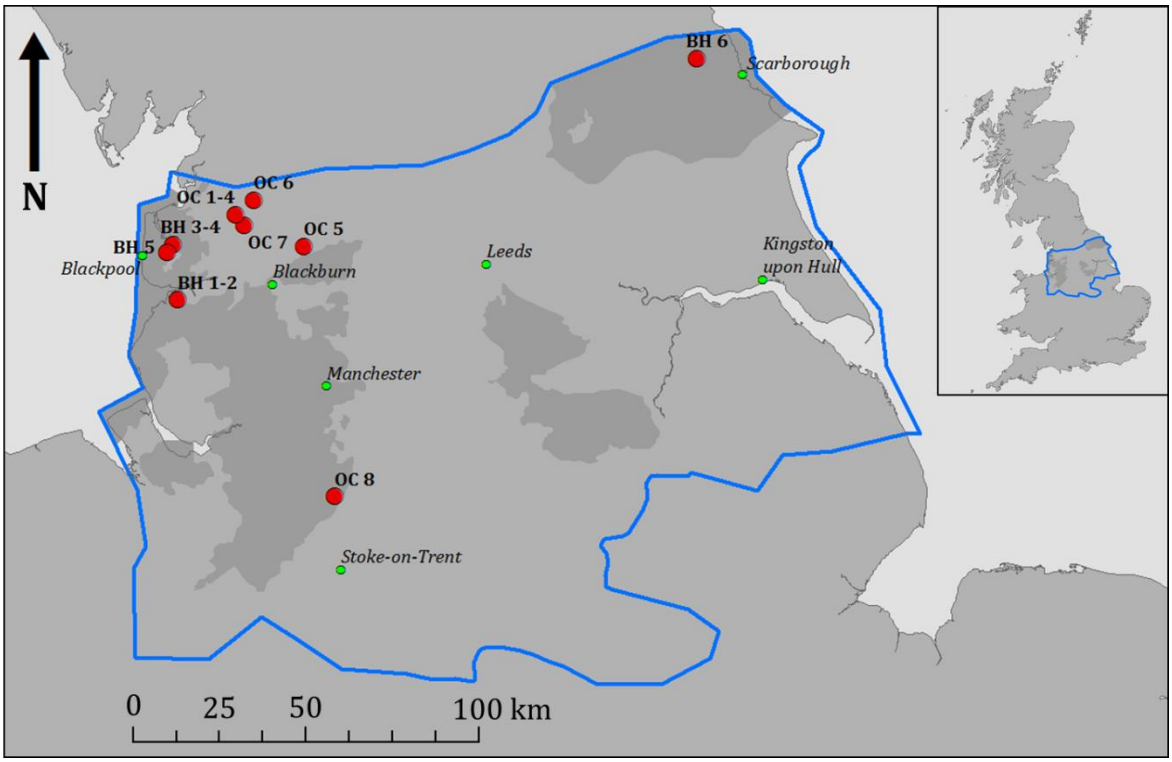

Figure 2.3: *Map of northern England showing all locations of outcrop and borehole samples. Outcrop samples are limited to the NW. The darker grey shaded area shows the extent of the subsurface Bowland*

Shale and the blue outline denotes the extent of the DECC 2013 report on the Bowland shale, adapted from (Andrews, 2013).

SAMPLE NAME	SAMPLE LOCATION	LITHOLOGY SAMPLED
OC 1	Hazelhurst Fell	Pendle Grit
OC 2	Hazelhurst Fell	Pendle Grit (shale rich)
OC 3	Hazelhurst Fell	Upper Bowland Shale
OC 4	Hazelhurst Fell	Upper Bowland Shale (sand rich)
OC 5	Sabden Quarry, Pendle Hill	Pendle Grit
OC 6	Sykes Quarry	Upper Bowland Shale/Pendleian Lst
OC 7	Wolf Fell	Upper Bowland Shale
OC 8	Congleton Quarry	Congleton Sandstone
BH 1	Becconsall 1Z 7030 ftTVD	Upper Bowland Shale
BH 2	Becconsall 1Z 7420 ftTVD	Lower Bowland Shale
BH 3	Grange Hill 7026 ftTVD	Upper Bowland Shale
BH 4	Grange Hill 8134 ftTVD	Upper Bowland Shale
BH 5	Preese Hall 1A 8885 ftTVD	Lower Bowland Shale
BH 6	Lockton 3 7049 ftTVD	Carboniferous Shale

Table 2.1: *Table showing a summary of all samples finalised for use in various experiments. 'Lithology Sampled' is based upon descriptions allocated to the rock in various references; for example, 'Carboniferous Shale' was not sub divided further in Lockton 3's End of Well Report. XRF mineralogy, TOC, TC, TIC and XRD for all samples can be seen in Section 2.4.*

2.2.1. Borehole Samples

Borehole samples were sourced from the BGS Core Store in Keyworth, Nottingham. Here, samples were in the form of core, cuttings or borehole specimens (larger blocks of cutting that are 5-20cm in size). Using cross sections, maps, drilling reports and the BGS open source borehole scan facility; wells were selected that penetrated the relevant shales. Using the BGS Core Store search facility, information was gathered on sample presence at depths relevant to the Carboniferous shales of interest. Cores were ordered and samples taken. Sample availability on certain samples was low, and thus only 1/3 of remaining samples could be taken. Core samples (samples that were blockier and boulder like) were the preferred type as cuttings often offered very small amounts of rock sample that may have also been contaminated due to washing at point of source, for example running through the mud shakers at wellhead.

Investigation of borehole data to ascertain what samples were available was highly variable and was dependent on the quality of the well metadata. More recent wells, examples being Preese Hall 1A (2010) and Becconsall 1Z (2011), provided comprehensive reports and logs in digital form. Older wells, such as Lockton 3 (1967), provided fewer comprehensive

reports usually in the form of scans. An example of the difference in data quality can be seen in Figure 2.4.

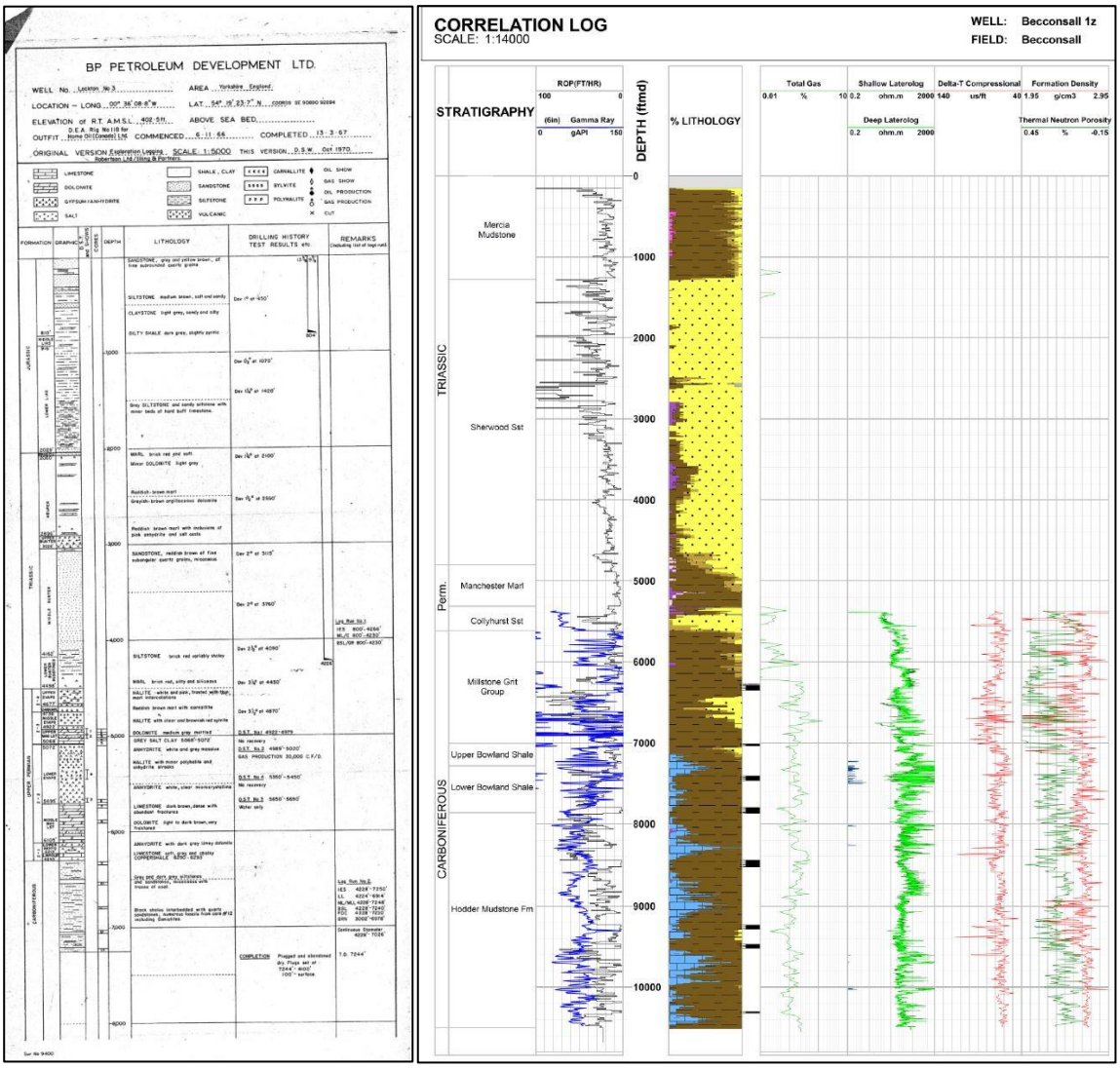

Figure 2.4: *Examples of the summary completion logs from Lockton 3 (left) and Becconsall 1Z (right). More modern logs are far more comprehensive and usually are less prone to mistakes. Images taken from BP Petroleum Development LTD, 1967 and Hird et al., 2011.Completion logs sourced from IHS and not publically available.*

Multiple samples were taken from 12 different wells. Due to the sample nature and availability, only 4 of the 12 wells were deemed fit for purpose within all experiments throughout this study, predominantly due to sample quantity and preparation (Table 2.2).

WELL	TYPE
Preese Hall 1A	Cuttings & Core
Lockton 3	Core
Becconsall 1Z	Cuttings & Core
Grange Hill 1Z	Cuttings & Core
Thistleton 1	Core
Kirby Misperton 3	Cuttings
Boulsworth 1	Borehole Specimen
Duggleby 1	Cuttings
High Hutton 1	Cuttings
Wessenden 1	Cuttings
Weeton 1	Cuttings
Roddlesworth 1	Cuttings

Table 2.2: *All borehole samples initially taken from the BGS. Those in green are the samples that were chosen for use in experiments and characterisation.*

The wells not used were not used because of poor quality samples, often due to minimal amounts of cuttings. Those wells that were used (highlighted in green in Table 2.2) typically contained large amounts of sample, enough for multiple experiments and testing. These samples were typically 1/3 of a 6 cm diameter core section. Some core sections were 11 cm in diameter (Lockton 3). Examples of the type of core sections provided are shown in Figure 2.5.

Figure 2.5: *Upper Bowland Shale borehole samples taken from BH 1 (Becconsall 1Z (left)) and BH 3 (Grange Hill 1Z (right)).*

As shown in Figure 2.3, there is a distinct lack of borehole sampling from the northeast of England. At the time of sample gathering, the area around Kirby Misperton, in the Vale of Pickering, was highly active in shale gas exploration. The current activity made samples such

as the current Kirby Misperton wells (KM 8 as an example) very difficult to obtain for confidentiality reasons. Other older wells in the area had not penetrated gas bearing Carboniferous rocks and hence why only one sample from a borehole was taken from this region.

2.2.2. Outcrop Samples

Outcrop samples were sourced from Lancashire, in particular, the Forest of Bowland area, north of Blackburn and northwest of Clitheroe. The outcropping geology in this whole area is what is known as the 'Bowland Series', consisting of Millstone grits, sandstones, limestones and shales (Lancashire County Council, 2015). Here, the relevant lithologies of the Pendle Grit, Upper Bowland Shale, Lower Bowland Shale and Hodderense Limestone are accessible at the surface.

To accurately ascertain where certain outcrops of the aforementioned lithologies existed, a literature search was conducted. Using BGS Sheet 67 (British Geological Survey, 1991) alongside the memoir for sheet 67 (Aitkenhead et al., 1992) and Lancashire County Councils Landscape Character Assessment of the Forest of Bowland (Chris Blandford Associates and Lancashire County Council, 2009) it was possible to pinpoint areas of interest to visit to obtain samples – as an example, Figure 2.6 shows locations OC 1 – 4 and OC 7.

Fieldwork took place in January 2017. The aim was to spend 1 day at 1-2 outcrops per day collecting samples. The reality, however, was the weather prevented a few sites from being accessed. This said, adequate amounts of sample were obtained from a good proportion of the previously proposed sites. In total 7 sites were visited. Of these 7 sites, 5 provided adequate outcrop of which 4 were used in all experimentation and characterisation. Two sites did not provide adequate outcrop due to dangerous terrain coupled with outcrop buried beneath quaternary cover. The locations of these samples can be viewed in Table 2.3 and Figure 2.3.

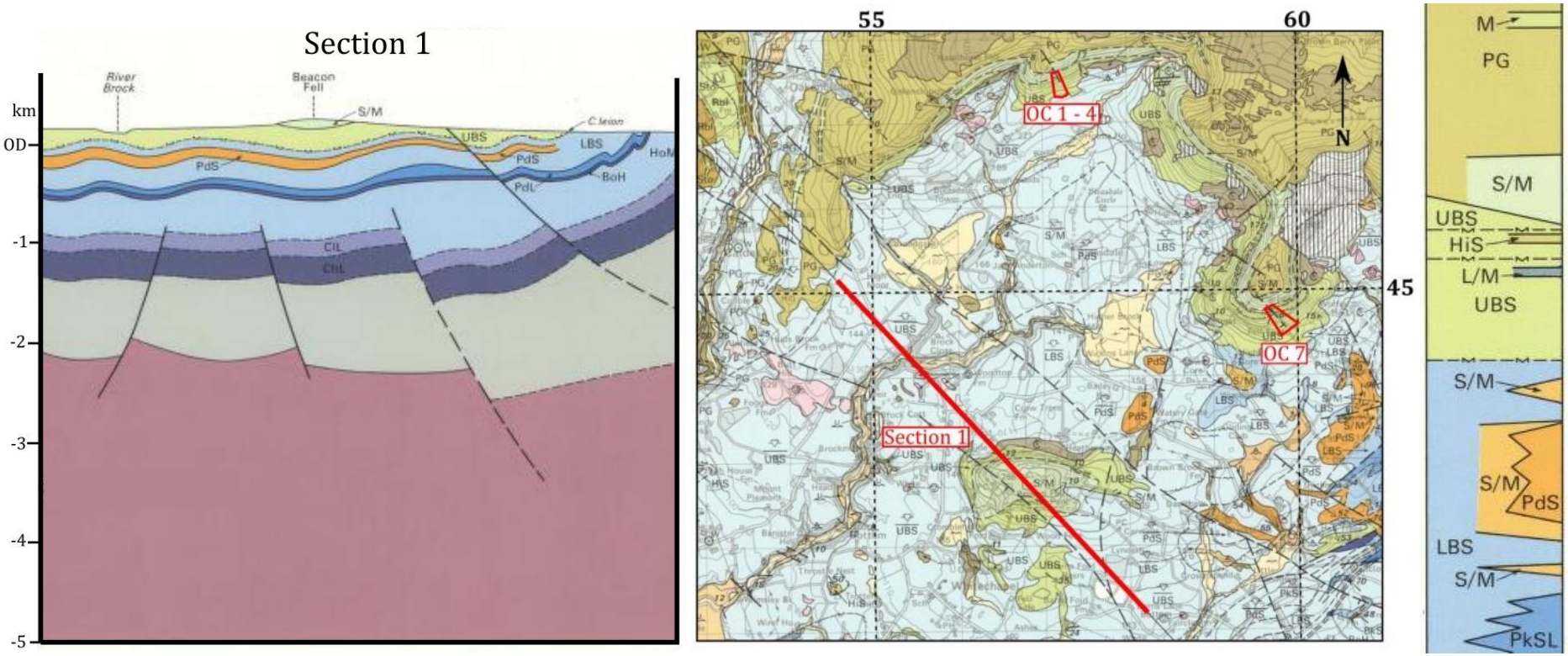

Figure 2.6: *Example of maps used to identify locations of interest for sample collection. Images are adapted from geological map and cross section seen in 1:50,000 BGS Memoir Sheet 67 Garstang (British Geological Survey, 1991). Upper Bowland Shale (UBS), Lower Bowland Shale (LBS), Pendle Grit (PG), Park Style Limestone (PkSL) and sandstones with mudstones, generally Pendleside Sandstones (PdS and S/M)*

LOCATION	SAMPLE TYPE	SAMPLE CODE	X	Y
Nick O' Pendle	Pendle Grit	OC 5	377243	438473
Langden Brook	Upper Bowland Shale	Not used	359883	449927
Disused Quarry Sykes (N)	Lower Bowland Shale	Innacessible	362788	451847
Wolf Fell	Upper Bowland Shale	OC 7	359839	444658
Disused Quarry Sykes (S)	Hodderense Limestone	OC 6	362756	451860
Hazelhurst Fell	Pendle Grit & Upper Bowland Shale	OC 1-4	357438	447705
Pendle Hill	Upper Bowland Shale	Innacessible	378684	441132

Table 2.3: *Table showing the locations selected for outcrop investigation. Of the 7 sites viewed, 6 provided available materials, 4 of which were used down the line.*

Multiple samples were taken from the Hazelhurst Fell outcrop area (denoted by 'OC 1-4' in Figure 2.2 and Figure 2.6. Here, due to interbedding, 4 different lithologies were able to be taken: OC 1) Pendle Grit (Figure 2.8), OC 2) Pendle Grit silty, OC 4) Upper Bowland Shale Sandy and OC 3) Upper Bowland Shale. Figure 2.7 shows a cross sectional image of where the lithologies lay at the Hazelhurst Fell area.

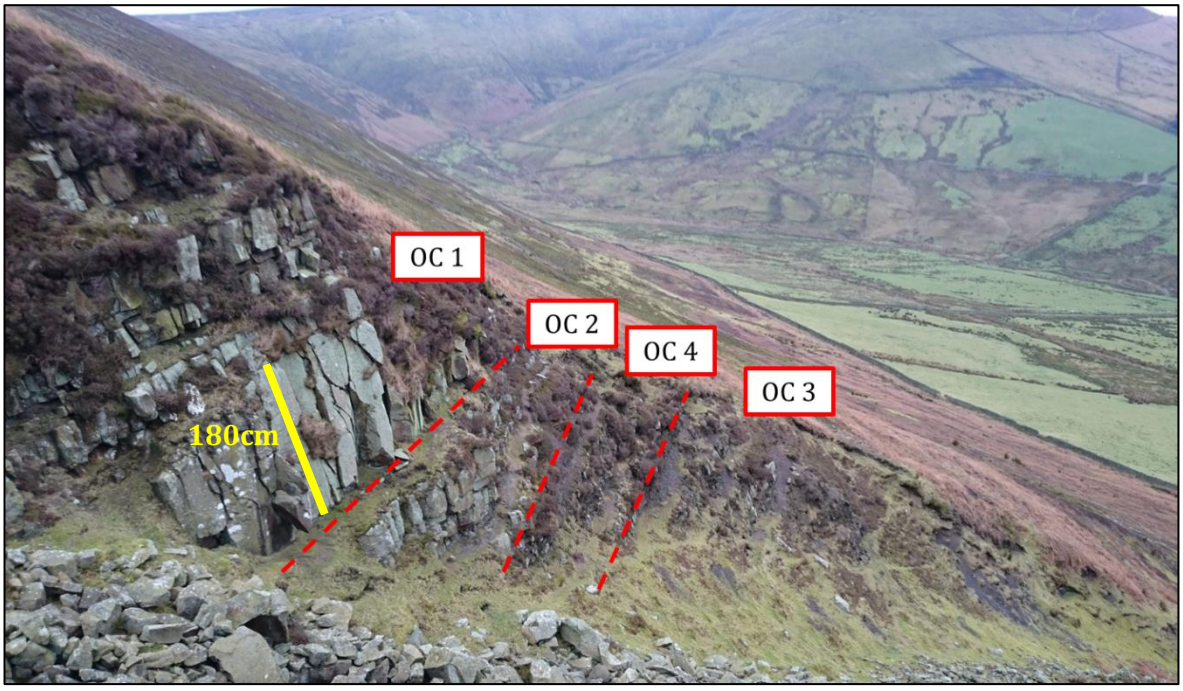

Figure 2.7: *View of Hazelhurst Fell outcrop sampling site, facing NE. Upper Bowland Shale is annotated as 'OC 3' at the base of the outcrop. From OC 3 to OC 1 (up the hill) the Upper Bowland Shale (UBS) becomes a siltier style of shale with siliclastics increasing until the Pendle Grid (OC 1) is reached. There is the occasional interbedded layer of pure shale or pure sandstone within these graded boundaries. The scale bar is drawn across a large continuous bed of Pendle Grit, the largest in this sequence at this location.*

Some locations were inaccessible (Table 2.3). At Pendle Hill this inaccessibility was due to dangerous terrain and weather on location. At the disused quarry, just north of Sykes quarry, no outcrop was available due to full cover by quaternary succession.

Figure 2.8: *Outcrop samples of OC 1 (Hazelhurst Fell, Pendle Grit (left)) and OC 7 (Wolf Fell, Upper Bowland Shale (right)) before removal of any weathered surfaces.*

As with all outcrop samples, examples shown in Figure 2.8, all weathered edges were removed and only fresh unaltered parts of the rock were used in all analyses.

2.2.3. Proppant Samples

Usually sand or resin coated ceramic particles (Proppant - Mitchell, 2015) is added to the fluid to "prop" open fractures to allow gas and fluids to flow more freely into the wellbore (Broderick et al., 2011). The particles are pumped downhole in suspension by means of either 1) a more viscous fluid or 2) higher pump and flow rates to keep particles energetic. To make experiments relevant to the UK shale gas industry, sand proppant was sourced that was used in the Preese Hall 1A (BH 5) well. According to Broderick et al., 2011, Preese Hall 1A used a mixture of both Congleton and Chelford sands. These Pleistocene age sands are unusual for glacial deposits in the fact that they are generally homogenous in size and largely free of impurities (BGS, 2009). The Cheshire deposits occur as irregular sheets which infill troughs in the underlying rocks, and they themselves are cut into by more impure and coarser sands (BGS et al., 2009). The Chelford sand is now thought to be highly limited and now usually earmarked for glass blowing but the Congleton Sand is much more abundant and used as foundry sand.

Samples of the Congleton Sand were obtained from Eaton Hall quarry in Congleton, Cheshire, with thanks to Tarmac Ltd for providing free samples. At the Eaton Hall quarry, the sand is dredged from beneath a 16 m deep artificial lake at a rate of 250 tonnes/hour. Sand is then sieved and graded before being sorted into dry and wet sand. The dry sand is dried in

large ovens at 60 ℃ for a number of hours. The sand that had the closes properties to fracking sand was the foundry sand, also known as WR416. The properties of this sand are shown in Table 2.4.

TYPICAL AGGREGATE PROPERTIES			XRF CHEMICAL ANALYSIS		
					%
pH	9.1	BS 1377-3:1990 (clause 9)	Iron oxide	as Fe_2O_3	0.32
			Calcium oxide	as CaO	0.42
			Silicon oxide	as SiO_2	96.14
SIEVE SIZE (mm)		PASSING (%)	Magnesium oxide	as MgO	0.12
1.000		100	Aluminium oxide	Al_2O_3	1.3
0.710		99.9	Phosphorus oxide	P_2O_5	0.05
0.500		99.5	Manganese oxide	MnO	<0.02
0.355		94.7	Sulphur oxide	SO_3	<0.01
0.250		50.2	Titanium oxide	TiO_2	0.04
0.212		25.8	Potassium oxide	K_2O	0.63
0.180		12.1	Sodium oxide	Na_2O	0.08
0.150		2.8	Loss on ignition	at 1000^oC	0.7
0.125		0.5			
0.090		0	PETROLOGICAL DESCRIPTION:		
0.063		0	Natural quartzose sand		
Pan		0	Particle shale:		
			Sub-angular to well rounded		
			Surface texture:		
			Rough to smooth		
			(March 2016 revision) Tarmac		

Table 2.4: *Table showing the properties of Congleton Sand Aggregate, type WR416.*

The dry sand, WR416, was chosen as proppant for testing at Durham shown in Table 2.4. This is a highly quartz rich clean sand with minimal calcite and a fairly uniform size (Figure 2.9). Minimal losses are seen upon ignition which is expected due to the high quartz content.

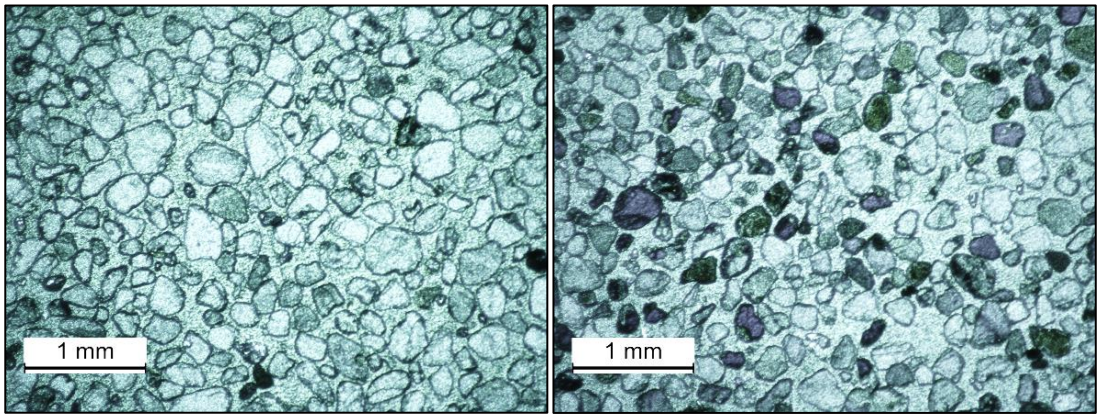

Figure 2.9: *Thin sections of OC 8 (Congleton Sand Proppant). Right hand image is shown under XPL (cross polarised light). Particles are both angular and rounded at an approximate 50:50 ratio.*

2.2.4. Sample Summary

Of all samples collected, 14 were deemed suitable for analysis and experimentation. Suitability depended on amount of sample available for replication, and type of sample. Of all samples deemed suitable, 6 were borehole samples while 8 were outcrop samples. All borehole samples used were core samples, this provided enough sample to grind down for various experimental analyses. Cuttings samples collected did not provide enough sample for multiple runs of experimentation. The majority of all samples were shale with 1 limestone and 3 sandstones also obtained.

2.2.5. Sample Preparation

Borehole samples (prefixed with BH) were washed of drilling muds. No cutting was necessary to remove weathered surfaces from the borehole samples. The storage of all borehole samples was within the Core Store at the BGS in Nottingham and so samples, although covered, were exposed to normal room temperature dry conditions and atmospheric pressures. Some samples may have cracked due to this change in pressure but conditions are unknown.

Outcrop samples had weathered surfaces removed using a rock saw to reveal fresh surfaces to provide sample with as little alteration or oxidation as possible.

Both outcrop (OC) and borehole (BH) samples were prepared by grinding into a fine powder of > 150 μm using a gyromill rock smasher. This powder was then dried overnight at 105 ^{o}C to remove excess moisture and volatiles. Samples were then rehydrated in a humid environment. After rehydration, between 60 g and 200 g of each sample was ready for use in multiple analyses. The preparation of powdered, drying and rehydrating shales conformed to American Society for Testing and Materials (ASTM) D1412-04 (2004) preparation of standards, methods that have been used in multiple studies, inclusive of, but not exclusive to, Ross and Bustin, (2009); Wiśniewska, (2012); Xiong et al, (2018) and (He et al., 2019). Fine

powder was used in all characterisation analysis methods (XRD, XRF, TGA and EA) as this was the requirement for each individual analysis.

RT and HPHT adsorption experiments, details in Section 3.3.1 and Section 4.5, used the fine powdered material. The use of the fine powder in these experiments was to ensure the most homogenous mass of rock available for reaction, inclusive of all minerals present in the rock itself. Using lumps, or cuttings of rock, for this type of experiment, especially over multiple individual experiments, may have meant that some samples were not 'homogeneously typical' – i.e. some samples of the same rock may have had higher proportions of certain minerals than others, such as veining or weathering. Powdered samples provided a representative high surface area for the interaction with PAM, as would be downhole (Xiong et al., 2018b).

Adsorb-desorb experiments used a different type of sample preparation. In the Ads-Des experiments powdered samples were not used, but instead a 1 cm cubed sample was used. The use of a cubed sample in these experiments was to have as consistent a possible surface area available for adsorption sites. The use of a cube of rock also allowed for consistent air drying of samples as part of the Ads-Des experimental procedure. The use of an identical cube for each of the adsorb-desorb experiments proved easier over experimental timescales that a PAM saturated powder. Details for the adsorb-desorb experiments are mentioned in Section 5.4. The powdering approach to the preparation of shale can alter the surface area by increasing it, alongside increasing the pore space available (He et al., 2019; Ross and Bustin, 2009). Accounting for this, and due to the fact established literature and studies use this particular method and procedure, it was chosen for this study. Surface area was not tested as part of this study.

2.3. Sample Characterisation

Characterisation included the composition, mineralogy, carbon content and organic content using a combination of X-ray fluorescence (XRF), X-ray diffraction (XRD) and carbon analysis by means of both thermogravimetric analysis (TGA) and total carbon Analysis using the elemental analyser (EA). The reason for this characterisation was so that particular rock characteristics could be attributed to behaviour observed from the adsorption or flow-back experiments. This chapter will be centred on this mineralogical analysis. All samples were analysed using all techniques mentioned in this section. The information gained from the characterisation can therefore be used in conjunction with all other analyses detailed within this study; room temperature adsorption (Chapter 3), HP-HT adsorption (Chapter 4), Adsorb-Desorb (Chapter 5), Colloid Analysis (Chapter 7) and finally, flow-back analysis (Chapter 6).

In terms of lithological characterisations, various studies have already considered the geochemistry and mineralogy of the Bowland Shales (or stratigraphic or similar units). Starting with the BGS memoirs, Aitkenhead et al., 1992 looks at general major and minor XRF

analyses data where available. Gross et al. (2015) analysed the organic petrography and mineral presences of the Bowland shales within the UK using the Duffield borehole, of which the TOC analysis is useful to this study, showing TOC's values ranged from between 1.25 % to 7.55 %. The TOC content of the Bowland shale is discussed in depth by Gross et al. (2015) and Konitzer et al. (2015). Newport et al., (2016) discusses the geochemistry of the Holywell shale in Wales, part of the Bowland Shale Unit, stating that TOC values ranged from 0.12 % to 10.31 % in the Upper Holywell Shale and between 0.63 % and 3.36 % in the Lower Holywell Shale across multiple sample locations. More general studies of shale gas in the UK have also been undertaken, encompassing all aspects from lithology, geochemistry, structure and exploitable potential. Such studies include the BGS & DECC's report on the Geology and Resource Estimation of the Carboniferous Bowland Shale (Andrews, 2013) and the Tyndall Centres 'Shale Gas: An Updated Assessment of Environmental and Climate Change Impacts' (Broderick et al., 2011).

2.3.1. Carbon Analysis

The carbon analysis for all samples was performed using a combination of data obtained from thermogravimetric analysis (TGA) and elemental analysis (EA). Losses upon ignition from the TGA (ambient to 1000 °C) were used to calculate organic carbon and inorganic carbon. Total loss on ignition was compared between both XRF data and losses observed from the TGA to verify all mass loss results (Digital Appendix B.2).

2.3.1.1. Elemental Analysis (EA)

To establish amounts of total carbon (TC) in each sample, CHN (carbon-hydrogen-nitrogen) analysis was performed. Total organic carbon (TOC) and total inorganic carbon (TIC) was established alongside data from the TGA. This CHNO analysis was undertaken using a COSTECH ECS 4010 Elemental Combustion System via a pneumatic auto-sampler. The machinery was only set up for CHN analysis, not oxygen. The system used two reactors: chromium (III) oxide/silvered cobaltous-cobaltic oxide alongside high purity copper wires at a temperature of 1020 °C. Helium was used as a carrier gas with a flow rate of 120-140 cm^3 min^{-1}.

The calibration for the CHN analysis comprised of a suite of acetanilide (C_8H_9NO) standards that ranged from 0.5-2.5 mg in weight. The curves for this calibration were based on linear and quadratic relationships, all with an r^2 >0.99.

All samples were prepared in triplicate by measuring between 1.5 and 2.5 mg of each powdered sample in a tin capsule. All samples were triplicated. During the sample run, as a check for drift and to calibrate to the original standards, an acetanilide procedural blank triplicate was placed every 24 single samples.

To understand what the typical ranges for the Bowland Shale and relevant lithologies were, a simple literature search was undertaken from both outcrop and borehole sources over the last 20-30 years. For this, 11 different sources (full details in Digital Appendix B.1) (Andrews, 2013; Armstrong et al., 1997; Gross et al., 2015; Kenomore et al., 2017; Konitzer et al., 2015; Maynard et al., 1991; Newport et al., 2016; Smith et al., 2010; Spears and Amin, 1981; U.S. Energy Information Administration, 2015) were combined which took results from 29 different boreholes, outcrops and horizons. Amongst them, TOC varied between 0 and 10 %, with an average of 3.97 %. Details of this compilation can be seen in Figure 2.10.

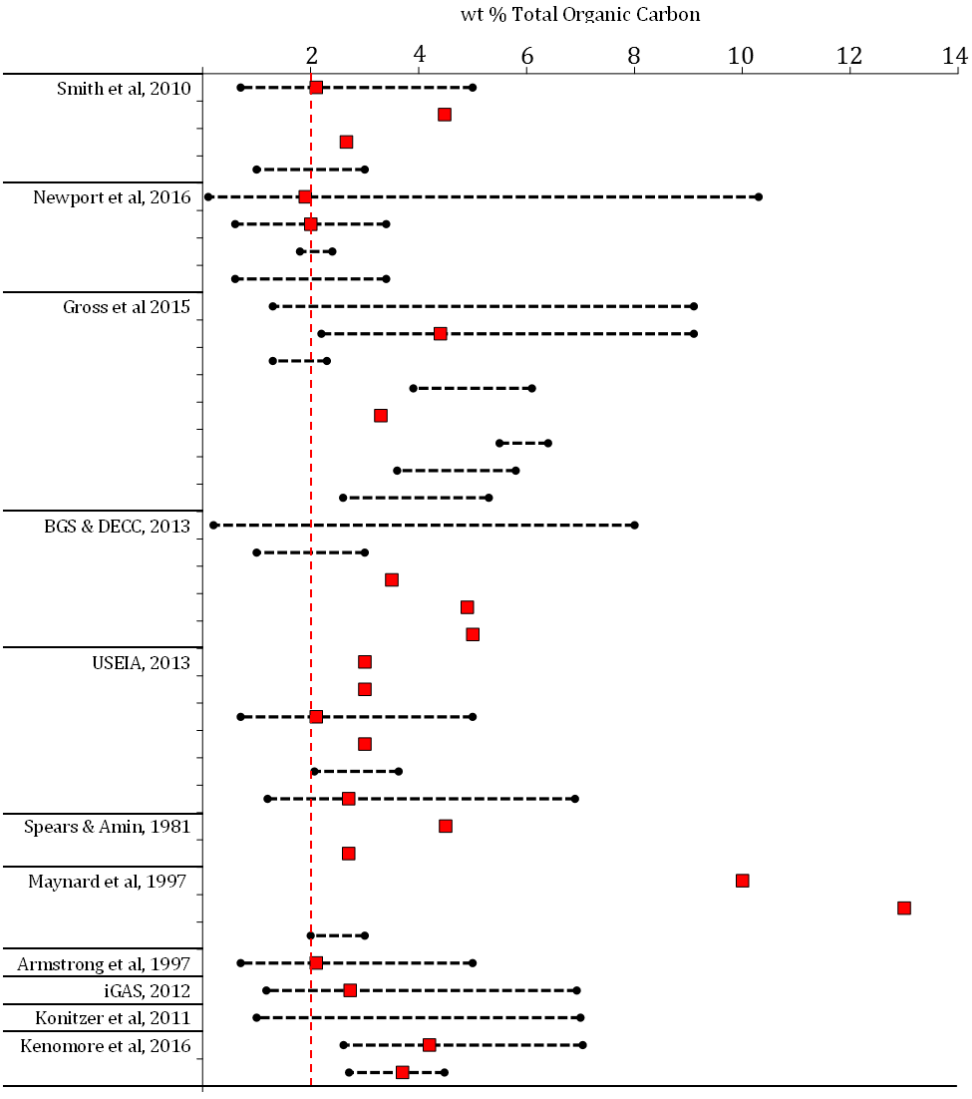

Figure 2.10: *Table which plots all the TOC values retrieved from a literature search of all available material regarding organic carbon within the UK Bowland Shales. Black lines and end markers denote highest and lowest values, with the red dots denoting the average published value. No values here have been calculated or averaged, all are only what was displayed in each relevant material, hence why some contain only averages, and other contain no averages. The red dashed line denotes the optimum 2 % TOC cut off for UK Namurian shales (Charpentier and Cook, 2011), explained in more detail in Section 2.4.4.1.*

2.3.1.2. Thermogravimetric Analysis

Thermogravimetric analysis (TGA) was used to assess the mass of volatile matter, organic matter, clay content and carbonate material within each sample. The TGA was conducted using an SGA i TGH 1200 high mass analyser (Instrument Specialists Inc, Wisconsin, USA). The powdered samples were measured to weights varying between 200 and 250 mg and loaded into the platinum hanging dish within the instrument. When the furnace was fully closed the sample was heated from ambient temperature to 1000 °C at a rate of 20 °C/min with a constant feed of N_2. Gas flow rate was set at 25 - 30 cc/min, purge flow rate 25 – 40 cc/min. Each sample took between 45 and 50 minutes to complete. Due to time constraints and limited sample availability no replicates were performed. A correlation of losses from XRF vs losses from TGA yielded an r^2 value of 0.9964 and thus TGA losses observed in Durham were deemed reliable.

Loss characteristics and temperature ranges were calculated using observations across all the samples and typical temperature range data observed in (Wang et al., 2009) and (Sutcu, 2007). This method cannot be used to account for individual minerals, just approximations based on recommended ranges. Example TGA thermal curves and derivatives can be observed in Appendix B and Digital Appendix B.2, data adapted from (Todor, 1976).

GENERAL RANGE	RANGE USED (for this study)	ATTRIBUTION
0-250°C	0-299°C	Moisture, volatiles
200-600°C	300-649°C	Structural water release from clays Decomposition of kerogen & organic matter Decomposition of pyrite (450-550°C)
600-950°C	650-980°C	Decompostion of carbonate minerals (Calcite, Dolomite, Aragonite)

Table 2.5: *Table adapted using data from Wang et al. (2009), Sutcu (2007) and Todor (1976), showing the general temperature ranges attributed to mineral decomposition alongside the ranges chosen for this study based upon all first losses seen using the first derivative.*

It is unlikely that the decomposition of pyrite was a major factor towards mass loss of any samples tested. Pyrite concentrations were negligible in all samples, however, if pyrite was abundant in a particular sample, it could not form hematite as the TGA is run in an N_2 environment (Wang et al., 2009).

2.3.2. X-Ray Fluorescence Analysis

X-Ray fluorescence (XRF) was performed by the University of Leicester. This analysis determines the weight percentage of major oxides and concentration (ppm or mg) of trace elements. The analysis was done on a PANalytical Axios Advanced X-Ray Fluorescence spectrometer that operates a 4Kw rhodium (Rh) anode end window super sharp ceramic X-ray tube. For this method, major oxides are determined on fusion beads, and traces are determined on pellets. All samples used powder that is prepared in Durham to <150 μm. Results are returned in the form of an MS Excel spreadsheet detailing all majors, minors and losses. All samples used are retained at Leicester University in case repeats need running.

2.3.3. X-Ray Diffraction Analysis

X-Ray diffraction (XRD) analysis was performed to assess mineral composition but primarily to qualitatively assess the clay types present in the samples. Again, the analysis required the same > 150μm powder as XRF. Each powdered sample was analysed using a Bruker D8 Advance diffractometer using a wavelength of 1.5406 nm and CuKα radiation. Samples were pressed into 1 mm deep resin discs with a radius of 1.25 mm to preserve a smooth surface for diffractions. An example of one of these resin discs is shown in Figure 2.11.

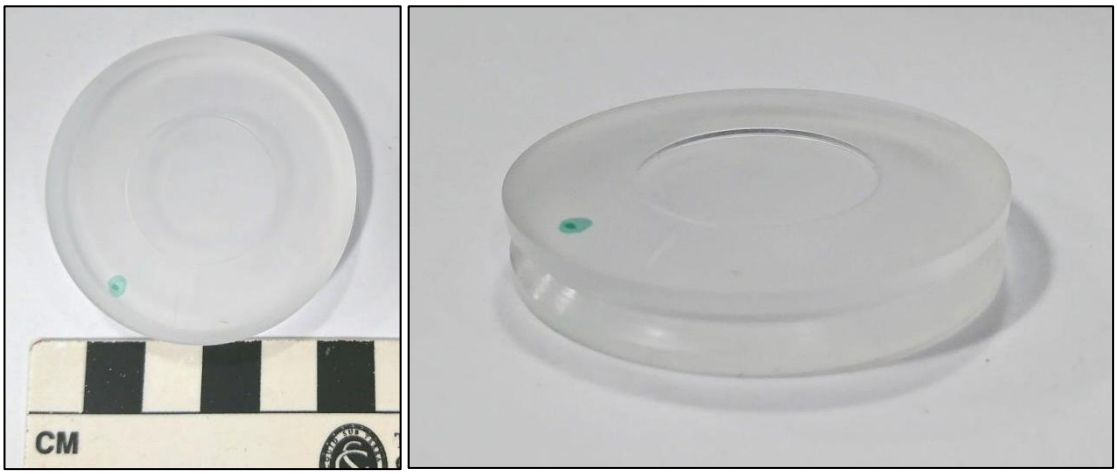

Figure 2.11: *Image of one resin disc for XRD analysis. The powders are pressed fully into the inset in the centre of the disc, ensuring a flush contact with the surrounding resin.*

All samples were measured with random orientations of grains. Samples were scanned from 2° to 90°2θ (Figure 2.12) with a time-step of 0.350 seconds and an increment of 0.02°. Each sample took approximately 28 minutes to complete.

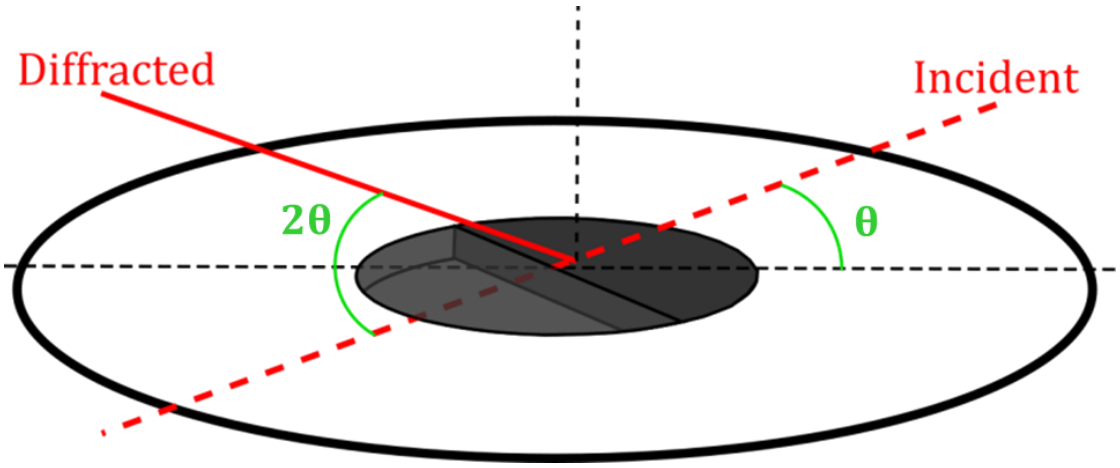

Figure 2.12: *Schematic of XRD resin disc shown in Figure 2.11 showing the incident and diffracted X-rays in terms of the θ (theta) and 2 θ angles.*

This study used both quartz and barite as internal standards both for the method of analysis in the Bruker D8 Advanced Diffractometer and each sample calibration. Quartz is not a clay mineral, but will often occur in the clay-size fraction of a sample (Moore and Reynolds Jr, 1997). Quartz has a distinctive and invariant signal pattern, with the principle 100 peak occurring at 26.65 °2 θ (*d* = 3.343 Å) (Å = angstrom) and can be readily observed when in quantities > 1 wt% (Brindley and Brown, 1984). This peak, and quartz's secondary peak at 20.85 °2 θ (*d* = 4.25 Å) can be used an internal standard for moderate accuracy.

The second internal standard that was used to assess machine accuracy was the sulphate barite. A 1-5cm thick barite vein was encountered at fieldwork site OC 6 and sampled for adsorption experiments. This sample did not actually end up being used in the adsorption experiments, but was instead used as another good calibrator for the XRD results profiles. As this sample was almost pure Barite ($BaSO_4$) there would not be much influence from other strong mixed layer peaks.

Non-clay minerals analysed for were: Quartz, Calcite, Dolomite, Aragonite, Orthoclase, Microcline, Plagioclase, Pyrite, Anhydrite and Gypsum. Clay minerals analysed were Chlorite, Vermicullite, Smectite, Montmorillonite, Kaolinite, Dickite, Illite and Illite/Smectite mixed layer.

The degrees 2θ range was chosen to provide enough range to identify primary peaks for clay minerals. Clay minerals (as listed above) have their primary peaks in the lower end of the spectrum, often between 2 and 20° 2θ. The *d* spacing 060 values for clays which are used to distinguish between dioctahedral and trioctahedral types, were present in most samples and using the various literatures listed below to cross reference, proved very useful for the identification of the certain desired clay types (Moore and Reynolds Jr, 1997). However, often in random oriented powders, these 060 spacing peaks are often hidden in the larger matrix

and can be very hard to identify. Clay peaks typically have weak intensity and large breadth and so can be difficult to identify alongside other more prominent minerals, i.e. quartz and calcite, in a mixed mineral aggregate (Moore and Reynolds Jr, 1997). Confirmation of each mineral phase was accomplished by using at least 2 major reflections and 2 minor reflections. Occasionally 1 minor reflection was used when peaks reflected by other minerals were suspected of obscuring the relevant peaks being searched. Peaks observed were cross referenced against five different reference databases: 1) diffracEVAL software database; 2) Moore and Reynolds Jr (1997), 3) Brindley and Brown (1984), 4) mindat.org mineralogy database; and 5) webmineral.com mineralogy database.

Using this range of sources for identification, results could be plotted on profiles using both degrees 2θ and '*d* spacings'. Conversion between 2θ and '*d* spacings' was completed using a method from the USGS with an adapted Bragg equation (Equation 2.1).

$$\boldsymbol{d = \frac{\lambda}{(2.0 \times \sin(0.5 \times 2\,\theta \times D2R))}} \qquad \textbf{Equation 2.1}$$

Equation 2.1 shows the adapted Braggs law equation to easily convert from 2θ to *d*. This method is adapted from the USGS (Poppe et al., 2002); λ is the wavelength of the rays (1.5406 nm) and D2R is an abbreviation for the conversion factor between degrees and radians, used as the value *0.0174532925199433*. The value must be exact to ensure no rounding offsets any identifiable peaks. Using this equation based on degrees 2 θ, numerical data is easily converted to *d* spacings. These *d* spacings values are also used to cross reference data amongst some of the multiple literature sources cited.

2.4. Results

Here all results from the elemental analysis, thermogravimetric analysis, XRF analysis and XRD analysis are presented. All results are shown where necessary and practical; however in some occurrences, due to the sheer number of data, some full suites of data are shown in the Appendices, with only examples selected here. Specific Appendices are referred to in the text where relevant.

2.4.1. Carbon Analysis

The full suite of results from both the TGA and Elemental Analyser are combined in this section to give details of TC, TIC and TOC. Total Carbon was measured only on the elemental

analyser whilst losses on ignition we measured with TGA and both organic carbon and inorganic carbon calculated from here.

2.4.1.1. Elemental Analysis

For all the samples measured, total carbon varied between 0.07 wt % and 12.04 wt % (Table 2.7)

SAMPLE	NITROGEN	CARBON	HYDROGEN	CARBON		
	wt%	wt%	wt%	Mean wt%	SD	RSD
BH 1	0.17	4.33	0.65	4.33	0.19	4.30
BH 2	0.08	9.58	0.54	9.58	0.22	2.30
BH 2	0.25	3.94	0.99	3.94	0.07	1.69
BH 3	0.07	5.45	0.50	5.45	0.22	4.10
BH 4	0.08	4.54	0.57	4.54	0.05	1.09
BH 5	0.21	4.56	0.70	4.56	0.07	1.55
BH 6	0.15	1.60	0.91	1.60	0.03	1.91
OC 1	0.14	0.12	0.37	0.12	0.04	30.05
OC 2	0.05	0.14	0.57	0.14	0.01	7.14
OC 3	0.12	4.71	0.59	4.71	0.01	0.24
OC 4	0.12	1.51	0.83	1.51	0.12	7.81
OC 5	0.10	0.07	0.54	0.07	0.02	28.39
OC 6	0.08	12.04	0.45	12.04	0.03	0.21
OC 7	0.22	1.65	0.74	1.65	0.01	0.61
OC 8	0.12	0.07	0.40	0.07	0.02	24.74

Table 2.6: *Total carbon data for all samples analysed with the elemental analyser. 'SD' denotes standard deviation and 'RSD' denotes relative standard deviation.*

Samples did not exceed about 12 % total carbon and most relative standard deviations (RSD) are low. RSD values for samples OC 1, OC 5 and OC 8 are the highest errors observed. The most likely reason for this error is the fact that these samples contained almost zero carbon and thus the standards used for the whole dataset were anomalous to this small cluster of samples. In short, the value of the lower acetanilide standard was still too high and so the machine would have struggled to constrain exact carbon values for these samples. These samples however, cross referenced with the other characterisation techniques used, are very silica rich based samples with almost no trace of hydrocarbons in the system (Table 2.6 and Table 2.9).

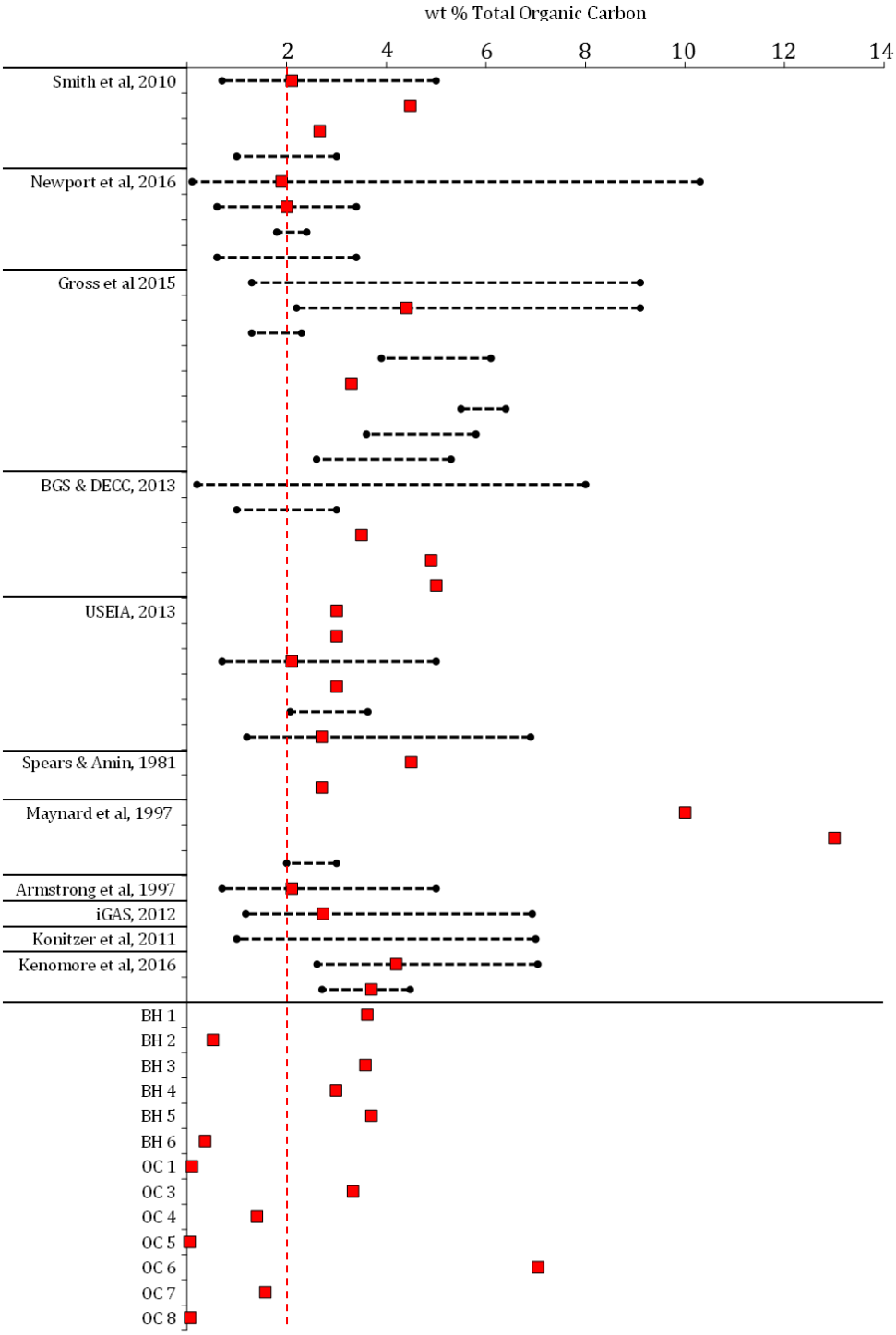

Figure 2.13: *Adapted version of Figure 2.10 this time showing all results from TOC analyses conducted on samples for this project here at Durham. Red line denotes the 2 % minimum requirements 'cut-off' for TOC for a successfully viable shale gas exploitation.*

Total carbon values analysed for this study (Figure 2.13) are within the typical range of carbon that would produce TOC values similar to those seen in the literature e.g., Andrews, 2014; Kenomore et al., 2017; Maynard et al., 1991; Spears and Amin, 1981. The majority of all

shale type samples (BH 1, BH 3, BH 4, BH 5, OC 3 and OC 6) have TOC values that sit above the 2 % 'minimum requirements' cut off for Namurian shales (Charpentier and Cook, 2011). Most sandstone based samples (OC 1, OC 5 and OC 8) have negligible carbon both inorganic and organic. The 2 % TOC cut off is based Andrews, (2013) literature. Using data from Charpentier and Cook, (2011), Gilman and Robinson, (2011), well legacy data and a DECC commissioned study discussed 2 % TOC is concluded to be a viable minimum for well exploitation. Other studies, such as (Jarvie, 2012) state a 1 % cut off, but discuss average TOC values for the top 10 shales in the USA, with their reported TOC values ranging between 0.93 % and 5.34 % (Andrews, 2014; Jarvie, 2012).

2.4.1.2. Thermogravimetric Analysis (TGA)

Using all data, average threshold values were selected for volatiles and residual water (0 - 300 ˚C) with water loss usually below 200 ˚C, organic matter (300 – 650 ˚C) and $CaCO_3$ (650 - 980 ˚C). Results from the TGA are shown in Table 2.7.

SAMPLE	0-200 °C	200-400 °C	400-600 °C	600-800 °C	800-1000 °C	TOTAL LOSS	300-650 °C	650-980 °C	TOTAL LOSS
BH 1	0.815462	0.306612	2.327748	3.80789	2.906726	10.164438	3.307286	5.92794	9.235226
BH 2	0.471942	0.131052	1.299566	3.619672	25.242122	30.764354	1.780324	28.464288	30.244612
BH 3	0.329966	0.10633	1.074806	3.516124	12.330406	17.357632	1.450518	15.555444	17.005962
BH 4	0.277476	0.08079	0.87277	3.588584	9.601464	14.421084	1.275396	12.863458	14.138854
BH 5	1.086522	0.230698	2.913292	4.723332	3.394238	12.348082	4.089972	7.090864	11.180836
BH 6	1.304422	0.313172	2.343672	6.3637	5.068948	15.393914	3.711176	10.313078	14.024254
OC 1	0.30369	0.112176	0.683838	0.275796	0.016166	1.391666	0.883034	0.157848	1.040882
OC 2									
OC 3	0.696012	0.3399	2.446158	4.956398	7.206918	15.645386	3.33132	11.525242	14.856562
OC 4	1.337316	0.498012	4.111978	1.587148	0.166622	7.701076	5.27718	0.90615	6.18333
OC 5	0.316746	0.11944	0.511678	0.25567	0.021552	1.225086	0.694732	0.15107	0.845802
OC 6	0.183888	0.076326	0.433162	3.364988	38.53389	42.592254	0.639536	41.640946	42.280482
OC 7	2.094188	0.60903	2.63109	1.09673	0.119728	6.550766	3.584814	0.635166	4.21998
OC 8	0.072854	0.060742	0.110648	0.041706	0.009464	0.295414	0.161404	0.036214	0.197618

Table 2.7: *Mass losses from TGA shown in 200 ˚C intervals and organic matter (300-650 °C) and carbonate intervals (650-980 °C). Samples are ordered by sample name.*

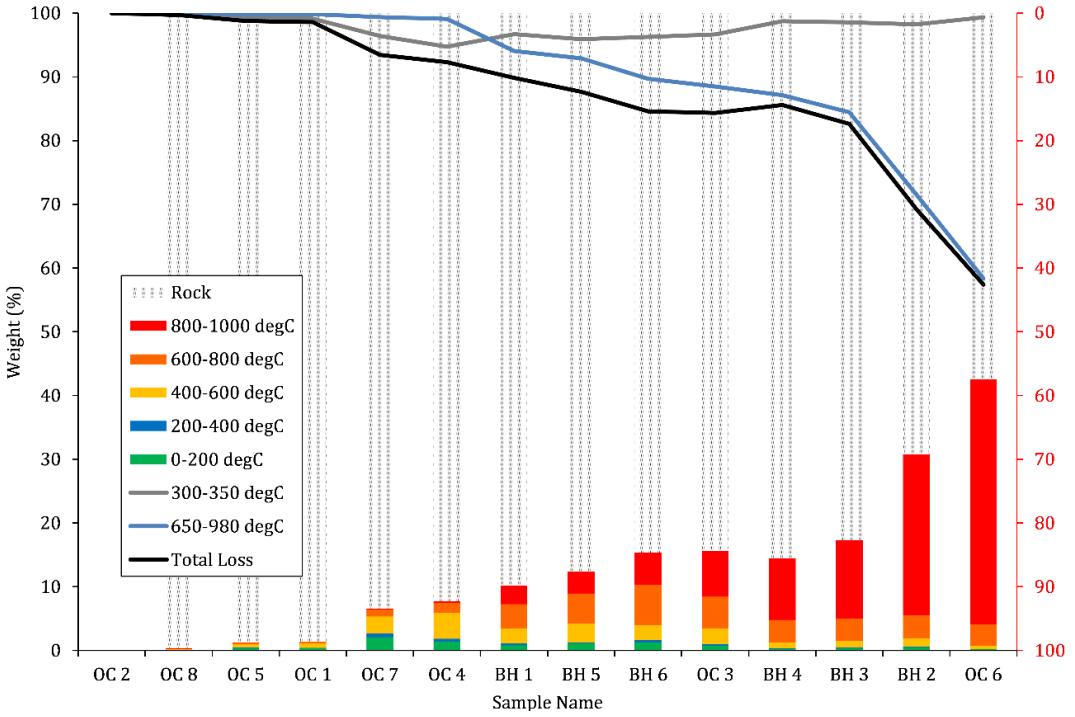

Figure 2.14: *All losses for all samples based on wt % losses seen at sequential 200 °C intervals. Samples here have been ordered by total losses observed in the carbonate window. Bar columns refer to the black left hand y axis (weight %). Lines represent the sample losses in the organic and carbonate windows (300-350 and 650-980 °C respectively and refer to the red axis (right)*

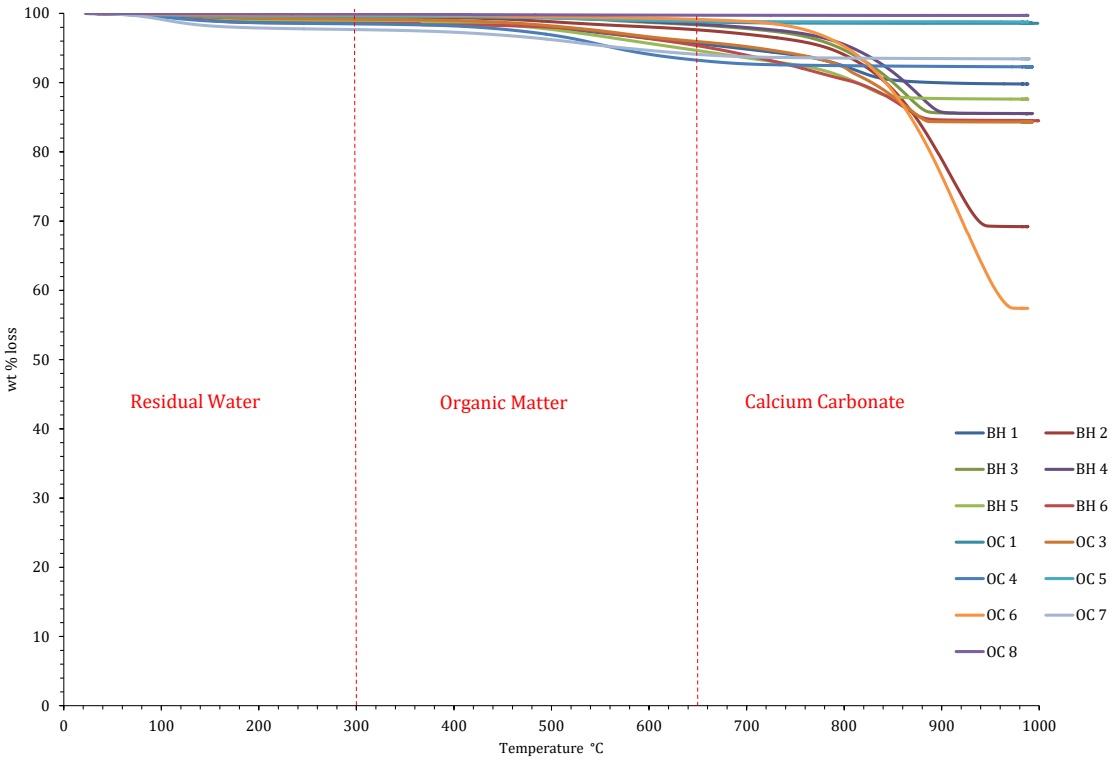

Figure 2.15: *All TGA curves, averaged over each individual temperature signature, for all samples. Example reference curves from Todor (1976) can be observed in Appendix B.*

Nearly all samples lose the most mass between 650 and 980 ˚C – and this is taken as loss due to presence of carbonates. Mass losses for organic matter between 300 and 650 ˚C range from 0.1 % to 10.9 % whereas for carbonate material between 650 and 980 ˚C mass losses range from 0.03 % to 41.6 %.

Sample OC 6, carbonate rich shale, loses just over 41 % of its mass at temperatures greater than 650 ˚C. The same sample, OC 6, loses less than 1 % of its mass in the window for organic matter between 300 and 650 ˚C (Table 2.7). Sample BH 6 has the most organic matter mass loss at 10.9 % with a small carbonate loss of 1.3 %, however samples such as BH 5 have 4.09 % of organic matter loss coupled with an even larger carbonate loss of 7.09 %.

2.4.1.3. Carbon Analysis Conclusions

The TOC values vary between 0.05 % and 7.04 % for all samples - all data is given in Table 2.9 and shown in Figure 2.16. Borehole samples generally have a higher TOC and TIC, but this is biased due to the fact that core was actually sampled; it was obviously in a zone of interest and of high TOC. A comparison of data obtained in Durham for the same samples analysed by operators is shown in Table 2.8. Most TOC values for all samples in the subset sampled in this study, in particular the shale samples, sit within the optimum organic carbon window which makes reservoirs feasible for exploration and exploitation. Andrews, (2013), suggests that the optimum cut off for UK Namurian shales is > 2 % using findings from Charpentier and Cook, 2011 and Gilman and Robinson, 2011.

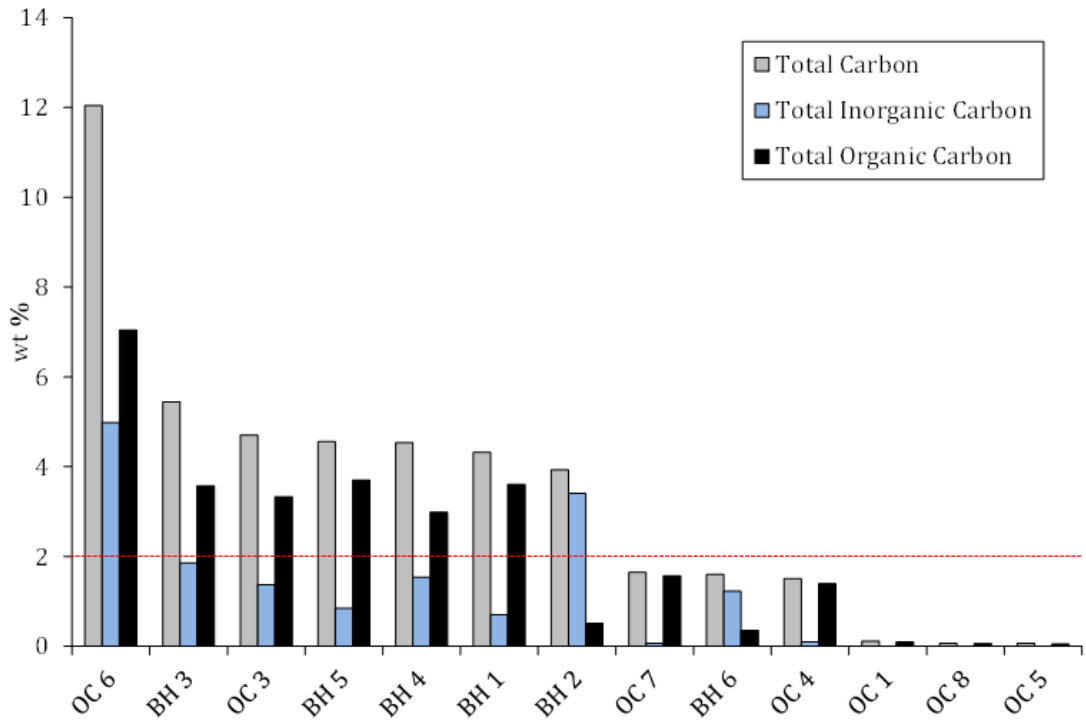

Figure 2.16: *All carbon values for all samples using data derived from both elemental analysis (TC) and thermogravimetric analysis (TOC and TIC). The red line denotes the > 2 % cut off for Namurian UK shales.*

WELL Sample	DURHAM ANALYSIS (TGA, EA)	EOWR Average (Maximum)
BH 1	3.62 %	2.80 % (3.52 %)
BH 3	3.58 %	2.12 % (3.15 %)
BH 5	3.70 %	(3.16 %)

Table 2.8: *Comparison TOC data chart for 3 borehole samples. 'Durham Analysis' represents data from both the TGA and EA whilst 'EOWR' represents data taken from the representative wells End of Well Report Summaries. No average data was available from BH 5 EOWR.*

SAMPLE	TC	TIC	TOC
BH 1	4.32	0.711	3.615
BH 2	3.93	3.41	0.52
BH 3	5.45	1.86	3.58
BH 4	4.54	1.54	2.99
BH 5	4.56	0.85	3.7
BH 6	1.6	1.23	0.36
OC 1	0.12	0.01	0.1
OC 3	4.71	1.38	3.33
OC 4	1.51	0.1	1.4
OC 5	0.07	0.01	0.05
OC 6	12.04	4.99	7.04
OC 7	1.65	0.07	1.57
OC 8	0.07	0.004	0.06

Table 2.9: *All carbon type values (wt %) for all samples, derived from elemental analysis (TC) and TGA (TIC and TOC)*

2.4.2. X-Ray Fluorescence

Both major and minor mineral oxides are displayed in Table 2.10. Only one measurement per sample was made and so no error was calculated in the analyses. The external technician who measured the samples at Leicester University assured us that error using this method was commonly low, and thus no replications of samples were undertaken: triplicates for each sample to get an average reading.

SAMPLE	SiO_2	TiO_2	Al_2O_3	Fe_2O_3	MnO	wt % MgO	CaO	Na_2O	K_2O	P_2O_5	SO_3
BH 1	67.18	0.28	7.85	3.27	0.04	1.08	7.12	0.36	1.470	0.084	2.281
BH 2	22.80	0.12	3.02	2.01	0.02	1.12	36.85	0.13	0.393	0.066	3.819
BH 3	54.75	0.17	3.11	2.52	0.03	2.55	17.20	0.42	0.421	0.073	0.880
BH 4	60.50	0.22	2.88	2.02	0.02	1.12	15.97	0.48	0.450	0.085	1.360
BH 5	59.46	0.42	8.75	2.64	0.01	0.77	10.72	0.60	1.452	0.995	2.827
BH 6	46.41	0.75	17.42	16.15	0.19	2.01	1.00	0.73	1.566	0.253	0.138
OC 1	90.79	0.14	4.90	0.55	0.00	0.08	0.01	0.17	1.307	0.023	0.005
OC 2	87.11	0.31	7.52	0.46	0.08	0.18	0.02	0.41	1.501	0.072	0.008
OC 3	56.69	0.31	5.70	2.72	0.08	2.59	13.04	0.17	1.073	0.136	2.632
OC 4	70.38	0.90	17.25	0.84	0.01	0.56	0.03	0.31	2.733	0.099	0.008
OC 5	89.76	0.28	5.19	0.99	0.01	0.13	0.02	0.63	1.083	0.023	0.004
OC 6	2.65	0.01	0.27	0.17	0.02	1.03	52.87	<0.004	0.019	0.004	0.289
OC 7	78.95	0.41	9.36	3.92	0.01	0.45	0.02	0.21	1.373	0.126	0.010
OC 8	98.72	0.04	1.41	0.21	<0.001	0.07	0.08	0.16	0.670	0.012	0.005

Table 2.10: *All XRF data separated by sample name for both major and minor minerals.*

	BH 1	BH 2	BH 3	BH 4	BH 5	BH 6	OC 1	OC 2	OC 3	OC 4	OC 5	OC 6	OC 7	OC 8
Si/Al	31/4	11/2	26/2	28/1	28/4	22/9	21/1	41/4	13/1	4/1	42/3	1/0	9/1	1/0
	7.75	5.5	13	28	7	2.44	21	10.25	13	4	14	*100*	9	*100*
	BH 6	OC 4	BH 2	BH 5	BH 1	OC 7	OC 2	BH 3	OC 3	OC 5	OC 1	BH 4	OC 6	OC 8
Si/Al	22/9	4/1	11/2	28/4	31/4	9/1	41/4	26/2	13/1	42/3	21/1	28/1	*1/0*	*1/0*
	2.44	4	5.5	7	7.75	9	10.25	13	13	14	21	28	*100*	*100*

Table 2.11: *Si/Al ratios calculated for all samples derived from SiO_2 and Al_2O_3 XRF results. Results ordered by sample name in upper rows and by Si/Al ratio (low to high) in lower rows.*

As is typical with shales, samples contain large amounts of quartz, up to 89 %, except OC 8, clean glacial sand. The three major oxides, SiO_2, Al_2O_3 and CaO were used as proxies for the three main mineral phases: quartz, clays and carbonates respectively (Ross and Bustin, 2009). Using the Si/Al ratio as a proxy for clay content (Newport et al., 2016), samples containing the most clay can be estimated. Sample BH 1 exhibits the lowest Si/Al ratio of 2.44 (22/9) indicating a higher clay content. Linking this data for BH 1 to the qualitative XRD results (Table 2.13) we see that BH 1 has one of the higher proportions of clays present; chlorite, kaolinite and illite. Samples OC 7 and OC 8 exhibit negligible amounts of clay, however sample OC 7 shows nearly seven times the amount of Al_2O_3 which XRD analysis has shown to be clays present in the form of kaolinite and illite (Table 2.13). OC 6, a calcite rich limestone-shale is estimated to have the lowest clay content of all samples less that a 1/0 ratio. The lack of clay content for sample OC 6 is backed up by XRD (diffractograms observed in Appendix B), with results showing no clays present.

2.4.3. X-Ray Diffraction

All X-Ray diffractograms can be viewed in Appendix B and Digital Appendix B.4. Quartz was present in all samples, with primary and secondary peaks observed. Using samples OC 8, foundry sand proppant, a calibration was made (Figure 2.17).

QUARTZ			BARITE		
d	I	2 θ	d	I	2 θ
4.27	22	20.8	4.4	16	20.2
3.342	100	26.67	4.34	30	20.47
2.457	8	36.57	3.9	50	22.81
2.282	8	39.49	3.77	12	23.58
2.237	4	40.32	3.58	30	24.89
2.128	6	42.5	3.45	100	25.86
1.979	4	45.83	3.32	70	26.86
1.659	2	55.38	3.1	95	28.77
1.453	1	64.04	2.84	50	31.55

Table 2.12: *Typical diffraction data for quartz and barite ordered by d spacing value. Data adapted from (Moore and Reynolds Jr, 1997). 'I' displays the intensity. All values <100 are taken as a ratio of 100, with 100 being the strongest and most prominent peak.*

Peaks observed in the barite sample match those from reference material in both degrees 2θ and intensity (I). Samples OC 8 and OC 6 contain the least amount of mixed minerals and display (Figure 2.17) the most prominent peaks for both quartz and barite (used as internal standards). All samples were measured twice, between 10 and 90 ° 2 θ and between 2 and 90 °2 θ. No erroneous peaks were measured between these two sets.

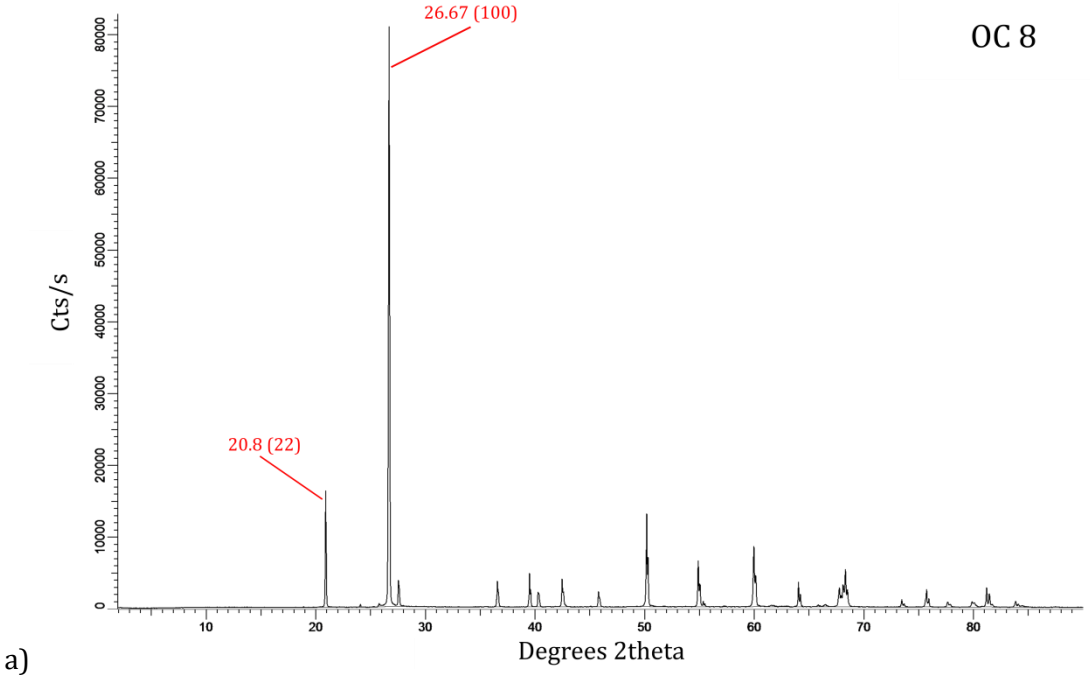

a)

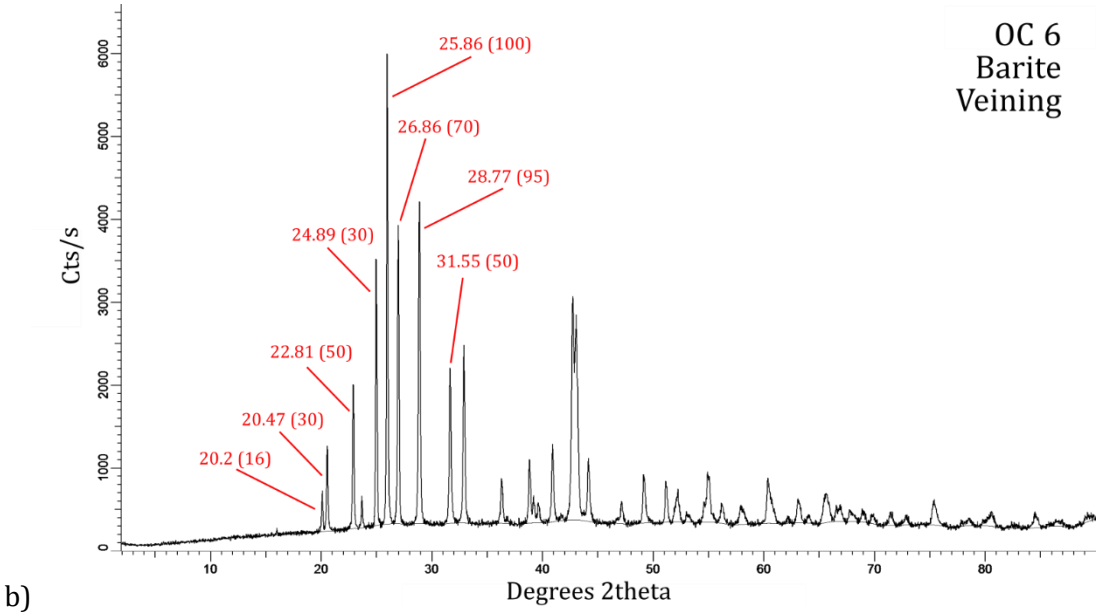

b)

Figure 2.17: *Diffractograms for sample OC 8 (a) and barite rich veining from OC 6 (b) displayed in cts/s (counts per second). For OC 8, only prominent quartz peaks are present with very minimal background interference suggesting a purer sample. The barite veining for OC 6 has slightly higher background interference, but still very low. Sample may be contaminated with other minerals, inclusive of clays and carbon; however, Barite peaks are still clearly visible in the correct positions and intensities as detailed in Table 2.12.The unbracketed value represent the degrees 2 θ value, whilst the bracketed value represents the peak intensity as a ratio of 100, i.e. (100) is the strongest peak, and (16) would represent an intensity of 16 % of 100.*

Table 2.13 exhibits the qualitative analysis results for all samples in the order of the sample name and type. The differentiation detailed in the caption between 'present', 'likely present', 'negligible presence' and 'not present' is derived from the fact that some major peaks may obscure minor peaks of other minerals. Differentiation between the presence and absence of certain minerals is especially likely in mixed mineral aggregates, of which all samples are in this study.

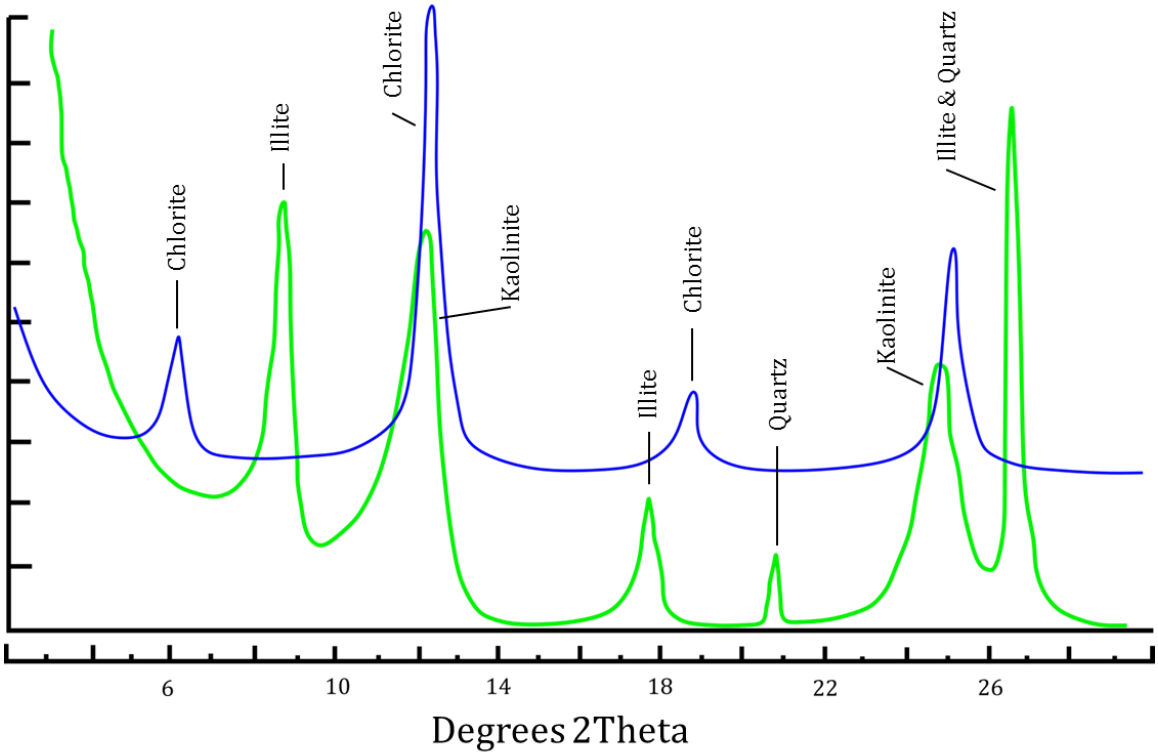

Figure 2.18: *Typical common clay diffractogram patterns for chlorite, illite, kaolinite and quartz. Diffraction pattern lines adapted from (Moore and Reynolds Jr, 1997). The blue and green lines represent two different example sample diffraction patterns adapted from the reference.*

The 00*l*, or basal, reflections for the clays of interest are shown in Figure 2.18. These reflections are the most prominent peaks for the clays sought and the ones used in the main identification of the clay types where possible.

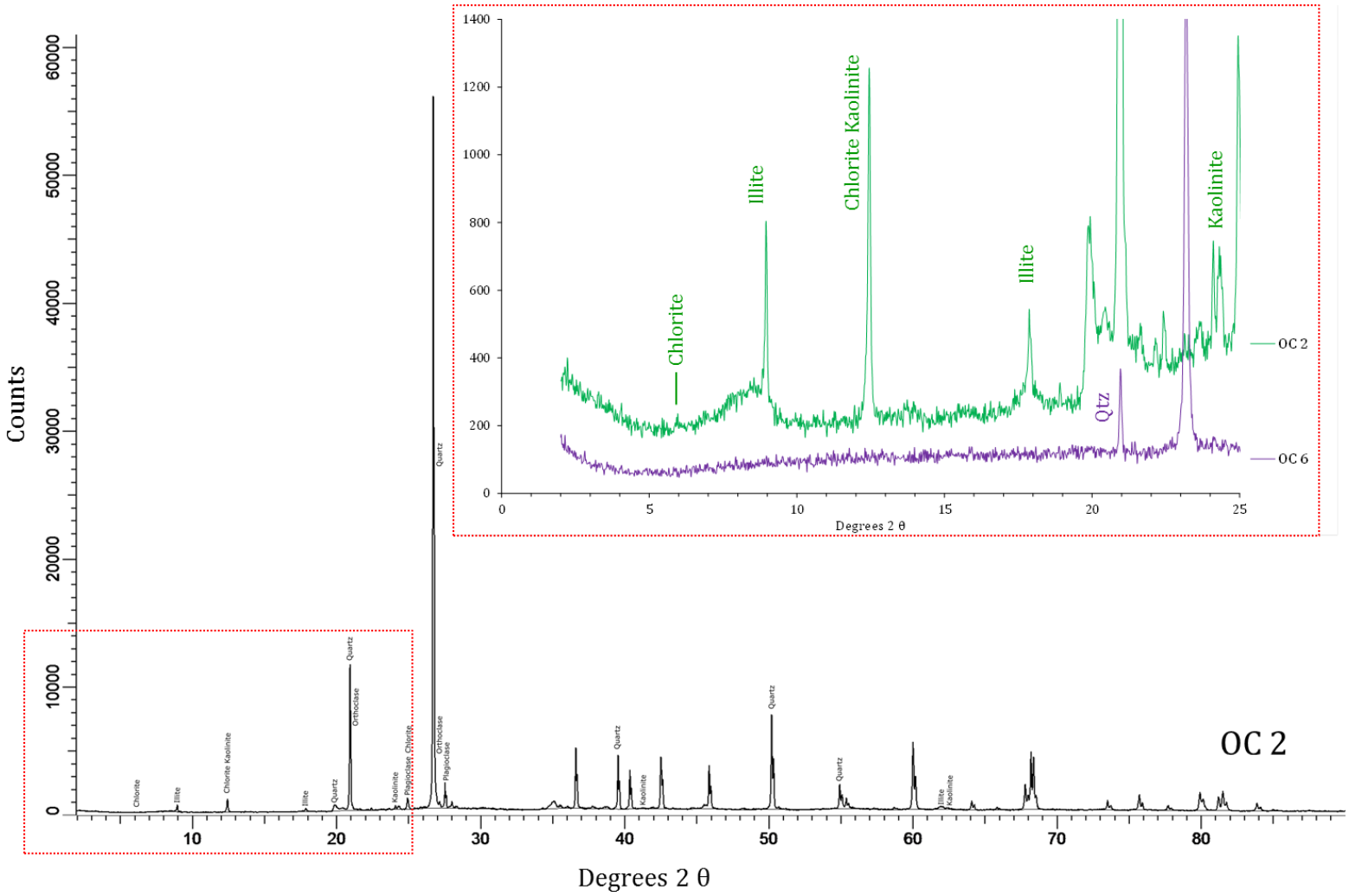

Figure 2.19: *Example XRD diffractogram of sample OC 2 (Hazelhurst Fell Pendle Grit (Silty)). The full range from 2 – 90 ˚2 θ is shown on the main image whilst a subsection from 2 – 25 ˚2 θ is shown in the image top right. This subsection image shows the difference between a sample that contains clays (OC 2) and a sample that contains minimal clays (OC 6). Please note the reduction in scale on the y axis from ~ 60,000 cts to 1400 cts in order to make clay peak intensities visible. Data from this can be cross referenced with reference patterns seen in Figure 2.18*

	SAMPLE	OC 1	OC 2	OC 3	OC 4	OC 5	OC 6	OC 7	OC 8	BH 1	BH 2	BH 3	BH 4	BH 5	BH 6
		sst	*sst/sh*	*sh*	*sh/sst*	*sst*	*lst*	*sh*	*sst*	*sh*	*sh*	*sh*	*sh*	*sh*	*sh*
Silicas	Quartz	***XXXX***	***XXXX***	***XXXX***	***XXXX***	***XXXX***	***XXXX***	***XXXX***	***XXXX***	***XXXX***	***XXXX***	***XXXX***	***XXXX***	***XXXX***	***XXXX***
Carbonates	Calcite	*x*	**-**	***XXXX***	-	***XXXX***	***XXXX***	-	*x*	***XXXX***	***XXXX***	***XXXX***	***XXXX***	***XXXX***	*XX*
	Dolomite	*x*	**-**	*XX*	-	-	***XXXX***	-	*XX*	***XXXX***	*XX*	*XX*	*XX*	-	*XX*
	Aragonite	-	***x***	*XX*	-	-	-	*x*	*XX*	-	-	-	*XX*	*XX*	*x*
Feldspars	Orthoclase	*XX*	***XX***	*XX*	-	***XXXX***	*XX*	-	***XXXX***	***XXXX***	***XXXX***	***XXXX***	*XX*	*XX*	*XX*
	Microcline	*x*	***XX***	*XX*	*x*	*XX*	*x*	*XX*	***XXXX***	*x*	*x*	*x*	*x*	***XXXX***	*x*
	Plagioclase	***XXXX***	***XXXX***	*XX*	*XX*	***XXXX***	-	*XX*	*x*	*XX*	***XXXX***	***XXXX***	***XXXX***	*x*	*XX*
Sulphides	Pyrite	-	***x***	***XXXX***	-	-	*XX*	*x*	-	***XXXX***	***XXXX***	***XXXX***	***XXXX***	***XXXX***	*x*
Sulphates	Anhydrite	-	**-**	*x*	-	-	-	-	-	-	-	*x*	*XX*	-	-
	Gypsum	-	**-**	-	-	-	-	-	-	-	-	-	-	-	-
Clays	Chlorite	-	***XX***	-	-	-	*XX*	-	-	***XXXX***	***XXXX***	-	-	-	***XXXX***
	Vermicullite	-	***x***	-	-	-	-	-	-	***XXXX***	***XXXX***	-	-	*x*	*x*
	Smectite	-	**-**	-	-	*x*	-	-	-	-	-	*x*	-	*x*	*x*
	Montmorillonite	-	***x***	-	***XXXX***	*XX*	-	-	-	*XX*	-	-	-	-	-
	Kaolinite	***XXXX***	***XXXX***	***XXXX***	***XXXX***	***XXXX***	-	***XXXX***	-	***XXXX***	*XX*	-	*x*	-	***XXXX***
	Dickite	*XX*	***x***	-	-	-	-	-	-	*XX*	-	-	*XX*	-	-
	Illite	-	***XXXX***	***XXXX***	***XXXX***	***XXXX***	-	***XXXX***	-	-	-	***XXXX***	***XXXX***	***XXXX***	***XXXX***
	Illite/Smectite	-	***x***	*x*	*x*	***XXXX***	-	*XX*	-	-	*x*	*x*	***XXXX***	*x*	*x*

Table 2.13: *Qualitative mineralogical compositional analysis for all samples included in this study. XXXX = present (dominant), XX = likely present (accessory), x = negligible presence (minor) and - = not present. Samples are named as per 'naming convention' seen in section XXX. 'sst' = sandstone lithology, 'sh' = shale lithology and 'sst/sh' or 'sh/sst' = sandstone and shale mix with the former labelled being the dominant lithology type.*

Where present, quartz has the most dominant, sharp and intense peaks making it easy to identify. On the other hand, feldspars such as plagioclase and orthoclase are difficult to identify because they contain variable compositions and have small primary peaks (Moore and Reynolds Jr, 1997). The most prominent peaks for feldspar lie very close to the major quartz peak at 26.67 ° 2 θ, obscuring its identification. Pyrite is another common mineral which can be difficult to identify. Pyrite (FeS_2), if present, can produce higher background signals on the diffractogram due to the CuKα incident radiation that is ideal for exciting fluorescent radiation from iron (Moore and Reynolds Jr, 1997).

Quartz is present in all samples analysed. The two most dominant quartz peaks were observed in all sample patterns. XRF data confirms this with samples ranging from 2.65 wt % (OC 6) SiO_2 to 98.72 wt % SiO_2 (OC 8). Calcite is confirmed across the majority of samples (OC 3, OC 5, OC 6, BH 1, BH 2, BH 3, BH 4 and BH 5) and is commonly associated with clay minerals. Calcite presence was ubiquitous, but samples were cross referenced with XRF results to ensure that potential peaks close to far more intense quartz peaks, would have also been calcite. Unsurprisingly, OC 6, limestone rich shale, contains the largest amount of carbonate material. Prominent peaks between the two in degrees 2θ are Qtz 29.4 / Cal 29.43, Qtz 35.9/ Cal 39.43, Qtz 43.12 / Cal 43.18 and Qtz 48.5 / Cal 48.5. Feldspars, particularly orthoclase and plagioclase are found in most samples. All three types of feldspar sought in the analysis, inclusive of microcline, are more dominant in the sandier lithologies such as OC 2, OC 5 and OC 8. Sulfides, such as pyrite are most abundant in the borehole samples: BH 1, BH 2, BH 3, BH 4 and BH 5. Pyrite occurs commonly as the product of dissolved sulphates, decomposable organic matter and reactive detrital iron minerals (Berner, 1984) from the microbial reduction of seawater sulphates (Shawar et al., 2018). Iron content of predominantly terrigenous samples from depth can be seen by using hematite (Fe_2O_3) from XRF results. Sulphates such as anhydrite and gypsum are uncommon, only three samples potentially contained anhydrite (OC 3, BH 3 and BH 4), although this was very low probability for OC 3 and BH 3. No gypsum peaks were observed in any of the samples.

The most common clay minerals within shales include illite, illite/smectite, smectite, kaolinite and chlorite (Chermak and Schreiber, 2014), the most abundant for the Bowland shale are kaolinite and illite (Gross et al., 2015). Using the Si/Al ratio as a rule for an estimation of the clay content, clay presence can be anticipated in some samples. The most common types of clay present in the study samples are kaolinite, present in 9 of the samples, and illite, present in a different 9 samples. Dickite and smectite appear to be the least common clay types having potential occurrences in 4 samples each. Complete clay content could not be calculated due to the qualitative nature of this analysis; however, an estimation of clay content can be ascertained through the Si/Al ratio (Table 2.11). All types of clays detected are more prominent in the shale type lithologies, rather than the silica type ones such as OC 1 and OC 8.

2.5. Discussion

Carbon analysis showed that samples contained up to 12.04 % of total carbon. When these figures were broken down into organic carbon and inorganic carbon amounts were up to 4.99 % and 7.04 %, respectively. Chiefly, organic carbon amongst all samples sat between 0.05 % and 7.04 %, sitting within the range of a study from Gross et al., (2015) (1.25 % to 7.55 %) and well within study results from Newport et al., (2016) which reported values ranging from 0.12 % to 10.31 % across the Upper and Lower Hollywell shales. Six samples sit above the suggested Namurian shale TOC cut off of > 2 % (Andrews, 2013; Charpentier and Cook, 2011; Gilman and Robinson, 2011) for exploitable shale gas units. Of these six samples, five were purely shale lithologies with the one remaining a more calcite rich shale, or limestone. Inorganic carbon ranged from 0.004 % in OC 8 to 4.99 % in OC 6. As expected, from these values, OC 8 showed the least drop in wt % (only 0.03 wt %) on the TGA in the carbonate window between 650 and 980 ^{o}C. Sample OC 6 on the other hand showed the greatest mass reduction between 650 and 980 ^{o}C at 41.64 % loss. This was confirmed by carbonate content as shown in the XRF results for OC 6 showing a wt % of 52.87 % CaO, the highest of all samples. Overall, the more shale type samples (examples being BH 1, BH 3, BH 5 and OC 3) exhibit more TOC. Samples which are lesser shale and more sandstone or limestone (e.g. OC 1, OC 5 and BH 6) exhibit much less TOC, but proportionally slightly higher TIC.

In terms of mineralogy, all samples contained large amounts of quartz (22.8 % - 98.72 %) apart from the limestone (OC 6) which contained only 2.65 % SiO_2. In general the more shale type lithologies contained the higher concentrations of Al_2O_3 and MgO, a proxy for clay content. This data fell in line with Al/Si ratios calculated from the XRF data showing that the sandier lithologies exhibited lower concentrations of Al_2O_3 and MgO which was concluded further with the sandier lithologies generally exhibiting a higher Si/Al ratio (e.g. being OC 1, OC 5 and OC 8).

Clay type, alongside some common mineral types based upon the general lithologies of the samples is shown in the XRD results. Although only qualitative (XRD is usually only semi-quantitative) it was useful to identify the types of clay present in each sample, and whether in fact there were multiple clays present, or none at all. As discussed, and in line with the literature (Gross et al., 2015), the most common types of clay present were kaolinite and illite with at least either or both types present in 11 samples. Again, sandier or more carbonate rich samples lacked clays. This was reflected in both the Si/Al ratios and the XRD results. For example, OC 6, OC 1 and BH 3 exhibit high Si/Al ratios showing low clay content and this is backed up by having negligible clays identified in the XRD diffractograms.

Overall the samples chosen for this study, whilst selected for their suitability, have been also deemed typical of shale gas exploitable units when compared to available literature. Borehole

samples are typical of exploitable units, and have been drilled for that exact reason. Outcrop units are of use as analogues to the subsurface Bowland Shale, Pendle Grit and Hodderense Limestone.

2.6. Conclusions

Results and various data from this chapter, either quantitative or qualitative, will be used throughout the remainder of this study. Using statistical analyses, analytical (XRF and TOC etc) and categorical (XRD) values will be analysed in conjunction with adsorption, desorption and fluid analysis results shown further along in this study, Chapters 3, 4, 5 and 6. Ultimately, the aim of this is to be able to link adsorption, desorption, colloid and flow-back fluid data to particular characteristics of the samples. For example, statistical analysis will be able to show us if certain sample features promote or increase adsorption, or if certain samples with higher concentrations of a certain substance release more of that substance into a flow-back fluid, or does the PAM inhibit this process. Furthermore, results from the characterisation within this study will be able to be used to inform the wider general understanding of the geochemistry and minerology of the Upper and Lower Shales, Hodderense Limestone and Pendle Grit. Data here would inform a more regional approach as samples are spread over a large geographical area, rather than over a depth interval, much like most of the available literature.

3. The Adsorption of Polyacrylamide at Room Temperature

3.1. Introduction

Chapter 2 developed the context of the samples and their relevance to the UK industry, and characterised their properties in terms of mineralogy and organic and inorganic carbon. Having a UK context for the study was key and in line with the project outline to accurately assess the baseline and effects before any major fracking operations began. The purpose of this chapter is to analyse how much non-ionic polyacrylamide (PAM), a common friction reducer (Blondes et al., 2017; Xiong et al., 2018b), is likely to be adsorbed to the shale surface. Based upon the results of the adsorption experiments, what environmental concerns are likely to arise because of this?

All methods and results in this chapter were presented at EGU General Assembly 2018 as part of a poster and at UDSIG UK (Use of the Deep Subsurface in the UK) conference at the Geological Society in 2018, as part of a presentation. Results were also summarised in poster form at an Environment Agency Knowledge Exchange event in Bristol, 2019. Posters can be viewed in the Digital Appendices.

3.2. Aims and Objectives

The aim of this chapter was to understand the behaviour of PAM in the presence of shale, and other rock types associated with the Bowland shale, particularly in terms of adsorption. Essentially, measuring how much aqueous PAM remained in solution, and how much was removed via means of adsorption. To be able to understand the adsorption behaviour of PAM in the presence of a shale, sandstone or limestone, it was deemed best to experiment with samples at room temperature and room pressure conditions first, before examining adsorption at conditions more akin to those that would be experienced at depth (Chapter 4). In these room temperature experiments (RT) the temperature ranged from 17 to 25 ˚C with the pressure remaining at atmospheric (101 kPa). By using one of the two onshore wells fracked in the UK, Preese Hall 1A (using 430 mg/L of PAM) as a proxy to this entire study (Broderick et al., 2011), a range of PAM slick-water concentrations were produced. The range of slick-water concentrations (15.625 mg/L – 1000 mg/L) encompassed the typical operational range of slick-water concentrations (30 – 2140 mg/L (Aften and Watson, 2009; Stringfellow et al., 2014)), and the Preese Hall 1A proxy.

Aqueous PAM was measured before and after the experiments and PAM removal was calculated by means of plotting data on three types of isotherm; Linear, Freundlich and

Langmuir. Isotherms were then chosen based upon the best statistical fits and then these were subsequently statistically analysed against quantitative data from the shale characterisation seen in Chapter 2 to see which factors were the major influencers of adsorption.

3.3. Room Temperature Adsorption Experiments

To be able to provide a range of PAM concentrations that are typical of the concentrations used in the shale gas industry (typically between 30 and 2140 mg/L for cationic, anionic and non-ionic forms (Aften and Watson, 2009; Stringfellow et al., 2014) a series of 8 concentrations were produced via the serial dilution of a single 1000 mg/L solution of a non-ionic PAM slick-water. The most useful proxy for this study was the Preese Hall 1A fracking fluid that used a concentration of 430 mg/L, which also used the non-ionic form of PAM (Broderick et al., 2011).

For the purposes of all adsorption experiments detailed in this thesis, a single sample of rock is referred to as a "rock sample"; a series of 8 slick-water dilutions containing the same rock sample is referred to as a "Sample Batch" and an individual vial of any dilution containing any sample of rock is referred to as a "Sample".

Initially a 1000 mg/L PAM solution was produced by adding 1000 mg of non-ionic granular PAM to 1 L of mains tap water, taken from the laboratory cold tap (Northumbrian Water supplied). Tap water, and PAM tap water (slick-water), were analysed for metals later in this study in Section 6.6.1. This solution was agitated at 400 rpm and left to fully mix overnight at room temperature. At least 40-60 minutes was required for full dissolution of a powdered or beaded form of Polyacrylamide (SNF FLOEGER), however an overnight period was selected to ensure full dissolution as some particles of granular PAM were observed after this 60 minute timescale.

From this 1000 mg/L solution (0.1 %), serial dilutions were taken with solutions halved each time to produce to the initial concentrations for adsorption seen in Figure 3.1. These 40 ml volume dilutions were prepared in 50 ml glass vials with snap plastic caps. At least one hour was needed for both water and PAM fluids to mix thoroughly to produce the 1000 mg/L non-ionic PAM solution.

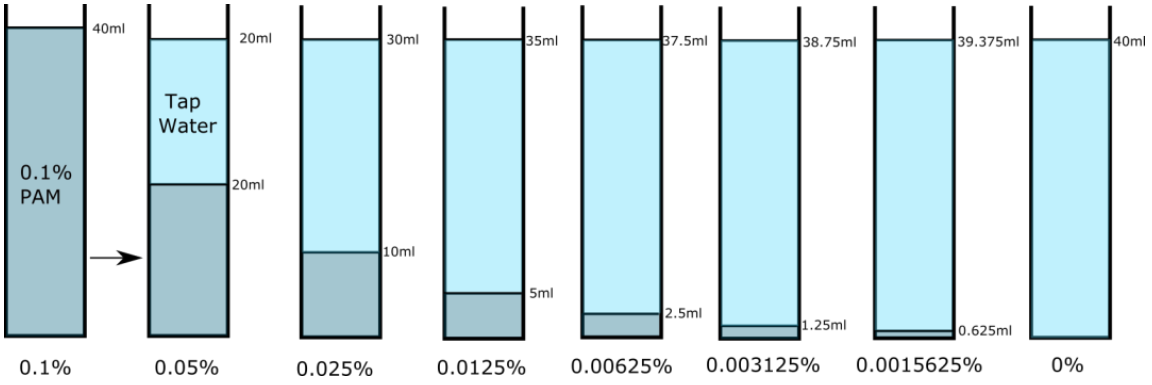

Figure 3.1: *All concentrations of 40 ml PAM fluids as shown as a dilution of a 1000 mg/L (0.1 %) solution. The set shown is a full set used for a sample batch, or standard batch. For standards, no sample is added, for samples, 1 g of powder of the same sample is added to each glass vial.*

In a sample batch, 1 g of powdered rock sample was placed into each glass vial, leaving 8 PAM dilutions each containing 1 g of the same sample of rock. One set of 8 dilutions (Figure 3.1) contains no rock sample as these were used as the standards for the experiment. Every time a new 1000 mg/L slick-water solution was made, a new set of standards was run with the new fluid. Using a new set of standards for each 1000 mg/L fluid produced limited the degradation or storage issues with a colloidal viscous fluid such as a PAM emulsion.

For each experimental run, one sample batch of standards was required alongside two sample batches of 1 rock type (these act as duplicates). So, in simple terms, for one rock sample to be analysed there needed to be 8 concentrations containing no rock sample that acted as standards and then at least 8 concentrations containing a sample, which were then duplicated (Figure 3.2). As many sample batches as was possible were run against one sample batch of standards. The adsorption procedure for this analysis, and the preparation of fluids for the *N*-Bromination method, takes place over a three-day period in total from initial submergence in the PAM rich fluid to analysis on the spectrophotometer. Each sample run contained a blank with 0 mg/L PAM that was 100 % tap water from Durham. This blank accounted for dissolved organic matter (DOM) within the sample. No exact quantities of DOM or TOC were measured within the tap water samples themselves as quantities of PAM, the lowest PAM concentration being 15.625 mg/L, would outweigh the effects from DOM or TOC. Typical UK untreated values of DOC range between 0.056 and 15 mgC/L (Worrall and Burt, 2007) and treated values ranging between 0.50 and 4 mg/L (Anglian Water, 2018; Northumbrian Water Ltd, 2017).

The addition of 1000 mg of granular non-ionic PAM (after 24 hours mixing) to a 1 L tap water (TW) solution produces a near-neutral solution at 7.46 pH and conductivity of 1215 µS/cm, measured at 20.1 °C. To compare, adding the same amount of PAM to 1 L of DI water solution produced a solution with a pH of 7.84 with conductivity of 1095 µS/cm. After two

weeks at room temperature both solutions the DI PAM fluid had a pH of 7.52 and a conductivity of 1098 μS/cm and the TW PAM solution had a pH of 7.29 and a conductivity of 1228 μS/cm.

3.3.1. Experimental Procedure

Day 1: 1000 mg of non-ionic granular polyacrylamide (Acros Organics CAS 9003-05-8) is mixed with 1 L of mains tap water. This mixture is placed on a shaker table for 1 hour at 400 rpm and left overnight to fully mix.

Day 2: This 1000 mg/L solution is placed briefly on the shaker table again at 400 rpm to ensure full mixing. From here, the solution is serially diluted, halving each time, with mains tap water to produce 8 varying concentrations of PAM slick-water ranging from 1000 mg/L to 15.625 mg/L and then a 0 mg/L blank, as shown in Figure 3.2. These new dilutions are placed on the shaker table for 1 hour at 400 rpm to ensure both liquids are fully mixed. After this, 1 g of powdered rock material is placed into each dilution producing a run of "sample batches". This rock and fluid mixture is placed again onto the shaker table for 1 hour at 400 rpm and left overnight for adsorption to occur. The agitation allows as much of the shale surface adsorption sites to be available to adsorb aqueous PAM, in the most consistent way for all fluid concentrations.

Day 3: In the morning, samples are briefly agitated again on the shaker table at 400 rpm to account for overnight settling. Sample fluids are then syphoned off from the shale mixture and filtered into a centrifuge tube using 30 ml disposable syringes and luer lock compatible syringe filters with a 0.45 μm cellulose acetate membrane. This filtration ensures no shale particles enter the fluid. Of this filtered fluid, 2 ml is then added to 18 ml of mains tap water to dilute the concentrations tenfold. This tenfold dilution brings the fluids into a range that can be competently measured on the spectrophotometer. Fluid dilutions are again left overnight to ensure a full mix between the soluble granular non–ionic PAM and the water. The remaining filtered fluid is kept in the centrifuge tube and frozen in storage to be used in the ICP "flowback" analysis, methods and results shown in Section 6.6.2 of this thesis.

Day 4: After full dilutions of both standards and sample batches, the *N*-Bromination method is undertaken – detailed in the next section. Any waste fluids deemed hazardous, containing substances like cadmium and bromine for example, were stored for specialist disposal.

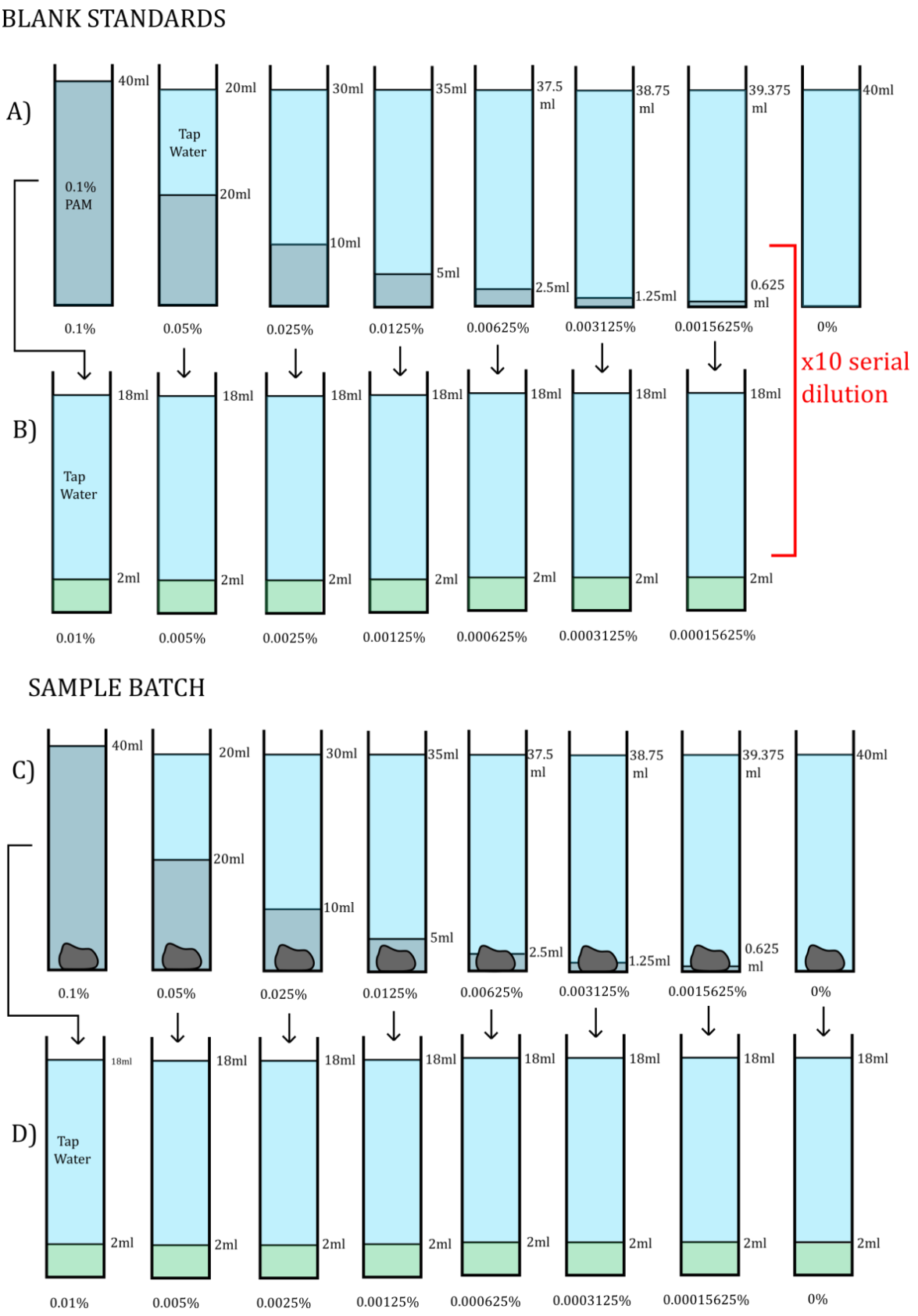

Figure 3.2: *The dilution process for each batch of standards and each sample batch. A) the initial range of concentrations produced from the 1000 mg/L PAM slick-water solution as standards; B) The tenfold dilution of the initial concentrations to bring them into a measurable range for the spectrophotometer; C) the exact same dilutions for 'A' as a "sample batch", all samples seen in 'C' (one run) will be one rock type; D) the same tenfold dilution factor as 'B', just filtered away from samples. Rows 'B' and 'D' are the dilutions of which 2 ml is sampled and mixed for measurement during the N-Bromination method.*

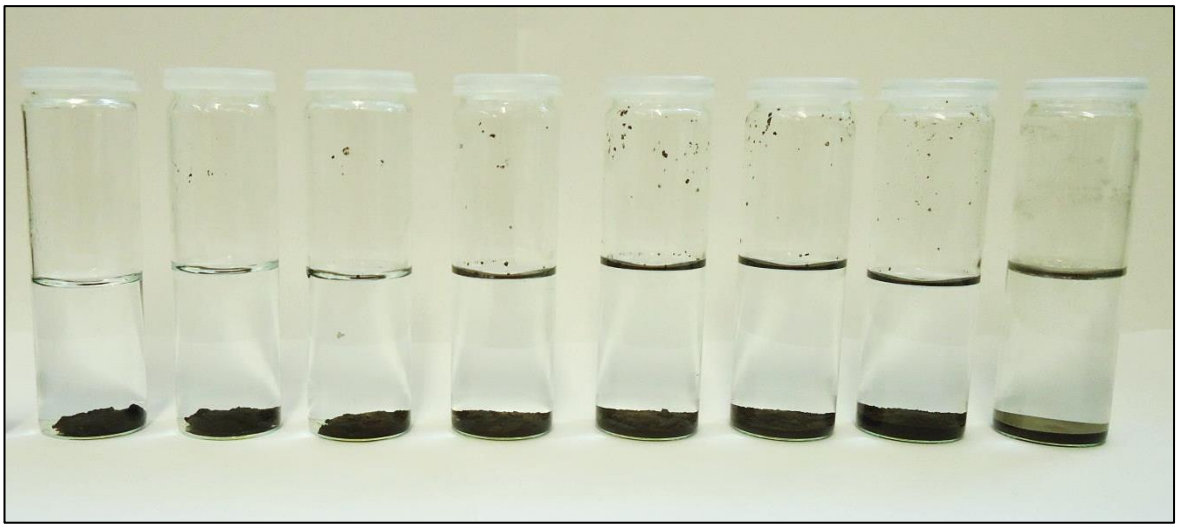

Figure 3.3: *One room temperature sample batch for sample BH 5. From left to right samples range from 1000 mg/L PAM to 0 mg/L PAM in the concentration ranges observed in Figure 3.2.*

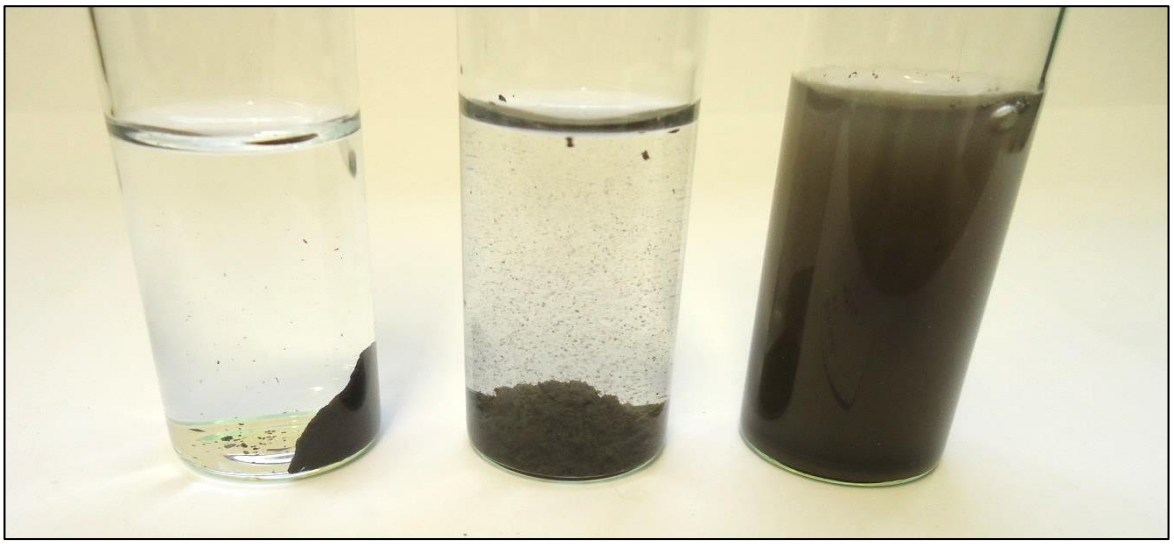

Figure 3.4: *A sample of BH 5 duplicate run. From left to right concentrations are 1000 mg/L PAM, 125 mg/L PAM and 0 mg/L PAM. The effect of higher concentrations of PAM are both acting to increase the hydrophobicity of the shale, preventing maximum surface coverage available, but also to bind the shale together into larger particles allowing material to settle quicker.*

Figure 3.3 shows a sample batch for BH 5 after some of the fluid has been decanted and filtered for analysis. From both Figure 3.3 and Figure 3.4 the hydrophobicity of the powdered rock can be observed in the higher concentration PAM fluids (far left on the images). The lower the PAM concentration within the slick-water fluid, the less the impact of the hydrophobicity of the shale; however, the suspension of particles is prolonged as they are not able to bind into larger particles that sink more easily, which is exactly the role PAM was initially designed for

in irrigation and agricultural applications. Figure 3.4 shows three concentrations of a PAM rich fluid after five minutes of agitation on a shaker table at 400 rpm, illustrating the hydrophobicity at larger PAM concentrations, and the particle binding issues faced in lower PAM concentrations.

3.3.2. The Analysis of Aqueous Polyacrylamide (PAM) – N-Bromination Method

Aqueous polyacrylamide was measured frequently throughout this study in all room temperature, HPHT, colloid and adsorb-desorb experiments. The method used in this study is one derived from Lu and Wu (2001), a method that determines aqueous polyacrylamide present in samples that contain dissolved organic matter. The particular method is called the *N*-Bromination method (*N*-Bromo). This method was derived and adapted from 3 previous studies; Scoggins and Miller (1979); Taylor (1993); Taylor et al (1998). Lu and Wu (2001) is one of the most recent studies looking at the analysis of PAM using this method. Furthermore, the fluid volumes being dealt with by Lu and Wu (2008) are similar to the fluid volumes used in this study, thus ideally suited.

Due to the concentrations of all samples in this study (1000 mg/L to 15.625 mg/L PAM fluids) all samples containing aqueous PAM were diluted tenfold before *N*-Bromo analysis to sit within the necessary analytical range of the spectrophotometer used. The method detailed here will be referred back to throughout the remaining chapters of this thesis, as explained above.

3.3.3. Reagents and chemicals used

All waters used in the production of the reagents were taken from a Milli-Q DI system. The Polyacrylamide used in all experiments was granular non-ionic poly(acrylamide) provided by Acros Organics (CAS 9003-05-8). Bromine used was Sigma Aldrich EMSURE®. Acros Organics supplied the Sodium Formate (99%) and Oxamide (98%). BDH Chemicals®, via VWR®, supplied the Sodium Hydroxide (99%), potato starch and glacial acetic acid (100%). Cadmium Iodide used was 98 % strength supplied by Alfa Aesar®. Filter paper used was Whatman No.5 qualitative 185 mm diameter circles.

3.3.4. Reagent Production

The *N*-Bromo method specified uses a series of 6 different fluids, 4 that are reagents, used in a certain order to determine the total concentration of amide groups at a wavelength

of 570 nm on the spectrophotometer. Four different reagents are used in this method. Reagent preparations below are re-written from Lu and Wu (2001); Scoggins and Miller (1979).

3.3.4.1. 1 M HOAC-NaOAc (Acetic Acid Buffer Solution)

A glass beaker is filled with 300 ml DI water, to which 28.9 ml of glacial acetic acid is added. The pH of this solution is then adjusted (increased) to 3.5 by the addition of a variable amount of 1 % NaOH solution. A 6 ml oxamide solution of 50 mg/L is then added, before bringing the whole solution total to 500 ml with the addition of more DI water.

3.3.4.2. 0.04 M Bromine Water Solution

Bromine water solution is produced by adding 3.20 g of liquid Br_2 to 300 ml of DI water. Once there is complete dissolution of the Bromine, the whole solution is topped up to 500ml with the addition of more DI water.

3.3.4.3. 0.08 M Sodium Formate Solution

Sodium Formate solution is produced by adding 2.72 g of sodium formate to 500 ml of DI water and mixing thoroughly.

3.3.4.4. 0.25 % starch – 0.03 M Cadmium Iodide Solution

The preparation for the starch-cadmium iodide solution is done by bringing 300 ml of DI to the boil. Whilst boiling, add 1.25 g of water-soluble linear starch that has been wetted with 5 ml of DI water. Stir this DI water and starch solution until clear and at the same time remove from the heat. The solution is then allowed to cool to room temperature. When cool, 5.49 g of Cadmium Iodide (CdI_2) is added and stirred until fully dissolved. The volume is then brought to 500 ml by the addition of more DI water. The mixture is then filtered through fine filter paper (Whatman No.42) to remove any insoluble particles. The solution is then stored in a brown glass bottle to protect light sensitive elements.

3.3.5. N-Bromination Analysis Procedure

Before the analysis procedure could start, all raw samples needed to be diluted tenfold to be within the working range of the spectrophotometer due to the concentrations used in this experiment.

Two millilitres of each diluted water sample (thought to contain aqueous PAM) was pipetted into a 20 ml glass test tube and allowed to settle. Once settled, 1 ml of HOAC-NaOAc

buffer solution was added, mixed and then followed by 1 ml of bromine water solution. The solution was then thoroughly mixed and left to react at room temperature for 40 minutes. After 40 minutes, 1 ml of sodium formate solution is added to the mixture and allowed to mix for 5 minutes. Finally, 1 ml of starch-CDI_2 solution was added, mixed, and the sample left for 10 minutes to fully react. Upon the addition of the starch reagent, if PAM was present, the solution will develop a blue complex dependent on the amount of PAM present. This final blue mixture remains stable for ~ 90 minutes which is more than enough time for sample analysis (Lu and Wu, 2001).

Each mixed solution was then measured on a Jenway 6505 UV/Vis spectrophotometer at a wavelength of 570 nm (Lu and Wu, 2001) in quartz cuvettes with a 1 cm length light path. Diluted samples exhibited adsorption values (unitless) of no more than 2.5, in the higher end of the working capability of the spectrophotometer. All samples were duplicated and all duplicates were measured twice with an average absorbance reading used as the final result.

3.3.6. How does N-Bromination work?

The *N*-Bromination method works by the formation of an N-Bromo amide which then converts iodide to iodine. The N-Bromo amide is in turn then measured as a starch-tri-iodide complex (Taylor, 1993). Reaction mechanisms for each step of the *N*-Bromination method are outlined in Equation 3.1 through 3.5 (below).

The amide groups of PAM are converted to *N*-Bromo amides via a reaction with the 0.04 M Bromine solution (Equation 3.1). Any excess bromine that remains from this is removed via the addition of the sodium formate solution (Equation 3.2). These *N*-Bromo amides then convert iodide to iodine when the starch-CdI_2 reagent is added (Equation 3.3 and 3.4). This iodine is what is then measured as the starch-triiodide complex (Equation 3.5) (Lu and Wu, 2001; Scoggins and Miller, 1979; Taylor, 1993).

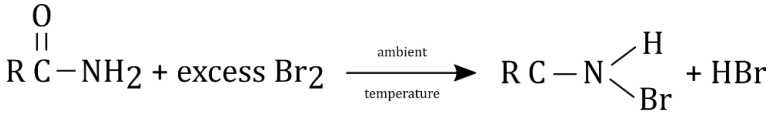

Equation 3.1

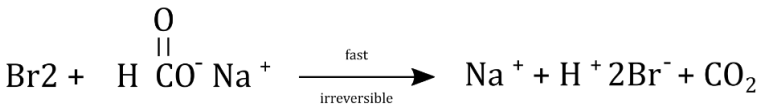

Equation 3.2

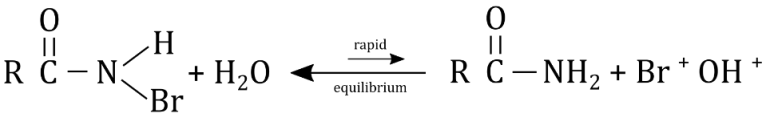

Equation 3.3

$$Br + OH^{+} + 2I^{-} + 2H^{+} \xrightarrow{fast} I_2 + HBr + H_2O$$

Equation 3.4

$$I_2 + I^{-} + starch \xrightarrow{fast} I_3^{-} - starch\ (blue\ complex)$$

Equation 3.5

As a general rule, when the *N*-Bromination process is complete, the bluer the fluid sample, the more aqueous PAM it contains. This can be viewed in Figure 3.5, an image that shows standards and a sample batch waiting to be analysed in the spectrophotometer after *N*-Bromination mixing has been performed.

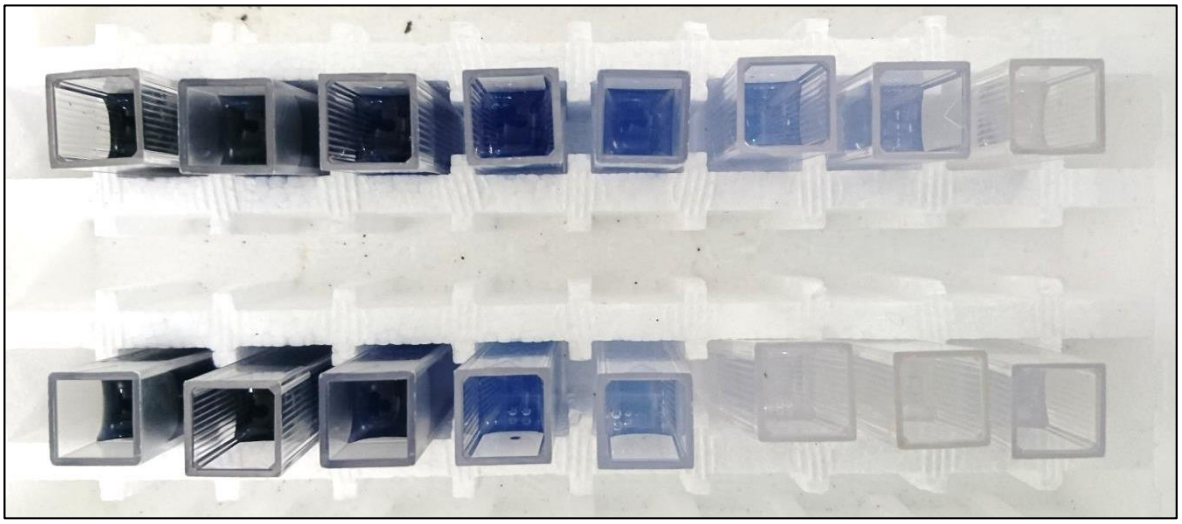

Figure 3.5: *An example of the blue complex developed by the conversion of iodide to iodine when a starch reagent is introduced. Each of these cuvettes contains 4 ml of sample and reagents that have reacted with aqueous PAM. The samples in the upper row are a batch of standards that have contained no rock type. The sample row below is an example of a sample batch. Each cuvette on the far right of each row contains 0 % PAM, hence the completely translucent matrix.*

3.4. Adsorption Isotherm Methodology

To understand the results of the aforementioned tests fully, in terms of amounts adsorbed and amounts of PAM removed, all data was plotted on three isotherms: linear, Freundlich and Langmuir.

The simplest of the three isotherms considered was the linear isotherm, also equivalent to Henry's adsorption isotherm;

$$\boldsymbol{C_s = K_d\, C_a}$$

Equation 3.6

For the linear isotherm (Equation 3.6), C_s is the adsorbed concentration of the adsorbate (mg/kg); K_d is the adsorption coefficient, and C_a the original aqueous concentration of the adsorbate (mg/L). The linear isotherm is typically associated with the initial parts of many of the two to three term isotherms (e.g. Freundlich and Langmuir isotherms). Typically, a linear isotherm is valid for adsorption where there are low surface coverages. The adsorption energy is independent of the coverage.

The Freundlich isotherm, developed in 1906, is an empirical model that can be applied to non-ideal sorption on heterogeneous surfaces, as well as multilayer adsorption (Ho et al., 2002). It is not restricted to monolayer adsorption and accounts for heterogeneity of adsorption sites (Foo and Hameed, 2010). It was historically developed for adsorption to activated charcoal and demonstrated how the ratio of the adsorbate onto a given mass of adsorbent to the solute was not constant with varying concentrations of solutions (Ahmaruzzaman, 2008; Foo and Hameed, 2010).

$$C_s = K_f C_a^{\frac{1}{n}} \qquad \textbf{Equation 3.7}$$

For the Freundlich isotherm (Equation 3.7), K_f is the Freundlich coefficient; and n is the Freundlich constant. The Freundlich isotherm assumes heterogeneous sites and multiple layers of adsorption.

The Langmuir isotherm is the third isotherm used in this study. It was originally developed to describe gas-solid-phase adsorption onto activated carbon (Foo and Hameed, 2010). This isotherm assumes monolayer adsorption where the adsorption layer is only one molecule in thickness (Foo and Hameed, 2010). At low sorbate concentrations the Langmuir effectively reduces to a linear isotherm (Kundu and Gupta, 2006).

$$\frac{C_a}{C_s} = \frac{1}{bk} + \frac{C_a}{b} \qquad \textbf{Equation 3.8}$$

For the Langmuir isotherm (Equation 3.8) all nomenclature remains the same as for the Freundlich isotherm with *k* being the Langmuir coefficient and the addition of b which represents the concentration at maximum coverage (mg/kg). This 'maximum coverage' can sometimes be referred to as the adsorption capacity and is the amount of PAM in mg that can be adsorbed per kg of available rock at equilibrium. Using the linear form of the Langmuir isotherm, 1/gradient is used to calculate this maximum coverage. The maximum coverage is however the averaged value for all the data on the isotherm, not the capacity at the maximum value.

These three isotherms were selected because of the range of adsorption types they can represent. All data was plotted against these three different isotherms with variability in fits due to the type of adsorption occurring.

3.5. Statistical Analysis

Due to the relatively small datasets for each sample and their relevant duplicates, statistical analysis was conducted on the results of all adsorption isotherms plotted. Isotherms were fitted to the results from all adsorption measurements by using equations 3.6 to 3.8 and the calculated aqueous and adsorbed PAM concentrations shown in Table 3.3. Stepwise linear regression was performed on all isotherm data (K values and maximum coverages) against all available quantitative data from the shale characterisation (XRF and carbon analysis (Section 2.3). The adsorption coefficient (K) is used as the statistical response value for both the Linear and Freundlich isotherms while both the concentrations at maximum coverage (maximum coverage) *and* the adsorption coefficient (K) were used as statistical response values in regression for the Langmuir isotherm. The predictors for the regression runs were the numerical values from the characterisation techniques; XRF oxides, TOC, TIC, TC and Si/Al ratios. The resulting regression was tested for significance (P-value) and the VIF (Variance Inflation Factor). The VIF predicts multicollinearity, the phenomenon whereby one predictor can be used to predict another, resulting in redundant data. Here, values range from between 1 and 5, with 1 moderately correlated and 5 + highly correlated. Ultimately a VIF greater than 10 usually indicates high correlation and thus cause for concern.

Analysis of variance (ANOVA) was used with the XRD data as it was not a continuous variable, only the four presence categories explained in Chapter 2 were used.

3.6. Adsorption Calibration

As mentioned previously, the analysis of aqueous PAM still present in the slick-water fluid after 24 hours of overnight adsorption was done by means of the *N*-Bromination method (Lu and Wu, 2001; Scoggins and Miller, 1979). As discussed in Section 4.3.1 the original PAM supernatants were diluted tenfold (i.e. 2 ml of a 1000 mg/L solution is added to 18 ml of blank matrix tap water to produce a 100 mg/L solution) to bring them to within the analytical range of the spectrophotometer.

For each run of experiments, essentially each time a new 1000 mg/L PAM slick-water fluid was made, a new set of standards were analysed using that fluid. This analysis produced 8 quantitative results for a range of PAM concentrations up to 1000 mg/L that are measured

at 570 nm on a Jenway 6505 UV/Vis spectrophotometer. The results of a typical set of standards are seen in Figure 3.6. Results for all standards for each experiment run, inclusive of the 0-250 mg/L and 0-1000 mg/L curves, are given in Digital Appendix C.1.

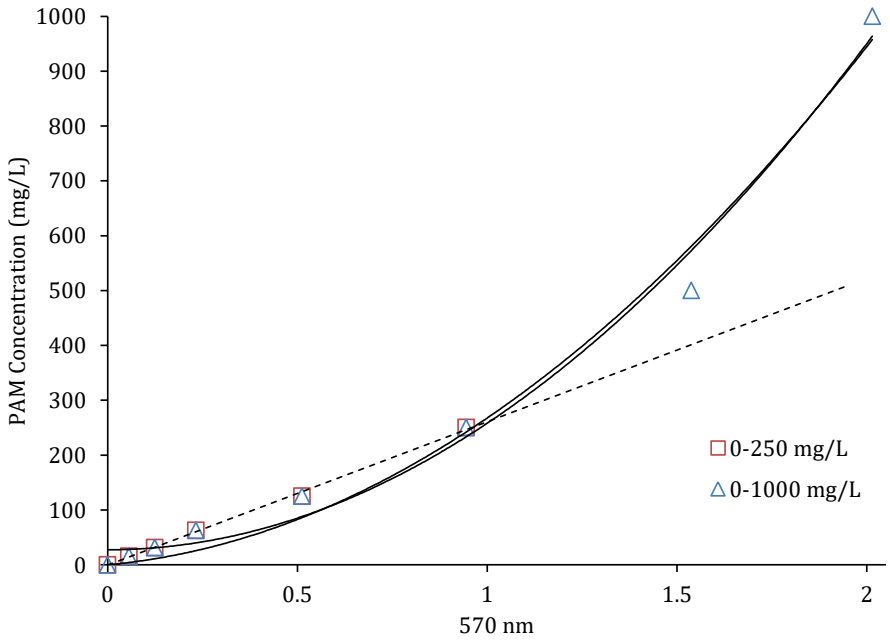

Figure 3.6: *Calibration curve of PAM standards taken from the batch experiment which analysed samples OC 2 and OC 4. The x axis is the value read on the spectrophotometer at a wavelength of 570 nm. Absorbency values for PAM concentrations that are higher than 250 mg/L deviate from the linear portion seen at concentrations up to 250 mg/L. To account for this, three calibrations were used; linear, polynomial (c = 0) and polynomial (c ≠ 0). Significance of these fits was tested via a t-test. Values of adsorbancy on the spectrophotometer are unitless.*

Results of the sample batches were calibrated against three calibrations from the standards. One linear calibration accounted for all data between 0 mg/L and 250 mg/L; and two polynomial fits accounted for all data from 0 mg/L to 1000 mg/L. Using these two calibration ranges would remove non-linearity between 250 mg/L and 1000 mg/L. Using only one of these calibrations may ignore large portions of data at either end of the concentration range (Figure 3.6). Using solely the 0-1000 mg/L calibration may underestimate a large amount of data in the lower concentration range, whereas using solely a linear calibration would underestimate data in concentration ranges above 250 mg/L. Logarithmic and exponential calibration curves were avoided as they provided highly variable, sometimes sigmoidal trends, which were very sensitive to the concentrations of the standards used.

To check the statistical difference in results between all three approaches to calibration, a simple two sample t-test was performed on a subset of the standards calibrated for all room temperature adsorption runs. Details of this t-test can be seen in Table 3.1.

EXAMPLE 1			
CONCENTRATION	Linear mg/L	Polynomial c = 0 (mg/L)	Polynomial c ≠ 0 (mg/L)
250 mg/L	236.74	239.5	239.19
125 mg/L	*147.78*	*145.7*	*146.07*
62.5 mg/L	60.04	57.54	58.65
31.25 mg/L	30.59	28.92	30.29
15.625 mg/L	8.91	8.15	9.73
0 mg/L	0	0	0
	Linear vs Polynomial (c = 0)	Linear vs Polynomial (c ≠ 0)	Polynomial (c = 0) vs Polynomial (c ≠ 0)
T-VALUE	0.01	0	-0.01
P-VALUE	0.99	1	0.99
EXAMPLE 2			
CONCENTRATION	Linear mg/L	Polynomial c = 0 (mg/L)	Polynomial c ≠ 0 (mg/L)
250 mg/L	246.22	242.13	233.29
125 mg/L	*133.15*	85.92	87.92
62.5 mg/L	60.08	25.71	39.89
31.25 mg/L	31.71	10.96	30.95
15.625 mg/L	13.93	4.17	*28.12*
0 mg/L	0	0	0
	Linear vs Polynomial (c = 0)	Linear vs Polynomial (c ≠ 0)	Polynomial (c = 0) vs Polynomial (c ≠ 0)
T-VALUE	0.36	0.21	-0.17
P-VALUE	0.729	0.839	0.872

Table 3.1: *Table showing the statistical t-test for calibration lines used to determine aqueous and adsorbed PAM concentrations. Each column refers to the mg/L of aqueous PAM found in the fluid depending on the calibration line it was derived from. Italics indicate where the calculated concentration is larger than the initial concentration, indicating calibration error.*

The t-test estimates the difference between both sets of means. Using a significance level (or alpha (α)) of 0.05, as is typical for this test, isotherms are tested as; 1) linear vs polynomial (c = 0), 2) linear vs polynomial (c ≠ 0) and 3) polynomial (c = 0) vs polynomial (c ≠ 0). If the P-value is ≤ 0.05 then the difference between these means is statistically significant and it rejects the null hypothesis (the hypothesis that there is no significant difference between specified populations). The reverse is also true, if the P-value > 0.05 then the difference between means is no statistically significant and so it fails to reject the null hypothesis. The t-value on the other hand measures the size of the difference relative to the variation in data. The greater the magnitude of this t-value, the larger the evidence is against the null hypothesis. Based upon this, the data we see in Table 3.1 suggests no significant statistical difference between either of the calibration lines used, but in order to not lose large portions of data from the analysis, both types of calibrations were used, linear and polynomial. All data for all

adsorption runs were used in all three isotherms and the best fitting isotherm selected for each run based on the available data.

Once calibration data was complete, regressions were performed on all three calibration lines to give aqueous concentrations of PAM. Using the same calibration data used in Figure 3.6, data in Table 3.2 shows the minor differences in the data obtained using the regression equations.

		AQUEOUS CONCENTRATIONS (mg/L)					
		0-250 mg/L CALIBRATION			0-1000 mg/L CALIBRATION		
PAM Conc (mg/L)	570nm avg	Linear	Polynomial (c ≠ 0)	Polynomial (c = 0)	Linear	Polynomial (c ≠ 0)	Polynomial (c = 0)
1000	2.0145				812.247	908.023	904.360
500	1.5375				*602.420*	*532.198*	*541.010*
250	0.9445	241.364	242.191	242.097	*355.448*	222.957	231.457
125	0.512	124.108	118.244	119.149	*157.118*	78.830	75.341
62.5	0.2325	56.919	53.266	52.971	43.471	38.076	23.006
31.25	0.124	20.971	20.311	18.843	*-17.332*	28.788	6.111
15.625	0.056	6.330	7.250	5.199	*-42.096*	*27.505*	1.449
0	0	*0.709*	*2.292*	0.000	*-51.603*	*27.397*	0.000

Table 3.2: *One set of aqueous concentrations derived from each calibration line based upon the standards and data seen in Figure 3.6 for sample OC 2 (1). Where the calibration has failed, i.e aqueous concentration is greater than initial concentration of < 0, data has been rejected (grey and highlighted). All values at 0 mg/L concentration were overridden to a zero value as this was a known value of aqueous PAM.*

For each set of standards run, the calibration was made from the best fitting curve for the relevant sample and initial PAM concentration. Adsorbed concentration was calculated by subtracting initial concentration from aqueous concentration. The process of converting the raw aqueous and adsorbed data into Linear, Freundlich and Langmuir isotherms is summarised in Table 3.3.

Column		*a*	*b*	*c*	*d*	*e*	*f*	*g*	*h*	*i*	*j*	*k*
							LINEAR		FREUNDLICH		LANGMUIR	
Initial Conc	Aq conc	Initial Conc	Aqueous Conc	Ads conc	Ads Conc	% removal	Aq conc	Ads conc	Log (aq)	Log (ads)	Aq	Aq/Ads
%	%	mg/L	mg/L	%	mg/kg	%	mg/L	mg/kg	Log (mg/L)	Log (mg/kg)	mg/L	mg/L / mg/kg
0.100	0.08499929	1000.000	849.993	0.015	15000.709	15.001	849.993	15000.709	2.929	4.176	849.993	0.057
0.050	0.04873996	500.000	487.400	0.001	1260.039	2.520	487.400	1260.039	2.688	3.100	487.400	0.387
0.025	0.02082955	250.000	208.295	0.004	4170.454	16.682	208.295	4170.454	2.319	3.620	208.295	0.050
0.0125	0.01090633	125.000	109.063	0.002	1593.670	12.749	109.063	1593.670	2.038	3.202	109.063	0.068
0.00625	0.00343966	62.500	34.397	0.003	2810.337	44.965	34.397	2810.337	1.537	3.449	34.397	0.012
0.003125	0.00103081	31.250	10.308	0.002	2094.192	67.014	10.308	2094.192	1.013	3.321	10.308	0.005
0.0015625	0.00016568	15.625	1.657	0.001	1396.820	89.396	1.657	1396.820	0.219	3.145	1.657	0.001
0.000	0.000	0.000	0.000	0.000	0.000	0.000	0.000	0.000	0.000	0.000	0.000	0.000

Column

a	Initial conc x 10000 to convert from % to mg/L
b	Aq conc x 10000 to convert from % to mg/L
c	Initial conc - Aq Conc
d	1000 x *c* x 1000 (dilution factor and % to mg/L)
e	((*a* - *b*)/*a*) x 100
f	column *b*
g	column *d*
h	log *f*
i	log *g*
j	column *f*
k	column *f* / column *g*

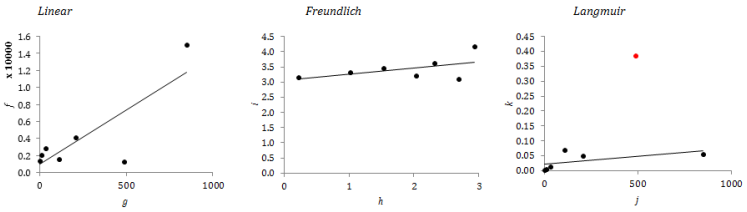

Table 3.3: *Example step by step isotherm calculation guide for sample BH 5 (2).*

Raw data was plotted directly onto the isotherms. Erroneous data, as shown in red in Table 3.3, was highlighted by cross referencing with sample duplicates where data was available. This data was then removed before statistical analyses such as regression or t-testing was performed thus to not invalidate or skew the final results.

3.7. Results

Isotherms were grouped into two main sets; a set of the three isotherm types explained previously for the 0-250 mg/L calibration, and a set of the same three isotherm types for the 0-1000 mg/L calibration. Erroneous data, which did not match between sample duplicates, was removed before fitting of the isotherms. Erroneous data was counted as data points that showed results off the trend by a large margin, or away from the main bulk of data that was present in both duplicates. Where no data was available to cross reference with, potential erroneous data was left as it could not be 100 % confirmed this data was due to random error or adsorption behaviour.

In total, using all calibrated samples and their duplicates, 162 isotherms were produced. One of the major issues faced was the calculated final concentrations that were greater than the initial aqueous concentration of PAM. These results, either > PAM initial concentrations or < 0 mg/L were removed from the final isotherms. R^2_{adj} values were used for all fit calculations, due to the small dataset within each isotherm (up to 7 data points as a maximum). The adjusted R^2_{adj} value is essentially an R^2 value which accounts for the number of predictors within the

model, something which the regular R^2 does not include. The R^2_{adj} value within these models will never be greater than the normal R^2 value as we are dealing with such a small dataset per sample. All samples were treated separately throughout the results section.

SAMPLE	0 - 250 mg/L									0 - 1000 mg/L								
	Linear			Freundlich			Langmuir			Linear			Freundlich			Langmuir		
	Aq	r^2 adj	P-value	Log (Ads)	r^2 adj	P-value	Aq/Ads	r^2 adj	P-value	Aq	r^2 adj	P-value	Log (Ads)	r^2 adj	P-value	Aq/Ads	r^2 adj	P-Value
BH 1 (1)	Regression Equation Coef (const) SE Coef	- -	-	-	2.706 - *0.009* Log (aq) 0.224 0.124	*0.00%*	-	- -	-									
BH 1 (2)		- -	-	-	2.499 + *0.127* Log (aq) 0.518 0.301	*0.00%*	-	- -	-									
BH 2 (1)		534 - *0.315* Aq 109 0.868	0.00%	0.741	2.706 - *0.009* Log (aq) 0.224 0.124	*0.00%*	0.946	*-0.0058* +0.0022 Aq 0 .0272 0.0002	96.33%	0.002	2619 + 4.92 Aq 894 2.29	42.01%	0.098	3.148 + 0.199 Log (aq) 0.241 0.13	21.29%	0.200	0.0211 + 0.0001 Aq 0.0253 0.0001	39.59%	0.107
BH 2 (2)		438 + 1.62 Aq 192 1.54	3.43%	0.403	2.499 + *0.127* Log (aq) 0.518 0.301	*0.00%*	0.714	*0.0639* +0.0010 Aq 0.0718 0.0006	38.72%	0.231	2788 + *1.31* Aq 652 1.61	0	0.462	3.212 + 0.1424 Log (aq) 0.163 0.0872	25.02%	0.178	0.0077 + 0.0002 Aq 0.0101 0.0	94.99%	0.001
BH 3 (1)		828.7 - 6.642 Aq 35.7 0.973	95.80%	0.093	3.155 - 0.273 Log (aq) 0.185 0.132	62.00%	0.287	*-0.0166* + 0.0025 Aq 0.0125 0.0003	96.29%	0.087	2083 + 6.98 Aq 1066 2.76	51.87%	0.065	3.200 + *0.097* Log (aq) 0.496 0.266	0%	0.734	0.127 + *0.0001* Aq 0.176 0.0005	0.00%	0.760
BH 3 (2)		794 - *1.06* Aq 202 1.4	0.00%	0.586	3.057 - 0.1429 Log (aq) 0.14 0.0791	53.11%	0.322	*0.0003* + 0.0017 Aq 0.0060 0.0	99.89%	0.015	2936 - 2.53 Aq 712 1.7	19.43%	0.212	3.531 - *0.164* Log (aq) 0.342 0.182	0%	0.419	*-0.1315* + 0.0026 Aq 0.0963 0.0002	96.21%	0.000
BH 4 (1)		135.7 + 3.266 Aq - -	-	-	1.405 + 0.6550 Log (aq) - -	*100%*	-	*0.1072+0.0006 Aq* - -	*100%*	-	1189 + 9.85 Aq 1061 2.72	66.90%	0.015	3.124 + *0.153* Log (aq) 0.33 0.164	0%	0.394	0.0591 + 0.0001 Aq 0.0497 0.0001	0%	0.504
BH 4 (2)		245.6 + 0.3804 Aq - -	-	-	2.283 + 0.1034 Log (aq) - -	*100%*	-	*0.0145+0.0029 Aq* - -	*100%*	-	2100 + 10.087 Aq 282 0.705	98.07%	0.001	3.098 + 0.2770 Log (aq) 0.12 0.0679	79.66%	0.027	0.0087 + 0.0001 Aq 0.0059 0.0	88.32%	0.011
BH 5 (1)		942 + 28.90 Aq 288 5.76	88.96%	0.038	2.512 + 0.531 Log (aq) 0.182 0.124	85.13%	0.051	0.0075 + 0.0002 Aq 0.0021 0.0	88.97%	0.037	*432* + 16.92 Aq 1257 3.48	81.88%	0.008	3.110 + *0.086* Log (aq) 0.531 0.276	0%	0.772	*0.248* + *0.0002* Aq 0.351 0.0009	0%	0.872
BH 5 (2)		1528 + 13.56 Aq 518 4.99	61.45%	0.073	2.612 + 0.455 Log (aq) 0.239 0.144	69.27%	0.051	0.0078 + 0.0002 Aq 0.0032 0.0	91.83%	0.007	*967* + 12.67 Aq 1541 4.04	59.53%	0.026	3.063 + 0.202 Log (aq) 0.302 0.149	12.22%	0.234	*0.0369* + 0.0002 Aq 0.066 0.0002	3.08%	0.325
BH 6 (1)		1402 + 12.93 Aq 498 4.74	61.72%	0.072	2.536 + 0.4813 Log (aq) 0.12 0.0717	91.68%	0.007	0.0075 + 0.0002 Aq 0.0012 0.0	98.97%	0.000	3869 + *2.58* Aq 1543 3.59	0%	0.052	2.650 + 0.436 Log (aq) 0.73 0.353	11.63%	0.305	0.0156 + 0.0002 Aq 0.0138 0.0	83.98%	0.018
BH 6 (2)		1609 + 12.01 Aq 710 6.79	34.72%	0.175	2.482 + 0.521 Log (aq) 0.237 0.142	75.78%	0.035	0.0070 + 0.0002 Aq 0.0028 0.0	94.93%	0.003	3034 + 15.69 Aq 1392 3.61	81.76%	0.022	2.246 + 0.693 Log (aq) 0.694 0.34	44.14%	0.134	0.0238 + 0.0 Aq 0.013 0.0	0%	0.394
OC 1 (1)		-4476 + 324.4 Aq - -	-	-	-9.153 + 9.799 Log (aq) - -	*100%*	-	*0.4428 - 0.0240 Aq* - -	*100%*	-	-5052 + 348.5 Aq - -	-	-	-12.93 + 12.72 Log (aq) - -	-	-	0.8213 - 0.0443 Aq - -	-	-
OC 1 (2)		-4003 + 349.4 Aq - -	-	-	-4.372 + 6.297 Log (aq) - -	*100%*	-	*0.1377 - 0.0080 Aq* - -	*100%*	-	-4623 + 375.4 Aq - -	-	-	-6.208 + 7.741 Log (aq) - -	-	-	0.2035 - 0.0118 Aq - -	-	-
OC 2 (1)		943.4 - 0.919 Aq 96.6 0.784	8.53%	0.326	3.043 - 0.0676 Log (aq) 0.112 0.064	2.87%	0.368	*-0.0029* + 0.0013 Aq 0.0094 0.0		0.000	2531 + 7.31 Aq 847 2.21	66.47%	0.030	3.189 + 0.206 Log (aq) 0.195 0.106	35.72%	0.124	*0.0189* + 0.0001 Aq 0.0217 0.0001	32.58%	0.138
OC 2 (2)		953.1 + 0.1315 Aq - -	-	-	2.953 + 0.0167 Log (aq) - -	*100%*	-	*0.0018 + 0.001 Aq* - -	*100%*	-	1738 + 12.07 Aq 789 2.13	86.12%	0.005	2.884 + 0.345 Log (aq) 0.25 0.132	53.86%	0.059	0.0212 + 0.0001 Aq 0.0185 0.0001	18.67%	0.217
OC 3 (1)		*559* + 39.68 Aq 858 9.63	79.98%	0.026	*1.12* + 1.273 Log (aq) 1.16 0.694	37.14%	0.164	0.1037 - 0.0006 Aq 0.076 0.0009	0	0.546	1290 + 22.09 Aq 757 2.16	94.52%	0.000	2.394 + 0.614 Log (aq) 0.267 0.132	77.60%	0.005	0.0200 + 0.0 Aq 0.0079 0.0	21.32%	0.166
OC 3 (2)		- -	-	-	- -	-	-	- -	-	-	- -	-	-	- -	-	-	- -	-	-
OC 4 (1)		895 + 19.84 Aq 661 6.48	67.64%	0.055	2.733 + 0.354 Log (aq) 0.257 0.154	51.77%	0.105	*0.0127* + 0.0002 Aq 0.0152 0.0001	20.20%	0.251	*2738* + 18.45 Aq 2976 8.48	38.37%	0.081	3.334 + *0.138* Log (aq) 0.439 0.229	0%	0.573	*0.043* + 0.0007 Aq 0.23 0.0007	2.48%	0.332
OC 4 (2)		791 + 9.660 Aq 111 0.865	98.41%	0.057	2.5178 + 0.4034 Log (aq) 0.0124 0.0076	99.93%	0.012	0.0102+ 0.0003 Aq 0.0024 0.0	99.18%	0.041	2286 + 13.65 Aq 402 1.01	97.84%	0.001	3.0758 + 0.3236 Log (aq) 0.097 0.0508	90.82%	0.008	0.0099 + 0.0001 Aq 0.0068 0.0	76.80%	0.033
OC 5 (1)		582 + 1.97 Aq 189 1.39	25.34%	0.291	2.663 + *0.118* Log (aq) 0.335 0.18	*0.00%*	0.578	0.0363 + 0.0008 Aq 0.0343 0.0003	76.82%	0.081	2987 + 3.70 Aq 829 2.11	29.35%	0.154	3.136 + 0.2293 Log (aq) 0.15 0.0808	58.51%	0.047	0.0084 + 0.0002Aq 0.0084 0.0	90.96%	0.002
OC 5 (2)		485 + 3.33 Aq 187 1.54	47.77%	0.120	2.374 + *0.261* Log (aq) 0.517 0.29	*0.00%*	0.434	0.0605 + 0.0006 Aq 0.0367 0.0003	36.99%	0.165	3066 + 4.44 Aq 819 2.1	41.09%	0.102	3.143 + 0.2417 Log (aq) 0.138 0.0748	65.40%	0.032	0.0078 + 0.0001 Aq 0.0076 0.0	90.83%	0.002
OC 6 (1)		749.2 + 0.303 Aq 85.9 0.698	*0.00%*	0.693	2.748 + 0.0805 Log (aq) 0.101 0.0571	19.87%	0.253	*-0.0049* + 0.0013 Aq 0.0084 0.0	98.94%	0.000	2944 + 5.03 Aq 862 2.22	45.38%	0.086	3.160 + 0.2274 Log (aq) 0.176 0.0955	48.26%	0.076	0.0116 + 0.0001 Aq 0.0127 0.0	74.17%	0.017
OC 6 (2)		611.0 - 4.25 Aq 90.2 1.13	86.67%	0.166	3.403 - 0.598 Log (aq) 0.288 0.171	84.85%	0.177	*-0.168* + 0.0092 Aq 0.206 0.0026	85.38%	0.174	2795 + *0.83* Aq 1100 2.47	0%	0.759	3.239 + *0.089* Log (aq) 0.356 0.177	0%	0.651	*0.0354* + 0.0003 Aq 0.0497 0.0001	50.44%	0.110
OC 7 (1)		782.5 + 9.115 Aq - -	-	-	2.817 + 0.1302 Log (aq) - -	-	-	0.0017 + 0.0009 Aq - -	-	-	- -	-	-	- -	-	-	- -	-	-
OC 7 (2)		1718 + *0.10* Aq 290 4.94	*0.00%*	0.985	3.185 + *0.0362* Log (aq) 0.104 0.0737	*0.00%*	0.672	*0.0001* + 0.0006 Aq 0.0010 0.0	99.74%	0.001	1042 + 2.82 Aq 581 1.43	36.79%	0.119	1.470 + 0.746 Log (aq) 0.958 0.475	22.69%	0.943	0.231 + *0.0* Aq 0.153 0.0004	0.00%	0.191
OC 7C* (1)		734 + *0.66* Aq 213 3.24	*0.00%*	0.857	2.746 + *0.083* Log (aq) 0.255 0.16	*0.00%*	0.657	*-0.0030* + 0.0014 Aq 0.0139 0.0002	93.32%	0.023	734 + 0.66 Aq 213 3.24	0	0.857	2.746 + *0.083* Log (aq) 0.255 0.16	0%	0.657	-0.0030 + 0.0014 Aq 0.0139 0.0002	93.32%	0.023
OC 7C* (2)		*691* + 63.58 Aq 708 9.36	91.86%	0.007	2.647 + 0.577 Log (aq) 0.158 0.101	88.78%	0.011	0.0069 + 0.0001 Aq 0.0031 0.0	33.26%	0.182	*893* + 49.19 Aq 1478 5.13	93.81%	0.000	2.550 + 0.6521 Log (aq) 0.138 0.0707	93.33%	0.000	0.0103 + 0.0 Aq 0.0033 0.0	30.11%	0.117
OC 8 (1)		506 + 9.60 Aq 170 1.47	93.29%	0.023	2.137 + 0.536 Log (aq) 0.233 0.138	82.42%	0.006	0.0270 + 0.0 Aq 0.009 0.0	78.34%	0.004	2751 + 6.54 Aq 504 1.31	82.69%	0.008	3.094 + 0.274 Log (aq) 0.087 0.047	86.87%	0.004	0.008+ 0.0 Aq 0.004 0.0	94.86%	0.075

Table 3.4: *Summary table of the statistical analysis performed on all room temperature adsorption samples. It is divided up by calibration type (0-250 mg/L (left) and 0-1000 mg/L (right)) and then by isotherm type (Linear, Freundlich and Langmuir from left to right for each calibration). The R^2_{adj} is a measure of the fit of the isotherm and the P-value represents the significant in relation to a 0.05 margin of error.*

Table 3.4: *Statistical Analysis summary for all room temperature adsorption experiments.*

A summary of the statistical analysis for all room temperature samples can be viewed in Table 3.4. Here, for each sample, the equation for the line, the R^2_{adj} fit and the significance are all present. For the purposes of this study, all fits that were classified as good displayed a > 60 % R^2_{adj}.

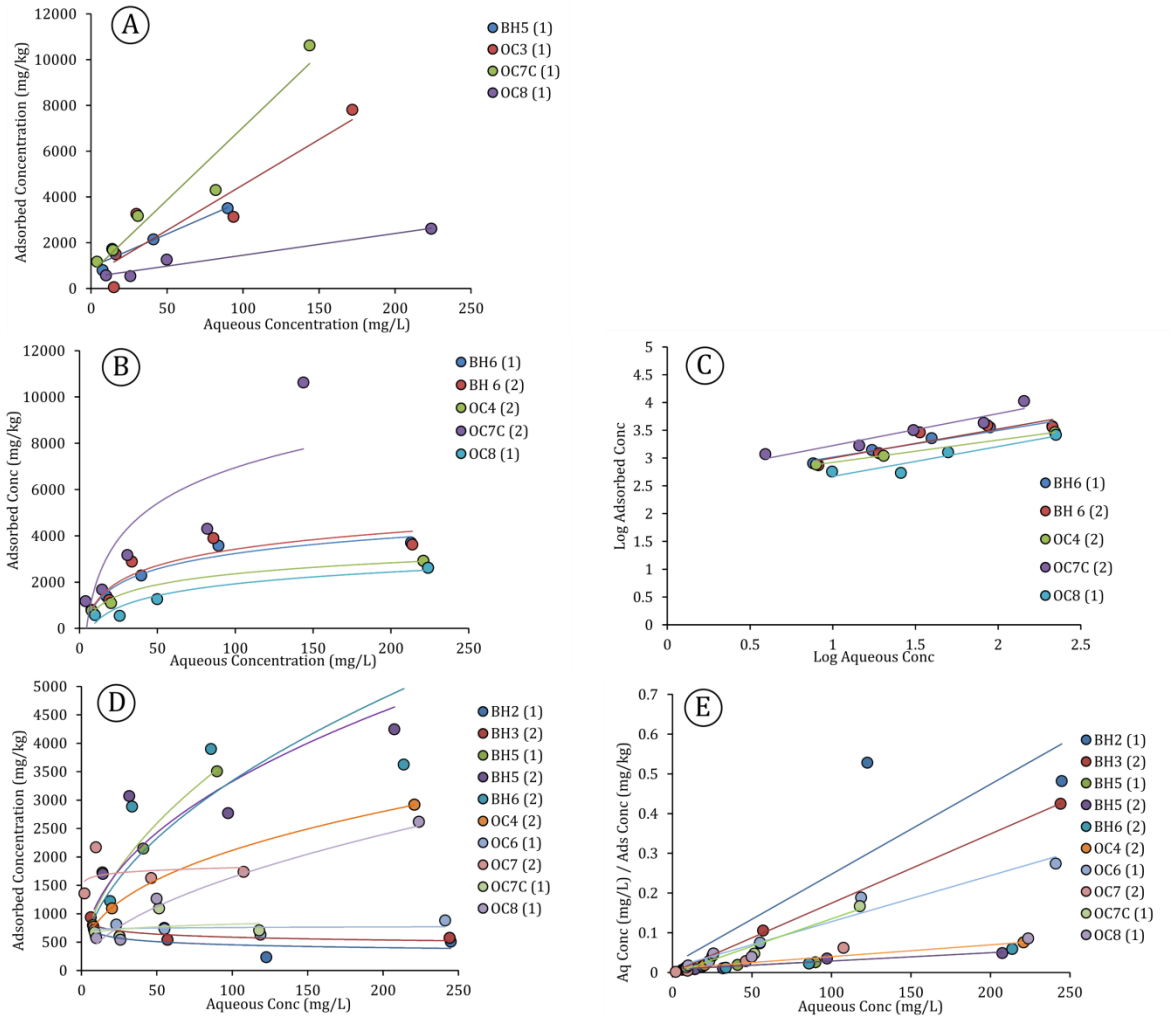

Figure 3.7: *All three types of isotherm for the statistically significant data for the 0-250 mg/L PAM concentrations. From top down; A is Linear, B is Freundlich and D is Langmuir. Charts B and D respectively are the non-linearised forms of both Freundlich and Langmuir. C is the linearised form of the Freundlich and E is the linearised form of the Langmuir isotherm. It is shown like this to help understand the profile of the raw data. The fits used for charts B and D are a logarithmic fit for Freundlich (B/C) and a Power-law fit for Langmuir (D/E).*

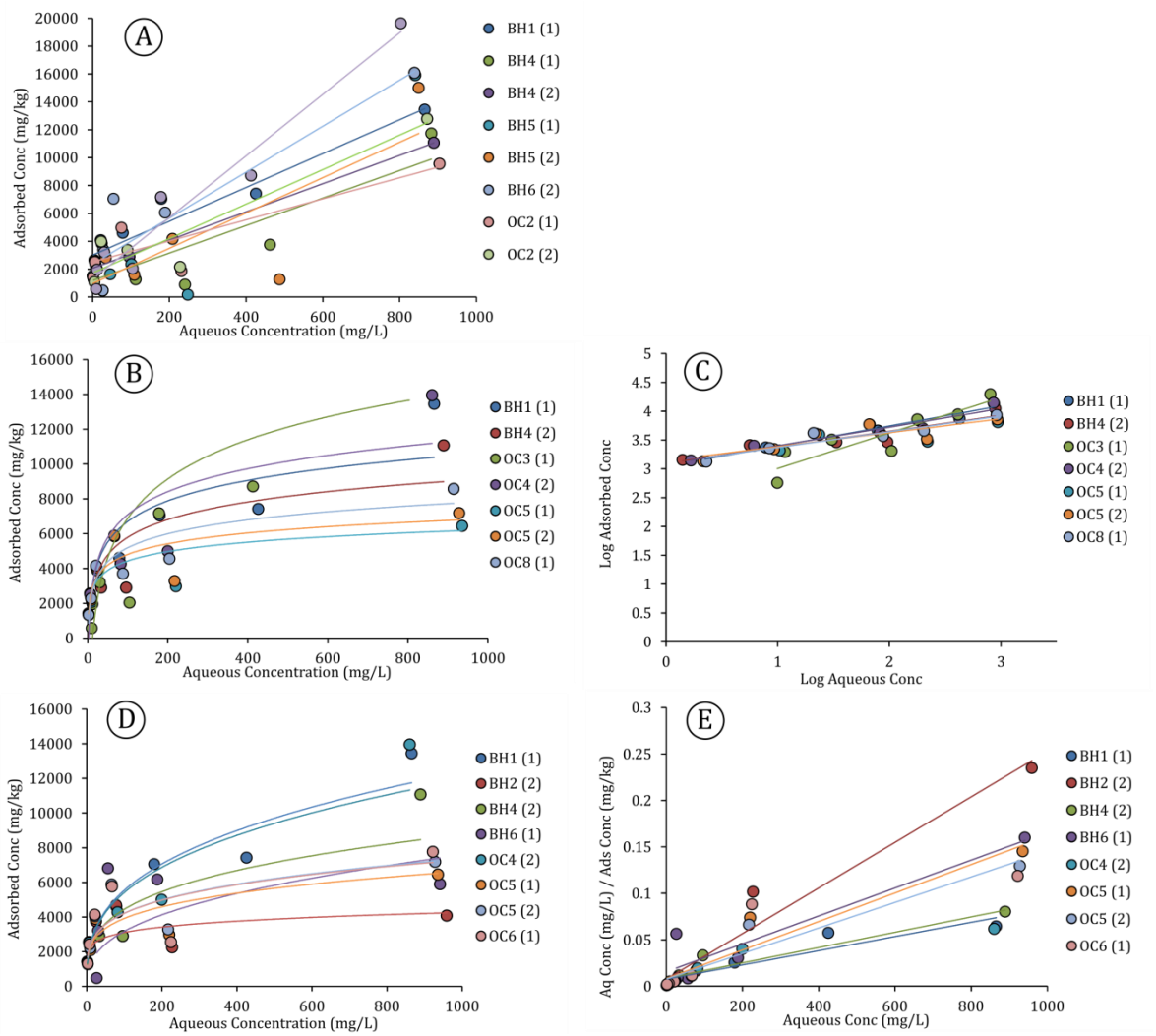

Figure 3.8: *All three types of isotherm for the statistically significant data for the 0-1000 mg/L PAM concentrations. From top down; A is Linear, B is Freundlich and D is Langmuir. Charts B and D respectively are the non-linearised forms of both Freundlich and Langmuir. C is the linearised form of the Freundlich and E is the linearised form of the Langmuir isotherm. It is shown like this to help understand the profile of the raw data. The fits used for charts B and D are a logarithmic fit for Freundlich (B) and a Power-law fit for Langmuir (D).*

Using the 0-250 mg/L calibration line, the linearised Langmuir isotherm offers the greatest number of rock samples with R^2_{adj} values both good and excellent, 13 and 10 samples, respectively. The Langmuir isotherm also gave the most number of statistically significant fits, 11 in total. All of these statistically significant Langmuir isotherms, apart from two (OC 8 (1) and BH 5 (1) had excellent R^2_{adj} fits. The linear isotherm for the 0-250 mg/L calibration offers far fewer statistically significant isotherms, only 4 in total out of 29. In terms of R^2_{adj} only 12 have fits > 60 % and only 3 of these are > 90 %. The Freundlich isotherm for the same calibration shows only 1 R^2_{adj} fit > 90 %, with only 8 as > 60 %. Of these, only 5 are statistically significant. Using the most linear calibration (0-250 mg/L), the Linear and Freundlich isotherms offer the poorest fits to the data, whereas the Langmuir offers a much better fit to the models.

Using the other calibration, the full suite of data between 0 and 1000 mg/L, there were more good and excellent fits, and much more statistically significant fits throughout, perhaps due to the larger number of data available for the analysis. The Linear and Langmuir isotherms resulted in the greatest number of statistically significant isotherms with 14 and 10 respectively. For the linear isotherm, 11 of these produced an R^2_{adj} > 60 % with 4 of these > 90 %. For the Langmuir isotherm, 10 samples produced an R^2_{adj} > 60 % whilst 5 were > 90 %. The Freundlich isotherm produced the lowest significance of all samples, with only 8 of significance and only 6 samples with an R^2_{adj} > 60 %, with 3 of these > 90 %.

During regression analysis, the 95 % confidence interval (CI) was calculated. This offers an 'error bar' for the spread of data for each isotherm (Figure 3.9). The 95 % CI takes into account all the data and plots it to a range where at least 95 % of the data will lie.

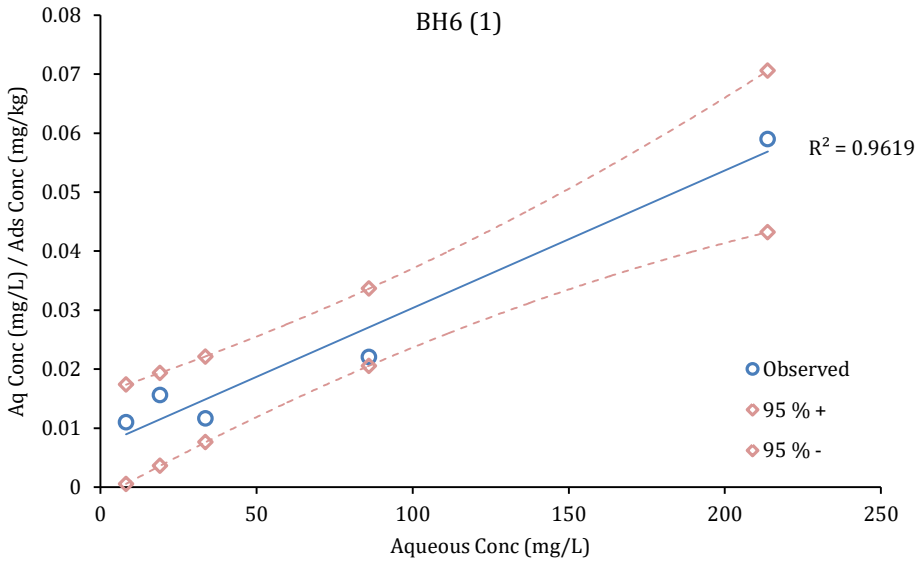

Figure 3.9: *0-250 mg/L Langmuir isotherm for sample BH6 (1) displaying the 95 % CI for the isotherm.*

Based upon this data, it is proposed that the Langmuir isotherm provides the best overall applicability to the type of adsorption, and the Freundlich the least applicable. The good performance of the Langmuir isotherm would imply that the predominant type of adsorption occurring is monolayer and to homogeneous available adsorption sites. Due to the fact it is monolayer on a finite amount of this homogenous material, a maximum coverage of this material is likely to exist, something that can be calculated from the Langmuir isotherm. The maximum coverage is, however, subject to a margin of error. When conducting a statistical analysis of the data, the 95 % confidence interval encompasses the value where 95 % of the data will fit. Maximum coverages observed in Table 3.5 use the gradient value, which is the average of all points on the isotherm. The values for the 95 % CI for isotherms, and the maximum coverages associated with these are viewed in Digital Appendices C.2 and C.3.

3.7.1. Concentration at Maximum Coverage (Adsorption Capacity)

The concentration at maximum coverage of the adsorptive material can be calculated by using the Langmuir isotherm. The maximum coverage is calculated from the gradient of the linearized form of the relevant Langmuir isotherm (Equation 3.3). The concentration at maximum coverage, sometimes referred to as the adsorption capacity, is the amount of adsorbate (PAM in this case) in mg that can be adsorbed per kg of available rock at equilibrium. Using the fits of the Langmuir isotherms, across both calibrations and only using the statistically significant data, maximum coverages range from 394 mg/kg to a maximum of 15,365 mg/kg.

LITHOLOGY TYPE	SAMPLE	CONCENTRATION AT MAXIMUM COVERAGE (mg/kg) (Room Temperature)
LBS	BH 2 (1)	441
UBS	BH 3 (2)	574
UBS	OC 7 (2)	1723
Sand	OC 8	3769
LBS	BH 2 (2)	4079
LBS	BH 5 (1 & 2)	4686 - 4754
Carboniferous Shale	BH 6 (1 & 2)	4287 - 6654
Pendle Grit	OC 5 (1 & 2)	6518 - 7276
UBS/Lst	OC 6 (1)	7818
UBS	BH 4 (2)	12126
UBS (silty)	OC 4 (2)	3365 - 15365

Table 3.5: *All maximum coverages (or adsorption capacities) for samples that exhibit 'good' statistical significance. Where there is a range, this means that both sample duplicates were classed as 'good' data. Lower Bowland Shale (LBS), Upper Bowland Shale (UBS), Limestone (Lst).*

Table 3.5 shows all calculated maximum coverages. There is large variation both between all samples and samples of the same type. Some sample duplicates were ruled out as they were not statistically significant, with errors > 0.05. Only 5 samples, inclusive of their duplicates, showed statistical significance in both duplicates and thus could be used in the calculation, BH 5, BH 6 and OC 5. Here, maximum coverages ranged from 4686 mg/kg to 7276 mg/kg. The majority of the significant data with high maximum coverages were shales, either designated as Upper Bowland Shales (UBS), Lower Bowland Shales (LBS) or Carboniferous Shales. Two samples were sand rich (OC 5 and OC 8) with OC 4 exhibiting the highest coverage of all samples and being a silty version of the Upper Bowland Shale.

3.7.2. Percentage Removal of Aqueous PAM

To further place the amount of PAM that has been adsorbed onto the surface of the rock samples into context, the removal of PAM as a percentage of the amount present was calculated. This was simply calculated across all individual samples and concentrations, regardless of statistical significance or fit.

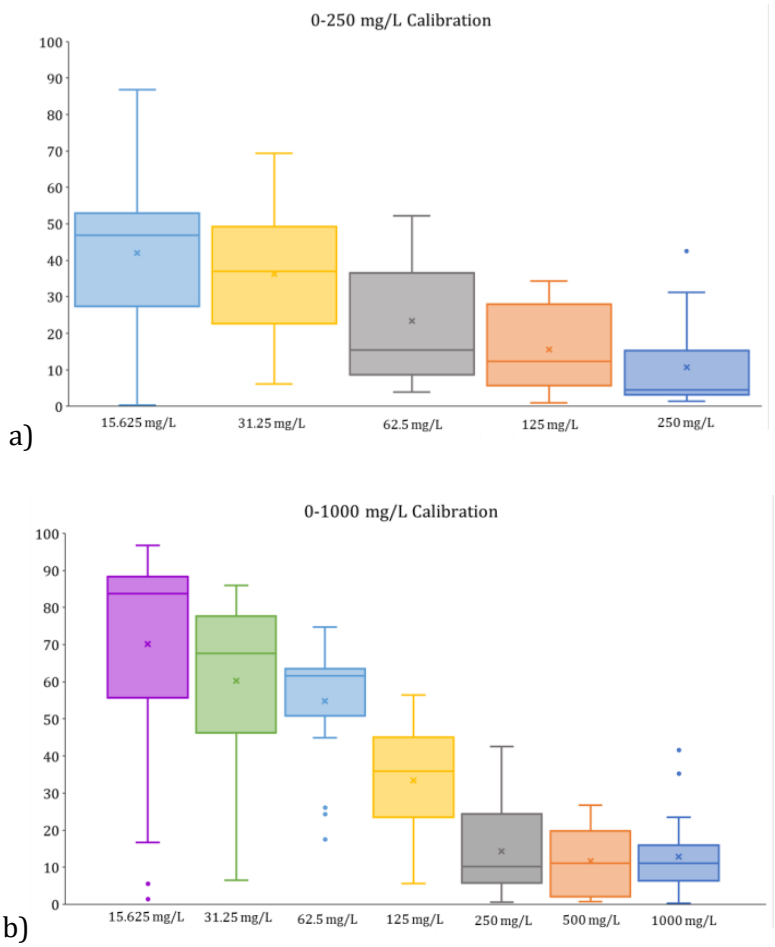

Figure 3.10: *Box and whisker plots showing the percentage removal of PAM from all samples using both calibration techniques (0-250 mg/L (a)*

and 0-1000 mg/L (b)). The mean for each concentration subset is denoted by an 'x' and all outliers from the general model by a dot.

Figure 3.10 shows that up to 97 % of aqueous PAM can be removed from the fluid by means of adsorption. Overall, there is a pattern observed in the bulk amount of data for each fluid concentration, higher at lower concentrations and substantially smaller at higher concentrations of PAM. These data do, however, contain large ranges between samples at the same concentration, and some outliers. Some samples of the same concentration may sit at 10 % removal, whilst others may sit at 80 % removal, but it is the bulk of the data that is important. The overall reduction in percentage removal with increasing concentration, seen in Figure 3.10 suggests monolayer adsorption. At lower concentrations, such as 15.625 mg/L and 31.25 mg/L, the adsorbent is able to remove most of the aqueous PAM. At higher and more viscous concentrations of PAM, all available adsorption sites become full and so no other aqueous PAM can be removed, providing monolayer adsorption is occurring, and so a lower proportion of the original PAM is removed.

3.7.3. Statistical Analysis

To see if the quantitative characteristics of the shales affected the adsorption behaviour and capacity (maximum coverage) of the samples, statistical analysis of adsorption results was conducted against all numerical values from the shale characterisation methods.

Stepwise linear regression was performed using both sets of results from the differing calibrations (0-250 mg/L and 0-1000 mg/L) and only performed where there were R^2_{adj} fits. The Linear and Freundlich isotherms used the adsorption coefficient, K, as the response whereas the Langmuir isotherm used the K value alongside the maximum coverage value as its response. These data were analysed against all numerical values from the XRF, TGA and carbon analyses.

CALIBRATION	ISOTHERM	RESPONSE	PREDICTOR	P-VALUE	VIF	r^2 adj	SLOPE
0-250 mg/L	Linear	K		n/a			
	Freundlich	K		n/a			
	Langmuir	K		n/a			
		Maximum Coverage	TiO_2	0.027	12.41	99.72%	+
			Na_2O	0	1.5		+
			SO_3	0.001	2.52		+
			Loss 300-650°C	0	7.69		+
			Total Carbon	0.004	2.41		-
0-1000 mg/L	Linear	K	SiO_2	0.011	2.25	99.87%	-
			MgO	0.001	2.08		+
			CaO	0.001	3.44		+
			Loss 300-650°C	0	3.5		+
	Freundlich	K	MgO	0.002	2.35	96.40%	-
			Total Carbon	0.025	2.35		-
	Langmuir	K		n/a			
		Maximum Coverage		n/a			

Table 3.6: *Stepwise Linear regression results for all room temperatures using data with 'good' fits from* $\boldsymbol{R^2_{adj}}$ *values. '+' and '-' symbols denote whether the gradient is positive or negative towards increasing K or maximum coverage.*

All results using the stepwise linear regression method are shown in Table 3.6. Organic matter and carbon, inclusive of that which is found in $CaCO_3$, influences the adsorptive capacity of the rock samples (Table 3.6). MgO appears twice for Linear and Freundlich isotherms with low VIF (Variance Inflation Factor) and significance (P-value) less than the limit of 0.05. With the exception of TiO_2 for a 0-250 mg/L Langmuir isotherm, VIF's are typically < 10 showing that the majority of all data displayed shows low multicollinearity. Example plots for some of this data can be found in Figure 3.11 and Figure 3.12.

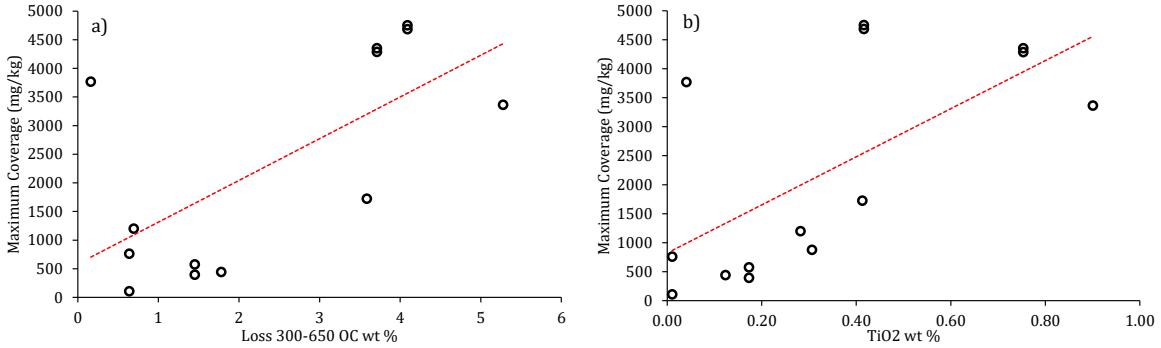

Figure 3.11: *Example linear regression patterns for 300-650 ºC losses (a) and TiO_2 (b) for the 0-250 mg/L Langmuir isotherm data, displayed in Table 3.6.*

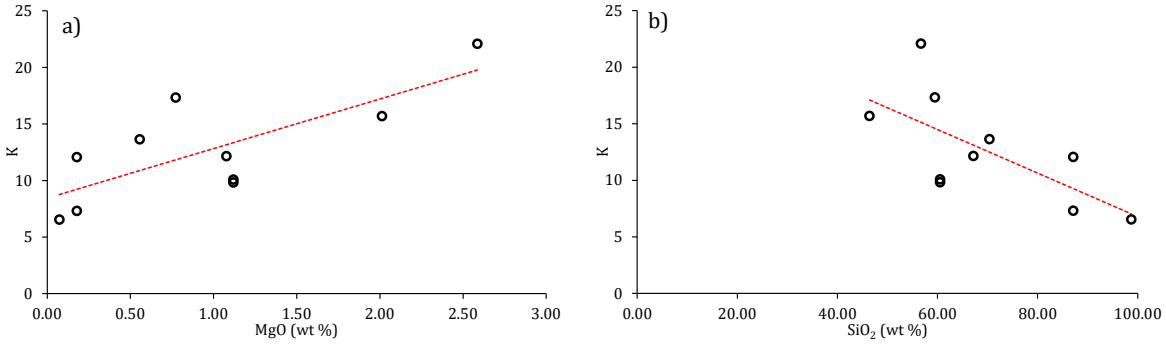

Figure 3.12: *Example linear regression patterns for MgO (a) and SiO_2 (b) for the 0-1000 mg/L linear isotherm data, displayed in Table 3.6.*

To show how the presence or absence of certain minerals had an influence on the adsorption, a different method of statistical analysis was used for the qualitative XRD data. Here, categorical stepwise analysis of variance (ANOVA) was used. This technique used the four categories shown in Table 2.13 from Chapter 2, the XRD data: 'present', 'likely present', 'negligible presence' and 'not present' and plotted them against the responses of K and maximum coverage (Table 3.7).

CALIBRATION	ISOTHERM	RESPONSE	FACTOR	PRESENCE	P-VALUE	VIF	r^2 ADJUSTED
0-250 m/L	Linear	K	Kaolinite	Not Present	0.033	1.85	74.68%
	Freundlich	K	Plagioclase	Likely	0	2.06	95.42%
				Not Present	0.005	2.78	
				Present	0.001	4.58	
			Anhydrite	Not Present	0.044	2	
	Langmuir	K	Anhydrite	Not Present	0.035	1.1	65.53%
			Illite/Smectite	Likely	0.001	3.55	
				Present	0.15	3.55	
		Maximum Coverage	Orthoclase	Likely	0.014	3.69	98.61%
			Plagioclase	Likely	0	3.61	
				Not Present	0.003	10.78	
				Present	0.001	9.8	
			Illite/Smectite	Likely	0.004	7.75	
				Present	0.003	5.03	
0-1000 mg/L	Linear	K	Anhydrite	Likely	0.039	1.03	68.71%
				Not Present	0.03	1.12	
			Smectite	Not Present	0.032	1.12	
	Freundlich	K	Anhydrite	Likely	0.007	1.17	96.69%
				Not Present	0.005	1.24	
	Langmuir	K	n/a				
		Maximum Coverage	n/a				

Table 3.7: *Results for categorical stepwise ANOVA for all qualitative XRD data. Responses used were from all ranges of isotherm where the* $\boldsymbol{R^2_{adj}}$ *values were 'good' or greater. Results only show the categories with significant fits either for the presence or absence of the minerals stated.*

Factors used in the model were based upon the quantitative results for each of the minerals sought (Table 2.13). One potential major contributor related to adsorption is the presence or potential presence of illite/smectite using the 0-250 mg/L calibrated Langmuir isotherm.

3.8. Discussion

Overall, of the lithologies analysed, shales are especially good adsorbents of the non-ionic PAM. The removal of PAM from solution is highly dependent on the concentration at maximum coverage of each individual shale or sandstone sample, and also the type of PAM. This study used non-ionic PAM, but cationic and anionic PAM may yield different adsorption

results. Even at relatively low maximum coverages ranging from 0 -1000 mg/kg (detailed in Table 3.5), relatively low concentrations of non-ionic PAM slick-water concentrations do not require a large amount of rock to potentially be almost fully adsorbed.

Results at room temperature show that, using the Langmuir isotherm, concentration at maximum coverage ranged between 441 mg/kg (BH 2) and 15,365 mg/kg (OC 4) (Table 3.5). Based on the statistical results, the most significant controls on the amount adsorbed and the concentration at maximum coverage are, predominantly, the carbon (inclusive of organic and inorganic carbon), and clay content, in particular the amount of illite/smectite. Other controls upon the adsorption, which have not been measured in this study, are the pH and salinity of the fluids. Higher salinities and lower pH's suppress electrostatic interactions (Xiong et al., 2018b). The NaCl content however can affect different types of PAM in different ways. For non-ionic PAM, adsorption is thought to be independent of NaCl content, but adsorption of anionic PAM increases with NaCl content due to the formation of ion pairs between cations and negative sites on the clay surface (Lee et al., 1991). The pH measured in this study was near neutral, at 7.46 measured within 24 hours of mixing 1000 mg of non-ionic PAM, so the pH would have had minimal effect upon the adsorption (Wiśniewska et al., 2016) as no ionisation had occurred. If the pH of the fluids had been varied through the stages of the experiments it would have been expected that in more acidic solutions, increases in adsorption would have been observed (Wiśniewska et al., 2016) whereas in more alkali conditions, less adsorption would have occurred. This phenomenon, whereby less adsorption occurs with and increasing pH is because the rise of pH causes an increase in negative charge of the polymeric chains and thus stronger electrostatic repulsion between the carboxyl groups, particularly with anionic PAM (Wiśniewska et al., 2016). The result of the increased negative charge is that polyacrylamide chains with the solution become more expanded and cannot adsorb. The above characteristics can of course vary, dependent on shale mineralogy and clay content. The reverse is true however for the use of cationic PAM with reference to adsorption on kaolinite. Tekin et al (2005) explains that cationic PAM adsorption increases with increases in pH from 5.5 to 10.5, alongside temperature from 25 to 55 °C. Adsorption of cationic PAM increases as when the pH increases, PAM cations can associate more with negatively charged kaolinite surface because of increasing SiO^- groups (Tekin et al., 2005). Alongside this, for anionic and cationic PAM, the isoelectric point (the pH at where a particular molecule carriers no net electrical charge (Kozlowski, 2017) is crucial in determining how much adsorption can occur, and throughout which mechanisms it may occur. For anionic PAM, the isoelectric point is pH 8.5 and above or below primary mechanisms are chelation and hydrogen bonding (McGuire et al., 2006), whereas for a cationic PAM solution of 200 mg/L, the isoelectric point of kaolinite is ~ pH 8. Using a cationic PAM polymer as the friction reducer in this setting may have seen

increased levels of adsorption at moderate, room temperatures (19-25 °C) in a pH neutral setting.

The amount of shale required (in kilograms) to remove almost all of the aqueous PAM from solution can be estimated based upon these results. Typical shale has a density between 1.9 g/cm^3 and 2.7 g/cm^3. Below (Equation 3.9) is an example calculation detailing how much shale is required to remove all PAM from a desired concentration slick-water solution.

$$\frac{(Conc\ of\ PAM)\times(Fluid\ volume)}{Maximum\ coverage\ of\ shale} = mass\ of\ shale\ required\ (kg)$$

Equation 3.9

Using a case study example, a slick-water fluid of 430 mg/L PAM and 8399 m^3 in volume (Broderick et al., 2011) with an average maximum coverage of 4000 mg/kg (based upon an ideal homogenous shale-PAM interaction) would require nearly 903,000 kg of rock to remove all PAM from solution, as (Equation 3.4). A fracture volume between 8,000-10,000 m^3 would contain between 16 × 10^6 kg and 27 × 10^6 kg of rock, using typical shale densities (ref) in the range between 1.9 g/cm^3 and 2.7 g/cm^3 respectively. This amount is a significantly greater mass of rock than the mass needed for total adsorption. Particularly at lower PAM concentrations, not much shale is required to adsorb all PAM from solution, even at relatively low shale densities.

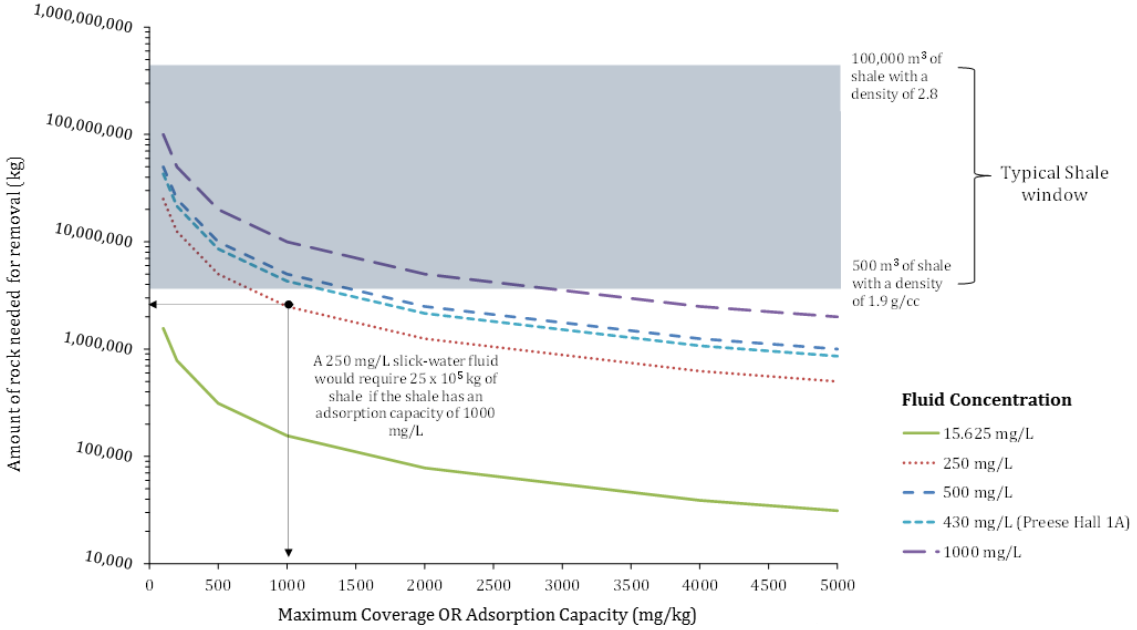

Figure 3.13: *A visual depiction of the estimated amounts of rock needed to remove 100 % of PAM from the fracking solution. The curved lines represent the different concentrations of a PAM slick-water fluid in mg/L at 100 % removal. The adsorption capacity on the x axis is the amount of PAM in mg that can be adsorbed per kilogram of available shale surface. The shaded grey area is an example of the amount of shale available in two relatively small fracks at both the lower and upper ends of typical shale densities (1.9 – 2.8 g/cc).*

In terms of percentage removal, results show that up to 97 % of any aqueous PAM can be removed from the solution by means of adsorption (Figure 3.11). Other studies, such as (Xiong et al., 2018b), state similar results such as 85 % PAM removed from solution by either adsorption or degradation. Furthermore, the lower the initial concentration of PAM within fluid, the greater the average percentage removal. The adsorption capacity is lower at higher concentrations, this result is similar to that of Guo et al. (1993) who stated that a maximum adsorption concentration was reached at 800 mg/L of PAM. This reduction in percentage removal from low concentrations to high concentrations is consistent with monolayer adsorption, and is governed by the adsorption sites on the shale becoming completely occupied by the adsorbate (Guo et al., 1993).

If all PAM has the potential to be removed from the fluid itself, how 'slick' does this water become over the timescale of a hydraulic fracture and during multiple frack stages? Waters that are returned to the surface are likely to contain nowhere near as much PAM as was initially added to the fracking fluid before it would have been pumped downhole. Therefore, a lot of PAM remains downhole with the potential to degrade chemically or physically. Degradation is likely to produce two products: acrylic and ammonium (Xiong et al., 2018b). Whilst it is important to understand the highly adsorbative nature of PAM, it should be noted that no kinetics were measured for the room temperature experiments, this study is based entirely upon overnight adsorption. These results demonstrate that large quantities of PAM

can be adsorbed per available kilogram of rock type, be it shale, sandstone or limestone, over a 24 hour period. In a real world situation, hydraulic fracturing does not just occur over 24 hours with fluid returning as flow-back over this period. In reality, hydraulic fracturing fluid can remain downhole for much more prolonged time periods undergoing further adsorption and/or other chemical reactions due to temperature, salinity, mineral type, pressure and decomposition.

Upon the flow-back and flushing stages of a frack, initial fluid input downhole can become more dilute and desorption could either be promoted or inhibited by the type of flush or geological situation. Adsorption rates of PAM as well as adsorption type could change due to the geological settings and time allowed for interaction.

3.9. Conclusions

Here PAM has been shown to be highly adsorptive on shale lithologies. The Langmuir isotherm performed the best of the isotherms used and at the conditions used in this experiment (room temperature and pressure) up to 15,365 mg/kg of PAM can be adsorbed per kilogram of available rock over a period of 16-17 hours (overnight). The most consistently adsorptive material was shale, potentially due to the generally higher clay and carbon content of this lithology type. On the whole, more shale samples exhibited much higher maximum coverages than other lithology types.

Overall, a higher maximum coverage within the sample seems to be controlled by a mixture of Al_2O_3 content, MgO content, Na_2O content and mass losses observed between 300 and 650 ˚C. It is likely that the clay content is also a primary control on the amount of PAM adsorbed by each sample; however, this cannot be pinpointed to an exact clay type due to the qualitative nature of the XRD and high error involved in the categorical stepwise regression of a non-numeric value.

The results show that, when fracking, it is overwhelmingly expected that PAM will be adsorbed in large quantities from slick-water fracking fluids. Due to adsorption and potential failure to desorb and return to the surface (discussed in Section 5.10 of this study), the PAM has the potential to degrade, desorb and ultimately over time migrate through strata or wellbores, active or historic.

The use of a different type of polymer friction reducer, primarily cationic or anionic PAM may have a distinct difference on the quantities of PAM adsorbed. Another major factor, one that can be known and estimated is the temperature of the shale gas basins within the UK. The effect of increasing temperatures, alongside pressures, on adsorption is investigated in the next chapter of this study.

4. The Adsorption of PAM in High Pressure High Temperature (HPHT) Environments

4.1. Introduction

The real conditions under which PAM will interact with shale rocks are quite distinct from those in the room temperature experiments with both higher pressures and higher temperatures present. To measure adsorption in conditions that had higher temperatures and higher pressures, a similar methodology was used to that applied in the room temperature experiments. Samples were prepared and diluted in the same way, and aqueous PAM was measured using the same *N*-Bromination method. The only major difference was that adsorption would occur overnight in a closed environment at higher pressures and higher temperatures than previously used with the conditions achieved using a batch reactor. The aim of this study was to assess whether these new conditions change the type of adsorption; or increase or decrease the adsorption capacity.

Throughout this chapter, room temperature experiments will be referred to as 'RT' and the high pressure high temperature experiment will be referred to as 'HPHT'. One experiment was run at 65 °C and 30 bar (3 MPa) as the HPHT experiment due to equipment problems towards the end of the project. The use of 'HPHT' is to distinguish between the RT experiments seen in Chapter 3, in terms of an oilfield definition (HPHT referring to temperatures > 177 °C and pressures > 103 MPa), this is not.

Results seen in this chapter were presented as part of a presentations at UDSIG UK (Use of the Deep Subsurface in the UK) conference at the Geological Society in 2018 as part of a presentation, and in poster form at an Environment Agency Knowledge Exchange event in Bristol, 2019. Posters can be viewed in the Digital Appendices.

4.2. Aims and Objectives

The aim of this chapter was to observe the adsorptive behaviour of the PAM in geological realistic conditions more realistic of the fracking environments that were considered in Chapter 3. These 'geologically realistic' conditions in the subsurface have higher pressures that are up to 69 MPa (un-fracked) and temperatures up to ~110 °C than the room temperature/atmospheric conditions used in the previous adsorption experiments. All of the four samples used in these experiments had already undergone RT adsorption tests (Chapter 3). It is important to understand that while these results are useful, they are still not the sorts of pressure conditions that the slick-water fracking fluids will experience when it is pumped

into rock at 3 – 5 km depths. On the UK continental shelf, subsurface pressures would be between 7000 and 10000 psi lithostatic pressure (48 – 103 MPa) and temperatures would range from 60 ˚C to 120 ˚C (Busby, 2010; Hird et al., 2011, 2012a).

4.3. Pressure Vessel Equipment

For the HPHT experiments, a custom made 3800 ml batch reactor was used. The setup was custom built by SciMED UK and comprised of Parr, Swagelok and SciMED components. The maximum capacity was 16 samples using 50 ml test tubes.

4.3.1. Batch reactor overview

The batch reactor mentioned above has a pressure tolerance of 13.1 MPa, and maximum operating pressure of 13.7 MPa. Laboratory restrictions meant the vessel could only be operated at a maximum of 80 % of its tolerance, approximately 10.95 MPa (1589 psiA). The system is setup to run using CO_2 as the pressurising gas. The vessel is surrounded by a heater with a maximum temperature of 450 ˚C. Due to the thickness of the steel casing on the vessel, approximately 1 inch thick, auto-calibration of the temperature for the vessel took at least 6 hours. The vessel has 1 inlet and 1 outlet valve. CO_2 is pumped in via the inlet, with the outlet shut, pressurising the vessel to the desired pressure. Once at pressure, pressure can be held within the vessel using a back pressure regulator (BPR) or by closing the system (inlets and outlets) completely. To de-pressurise, pressure is bled through the outlet valve using the BPR until it reaches atmospheric pressure. Once calibrated, when CO_2 is added and it reaches past the sublimation point, the heat reduces the risk of ice when CO_2 is added to the vessel at lower pressures, and also during rapid decompression at the end of an experiment.

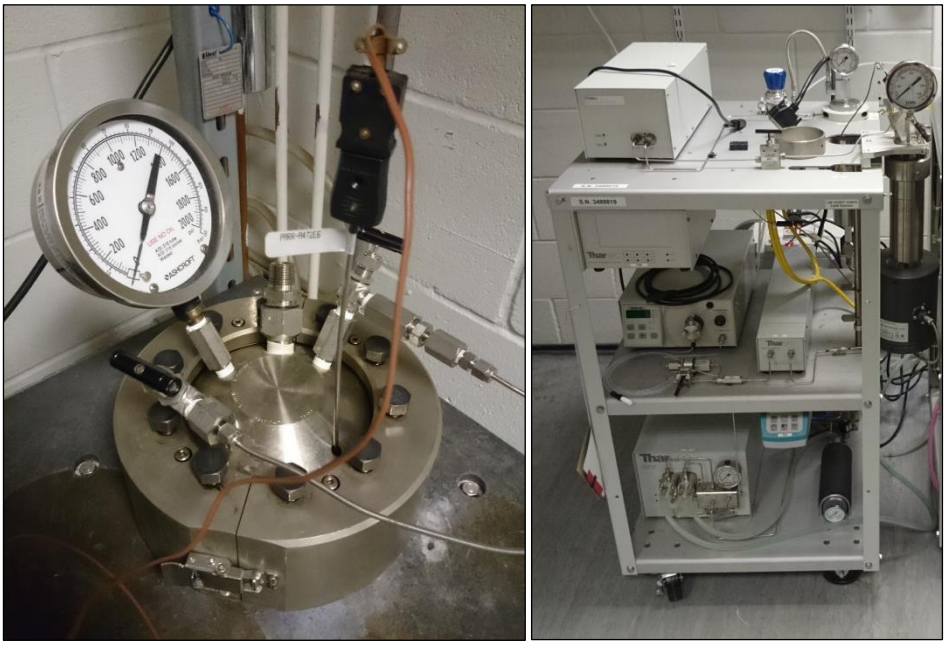

Figure 4.1: *Image of the 3800 ml batch reactor vessel (left) and the control unit and back pressure regulator (right). Vessel is pressurised by CO_2 and temperature controlled automatically by a thermocouple and heater unit surrounding the vessel.*

4.3.2. Reactor Vessel Limitations

The batch reactor is a large capacity vessel capable of ideally holding between 12 and 14 samples in 50 ml glass test tubes, but with the potential of up to 16. Based on this capacity, inclusive of blanks and duplicates necessary for calibration, the sample selection could only contain 4 samples containing rock - 8 test tubes – then with the 4 blanks this made up 12 glass test tubes inside the vessel. The primary limitation of the vessel is the pressure capacity compared to actual geological formation pressures. A comparison of the geological temperatures expected within the Bowland Basin, Northwest England and Northeast England can be viewed in Table 4.1. Typical subsurface pressures due to overburden (the compaction of the rock above the area of interest) (> ~ 8000 psi or ~ 55 mPa) could not be achieved using the hardware, but typical temperatures (50-110 ˚C) could be easily met. The reactor vessel system is setup for use with CO_2 as the pressurising gas. Using this gas may lead to a reduction in pH as any additional CO_2 within the fluid as increased CO_2 levels increase the amount of hydrogen ions within the water system (Turley et al., 2006). With this particular experimental rig, using nitrogen was not an option.

4.4. Samples Selected for HPHT Adsorption

Only 4 samples were selected for adsorption analysis in these experiments; OC 5, OC 7, BH 5 and BH 6. The reason for the selection of these samples was a combination of the results

from the RT experiments (Chapter 3), sample type and amount of sample available. Samples for these are listed below with characterisation data taken from Chapter 2.

- **OC 5:** A Pendle Grit silica rich sample containing low TOC (0.05 %) and 5.19 wt % Al_2O_3. Clays present are kaolinite, illite and illite/smectite. The sample exhibits good fits and statistical significance for all isotherms apart from the linear and has a high adsorption capacity at room temperature compared to the majority of other samples (6518 – 7276 mg/kg).
- **OC 7:** Upper Bowland Shale sample containing 1.57 % TOC and high levels of Al_2O_3 (9.36 wt%). Kaolinite and Illite are present with a lower Si/Al ratio suggesting high clay content. Sample OC 7 only has one good fit and significance for the 0-250 mg/L Langmuir isotherm. The sample exhibits low RT adsorption capacity (1723mg/kg) compared to the other samples in this study despite having higher TOC content and more clay type present.
- **BH 5:** Borehole sample of exploration strata (LBS). Sample contains moderate TOC (3.7 %), but the highest TOC of all samples used in the HPHT experiments, and high levels of Al_2O_3 (8.75 wt%). Illite is the only clay type present with a low Si/Al ratio. Sample exhibits good and significant fits for all isotherms using a 0-250 mg/L calibration, but only samples for the linear using a 0-1000 mg/L calibration. For the samples selected for HPHT analysis it has a moderate RT adsorption capacity of between 4686 and 4754 mg/kg.
- **BH 6:** Carboniferous shale borehole sample containing low TOC values (0.36 %) but the highest levels of Al_2O_3 (17.42 wt%). Multiple clays are present, foremost chlorite, kaolinite and illite, helping to maintain a very low Si/AL ratio of 2.44. Statistical analysis of the sample of the isotherms shows good fits and significance for at least one sample duplicate using each of the two calibrations and three isotherm types. RT adsorption capacities for this sample are moderate at between 4287 and 6654 mg/kg.

As in previous adsorption experiments in this study (Section 3.3), the respective sample was a 1 g powdered amount for each test tube.

4.5. HPHT Approach and Methodology

The method of sample preparation, sample dilution and spectrophotometric analysis remained exactly the same as the RT experiments, methods detailed in Chapter 3, Section 3.3. The only difference from the RT adsorption experiments throughout this whole process is the

addition of the batch reactor vessel for the 16 hours overnight adsorption in conditions that were not indicative of room temperatures and pressures. This addition ensured that the samples were pressurised and heated overnight in a closed environment, rather than being left at room temperature.

4.5.1. Temperature

Temperatures for the experiments were set to 65 ◦C. This temperature was seen as a reasonable proxy based upon temperature data seen directly from well reports used in the study and a literature citing data for England, particularly the Cheshire, Bowland and NE Basins (Table 4.1). To arrive at 65 °C, temperature data was collected from End of Well Reports, utilising wireline measurements, completion logs and 'TOGIP' analysis (Total Gas in Place) (Hird et al., 2012a, 2012b, 2011).

WELL NAME	BOWLAND SHALE	START DEPTH	END DEPTH	TEMPERATURE °C	
				WIRELINE	TOGIP ANALYSIS
Grange Hill 1Z	UBS	7175 ft	9580 ft	93	61.1 - 77.7
	LBS	9580 ft	10775 ft at TD	93	77.7 - 83.3
Becconsall 1Z	UBS	7005 ft	7283 ft	86.7	58.8 - 63.8
	LBS	7283 ft	7827 ft	86.7	63.8 - 68.8
Ince Marshes 1	Millstone Grit	3062 ft	4154 ft	42.2	n/a
Preese Hall 1A	UBS	6540 ft	8220 ft	70	n/a
	LBS	8220 ft	9100 ft at TD	70	n/a
Lockton 3	Carboniferous	6293 ft	7244 ft at TD	60	n/a

LITERATURE	BASIN / AREA	GEOTHERMAL GRADIENTS		TEMPERATURE °C (based upon top and base depths seen above)	
				Top	Base
Busby 2010	Cheshire Basin	27	°C / km	51	88
	NE England Basin	31.9	°C / km	60	70
	UK Average	26	°C / km	49	85
Downing and Gray (1986)	Bowland Basin	20	°C / km	38	65
	NE England	17.1-20	°C / km	33	44

Table 4.1: *Subsurface temperature ranges for depth intervals and basins in the NW Lancashire and NE England areas, based upon well data used in this study (Dowell and Schlumberger, 1966; Hird et al., 2012a, 2012b, 2011) and data relating to the UK geothermal gradient in general, and the Cheshire basin and NE England Basin (Busby, 2010; Downing and Gray, 1986)*

4.5.2. Pressure

Pressures needed to fracture rocks are dependent on the stress regimes and parameters surrounding the well bore, however pressure must exceed the fracture pressure of the surrounding rock. The pressure required to fracture rocks deep within the subsurface (> 2km vertical depth) cannot be matched using the batch reactor used in these experiments.

Preese Hall was fractured under a pressure of 55 MPa (~8000 psi or 551 bar (Gilbert, 2012)), with a fracture extension pressure of 56.33 MPa (8171 psi). Borehole pressures of between 49 MPa (7250 psi) and 60 MPa (8800 psi) from Preese Hall at depths between 2337 m and 2697 m are reported by De Pater and Baisch, (2011). Preston New Road wellsite actual fracture pressures are unavailable, but hydraulic fracture plan documents indicate an estimated maximum surface pumping pressure of 65.5 MPa (9500 psi) (Cuadrilla Resources, 2018a). Due to the unavailability to reach these pressure, 3 MPa was set as a starting pressure to further investigate how pressure may affect adsorption in comparison to the RT experiments. The initial aim was to further investigate pressure increases as the study progressed. Unfortunately, due to long delays in the setting up of the pressure rig, only one temperature and pressure could be tested. Future work would be ideally suited to testing increased temperatures and pressures.

4.5.3. Step by Step Method

In this step by step methodology, as per detailed in Chapter 3, Section 3.3.1, the 1000 mg/L PAM solution has already been diluted down into the relevant concentrations for each sample batch. For this analysis each sample batch contains samples that are run in the same PAM fluid concentrations. For example, 1 overnight batch would contain 4 samples and 2 blanks, with all fluids being the same concentrations (i.e. 250 mg/L). The reason behind this is that all samples will be closed into a sealed atmosphere. To accurately measure PAM concentrations, or any which may have transferred in a PAM rich vapour inside the vessel, all samples need to have a known consistent concentration.

In each run, four blanks were run alongside the samples (Figure 4.2):

- In vessel blanks: 40 ml of tap water with no PAM or sample & 40 ml of identical concentration PAM fluid (as is outside the vessel) with no sample.
- Outside vessel blanks: 40 ml of tap water with no PAM or sample & 40 ml of same concentration PAM fluid with no sample (run for the same period as the pressure vessel).

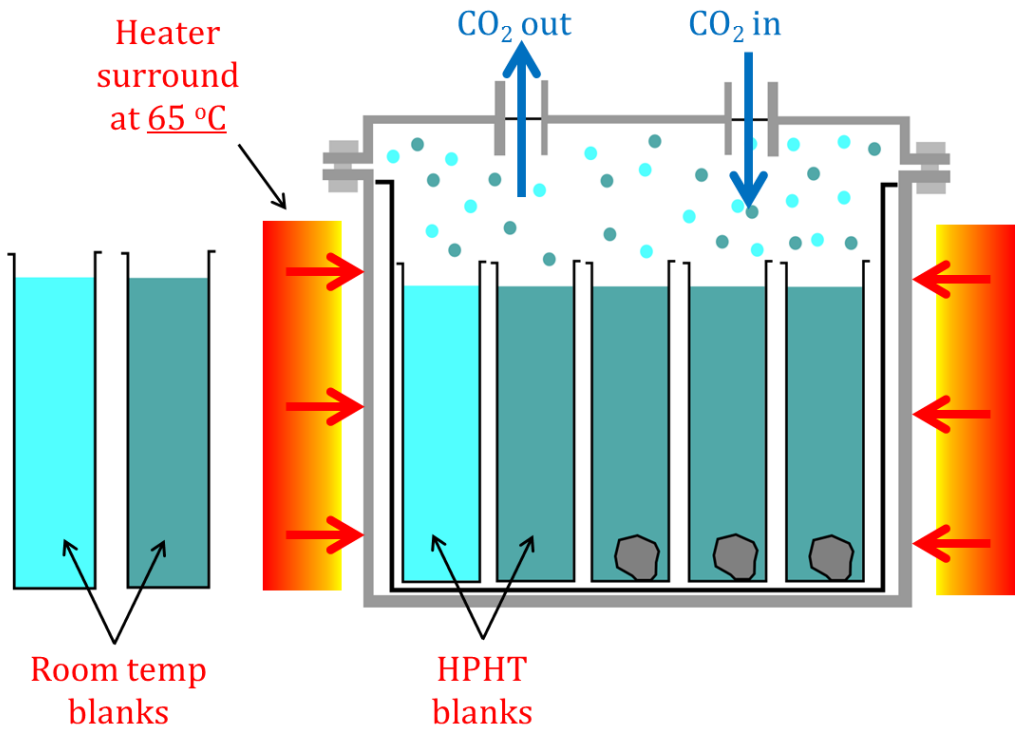

Figure 4.2: *Batch reactor vessel diagram. Heater is turned on to heat all vessel walls and components to the required temperature before CO_2 is added. Samples are place into the vessel, the vessel is sealed, and then CO_2 is pumped in to pressurise vessel. After 24 hours the pressure is bled off via an automated back pressure regulator (BPR) and samples removed.*

Day 1: Batch reactor temperature control is set to 65 ˚C and left to auto tune to the desired temperature. A 1000 mg/l PAM standard is diluted to the concentration needed for the batch being undertaken 10 times, 2 for each of the 4 samples and twice for each of the PAM blanks.

Day 2: 1g of powdered sample is placed into each of the 50 ml glass test tubes filled with 40 ml of PAM slick-water fluid, apart from the blanks. All samples and the two blanks are placed into the heated vessel and sealed in by screwing the lid down ensuring the seal is competent. CO_2 is pumped in to the desired pressure and the inlet is sealed, shutting in the vessel. This is left overnight. The two room temperature blanks are left outside the vessel overnight, much like for the RT experiment conditions.

Day 3: After 24 hours the pressure is bled off from the vessel using the BPR and vented into the fume cupboard. Using an ABEK 1 face mask filter system, primarily filtering for Ammonia gas, the vessel is unsealed, and the samples removed and placed into the fume cupboard. Immediately, the fluid is poured into separate glass vials away from shale present to prevent further room temperature adsorption from occurring. Samples are allowed to degas for at least 12 hours before filtering off sub-samples for analysis with 2 ml frozen for ICP analysis and 2 ml for PAM *N*-Bromination analysis.

Day 4: The 2 ml fluid sub-samples for PAM analyses are diluted to the relevant concentration and are analysed using the *N*-Bromination method. Fluids post analysis are disposed of into plastic bottles and kept in the fume cupboard until safe disposal.

4.6. HPHT Adsorption Isotherms

All results from the HPHT experiments were fitted to the same three isotherms as described in Section 3.4, i.e. linear, Freundlich and Langmuir isotherms.

4.7. HPHT Statistical Analysis Methodology

As per Section 3.5, linear regression was conducted on all isotherm results against all quantitative and qualitative data from the shale characterisation in Chapter 2. No categorical stepwise ANOVA could be conducted on the qualitative XRD results due to such a low sample size. Much like in the RT adsorption experiments (Section 3.5) statistical analysis was performed to see if quantitative and qualitative characteristics of the samples had a bearing on the adsorptive behaviour, this time at higher temperatures and pressures.

4.8. HPHT Adsorption Calibration

Calibration of the adsorption data from the standards used the same format as per Section 3.6. Two calibrations were made between 0 and 250 mg/L and 0 and 1000 mg/L.

For the HPHT experiments, multiple standards were used as it was discovered that PAM analysis was highly variable in these fluids. Prepared controls and standards included:

- 1 full suite of RT standards at the start of each experiment run – to calibrate a normal calibration line based on behaviour not influenced by temperature or pressure.
- 2 room temperature controls of the same concentration of those in the vessel, each run – to measure any differences between these standards and the ones in the vessel.
- 2 vessel controls with no sample within of the same concentration of those with samples, each run – to measure in comparison to the RT standards and primarily to account for aqueous PAM that may have transferred between vessels as a vapour when under pressure.
- 1 full suite of standards at the end of each experiment run – to calibrate again to all standards measured throughout the experiment as PAM can be highly unpredictable fluid in terms of full dissolution within a liquid.

Data was checked and erroneous measurements, data that strayed uncharacteristically away from the main trends seen in the duplicates, were removed. An average of the main data, ignoring erroneous data, was taken to produce a full suite of standards from 0-1000 mg/L (Figure 4.3).

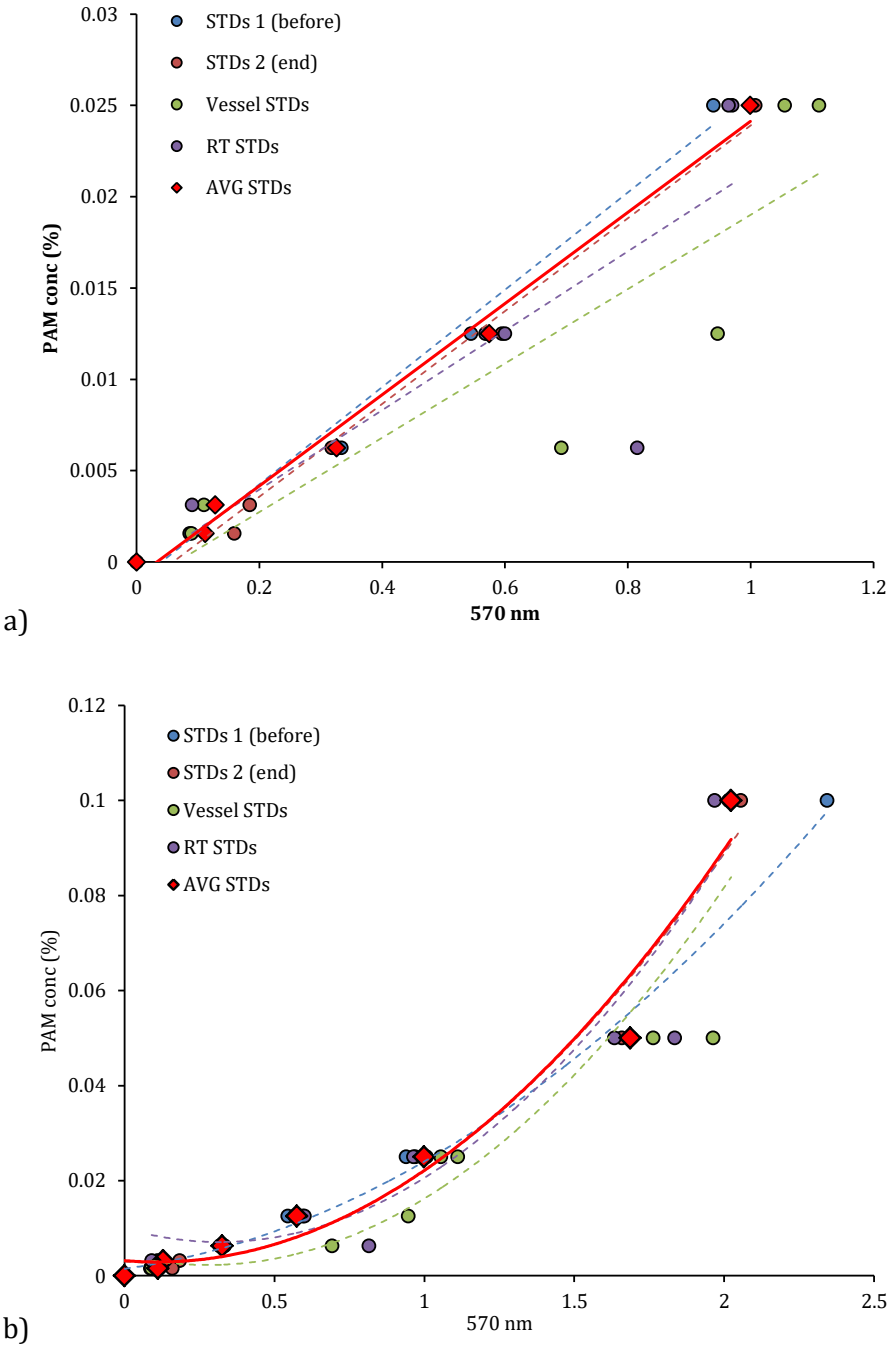

Figure 4.3: *Example of the standard calibrations for the 65 ˚C / 30 bar HPHT adsorption experiment. Variation can be seen between the different standards run. Erroneous data, predominantly seen between PAM concentrations of 0.025 % and 0.05 % (250 mg/L and 500 mg/L respectively), has been removed where deemed to be over saturated. The average of the remaining data was then taken to provide one set of values to be used as standards, seen here as red diamonds on both graphs. Lines of best fits used for demonstrations are linear (a) and polynomial (c ≠ 0) (b).*

EXAMPLE			
CONCENTRATION		0-250 mg/L calibration lines	
	Linear mg/L	Polynomial (c=0)	Polynomial (c≠0)
250 mg/L	0.02418	0.02499	0.02496
125 mg/L	0.01356	0.01984	0.01243
62.5 mg/L	0.00734	0.01812	0.00643
31.25 mg/L	0.00241	0.01743	0.00238
15.625 mg/L	0.00200	0.01740	0.00207
0 mg/L	0	0	0
		0-1000 mg/L calibration lines	
250 mg/L	0.03627	0.02327	0.02217
125 mg/L	0.01809	0.00821	0.00818
62.5 mg/L	0.00744	0.00293	0.00405
31.25 mg/L	-0.00101	0.00062	0.00292
15.625 mg/L	-0.00171	0.00050	0.00291
0 mg/L	0	0	0
	Linear 0-250 mg/L vs Linear 0-1000 mg/L	Polynomial (c=0) 0-250 mg/L vs Polynomial (c=0) 0-1000 mg/L	Polynomial (c≠0) 0-250 mg/L vs Polynomial (c≠0) 0-1000 mg/L
T-VALUE	-0.22	2.05	0.27
P-VALUE	0.829	0.07	0.796

Table 4.2: *Table showing the results of the t-test for similarity for both calibrations based upon standards data from the 65 ˚C / 30 bar HPHT experiment.*

Similar to Section 3.7.3, using an alpha (α) of 0.05 the results of the standards were tested for similarity using a t-test (Table 4.2). Data in Table 4.2 adheres to the null hypothesis rule, with the worst similarity in data between both calibrations using a polynomial fit with a set intercept of 0. The linear and polynomial ($c \neq 0$) fits have no significant difference between them. There is little significant difference between the calibration fits, and so the best one can be chosen for the approach, dependent on sample.

The standards and blanks used throughout the duration of the experiment were used to calibrate small variances seen in each of the experiments. The same 1000 mg/L fluid was used for all the experiments, however the storage of PAM is difficult, the polymer may vary over time in different temperatures and light settings, and thus multiple 1000 mg/L batches were made for each experiment run. Blanks within the vessel were used to calibrate to aqueous PAM that may have been in a vapour form within the vessel.

4.9. HPHT Adsorption Results

Results in this section refer to the HPHT experiment conducted at 30 bar and 65 ˚C. Analysis refers to similar quantifiable data as in Chapter 3, such as maximum coverages, percentage of aqueous PAM removed from solution and the statistical analyses run.

In total, 48 isotherms were produced based on the four samples in duplicate, three isotherm types and two calibration methods. Under these conditions, both R^2_{adj} fits and statistical significance favoured the 0-1000 mg/L calibration in the majority (Table 4.3).

SAMPLE		0 - 250 mg/L Linear			Freundlich			Langmuir		
		Aq	r^2 adj	P-value	Log (Ads)	r^2 adj	P-value	Aq/Ads	r^2 adj	P-value
BH 5 (1)	Regression Equation	1201 - *7.0* Aq	0%	0.839	2.97 - *0.024* Log (aq)	0%	0.980	*-0.0* + 0.001 Aq	84.13%	0.182
	Coef (const) SE Coef	896 27.1			1.01 0.758			0.012 0.0		
BH 5 (2)		1486 - 2.23 Aq	56.36%	0.309	3.398 - 0.175 Log (aq)	97.18%	0.076	*-0.009* + 0.001 Aq	99.90%	0.014
		167 1.18			0.038 0.021			0.003 0.0		
BH 6 (1)		*982 - 3.8* Aq	0%	0.924	2.43 + 0.27 Log (aq)	0%	0.880	*0.032 + 0.0* Aq	0.00%	0.694
		1074 31.8			1.92 1.4			0.048 0.001		
BH 6 (2)		*1284 - 2.706 Aq*	*100%*	-	*3.185 - 0.074 Log (aq)*	*100%*	-	*-0.002 + 0.001 Aq*	*100%*	-
		* *			* *			* *		
OC 5 (1)		*-1334* + 78.5 Aq	64.68%	0.126	*2.14 + 0.65* Log (aq)	0%	0.662	*0.153 - 0.001* Aq	0.00%	0.856
		2655 30.8			2.29 1.29			0.231 0.003		
OC 5 (2)		*-452* + 65.6 Aq	94.79%	0.103	1.869 + 0.933 Log (aq)	76.05%	0.225	*0.0* - 0.0 Aq	0.00%	0.914
		993 10.7			0.598 0.344			0.009 0.0		
OC 7 (1)		1383 - *12.7* Aq	0%	0.771	3.16 - 0.197 Log (aq)	0%	0.870	*0.005* + 0.001 Aq	71.94%	0.244
		1123 33.8			1.26 0.95			0.019 0.001		
OC 7 (2)		1435 + *17.1* Aq	0%	0.714	2.890 + *0.284* Log (aq)	0%	0.649	0.003 + 0.0 Aq	83.18%	0.187
		877 35.5			0.543 0.461			0.003 0.0		

SAMPLE		0 - 1000 mg/L Linear			Freundlich			Langmuir		
		Aq	r^2 adj	P-value	Log (Ads)	r^2 adj	P-value	Aq/Ads	r^2 adj	P-value
BH 5 (1)	Regression Equation	1687 + 16.81 Aq	80.07%	0.010	3.186 + 0.207 Log (aq)	8.22%	0.295	*0.035* + 0.0 Aq	0%	0.604
	Coef (const) SE Coef	1300 3.66			0.314 0.172			0.044 0.0		
BH 5 (2)		2306 + 11.94 Aq	87.80%	0.004	3.106 + 0.278 Log (aq)	50.91%	0.068	0.014 + 0.0 Aq	45.27%	0.086
		722 1.96			0.205 0.112			0.012 0.0		
BH 6 (1)		2767 + 8.86 Aq	88.49%	0.003	3.142 + 0.271 Log (aq)	73.08%	0.019	0.008 + 0.0 Aq	91.21%	0.002
		531 1.41			0.13 0.071			0.005 0.0		
BH 6 (2)		2475 + 12.98 Aq	94.38%	0.004	3.025 + 0.356 Log (aq)	73.54%	0.040	0.007 + 0.0 Aq	88.15%	0.012
		610 1.57			0.177 0.102			0.005 0.0		
OC 5 (1)		6542 + 19.39 Aq	60.20%	0.077	3.225 + 0.396 Log (aq)	78.08%	0.030	0.003 + 0.0 Aq	97.52%	0.001
		2602 7.3			0.188 0.101			0.001 0.0		
OC 5 (2)		2563 + 57.72 Aq	94.86%	0.001	2.872 + 0.564 Log (aq)	77.64%	0.013	0.007 + 0.0 Aq	9.12%	0.288
		1553 5.98			0.228 0.132			0.004 0.0		
OC 7 (1)		2362 + 16.37 Aq	96.86%	0.002	3.156 + 0.306 Log (aq)	64.90%	0.063	0.007 + 0.0 Aq	75%	0.037
		554 1.47			0.18 0.105			0.005 0.0		
OC 7 (2)		1793 + 54.32 Aq	97.43%	0.001	3.211 + 0.383 Log (aq)	63.37%	0.067	0.007 + 0.0 Aq	0%	0.405
		1258 4.39			0.22 0.136			0.006 0.0		

Table 4.3: *Summary table of the statistical analysis performed on all room temperature adsorption samples. The table is divided into calibration type (0-250 mg/L and 0-1000 mg/L) and then into isotherm type.* $\boldsymbol{R^2_{adj}}$ *represents the fits of the isotherm and the P-value represents the significance in relation to a 0.05 margin of error.*

All isotherm fits that were statistically significant at least at a probability of 0.05 and then those isotherms fits with R^2_{adj}> 60 % were classified as 'good fits' and all fits where R^2_{adj} > 90 % were classified as 'excellent'. The 0-1000 mg/L calibration had the most data linked by both good and excellent R^2_{adj} fits to statistical significance (< 0.05). Out of 8 samples in total for each, the linear isotherm produced 7 of statistical significance and 4 each for both the Freundlich and Langmuir isotherms. Using a 0-250 mg/L calibration, there were far fewer statistically significant fits. Only 1 Langmuir isotherm offered significance of < 0.05 while R^2_{adj}values were slightly better across all isotherms. The linear and Freundlich isotherms showed good fits for two samples each, whilst the Langmuir only showed good fits for 4 of the 8. Data from Table 4.3 has been plotted for all samples on Figure 4.4 and Figure 4.5.

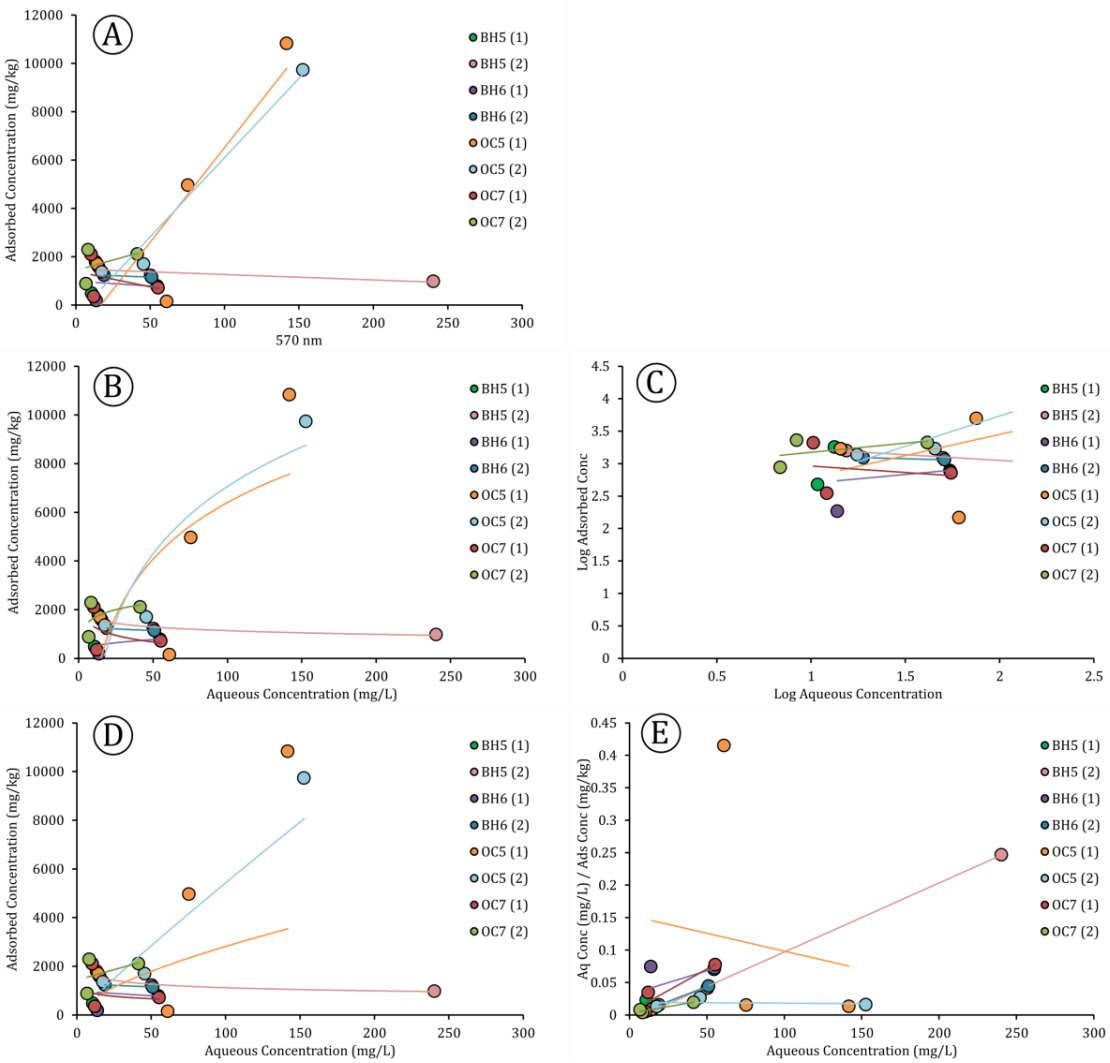

Figure 4.4: *All samples of HPHT #1 shown on the three different types of isotherm for the 0-250 mg/L calibration. Linear isotherm, B: Freundlich Isotherm, C: Linearised Fruendlich Isotherm, D: Langmuir Isotherm, E: Linearised Langmuir isotherm*

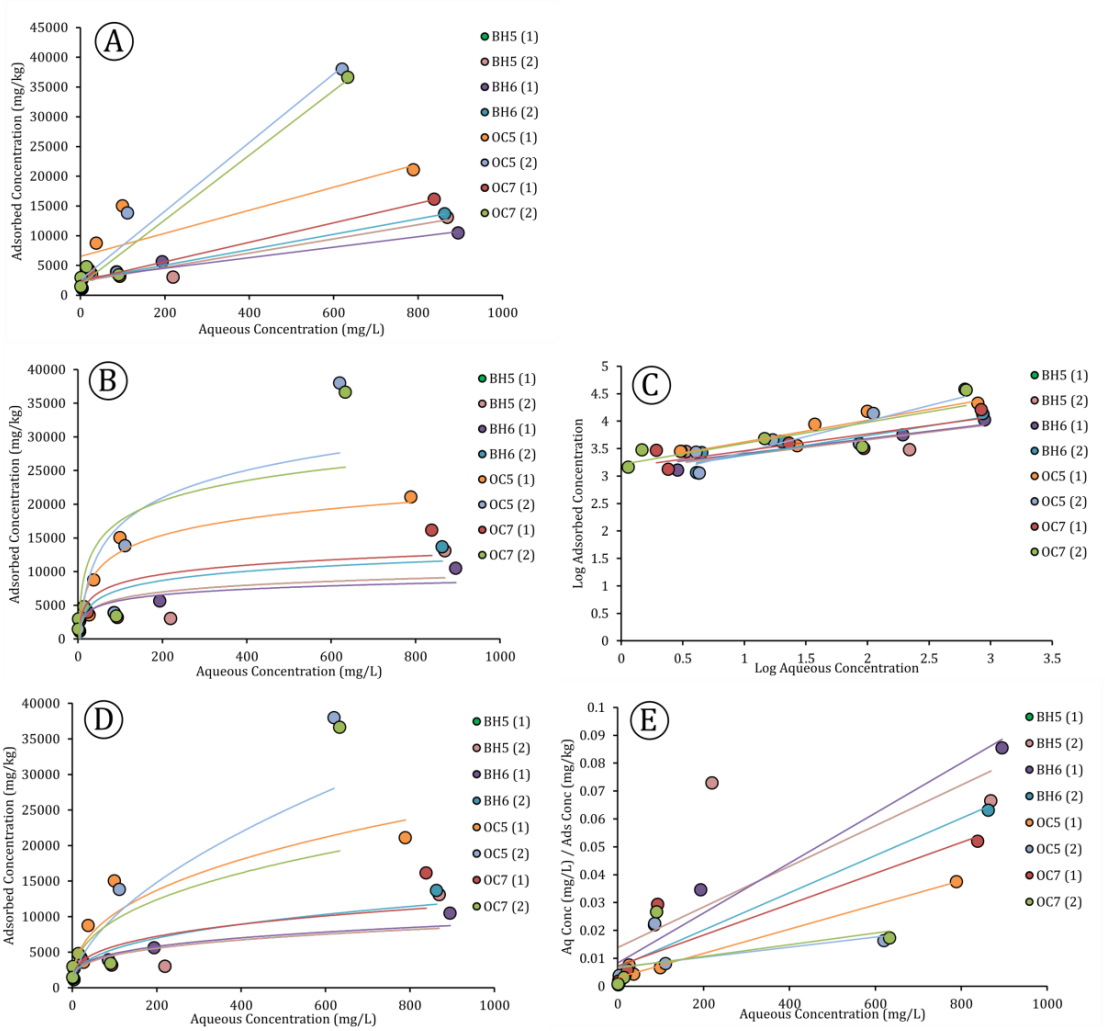

Figure 4.5: *All samples of HPHT #1 shown on the three different types of isotherm for the 0-1000 mg/L calibration. Linear isotherm, B: Freundlich Isotherm, C: Linearised Freundlich Isotherm, D: Langmuir Isotherm, E: Linearised Langmuir isotherm*

The 0-250 mg/L calibration line had the fewest R^2_{adj}fits and the fewest significant fits for all isotherms. Linear and Freundlich isotherms have only 2 fits that are classified as good and 1 each that is excellent. Neither linear or Freundlich produce fits that were significant. Using the 0-250 mg/L calibration, the Langmuir has slightly more 'good' fits, four in total, but still only one of these is classified as excellent. Only 1 Langmuir fit is statistically significant, that of BH5 (2).

Overall, the 0-1000 mg/L calibration has a higher proportion of good, excellent and statistically significant fits than the 0-250 mg/L calibration (Table 4.3). Starting with the Freundlich isotherm, this exhibits the worst of the 3 isotherms in terms of excellent and significant fits, only 6 good fits with no excellent fits, there were four significant Freundlich

isotherm fits. The Langmuir isotherms offers 4 with good fits, 2 of these being excellent whilst the linear isotherm offers 8 good fits with 4 excellent fits. In terms of statistical significance for the linear and Langmuir isotherms, the Linear performs the best with 7 significant fits to the Langmuirs' 4.

As per Section 3.7, the 95 % CI is calculated for the Langmuir isotherms. Data for these calculations are present in Digital Appendices D.2 and D.3. Maximum coverages calculated from these values are located in Digital Appendix D.1.

Based upon this data, it is proposed that the 0-1000 mg/L calibration is the best fit to the initial standard data. Any one of the three isotherms used for this calibration could be most applicable to the type of adsorption. The Freundlich is likely the least applicable due to the lower amount of good and excellent R^2_{adj} fits or lack of statistical significance compared to Linear and Langmuir. As with the RT experiments (Section 3.8) the Langmuir isotherm is the best overall description of the adsorption.

4.9.1. Concentration at Maximum Coverage (Adsorption Capacity)

As learnt earlier in this study, the Langmuir isotherm can be used to calculate the concentration at maximum coverage (adsorption capacity) – maximum coverages for HPHT #1 are shown in Table 4.4 and Figure 4.6.

LITHOLOGY TYPE	SAMPLE	CONCENTRATION AT MAXIMUM COVERAGE (Room Temperature)	CONCENTRATION AT MAXIMUM COVERAGE (HPHT #1)
UBS	OC 7 (2)	*1723*	18062
LBS	BH 5 (1 & 2)	*4686 - 4754*	940-14442
Carboniferous Shale	BH 6 (1 & 2)	*4287 - 6654*	11163 - 14983
Pendle Grit	OC 5 (1 & 2)	*6518 - 7276*	22972

Table 4.4: *All concentrations at maximum coverage (adsorption capacities) for all HPHT #1 samples (right) that exhibit statistical significance. These are compared against the maximum coverages observed in the same samples during the room temperature experiments (greyed out values). All values are shown in mg/kg.*

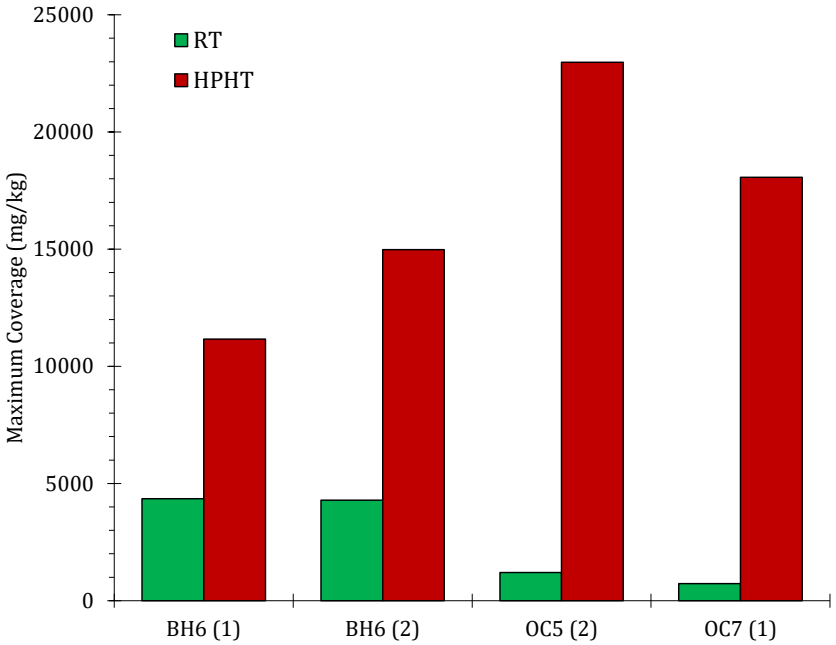

Figure 4.6: *HPHT concentration at maximum coverage for samples BH6, OC5 and OC7, alongside the comparative result for the room temperature experiment.*

Maximum coverages range from 940 mg/kg to 22972 mg/kg. The lowest value of maximum coverage (940 mg/kg) was sample BH 5 (2) for 0-250 mg/L calibration data. The BH5(2) samples was the only significant fit for 0-250 mg/L calibration: and this data may potentially be erroneous. Using only statistically significant data derived from the 0-1000 mg/L calibration, maximum coverage range was between 11163 mg/kg to 22972 mg/kg. In comparison to the same samples during room temperature examples, these values are between two and ten times larger than the values seen in the room temperature experiments (Figure 4.6). Based on the range of samples tested, this time the most silica rich sample (OC 5) exhibits the highest maximum coverage. Maximum coverages calculated using the 95 % CI can be viewed in Digital Appendices D.2 and D.3. The maximum coverage for the HPHT #1 samples are significantly larger than those of the room temperature experiments. Graphically, this is shown on Figure 4.7.

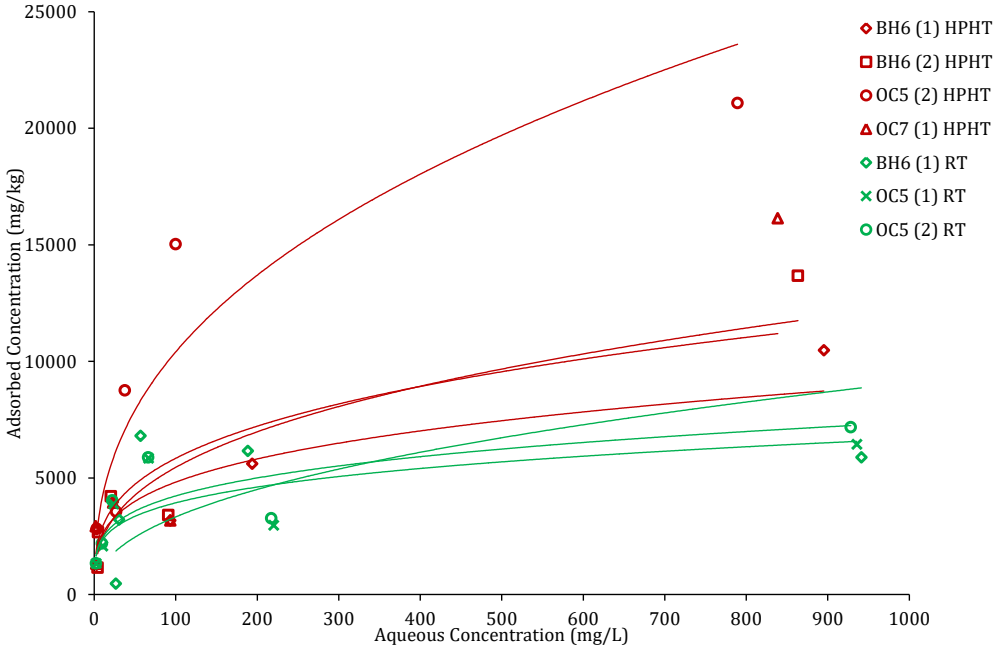

Figure 4.7: *Plot of the non linearised data for various samples using 0-1000 mg/L calibration Langmuir isotherm. The data is fitted using a power function to illustrate maximum coverage for the Langmuir isotherm. Comparison is made between the room temperature (RT) experiments and the HPHT#1 samples (HPHT).*

Fitting a power-law, best-fit to non linearised Langmuir isotherm data, the curves fitted (Figure 4.7) show that the HPHT #1 fits shown in red have consistently higher endpoints on the y axis, meaning that samples subjected to greater pressure and higher temperatures, than the RT samples, have higher concentrations at maximum coverages (or adsorbed concentrations).

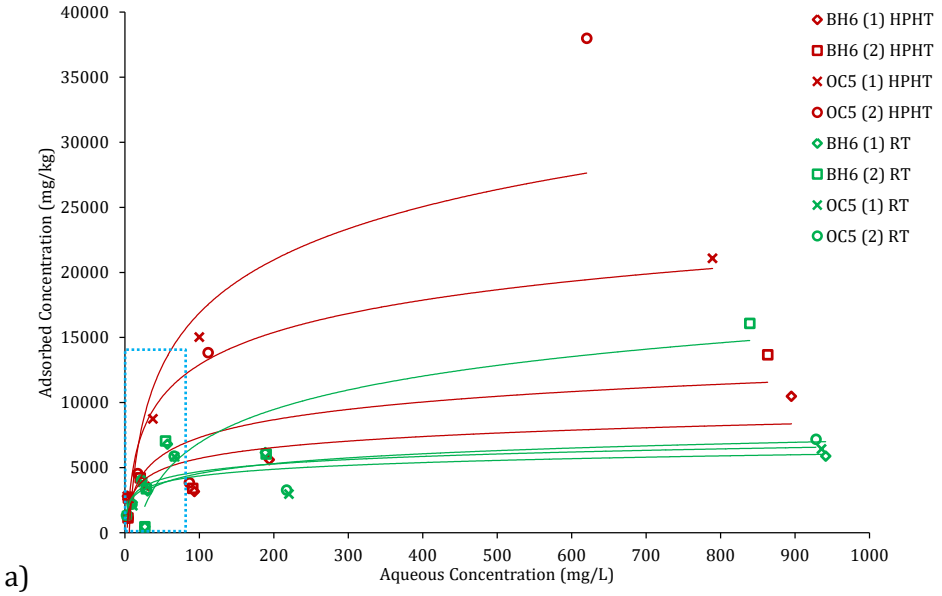

a)

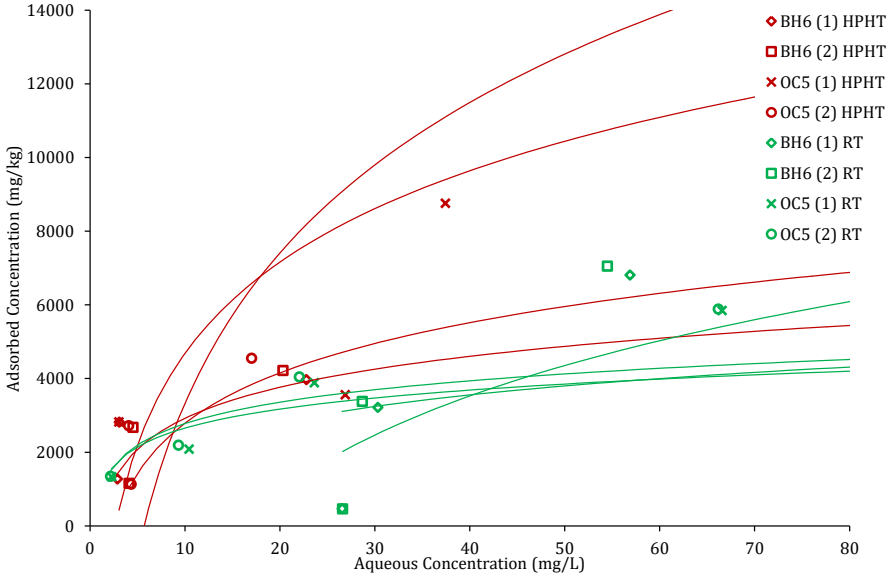

b)

Figure 4.8: *Non linearised Freundlich isotherms for both RT and HPHT #1 results. 'b' is a magnified section of the upper graph (a), as delineated by the blue highlighted box on the upper graph.*

Using Figure 4.8, Freundlich isotherms can be seen to favour lower concentrations. The uptake of the adsorbate, PAM, onto the rock surface seems to have not been largely affected by either increases in pressure or temperature (Table 4.5).

SAMPLE	RT	HPHT
BH 1 (1)		0.348
BH 1 (2)		0.418
BH 4 (2)		0.277
BH 5 (1)	0.243	0.452
BH 5 (2)	0.241	0.564
BH 6 (1)	0.436	0.270
BH 6 (2)	0.524	0.355
OC 3 (1)	1.272	0.614
OC 4 (1)	0.353	
OC 4 (2)	0.403	0.323
OC 5 (2)		0.241
OC 7 (2)	0.576	
OC 8	0.536	0.274

Table 4.5: *'Good' ($R^2_{adj} > 60$ %) data from the Freundlich isotherm showing the 1/n value, indicative of adsorption favourability, for the respective samples.*

The 1/n value (dimensionless) for the Freundlich adsorption isotherm (the gradient) assesses the degree of curvature of each individual isotherm. Values of 1/n typically range between 0 and 1. The gradient (1/n) value depends on adsorption intensity or surface heterogeneity (Foo and Hameed, 2010). On Freundlich isotherms, 1/n values are typically < 1, suggesting an L-type isotherm, indicative of both Freundlich and Langmuir (examples seen in Figure 4.8 and Figure 4.9), rather than what is classed as a C-type isotherm (completely linear and limitless). In summary, the higher the value of 1/n, calculated from the slope of the Freundlich isotherm (Figure 4.4 and Figure 4.5), the quicker the uptake of the adsorbate onto the adsorbent, at least in term of monolayer adsorption. Using Table 4.5, there was no observable statistical difference between the range of values for RT experiments and the HPHT experiments. Conducting a paired t-test on results from Table 4.5 display a p-value of 0.38, greater than the alpha level of 0.05, showing weak evidence against the null hypothesis and thus both datasets were not significantly different from each other.

4.9.2. Percentage Removal of Aqueous PAM

Percentage removal was plotted for all samples for data of the same concentration regardless of sample or significance (Figure 4.9).

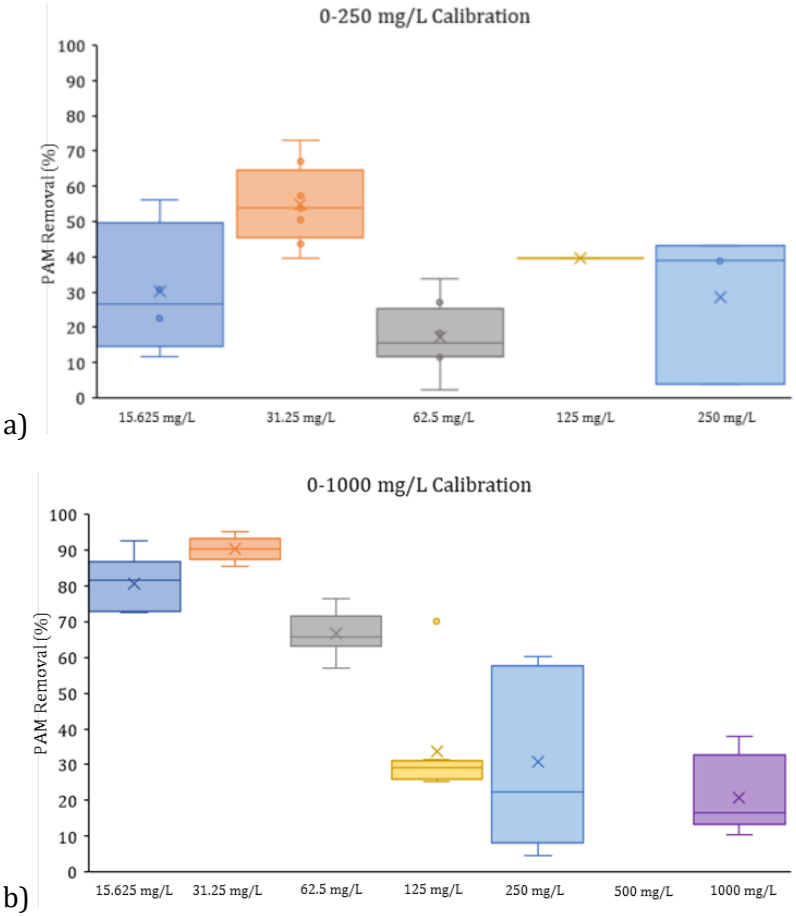

Figure 4.9: *Box and whisker plots showing the percentage removal of PAM for all samples in HPHT #1 using both calibration types. The mean concentration is denoted by an 'x' symbol and all outliers from the general model by a dot. A- 0-250 mg/L calibration, 'b' – 0-1000 mg/L calibration.*

Figure 4.9 shows that up to 95 % of aqueous PAM can be removed by means of adsorption at the elevated pressure and temperature used in this experiment. No pattern in percentage removal is observed using the 0-250mg/L calibration; however this is the data with the lowest number of statistically significant results (Table 4.3). The lack of pattern shown in Figure 4.9 is in comparison to data in 0-250 mg/L RT adsorption experiments where there was a pattern of reducing percentage removal with an increase in PAM concentration (Section 3.7.2). Data using the 0-1000 mg/L exhibits a similar pattern to that seen in Figure 3.10 (Section 3.7.2) with the RT adsorption results. The RT experiments, have a lower percentage of removal where higher concentrations of PAM are present and a higher percentage removal with the lower concentrations of PAM.

4.9.3. Statistical Analysis of Results

Sample size, the amount of samples used in experimentation, is a limitation for analysis of the HPHT results. By design, and hardware limitations, the sample size was small for this type of experiment, yielding fewer results. The size of the sample, the amount of data available for analysis, dictates the precision or confidence level of the analysis, and thus the smaller the size, the lower the confidence the user would have in the results of the analysis. Sometimes analyses do not work due to lack of responses or predictors.

Stepwise Linear regression was performed using both sets of results from the two different calibrations (0-250 mg/L and 0-1000 mg/L) ad only performed where R^2_{adj} fits were present. All fits were used in these analyses, whether or not they were classed as 'good' or 'excellent'. The Linear and Freundlich isotherms used the adsorption coefficient, the K value, as the response whereas the Langmuir isotherm used the K value alongside the maximum coverage value as its response. These data were analysed against all numerical values from the XRF, TGA and carbon analyses.

CALIBRATION	ISOTHERM	RESPONSE	PREDICTOR	P-VALUE	VIF	r^2 adj	SLOPE
0-250 mg/L	Linear	K	Loss 300-650°C	0	1	91.51%	-
	Freundlich	K	TOC	0.029	1	57.76%	+
	Langmuir	K	SO_3	0.112	1	31.10%	-
		Maximum Coverage	Loss 300-650°C	0.1	1	33.69%	+
0-1000 mg/L	Linear	K	Loss 650-980°C	0.075	1	34.16%	+
	Freundlich	K	n/a				
	Langmuir	K	TOC	0.141	1	21.06%	-
		Maximum Coverage	Total Losses	0.051	1	41.15%	-

Table 4.6: *Stepwise Linear regression results for all HPHT experiments using data with all fits (not including 0 % R^2_{adj} fits). '+' and '-' symbols denote the gradient either as positive or negative towards increasing K or maximum coverage.*

All results using this stepwise linear regression analysis are shown in Table 4.6. The VIF values of 1 suggest no multicollinearity between predictors. Table 4.6 exhibits predictors that influence the K or maximum coverage responses as loss data in temperature windows of 300-650 ˚C or 650-980 ˚C, or TOC. Losses attributed to temperatures between 300-650 ˚C appear twice, both using the 0-250 mg/L calibration. TOC appears once with the 0-250 mg/L calibration, also showing the lowest P-value, 0.029, for the whole dataset. TOC appears once using the 0-1000 mg/L (P-value 0.141) using the Langmuir isotherm, alongside losses seen

between 650 and 980 °C (P-value 0.075) using the linear isotherm, and total losses (P-value 0.051), also using the Langmuir isotherm. Example plots of the data shown in Table 4.6, can be seen in Figure 4.10 to 4.12.

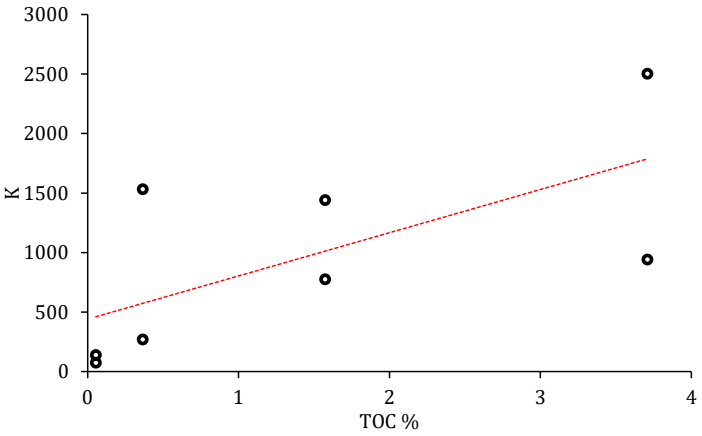

Figure 4.10: *Linear regression pattern for the 0-250 mg/L Freundlich isotherm displaying TOC against K from Table 4.6.*

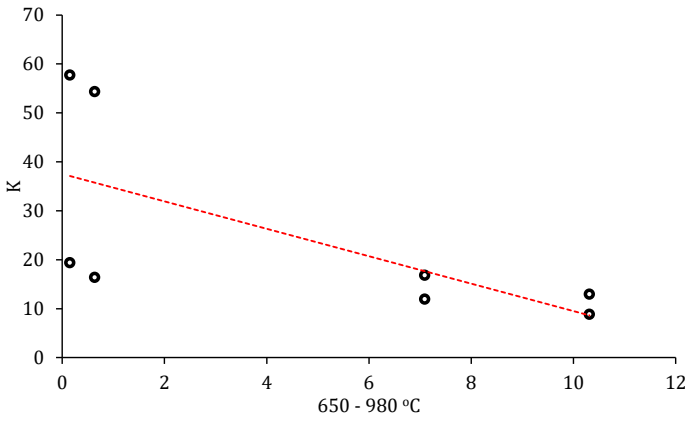

Figure 4.11: *Linear regression pattern for the 0-1000 mg/L linear isotherm displaying losses between 650 and 980 °C and K from Table 4.6.*

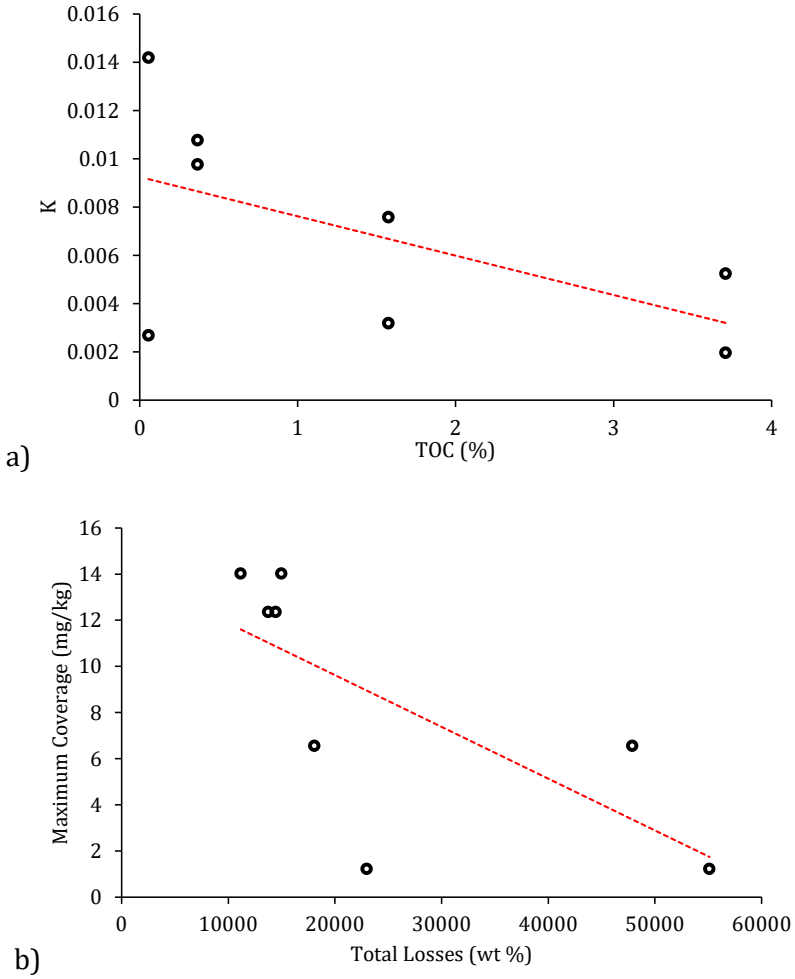

Figure 4.12: *Example linear regression patterns for the 0-1000 mg/L Langmuir isotherm displaying wt % for TOC against K (a) and total losses against maximum coverage (b).*

To understand if the presence or absence of certain minerals influenced the adsorption at higher pressures and temperatures to that of the RT experiments, ideally a categorical stepwise analysis of variance (ANOVA) would have been conducted on the quantitative XRD data. Unfortunately the dataset for the HPHT experiments was so small this analysis could not be conducted.

Using the Freundlich constant (1/n), no statistical relationship was found between the 1/n value or the quantitative or qualitative data.

4.10. Discussion

As for the RT adsorption experiments, both sand and shale rock samples exhibit highly adsorptive properties. The concentration at maximum coverage, calculated from these samples that have undergone adsorption in higher pressure and higher temperature conditions, can be up to 10 times the amount observed in the RT experiments (Figure 4.6). These data were collected using geologically realistic temperatures, but not geologically realistic pressures, thus showing that adsorption in large quantities (up to 22,000 mg/kg concentration at maximum coverage) is highly likely in the subsurface environments typical of gas shales in the UK such as the Lower Bowland Shale, based on the increase observed between the RT and HPHT results. The increase in concentration at maximum coverage, up to 22,972 mg/kg (Figure 4.6), shows us that even less rock would now be required to remove almost all aqueous PAM from the slick-water fluid by means of adsorption.

The limited sample size within the HPHT experiments, the total results, did hinder rigorous statistical analysis but in general, as with the RT experiments; losses and carbon percentages appear to be key factors in influencing adsorption. Statistical analysis of the XRD mineralogy produced no statistically significant relationships between the presence or absence of certain mineral types, in this case with 4 samples, this lack of any relationship is highly likely due to sample size. Regression analysis produced some results, albeit with limited statistically significant results, showing that potentially the main controls on the adsorption at these higher pressures and temperatures are the controlling factors of the mass losses observed both between 300 and 650 ˚C and 650 and 980 ˚C, i.e. TOC and carbonates (Table 4.6). The TOC data also provided two relationships using the Freundlich and Langmuir isotherms (Table 4.6). Using this data and linking it to the statistical analysis conducted on the RT experiments (Section 3.7.3), it is possible to conclude that similar controls may be accountable such as carbon content, inclusive of both organic and inorganic carbon. Clay type, likely to be another major factor, could not be checked due to the sample size being under the necessary amount for a useful analysis. The decrease in percentage PAM removed as the PAM concentration increases again suggests monolayer adsorption. Up to 95 % of aqueous PAM is removed from solution at the lowest PAM concentrations of 15.625 mg/L and 31.25 mg/L (Figure 4.9). Despite the HPHT experiments having fewer data, the trend in reduction of percentage removal from lower to higher initial PAM concentrations is similar to those observed in the RT adsorption results (Figure 3.11 Chapter 3, and Figure 4.9 Chapter 4). An increase in initial aqueous PAM slick-water concentration has the least PAM removed by adsorption, or from the other perspective, there is so much PAM in solution, all adsorption sites fill up quickly meaning no more PAM can adsorb, thus with larger initial PAM quantities in the fluid, larger amounts are left in solution after all adsorption sites have been filled.

Using Equation 3.9 (Section 3.8), the amount of shale required to remove all the aqueous PAM can be estimated at equilibrium. Taking the same 430 mg/L fluid used in Section 3.8, we can apply it to these more geologically realistic conditions with elevated temperatures and pressures. Using a frack volume the same as the volume of water used (8,399,000 L) against a rock type with a maximum coverage of 12,000 mg/kg (Table 4.4), only 301,000 kg of rock would be needed to remove all PAM from solution. If the maximum coverage is increased to the highest value seen in Table 4.4, 22,972 mg/kg, then the amount of rock required is a very small, 157,216 kg.

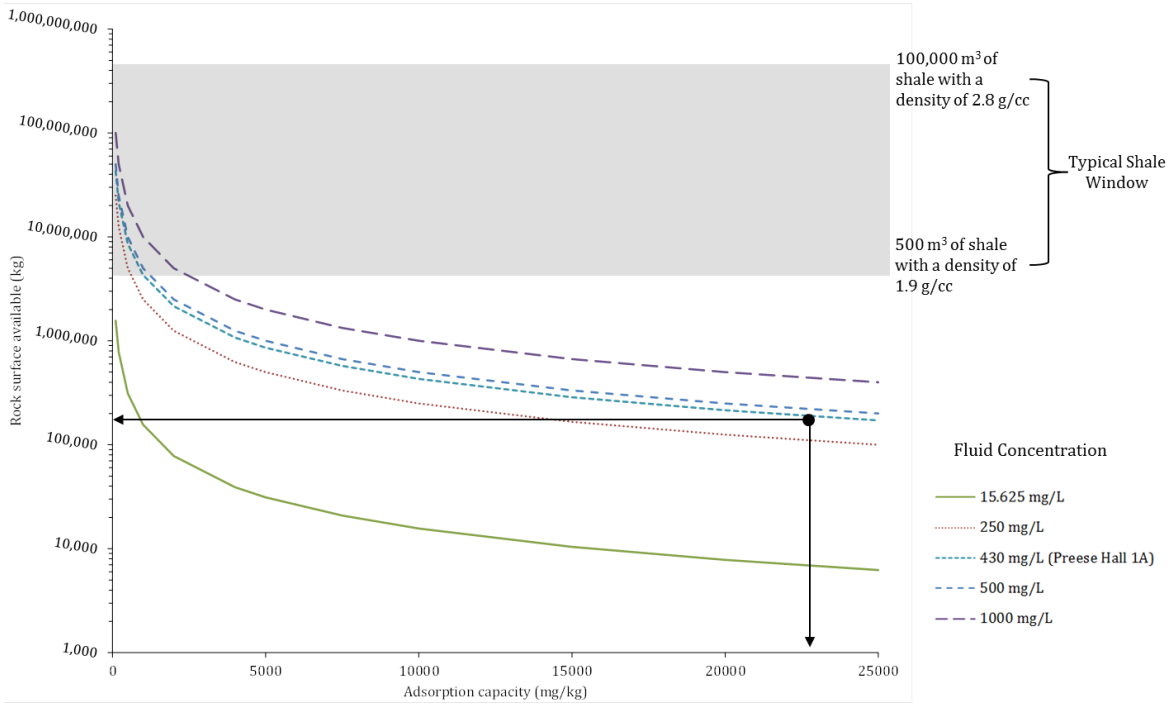

Figure 4.13: *An enhanced visualisation (from Figure 3.13) depicting the estimated amounts of rock needed to remove 100 % of all PAM from the fracking solution in the HPHT experiment. The curved lines represent the different concentrations of a PAM slick-water fluid in mg/L at 100 % removal. The adsorption capacity on the x axis is the amount of PAM in mg that can be adsorbed per kilogram of available shale surface. The shaded grey area is an example of the amount of shale available in two relatively small fracks at both the lower and upper ends of typical shale densities (1.9 – 2.8 g/cc). The black arrowed lines represent the amount of rock surface available to remove all PAM from solution at the specific adsorption capacity (maximum coverage based on Langmuir).*

Using Figure 4.13, it is easily shown that the higher maximum coverages found in the HPHT experiments require far less rock than in the RT experiments to remove nearly all aqueous PAM from solution. The arrows depicted on Figure 4.13 represent a rock type with a maximum coverage of 22,972 mg/kg, the highest maximum coverage observed in the results (Table 4.4). The amount of rock needed to remove all PAM at equilibrium is depicted as far lower than the shale window lower limit. This shale limit is a 500 m^3 frack with a low density

of 1.9 g/cm3, an almost unrealistically small hydraulic fracture that would, based on data shown, be able to remove nearly all aqueous PAM easily at equilibrium. Subsurface conditions, most likely higher pressures that are forcing more PAM onto the surface of the shales and potentially into pore spaces, are promoting this adsorption even further than at conditions indicative of room temperature. As observed in the RT experiments, the slick-water fluid will become less 'slick' overall, and certainly if it is re-used over multiple frack stages. Waters are again likely to contain considerably less PAM upon return to the surface and thus a lot is remaining downhole with the potential to degrade or migrate over time. Due to the adsorption ability of the PAM, results show, alongside literature, that its migration is highly likely limited within the subsurface environment (Guezennec et al., 2015).

The temperature, albeit relatively low still (< 100 °C) is indicative of UK onshore subsurface basins is likely to have had an impact upon the adsorption of the PAM, or at least the temperature change from room temperature seen in Chapter 3, to the 65 °C used in this part of the study. As is already known (Section 1.7), the effect of temperature on adsorption can be variable (Wiśniewska, 2012). With particular reference to shales, where clays are a principle component, swelling clays such as montmorillonites or smectites may increase in internal structure with temperatures up to 55 °C (Tekin et al., 2005). The same is true for kaolinite, enabling any PAM to penetrate further into the structure (Tekin et al., 2005). Temperature swelling may have occurred to the 4 samples analysed here, thus providing some explanation as to why concentrations at maximum coverage were observed as high as 22,972 mg/kg (Figure 4.6).

As mentioned earlier in this chapter, the addition of CO_2 into the system as a pressurising gas to produce near subsurface conditions may have led to a reduction in pH as increased CO_2 levels will increase the amount of hydrogen ions within the system (Turley et al., 2006).

FLUID	pH at 22.8 °C	
	Result 1	Result 2
0 mg/L PAM in vessel	7.74	7.76
250 mg/L PAM in vessel	7.56	7.51
0 mg/L PAM standard in vessel	7.65	7.63
250 mg/L PAM standard in vessel	7.54	7.51
0 mg/L PAM standard NOT in vessel	7.61	7.6
250 mg/L PAM standard NOT in vessel	7.42	7.4
Tap Water (no PAM)	7.55	7.58
DI Water (no PAM)	7.8	7.8

Table 4.7: *Recorded pH values post experiment for PAM fluids (250 mg/L) and fluids containing no PAM (0 mg/L) located both inside and outside the pressure vessel during the 250 mg/L PAM HPHT experiment.*

Under the particular conditions used in these HPHT experiments, 30 bar and 65 °C, and the non-ionic nature of the PAM, no acidic values were recorded, and fluids remained pH neutral. If fluids had become more acidic in nature then it would have been expected that potentially more adsorption would have occurred (Wiśniewska et al., 2016).

The degradation of PAM is thought to be generally temperature dependent and pressure/salinity independent (Xiong et al., 2018b). In the subsurface, any polymer degradation is likely to only mechanical (from operational pumping pressures), chemical, thermal or from biological degradation and not photo-degradation (Guezennec et al., 2015), and with salinity, higher in the deep subsurface (2-5 km depth), having little effect on the degradation of the PAM in terms of reducing its molecular weight (Xiong et al., 2018b). In an aqueous solution, such as a slick-water fracking fluid, polymers can be degraded both thermally and biologically (Rho et al., 1996), and PAM can degrade to acrylamide (AMD) under the right conditions. Typically, PAM does not degrade thermally until temperatures of ~200-250 °C are reached, and then degradation increases considerably with temperature increases (Xiong et al., 2018b; Yang, 1998). It is unlikely that any thermal degradation will have occurred in the HPHT experiments of this study as in shale gas environments in the UK the subsurface temperatures are unlikely to ever reach temperatures close to 200 °C. Studies have shown that also under the relatively low temperatures used in this study (~65 °C), acrylamide (a product of degradation) will not be present in detectable quantities. Caulfield et al., (2003) reported the

lack of acrylamide present in 'hot aqueous solutions at 95 °C, temperatures not unreasonable to subsurface basins of the onshore UK. Mechanical degradation of PAM, independent of adsorption, may likely occur due to the typically higher pump rates for slick-water fluids (Ferrer and Thurman, 2015). Mechanical degradation is caused by a shearing hydrodynamic field, which in turn leads to induced chain scissions which in turn leads to a decrease in the molecular weight of the PAM (Guezennec et al., 2015; Nguyen and Boger, 1998). While mechanical degradation could not be tested as part of these HPHT experiments, it is a potential degradation method in real-world operations; in turn this could affect the amounts of PAM adsorbed if some PAM had already degraded prior interacting with the shale surface. PAM adsorption may also reduce with increased flow (Lee and Fuller, 1985) and desorption increasing with an increasing flow velocity, neither of which could be tested within the remit of this study.

Biological degradation is entirely plausible within the geological setting of shale gas, and the use of mains tap water as the carrier fluid, for this study, Northumbrian Water mains fluid, as it would come into contact with microorganisms, however PAM is generally resistant to biodegradation as they are of high molecular weight (Guezennec et al., 2015). Having a higher molecular weight means that the PAM requires the presence of enzymes such as amidases to degrade the carbon chains, thus limiting biodegradation in low temperature, neutral settings (Caulfield et al., 2002; Guezennec et al., 2015). Although the degradation of the PAM to acrylamide could not be investigated, based upon the literature and geological setting for UK shale gas, it is unlikely that any hazardous amounts of AMD would be produced from slick-water concentrations of PAM. In terms of a hydraulic fracturing operation, mechanical degradation, due to the high pump rates, and thermal degradation would be the principal controls in this particular geological setting (neutral pH, low temperature, moderate salinity).

4.11. Conclusions

The HPHT experiments show that the aqueous PAM that makes up the friction reducer in the slick-water fluid is highly adsorptive to shale lithologies. At the conditions of the experiment, up to 22,972 mg/kg of aqueous PAM can be adsorbed per kg of rock available. No statistical analysis could however be conducted on the 1/n value due to limited sample size and this was also the case with the qualitative XRD data. No clay type could be pinpointed to adsorption.

Results here, at more geologically reasonable conditions, show that PAM once again would be adsorbed in large quantities. This data also suggests that due to the increase of PAM that is adsorbed, more PAM is likely to remain downhole. The potential for degradation to

acrylamide is limited, due to the relatively low temperature and neutral environment of the UK subsurface, and the experimentation methods.

5. The Desorption Properties of Adsorbed Polyacrylamide

5.1. Introduction

Alongside the previously outlined adsorption capacities of some of the shales, another key issue is how the adsorbed PAM may desorb off the shales and return in flow-back or produced fluids. This desorption could occur over day or weeklong timescales as a result of the flushing stages of a frack, or could occur over longer timescales such as years or decades. Typically, particularly in the United States, a hydraulic fracture consists of four main stages; 1) an acid stage consisting of water and usually HCl to clear the wellbore of debris; 2) the pad stage which initially open up the well bore to fluids before the frack; 3) the 'prop sequence stage' which is where fluid and proppant are pumped downhole under high pressure (the main frack stage); and 4) the flush stage (Holloway and Rudd, 2013; Speight, 2016). This flushing stage of a hydraulic fracture is commonly referred to as the final stage of a frack and is used to clean remaining aggregate, proppant or residual additives from the fractures (Al-Tailji et al., 2014; FracFocus, 2018; Holloway and Rudd, 2013; RigZone, 2019; Speight, 2016). Usually during this flushing stage freshwater, free from additives, is pumped down to remove these residuals. In this chapter this flushing stage is simulated in laboratory conditions so that adsorbed PAM that may desorb can be quantified. If amounts of desorbed PAM are minimal, this means that the adsorbed PAM is remaining on the surface of the samples and thus has the potential to degrade or de-polymerise to acrylic, acrylamide or ammonium. The experiments in this chapter were conducted at room temperature and at equilibrium. No rates of adsorption or desorption were measured. Adsorption and desorption experiments are referred to using 'Ads-Des'.

Results from this chapter were used in a project summary poster presented at an Environment Agency Knowledge Exchange event in Bristol, 2019. Posters can be viewed in the Digital Appendices.

5.2. Aims and Objectives

The aim of this chapter was to investigate whether adsorbed PAM can be desorbed off the shale surface if flushed using freshwater, as is typical in the industry (Al-Tailji et al., 2014). This flushing phase was simulated by soaking rock samples, that had aqueous PAM adsorbed to them, in freshwater and agitated over a similar time period to the adsorption experiments (see Section 3.3). Understanding the desorption behaviour of PAM to some of the same samples

used in the RT experiments will be key in understanding the potential polluting effects of PAM in the subsurface and potentially if this adsorbed PAM may affect reservoir permeability (Yang et al., 2018).

In this chapter, a subset of samples from the room temperature adsorption experiments were tested using a more constrained concentration range of PAM. A small range of lithology types were tested by using some of the same samples used in both the RT and HPHT adsorption experiments; OC 2, OC 6 and OC 7.

5.3. The study of PAM desorption

Due to the primary use of PAM in the agricultural and water treatment industries; there have been multiple studies on the PAM interactions with soil and clay type. Results generally conclude that little to no PAM can desorb either when kept wet or dry, and PAM can become irreversibly bonded (Nadler et al., 1992). The drying of samples producing irreversibly adsorbed PAM is something that is backed up by Green and Stott (2001). PAM can adsorb so well to soil samples that chemical solvents are needed for adequate desorption (Langenhoff, 2011). More recently there have been studies focussing on how PAM is used as a slick-water fluid fracking additive. Yang et al. (2018) discusses that adsorption and desorption capacities of PAM can vary with the addition of certain additives, particularly urea. The addition of urea can help against the decreasing of the permeability in the reservoir which the adsorbed PAM contributes to. Guo et al. (2018) states how adsorption capacities of PAM are high, and desorption can be aided by an increase in temperature, as would be the case in subsurface environments.

5.4. Adsorb-Desorb Sample Preparation and Methodology

The methodology for the "adsorb-desorb" experiments was conducted in a very similar way to the previous adsorption methods mentioned in both the RT and HPHT adsorption experiments (Sections 3.3.1 and 4.5). One major change in the methodology was to the sample type, in this experiment a 1 x 1 x 1 cm cube of the rock sample rather than 1 g of powder was used. Using a powdered 1 g sample in this type of experiment would have made it difficult to constrain the hydrophobicity and surface area. To best mitigate against the hydrophobic properties of a rock powder entering a viscous solution, and the necessary drying associated with the desorption experiments, cubes of rock were used. Cubed rock samples of equal size also mitigate against variation in the amount of surface area available for adsorption within each experiment whilst being inclusive of natural porosity or permeability of the shale that

would not be the case for powdered samples. Only 3 samples were selected for the full adsorb-desorb tests. Two samples were tested initially, OC 1 and OC 3, to ensure the method was robust. The samples selected were; OC 2, OC 6 and OC 7. Only outcrop samples could be used for this analysis based on the preparation of the 1 cm^3 rock cubes and the amount of sample availability.

There were some changes to the methodology from previous adsorption experiments. Firstly, in the room temperature and HPHT adsorption experiments, 1 g of a fine rock powder was used. In these desorption experiments 1 cm x 1 cm x 1 cm cube of rock was used. The use of this type of cube was to ensure, as best possible, the same amount of surface area for each sample. If a powder was used for this type of experiment there would be no means of obtaining how hydrophobic each 1 g of powder had become upon entering the fluid. Furthermore, it would be almost impossible to dry a consistent amount of powder to rehydrate and measure aqueous desorbed PAM that may be present.

Secondly, the desorption stage: after a sample was removed from a PAM slick-water fluid and any remaining aqueous PAM measured for adsorption, the sample was allowed to air dry. Air drying the rock sample mitigates against the transference of any aqueous PAM remaining on a wet sample into the new freshwater fluid, i.e not measuring abundant PAM that was not adsorbed in the first place. It is of course, highly unlikely that the subsurface would become dry, and any PAM that has not adsorbed, will return to the surface during a flushing or flowback stage. Once dry, this sample was then placed in to fresh water, agitated and left for the same time period that had been allowed for adsorption. After 12 hours the sample was removed and the fluid was analysed using the *N*-Bromination method, as detailed in Section 3.3.5 to assess for aqueous PAM that was desorbed.

Thirdly, to gain *only* an insight into the desorption properties of adsorbed PAM, only three concentrations of a PAM slick-water fluid were used; 15.625 mg/L, 62.5 mg/L and 250 mg/L. This would mean that samples can be calibrated to the 0-250 mg/L linear calibration.

5.4.1. Experimental Procedure

Step by step guidance below is linked to Figure 5.1 and Figure 5.2.

Day 1: The relevant PAM slick-water concentrations (15.625, 62.5, and 250 mg/L) were diluted down from an original 1000 mg/L PAM solution. A total of 40 ml of each diluted fluid was placed into a 50 ml glass vial. For each single sample there were 4 rock cubes, one placed into each respective concentration including a 0 mg/L blank. Samples were agitated on the shaker table at 400 rpm and left overnight for adsorption to occur, similar to the RT adsorption experiments.

Day 2: Cubed samples were removed from the slick-water fluids and left to air dry, ensuring no fluid was forcibly removed from the samples themselves. Once samples were fully dry, they were re-submerged in 40 ml of fresh water, agitated for 1 hour at 400 rpm and then left overnight to allow desorption to occur. Meanwhile, fluids from the adsorption stage of the experiment were diluted tenfold with 18 ml of fresh water to 2 ml of sample water and left to mix overnight.

Day 3: Original adsorption fluids that have been diluted were then analysed using the *N*-Bromination method providing adsorption results. Samples in the desorption phase of the experiment were removed from the fresh water glass vials. This freshwater fluid was diluted tenfold, to maintain consistency in the dilution of fluids measured on the spectrophotometer, and mixed.

Day 4: Diluted freshwater fluids from the desorption phase were analysed using the *N*-Bromination method to measure for aqueous PAM that would be present due to desorption.

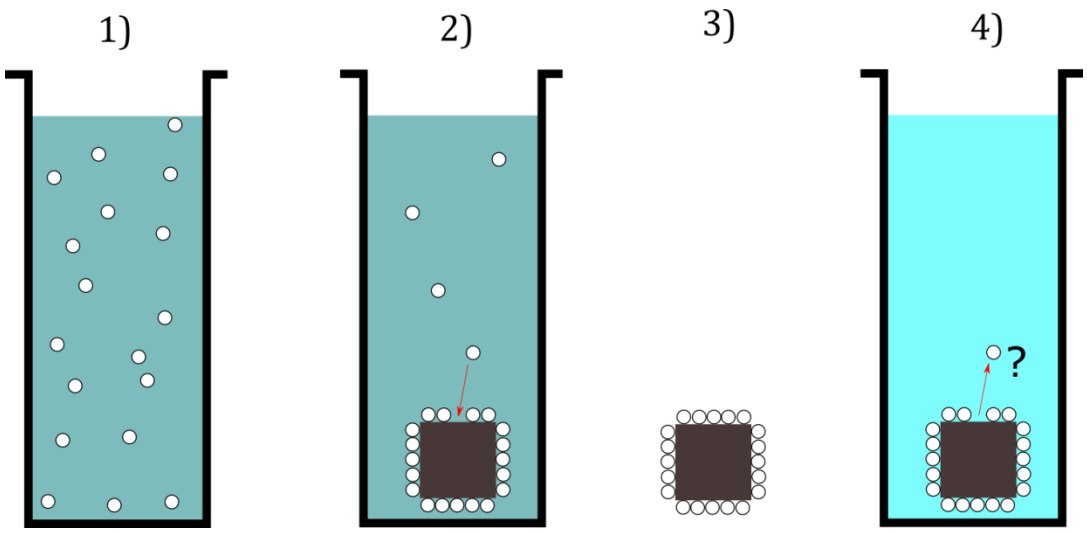

Figure 5.1: *A summarised diagram of the desorption experiment setup. 1) Aqueous PAM (white circles) is mixed into the relevant concentrations; 2) rock sample cube is added to the fluid and left overnight for adsorption to occur; 3) the rock sample is removed from the fluid and air dried and; 4) the sample is placed into a freshwater fluid, simulating the 'flush' stage and allowing for PAM to desorb back into solution.*

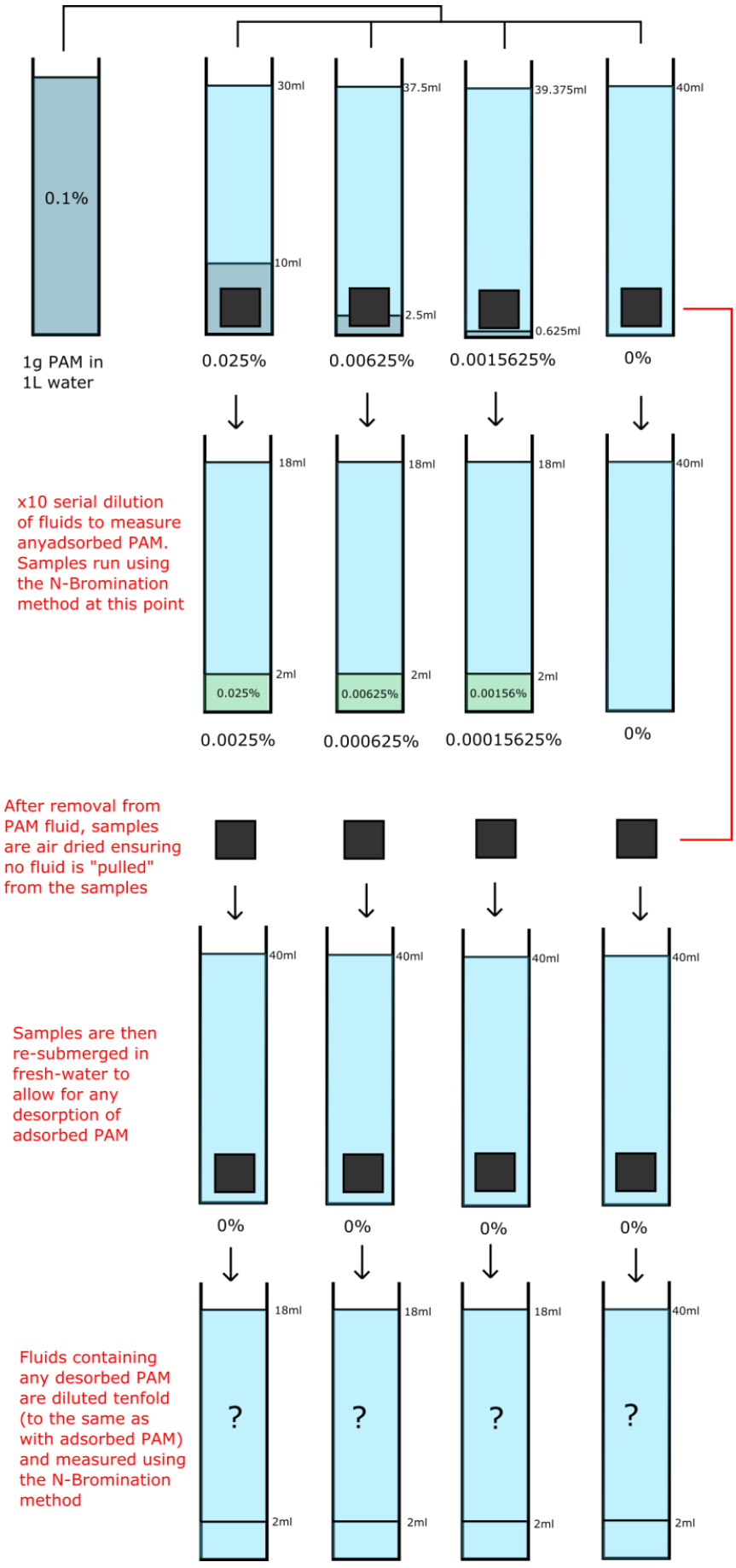

Figure 5.2: *Graphical diagram of the adsorb-desorb methodology as explained in Section 5.4.1.*

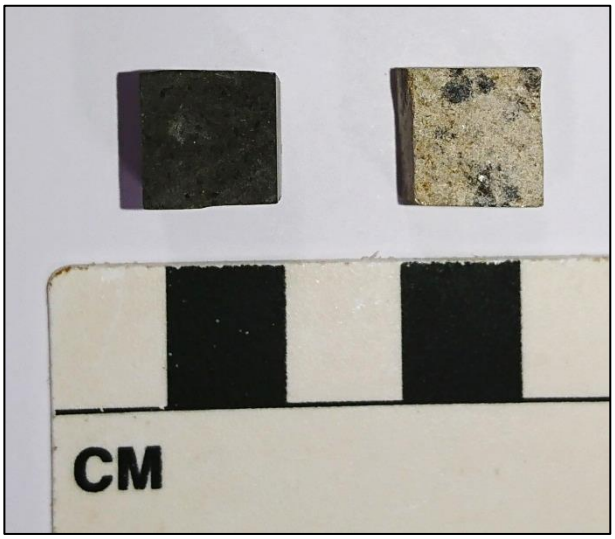

Figure 5.3: *Example 1 cm cubes used in the experiments for OC 7 (left) and OC 2 (right).*

Figure 5.4: *Example of an OC 7 sample saturated in 40 ml of a PAM rich fluid. From here, the sample is removed and air dried before being placed into 40 ml of freshwater in a similar setup to the one displayed.*

5.5. Adsorb-Desorb Isotherms

All the results from adsorb-desorb experiments were plotted on the same three isotherms as per the RT and HPHT experiments: linear, Freundlich and Langmuir. To plot these correctly, as samples were divided by size and not mass, sample weights needed to be accounted for. Instead of 1 g mass per sample, samples cube weights were averaged. Weight results are shown in Table 5.1.

SAMPLE	WEIGHT (g/cc)
OC 1	2.44
OC 2	2.87
OC 3	3.08
OC 6	4.12
OC 7	3.84

Table 5.1: *Average weights of all samples as 1 cm cubes used in the adsorb-desorb experiments.*

Upon creating the isotherms and results for adsorbed PAM in mg/kg, the weight values shown in Table 5.1 had to be used. Samples OC 1 and OC 3 are not included in these results here as they were used as test samples when refining the method.

5.6. Adsorb-Desorb Statistical Analysis Methodology

As per previous chapters, linear regression and ANOVA were conducted on all isotherm results. Unfortunately, statistical analysis could not be conducted against the quantitative and qualitative shale characterisation data due to limited number of samples used. An ANOVA was also conducted on value for percentage removal and amount adsorbed (mg/kg from a linear isotherm) for all types of experiment using the samples used in this chapter (OC 2, OC 6 and OC 7). Factor used for ANOVA analyses were:

1) Percentage Removal
    a. Sample Name (OC 2, OC 6 and OC 7 and duplicates thereof).
    b. Experiment Type (RT, HPHT and ADS-DES)
    c. Initial PAM concentration (15.625, 62.5 and 250 mg/L)

2) Adsorbed Concentration (mg/kg)

   a. Sample Name (OC 2, OC 6 and OC 7 and duplicates thereof).

   b. Experiment Type (RT, HPHT and ADS-DES)

   c. Initial PAM concentration (15.625, 62.5 and 250 mg/L)

Two ANOVA analyses were run. One run accounted for all experiment types, the other removed HPHT as there was only one sample (OC 7) that was used in both the HPHT and Ads-Des experiments. In the second analysis, Ads-Des samples were compared to the comparative RT sample.

5.7. Adsorb-Desorb Calibration

Due to the limited range of concentrations used in the adsorb-desorb experiments, a maximum concentration of 250 mg/L, only one linear calibration was used between 0 and 250 mg/L. One set of standards between 0 and 1000 mg/L was calibrated against in the spectrophotometer, maintaining consistency to all other experiments (Figure 5.5).

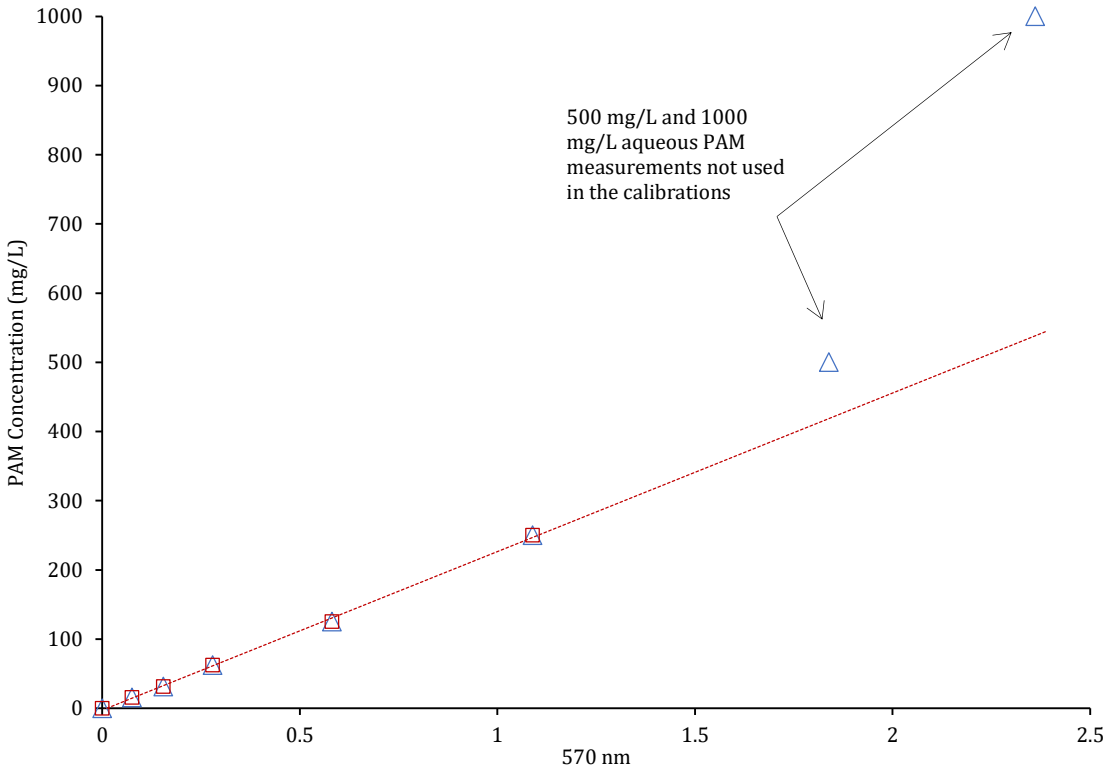

Figure 5.5: *Linear calibration used for the adsorb-desorb experiments. Standards were only calibrated between 0 and 250 mg/L as the highest concentration used in these experiments was 250 mg/L.*

The linear calibration was used as there was no statistically significant difference between data for either the linear, polynomial (c = 0) or polynomial (c ≠ 0) fits between 0 and 250 mg/L.

5.8. Adsorption Results

In total, after testing and method refinement, 3 samples and their duplicates were measured alongside a duplicated blank: there was a total of 18 isotherms to plot. Sample OC 7 (1) produced an anomalous data point, grossly off trend with the respect to the remaining sample and sample duplicate points, and so this was removed from the analysis (Figure 5.6) Least squares regression was performed on all isotherms (Table 5.2).

SAMPLE	0.0015625, 0.00625, 0.025 % PAM								
	LINEAR			FREUNDLICH			LANGMUIR		
	Aq	r^2 adj	P-VALUE	Log (Ads)	r^2 adj	P-VALUE	Aq/Ads	r^2 adj	P-VALUE
OC 2 (1)	221 + 6.20 Aq 209 1.71	85.95%	0.171	1.320 + 0.829 Log (aq) 0.386 0.221	86.75%	0.166	0.069 + 0.0 Aq 0.021 0.0	56.25%	0.31
OC 2 (2)	199.8 + 6.520 Aq 78.3 0.641	98.08%	0.062	1.658 + 0.660 Log (aq) 0.004 0.003	100.00%	0.002	0.052 + 0.0 Aq 0.011 0.0	91.61%	0.131
OC 6 (1)	690 + *1.46* Aq 589 4.87	0.00%	0.814	2.338 + *0.288* Log (aq) 0.958 0.611	0.00%	0.719	*0.029* + 0.0 Aq 0.031 0.0	84.02%	0.182
OC 6 (2)	75.51 + 8.1194 Aq 1.75 0.0159	100.00%	0.001	1.390 + 0.787 Log (aq) 0.104 0.061	98.81%	0.049	0.073 + 0.0 Aq 0.018 0.0	41.09%	0.365
OC 7 (1)	*-14.7* + 4.728 Aq 50.9 0.402	98.56%	0.054	*-0.344* + 1.483 Log (aq) 0.657 0.365	88.57%	0.154	0.594 - *0.002* Aq 0.333 0.003	0.00%	0.58
OC 7 (2)	71.0 + 7.728 Aq 56.7 0.5	99.17%	0.041	1.551 + 0.690 Log (aq) 0.271 0.157	90.14%	0.143	0.074 + 0.0 Aq 0.038 0.0	0.00%	0.541

Table 5.2: *Summary table of the statistical analysis performed on all the adsorb-desorb isotherm results. PAM concentrations used are displayed: 0.00156 %, 0.00625 % and 0.025 % PAM. Only one calibration type is used, the 0-250 mg/L for all isotherms; linear, Freundlich and Langmuir. Significance was tested with a 0.05 margin of error.*

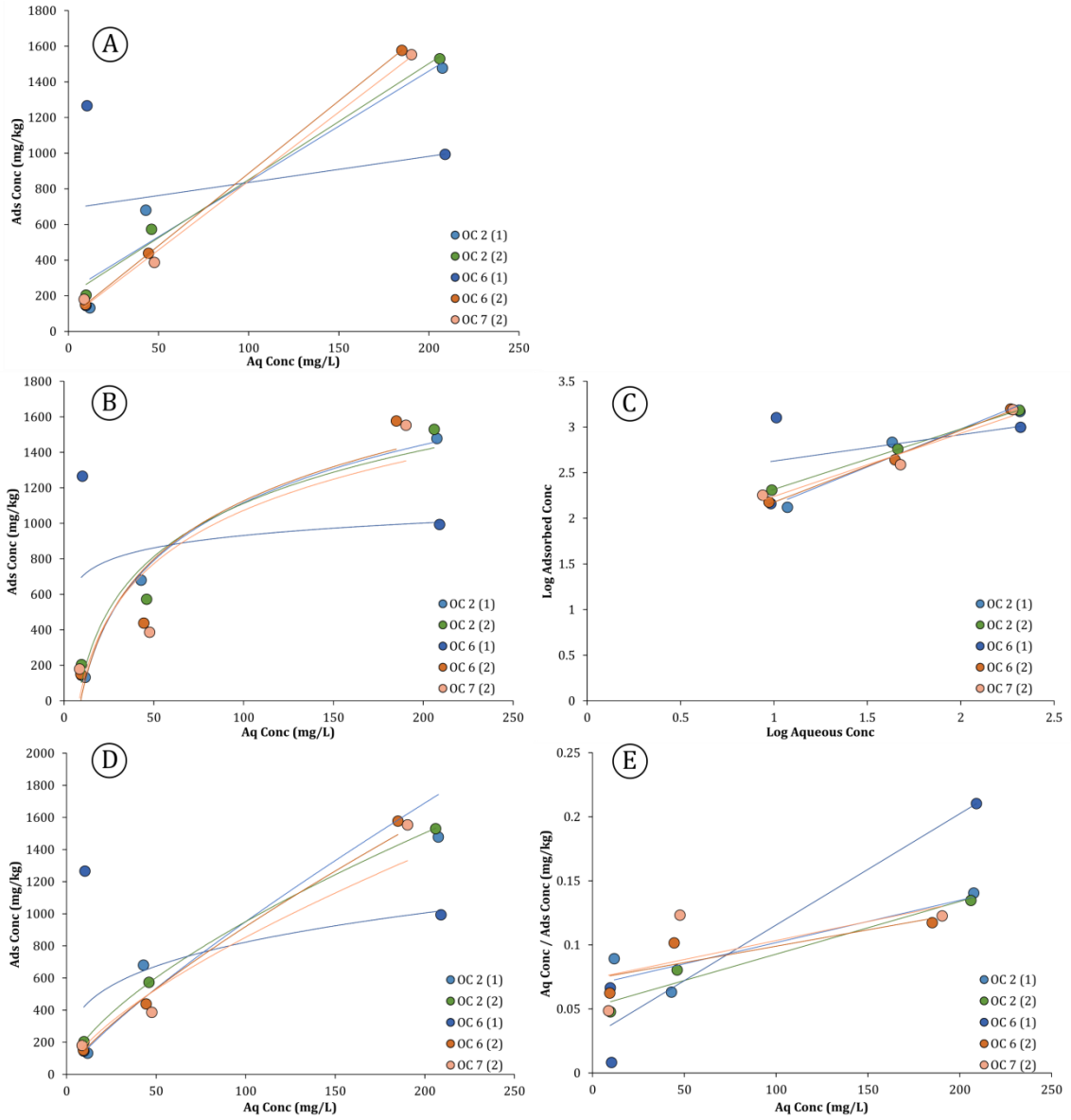

Figure 5.6: *All three types of isotherm for the adsorb-desorb data using a 0-250 mg/L calibration. From top down; A is linear, B and C are Freundlich and linearised Freundlich respectively and D and E are Langmuir and linearised Langmuir respectively.*

From the data (Table 5.2), the Langmuir isotherm offered the worst number of fits, 2 classified as good, and 1 of these as excellent. No fit for the Langmuir isotherm was found to be statistically significant. For both the linear and Freundlich isotherms, two isotherms showed significant fits and for both five isotherms were classified as having good R^2_{adj} fits. From this the linear isotherm produced 4 isotherms with excellent R^2_{adj} fits and Freundlich 3.

Although, not integral to the desorption analysis, maximum coverages can be estimated from the Langmuir isotherms (Table 5.4). Results here should be only treated as estimations due to the small size of the dataset and the lack of significant fit for this isotherm (Table 5.2).

LITHOLOGY TYPE	SAMPLE	MAXIMUM COVERAGE (Room Temperature)	MAXIMUM COVERAGE (HPHT #1)	MAXIMUM COVERAGE (Adsorb-Desorb)
LBS	BH 2 (1)	*441*		
UBS	BH 3 (2)	*574*		
UBS	OC 7 (2)	*1723*	*18062*	3373
Pendle Grit (silty)	OC 2 (1 & 2)			2429 - 3026
Sand	OC 8	*3769*		
LBS	BH 2 (2)	*4079*		
LBS	BH 5 (1 & 2)	*4686 - 4754*	*940-14442*	
Carboniferous Shale	BH 6 (1 & 2)	*4287 - 6654*	*11163 - 14983*	
Pendle Grit	OC 5 (1 & 2)	*6518 - 7276*	*22972*	
UBS/Lst	OC 6 (1)	*7818*		1151 - 3917
UBS	BH 4 (2)	*12126*		
UBS (silty)	OC 4 (2)	*3365 - 15365*		

Table 5.3: *Maximum coverages calculated from the Langmuir isotherms for the adsorb-desorb experiments. Results are estimates based upon the small statistical dataset input.*

Dependent on initial aqueous PAM concentration, 15.625, 62.5 or 250 mg/L, up to 83 % can be removed by means of adsorption (Figure 5.7).

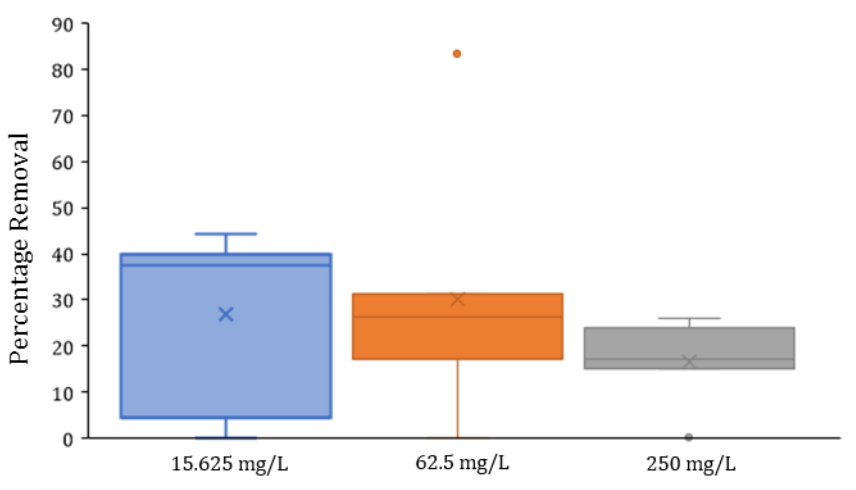

Figure 5.7: *Percentage removals for the concentrations used in the adsorb-desorb experiments. The mean percentage removal is denoted by an 'x' symbol and all outliers from the general model by a dot.*

It may be possible to conclude that percentage removal decreases with an increase in the initial aqueous PAM concentration, similar to observed results in the RT and HPHT adsorption experiments (Section 3.7.2 and 4.9.2). If true, the decrease in percentage removal with an increase in PAM concentration would suggest monolayer adsorption see discussion.

Comparison of the adsorbed concentrations (mg/kg) amongst all samples used in the ads-des, RT and HPHT experiments shows that there is no statistical significance between experiment type and adsorbed concentration (mg/kg) apart from with the 'initial PAM concentration (mg/L)'. Including and excluding the HPHT experiment as a factor the P-value for PAM concentration is 0.004 (including the HPHT factor) and 0.031 (excluding the HPHT factor) (Table 5.4). An increase in the amount adsorbed to the shale (mg/kg) would be expected alongside an increase in initial PAM concentration, simply because there is more available to adsorb before a maximum coverage is reached.

Comparing the percentage removal of the samples (OC 2, OC 6 and OC 7) to the same samples used in both the RT and HPHT experiments using ANOVA (Table 5.5) there is no statistically significant difference (at the 95 % probability of being zero) between experiment type and the percentage removed.

RT, HPHT & ADS-DES			RT & ADS-DES		
ANOVA	F-VALUE	P-VALUE	ANOVA	F-VALUE	P-VALUE
SAMPLE	0.16	0.952	SAMPLE	0.68	0.641
EXPT	0.33	0.726	EXPT	0.41	0.556
PAM (mg/L)	9.83	0.004	PAM (mg/L)	9.28	0.031
SAMPLE x PAM (mg/L)	0.94	0.525	SAMPLE x EXPT	0.48	0.755
			SAMPLE x PAM (mg/L)	1.35	0.41
			EXPT x PAM(mg/L)	7.98	0.04
MODEL SUMMARY			MODEL SUMMARY		
R^2	Adj R^2		R^2	Adj R^2	
71.58	30.23		95.8	73.77	

Table 5.4: *ANOVA results for the comparison of adsorbed concentration across all experiments involving samples OC2, OC 6 and OC 7 (left) and experiments removing the HPHT elements, where only one sample of the Ads-Des samples was used (right).*

RT, HPHT & ADS-DES			RT & ADS-DES		
ANOVA	F-VALUE	P-VALUE	ANOVA	F-VALUE	P-VALUE
SAMPLE	0.33	0.853	SAMPLE	0.41	0.793
EXPT	0.39	0.686	EXPT	0.31	0.605
PAM (mg/L)	2.41	0.135	PAM (mg/L)	4.08	0.108
SAMPLE x PAM (mg/L)	0.28	0.958	SAMPLE x EXPT	1.37	0.383
			SAMPLE x PAM (mg/L)	0.69	0.694
			EXPT x PAM (mg/L)	4.3	0.101
MODEL SUMMARY			MODEL SUMMARY		
R^2	Adj R^2		R^2	Adj R^2	
48.9	0		91.02	43.85	

Table 5.5: *ANOVA results for the comparison of percentage removal across all experiments involving samples OC2, OC 6 and OC 7 (left) and experiments removing the HPHT elements, where only one sample of the Ads-Des samples was used (right).*

Detailed versions of Table 5.4 and Table 5.5 are available in Digital Appendices E.2 and E.3 showing fitted means for all factors in the ANOVA models for each test.

5.9. Desorption Results

Using the 0-250 mg/L calibration, aqueous PAM that may be present in the fluid from the desorption phase will have been desorbed from the samples. In summary, for all samples, desorbed PAM was minimal; with some aqueous PAM being so negligible it was undetectable on the spectrophotometer. A full suite of results can be viewed in Table 5.6.

SAMPLE	INITIAL (mg/L)	REMAINING AQUEOUS (mg/L)	ADSORBED (mg/L)	% REMOVED (%)	DESORBED (mg/L)	% DESORBED (mg/L)
OC 2 (1)	15.625	11.800	3.825	24.482	n/a (0)	-
OC 2 (2)	15.625	9.738	5.887	37.676	n/a (0)	-
OC 6 (1)	15.625	9.624	6.001	38.409	2.752	45.851
OC 6 (2)	15.625	9.395	6.230	39.875	n/a (0)	-
OC 7 (2)	15.625	8.707	6.918	44.273	0.003	0.042
OC 2 (1)	62.5	42.953	19.547	31.276	n/a (0)	-
OC 2 (2)	62.5	46.045	16.455	26.328	n/a (0)	-
OC 6 (1)	62.5	10.311	52.189	83.503	n/a (0)	-
OC 6 (2)	62.5	44.441	18.059	28.894	0.690	3.821
OC 7 (2)	62.5	47.648	14.852	23.763	n/a (0)	-
OC 2 (1)	250	207.536	42.464	16.986	0.232	0.546
OC 2 (2)	250	206.047	43.953	17.581	n/a (0)	-
OC 6 (1)	250	209.025	40.975	16.390	n/a (0)	-
OC 6 (2)	250	184.973	65.027	26.011	0.919	1.413
OC 7 (2)	250	190.356	59.644	23.858	0.461	0.773

Table 5.6: *Results for amounts both adsorbed and desorbed for samples OC 2, OC 6 and OC 7. 'Adsorbed' denotes the concentration of adsorbed PAM to that sample, the difference between 'initial' and 'remaining aqueous' concentrations. '% removed' denotes the % of the original aqueous PAM concentration that has been removed from solution via adsorption. 'Desorbed' denotes the amount of adsorbed PAM that desorbs into the fresh-water fluid. 'Percentage desorbed' denotes the percentage of the adsorbed PAM that desorbs over the course of the experiment.*

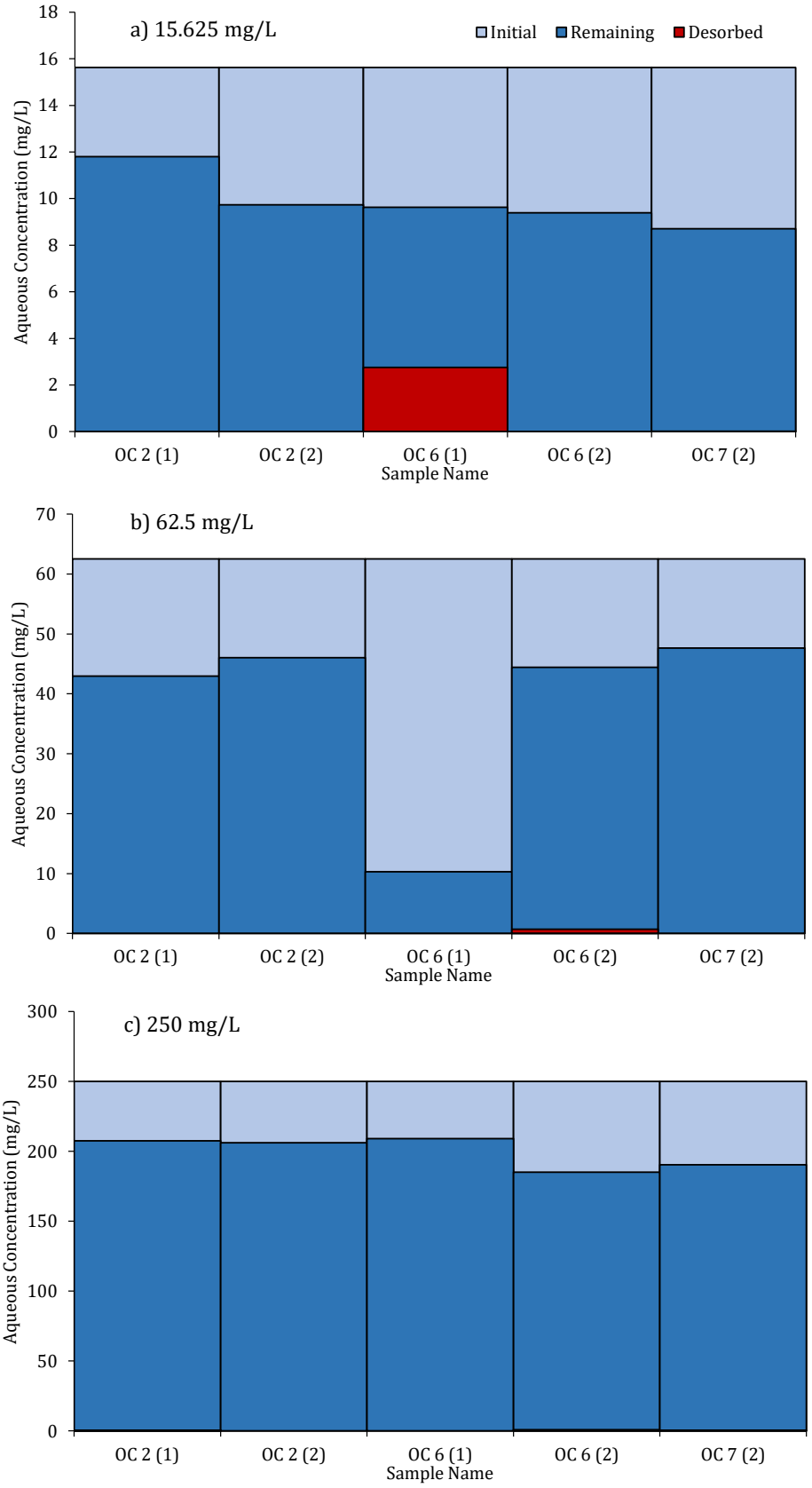

Figure 5.8: *Adsorption and desorption results in terms of remaining aqueous PAM initially, after adsorption, and after desorption (flushing). 'Original' denotes the initial aqueous PAM concentration; 'Remaining' denotes the aqueous PAM left in solution after quantities have been removed by adsorption and; 'Desorbed' denotes aqueous PAM that has been desorbed from the samples.*

In terms of desorption, after results were calibrated, negligible PAM is desorbed from these samples during the simulated flushing stages (Figure 5.8 and Table 5.6). After calibration, if some samples showed negative amounts desorbed, these were zeroed to account for unrealistic values. The maximum amount of PAM that was desorbed back into solution was 2.75 mg/L for sample OC 6 (1). This sample adsorbed ~ 6 mg/L of aqueous PAM after being submerged in a 15.625 mg/L PAM slick-water solution. This particular desorption result for OC 6 (1) was much higher than the typical results for all other samples. In general, between 0.919 and 0.002 mg/L of PAM were desorbed back into solution during the simulated flushing stages, irrespective of initial PAM concentration adsorbed. This equated to values between 0.042 % and 3.8 % of adsorbed PAM desorbed back into solution (Table 5.6). Results show no relationship between initial concentration of PAM and amount of PAM desorbed after flushing.

5.10. Discussion

Using 1 cm cubes to mitigate the problem of consistent surface area as best possible, the adsorption of aqueous PAM occurs as 'normal', similar to what has already been observed throughout this study so far. The uptake of PAM by the samples varies from 44 % removal in slick-water concentrations of 15.625 mg/L PAM to 26 % removal in slick-water concentrations of 250 mg/L PAM. Statistical analysis of the percentages removed show that there is no statistical difference between the types of experiment. A decrease in percentage removal occurring alongside an increase in initial PAM concentration is observed in RT. HPHT and Ads-Des experiments.

The more important result in this chapter is that the overwhelming proportion of adsorbed PAM did not desorb. PAM is unlikely to desorb in large quantities due to the large molecular sizes, long chained, flexible nature of PAM, making it unlikely that all segments can be detached from the adsorbate surface into the fluid (Stuart et al., 1980). Results in this study show that in the absolute highest case 45 % could be desorbed from a sample that has been saturated in a 15.625 mg/L fluid. Desorption ranges between 0.042 % and 3.8 % in the most likely cases. One result shows desorption of 45.81 %, but this is considerably larger than the remaining data. These data show that minimal PAM is desorbed from the rock during the flushing stages of a hydraulic fracture, and is likely to remain downhole. Data observed here matches conclusions met in other studies both on soil and shale stating that large scale desorption is unlikely, and potentially difficult without the aid of other additives. A study on soil, conducted by (Nadler et al., 1992), showed that a maximum of 10 % of adsorbed polymers desorbed back into solution, slightly greater yet similar amounts to this study (maximums of

3.8 % adsorbed PAM desorbed), and Nadler et al also observed that little to no desorption occurred if the soil was kept wet. Desorption in larger quantities, up to 10 % of adsorbed quantities, is more likely in lower polymer concentrations (Nadler et al., 1992). In the deep subsurface, a fluid rich environment, it can be proposed that minimal amounts of adsorbed PAM would desorbed back into solution based on data from this study, and cited studies such as Nadler et al, (1992). This result may be indicative of very low temperature environments (experiments in this chapter tested at room temperature) that PAM will remain adsorbed to the available rock surface and potentially desorb or degrade over much longer timescales. However, in higher temperatures up to 70 °C, similar to UK subsurface temperatures at 2-5km depth (Busby, 2010), PAM may be more likely to desorb. In temperatures greater than 70 °C, Guo et al., (2018) suggested that adsorption and desorption of the polymer interactions would reach dynamic equilibrium where no further adsorption would occur, reportedly stabilising at approximately 2.7 mg/g. Statistical analysis could not be conducted on the results due to the sample size and so no sample characteristics can be attributed to the amount both adsorbed and desorbed. However, due to the range of the sample type, shale (OC 7), limestone rich shale (OC 6) and 'shaley' sand (OC 2), it can loosely be concluded that there is no particular characteristic that can be attributed to the lack of desorption, particularly within the samples of interest in the UK shale gas industry; the Bowland Shale, Pendle or Millstone Grit and the Hodderense Limestone. Future work on the desorption of PAM in a hydraulic fracturing context could focus on how temperatures affect the desorption of the PAM from shale surface, and if desorption is minimal, how certain additives, such as urea (Yang et al., 2018), may be used to promote desorption if required.

5.11. Conclusions

In this part of the study, PAM continues to show high levels of adsorptivity to all samples used but this time with the linear and Freundlich isotherms performing the best of all isotherms. Estimated concentrations at maximum coverage sit within the ranges observed in the other room temperature experiments, (Section 3.7.1), up to 3917 mg/kg. Upon simulating the flushing stage of a frack at room temperature, negligible amounts of PAM desorb. A maximum of 0.919 mg/L PAM was desorbed from an adsorbed amount of 65 mg/L, equating to a 1.4 % desorption.

6. Metals Analysis of Flow-back Fluids

The data within this chapter was presented as part of a poster presentation at the BGS's UDSIG ("Use of the Deep Subsurface in the UK: What are the implications for groundwater?") conference at Burlington House, 11th-12th July 2018.

6.1. Introduction

This part of this study focusses primarily on the composition of the flow-back water from the samples of the room temperature (RT) (Chapter 3) and high-pressure high temperature (HPHT) (Chapter 4) adsorption experiments. As discussed in Section 3.3.1, some fluid was taken from the adsorption fluids and stored frozen to be analysed for metals. It is these fluids that are analysed in this section.

One of the most studied impacts of fracking is the potential for contamination from flow-back waters. Flow-back waters have the potential to contain multiple contaminants including: heavy metals, salinity and dissolved organic matter, and in general these increases are attributed to human activities (Alloway and Ayres, 1997; Wingenfelder et al., 2005). Contaminants, such as the aforementioned, are of key interest in the scientific community and for government and policy as they have the potential to endanger ecosystems, wildlife, agriculture and humans; and contaminate drinking water, even at trace levels (Mouser et al., 2016; Wang et al., 1999; Zhang et al., 2018). Multiple journal articles, reports and databases have been compiled studying flow-back water contamination, with the majority using examples in the USA (e.g., Chapman et al., 2012). Vengosh et al. (2013) used geochemical fingerprinting to delineate the impact of shale gas fluids on the environment, reviewing the majority of tight gas shales in the USA, and Warner et al (2013), explored how the discharge of wastewater has discernible impact upon local waterbodies, citing, for example, that chloride levels 1.7 km downstream were 2-10 times higher than recorded background levels. One of the largest databases for flow-back fluids is the USGS Produced Waters Database (Blondes et al., 2017) citing flow-back data for 114,943 wells located onshore, divided up by multiple factors including state, county, basin and geological period. Within this USGS database, full and thorough data is sparse as multiple wells do not show any data. Furthermore, not all parameters are reported for each well. Data within this study ranges from, but is not exclusively, conductivity, total dissolved solids, individual metals, nitrates and dissolved oxygen. A summary of USGS data that is relevant to this particular study can be viewed in Table 6.1. Multiple studies have looked at the compositions of fluids from US shales (Chapman et al., 2012; Maguire-Boyle & Barron, 2014; Kresse et al., 2012; and Shih et al., 2015) with other literature discussing the chemical composition of these US shales and how this may impact the returned fluids (Chermak and Schreiber, 2014; Phan et al., 2015). There is substantially less

literature regarding shale chemistry and produced waters specific to the UK. Multiple studies have looked at shale gas potential in the UK (eg. Andrews, 2013; Broderick et al., 2011; Jackson et al., 2014) some have considered the water quality implications. Parnell et al. (2016) studied how selenium enrichment in UK shales could impact ground waters, whilst Stuart (2012) assess groundwater impact from these type of operations specific to the UK. The M4 shale gas project assessed the wider implications for groundwater quality from a more European regulatory perspective (Jacobsen et al., 2015).

To date, only one source of UK specific flow-back water has been published: Preese Hall flow-back fluid data from 2011 can be found in (Broderick et al., 2011) and is summarised in Table 6.1.

ANALYTE	CONCENTRATION (mg/L)		
	MAX	MIN	AVG
Al	5290	0.0013	48.347
Ca	193359	0.01	5360.696
Cd	24	0.0001	0.216
Cu	130	0.0001	0.555
Fe	81800	0.00219	70.957
K	78196	0.03	811.171
Mg	137110	0.003	990.149
Mn	440.48	0.000101	6.81
Na	434403	0.1	26953.005
Pb	8187	0.00012	29.586
Si	5555	0.18	54.874
Zn	575	0.0001	11.479

Table 6.1: *Data from USGS produced waters database (Blondes et al., 2017) displaying reported minimum and maximum values, alongside the arithmetic average values for the analytes tested in this study. Data is displayed in mg/L.*

The majority of the determinant concentrations reported for the flow-back water from Preese Hall 1A lies above the tap water average (Table 7.2), suggesting a need for treatment before reuse.

DATE	07/04/2011	14/04/2011	28/04/2011	18/05/2011	14/06/2011	01/08/2011	17/08/2011	Mains Water Concentration (avg)
Time	13:20	13:30	11:10	14:00	09:55	11:00	09:30	
Conductivity 25 °C µs/cm	-	-	-	150614	133730	176000	-	- -
pH	-	-	-	6.35	7.06	6.33	-	7.54
Acrylamide µg/L	-	-	-	-	-	-	0.05	-
Lead as Pb µg/L	600	<10	<10	<40	<44.9	80.5	<100	<0.417
Mercury Hg µg/L	0.024	<0.01	<0.01	<0.01	0.012	0.09	0.038	<0.013
Cadmium Cd µg/L	1.29	<0.5	<0.5	<2	<1	6.02	<5	<0.04
Bromide mg/L	-	-	242	854	608	673	1020	<0.444
Chloride Ion mg/L	15400	34400	22200	75000	64300	58000	92800	13.5
Sodium Na µg/L	-	15100	9380	28400	23600	21700	34800	22.9
Potassium K mg/L	28.8	52.3	40.6	-	-	-	-	-
Magnesium mg/L	-	586	401	14770	1350	1370	2170	9.21
Phosphorus P mg/L	1.28	0.0771	<0.02	<0.1	<0.5	0.532	<0.2	-
Chromium Cr µg/L	25	4.03	<3	20.5	53.9	222	42.9	<0.349
Zinc Zn µg/L	565	51.5	<30	173	435	385	<300	-
Nickel Ni µg/L	20.3	<5	<5	<20	<20	<20	<50	1.2
Silver µg/L	-	-	<1	<20	<10	<20	99.4	-
Aluminium Al µg/L	596	<50	<50	<200	<100	1590	<500	<8.04
Arsenic As µg/L	6.2	<1	<1	<1	<1	2.3	<1	-
Iron Fe µg/L	66600	80700	51800	78600	112000	137000	88200	<7.62
Cobalt Co µg/L	-	-	4.96	<20	<50	<20	<50	-
Copper Cu µg/L	27.5	<10	12.4	36	<20	13.3	<50	-
Nitrogen N mg/L	10.7	52.5	33.4	98.8	77.8	47.9	121	-
Vanadium V µg/L	<4	<10	<2	<40	<100	<40	<100	-

Table 6.2: *Environment Agency analysis of dissolved salts analysis from Cuadrilla rig Preese Hall 1A. Data adapted from Environment Agency, 2011 and (Broderick et al., 2011)***.** *Metals highlighted in green are the ones analysed in this study '-'denotes no data.*

Data from the USGS shows many orders of variation in concentration (Table 7.1 - only data for the metals analysed in this study are shown), for example salinity based on sodium content can vary from between 0.1 mg/L to 434,403 mg/L, a substantially briny fluid. Very hazardous contaminants such as cadmium, lead and copper can reach maximum concentrations of 24, 8187 and 130 mg/L, respectively, all above the threshold limits for the United States Safe Drinking Water Act (EPA, 1974).

The composition of flow-back fluids may also be influenced by other variables within the subsurface, such as pH and redox state (Manju et al., 2002). Waters downhole and in the subsurface are generally less oxic than the waters being injected as part of fracking fluids (Manju et al., 2002). Typically, redox active metals such as Pb, Cd, Cu and Zn (analysed within this study) are more likely to mobilise in slightly acidic conditions, pH 5-6 and in slightly less oxic conditions (Chuan et al., 1996; Manju et al., 2002). Fluids used in this study were pH neutral, and remained neutral after HPHT experiments which used CO_2 as a pressurising gas.

Based upon some of the data seen in Table 6.1 and Table 6.2, concentrations of some metals return in great quantities, far above provided regulatory advice from multiple sources, it is of critical importance to fully mitigate and understand this risk for the future of fracking to continue safely and with greater support.

6.2. Aims and Objectives

The purpose of this chapter was to assess the potential contaminant concentrations that could return to the surface in flow-back fluid. The composition of flow-back fluids are scrutinized in the scientific community, and in the eyes of the government and the public. Policy is often shaped around the impact various contaminants may have on the wider environment. Assessing the concentrations of these contaminants could be considered in two ways, firstly, as direct results of metals increasing in fluids and returning immediately to the surface, and secondly, if metals are lost from the fracking fluid to the target formations. This study predominantly assesses the former but also assesses losses of contaminants. It must be noted that no other timescales, other than the time taken for the adsorption experiments discussed in Chapters 3 and 4, were measured, thus it was impossible to conclude if certain timescales would influence contamination or adsorbed contaminants would eventually return to the surface.

This chapter analyses all fluids taken from the RT adsorption and HPHT adsorption experiments (Chapters 3 and 4) to understand how PAM, and the rock types, influence the composition of the flow-back fluid. Fluids are analysed using ICP-OES (Inductively Coupled Optical Emission Spectroscopy). Results are then compared to multiple databases to see if certain concentrations should be of concern.

6.3. ICP-OES Theory

To measure environmental fluid samples for metals, there are typically two options available; ICP-MS and ICP-OES. The preferred method for this project was the ICP-OES method. The reason for this choice was simply because ICP-OES is a more robust against high values of TDS, typically ICP-OES can handle up to 30 % contamination whilst ICP-MS, can generally only handle TDS contamination to maximum limits of 0.2 % (Tyler, 1995). Typically, ICP-MS detection limits are up to 3 orders of magnitude higher than those of ICP-OES (Olesik, 1991), however, the contamination offered from tap water samples that have PAM and geological substances in could be high, making ICP-OES the preferred choice for this study.

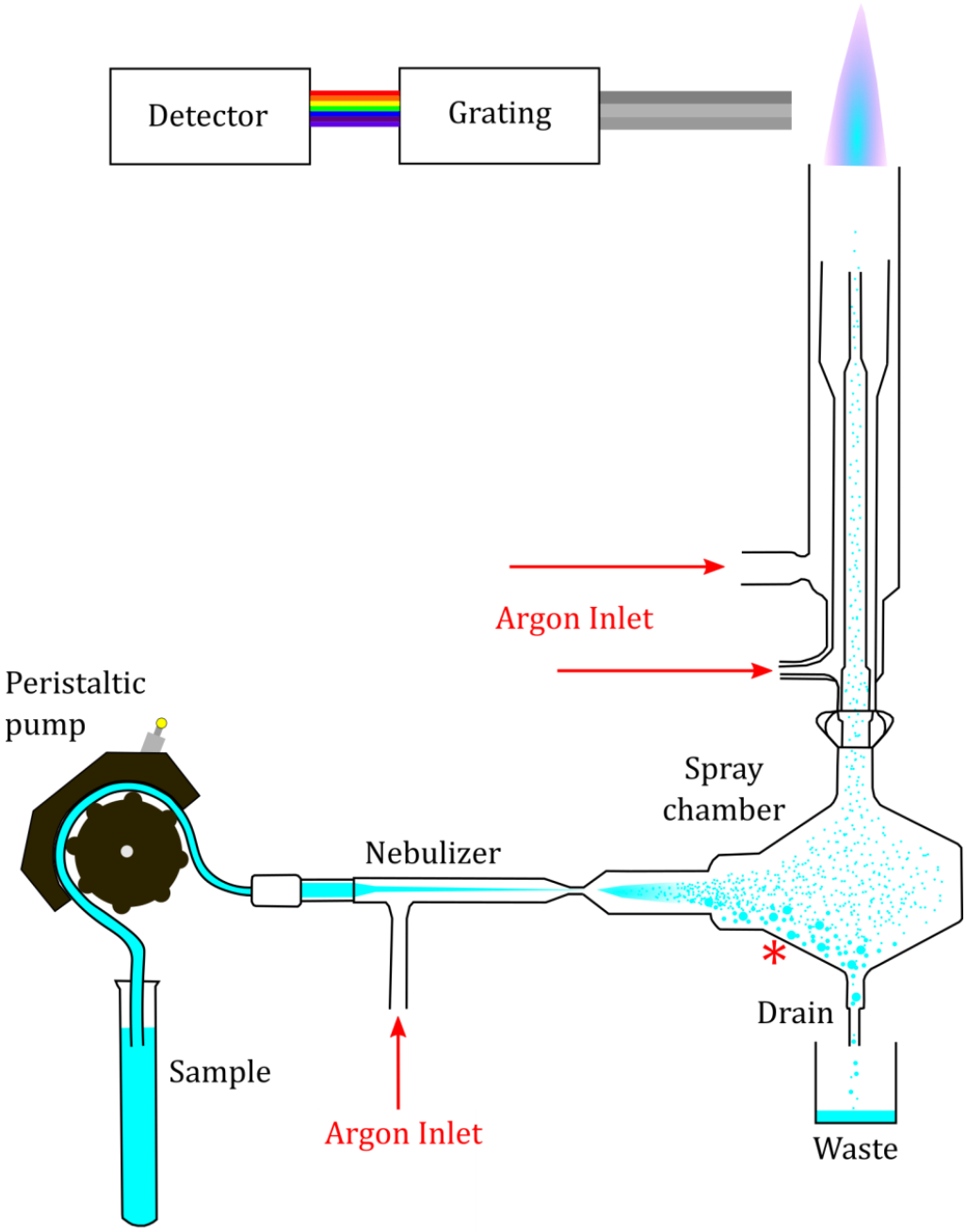

Figure 6.1: *An example diagram of a ICP-OES setup from sample to measured result. Diagram adapted from (Caruso et al., 2017).*

The basic principle of ICP-OES is as follows:

1) The sample is pumped via a peristaltic pump to the nebuliser.
2) The sample is nebulised and the resulting aerosol is then put through a spray chamber. Here, heavier or sticky clumps can fall into the waste chamber (denoted by the red *).
3) The spray is then sent through argon plasma that is generated by the argon gas passing through a high frequency electric current supplied by a coil at the end of the torch. The argon gas is here ionised and plasma is created. The plasma is then supplied at very high temperatures of 10000K.
4) When the sample spray is sent through the torch, desolvation, atomisation and ionisations of each sample take place. The electrons within the samples reach and 'excited' state.
5) When the electrons return to a lower energy position photons are emitted. The wavelengths of the photons are measured and then the result attached to the corresponding wavelengths of the analytes of interest.

For this full analysis to occur, samples needed to be at least 6 ml in quantity and would be run for 3 minutes per sample.

6.4. Adsorption Fluid Sample Preparation and Methodology

Fluids used in the ICP-OES analysis were taken from all adsorption experiments, both RT and HPHT reported in Chapters 3 and 4. The method described here for analysing metals using the ICP-OES is the identical method as was utilised for the colloid analysis of cadmium and sodium (Section 7). As previously mentioned, at least 1 ml of fluid from every single adsorption sample and stored frozen until it could be analysed by ICP. Freezing the sample would ensure no degradation or biological reactions would take place within the tap water samples. Samples were fully defrosted overnight before preparation and dilution with a ~7 % HNO_3 solution (nitric acid). Weak analytical nitric acid solution is normally used to stabilise the sample and the dissolution of metals present (Pappas, 2012).

6.4.1. Stock Preparation

Using a mixture of references, inclusive of the USGS flow back database (Blondes et al., 2017; Maguire-Boyle and Barron, 2014; Parnell et al., 2016; Shih et al., 2015), twelve major and trace metal contaminants were chosen for analysis within the flow-back fluids. These metals

were; aluminium, cadmium, calcium, copper, iron, lead, magnesium, manganese, potassium, silica, sodium and zinc.

The metals chosen would be present within the fluid and the rock within different concentration ranges, i.e, calcium or magnesium would be present in generally much larger concentrations than cadmium. To account for the likely ranges like the contaminants were divided into four different groups; “high case”, “mid case”, “low case” and “lowest case”. Due to the large range in sample type (shale, limestone and sandstone) a broad range needed to be covered so that low concentrations of the same analyte would be as detectable as higher concentrations of the same analytes but from a different sample.

For the purposes of this chapter, “stock” refers to the bulk fluid containing multiple analytes that has been produced with a mix of dilute 7 % HNO_3 and major stock solutions (Table 6.3). A “standard” is the calibration fluid produced in numerous concentration ranges derived from diluting down varying measurements of the “stock” solution (Table 6.4).

All bulk stock solutions were provided by the ICP laboratory at Durham University which were in turn sourced from manufacturers ROMIL Ltd. To produce the main stock solution, multiple measurements of pure stocks in high concentrations were added to a 7 % HNO_3 matrix, thus diluting them down into a matrix that could be easily diluted further for the production of standards. The bulk stock solution consisted of the aforementioned high, middle, low and lowest cases. The correct amount of manufacturer stock solution to be used in the bulk stock was calculated by using;

$$\boldsymbol{C_1 \times V_1 = C_2 \times V_2} \qquad \textbf{Equation 6.1}$$

For Equation 6.1; C_1 is the concentration of the pure manufacturer stock solution, V_1 is the volume to be taken from the manufacturer stock solution, C_2 is the final concentration of the diluted made stock and V_2 is the final volume of the stock solution being produced. Using this approach, a 40 ml stock solution was created (Table 6.3).

		STOCK SOLUTION				
	ELEMENT	STOCK VOL (ml)	STOCK SOLUTION (mg/L)	DILUTED STOCK VOL (ml)	VOL NEEDED FROM STOCK ml (µl)	CONC OF NEW STOCK (mg/L)
			C_1	V_2	V_1	C_2
High	Calcium (Ca)	100	10000	40	0.4	100
	Potassium (K)	100	10000	40	0.4	100
	Magnesium (Mg)	100	10000	40	0.4	100
	Sodium (Na)	100	10000	40	0.4	100
Mid	Aluminium (Al)	100	10000	40	0.1	25
	Iron (Fe)	100	10000	40	0.1	25
	Silicon (Si)	100	1000	40	1	25
Low	Copper (Cu)	100	1000	40	0.2	5
	Manganese (Mn)	100	1000	40	0.2	5
	Lead (Pb)	100	1000	40	0.2	5
	Zinc (Zn)	100	1000	40	0.2	5
Lowest	Cadmium (Cd)	100	1000	40	0.04	1

Table 6.3: *Stock solution created to be diluted further for the standards. 100 mg/L for Ca, K, Mg and Na; 25 mg/L for Al, Fe and Si; 5 mg/L for Cu, Mn, Pb and Zn and; 1mg/L for Cd.*

Using the measurements depicted in Table 6.3, a 40 ml bulk stock solution was produced containing 12 analytes in concentrations ranging from 1 to 100 mg/L. This solution would be diluted down to produce multiple standards for the purposes of creating a calibration line for ICP-OES analysis.

6.4.2. Standard Preparation

From the completed bulk stock solution, six standard solutions and a blank were produced for each run on the ICP. These standards and their concentrations can be viewed in Table 6.4. Each standard was made up as a dilution of 40 ml in a 50 ml polypropylene centrifuge tube with the addition of ~7 % nitric acid.

STANDARDS					
Name of Standard	High mg/L	Mid mg/L	Low mg/L	Lowest mg/L	Vol from stock (ml) decanted to produce 20 ml
"40"	40	10	2	0.4	8
"20"	20	5	1	0.2	4
"10"	10	2.5	0.5	0.1	2
"5"	5	1.25	0.25	0.05	1
"1"	1	0.25	0.05	0.01	0.2
"0.05"	0.05	0.0125	0.0025	0.0005	0.025 (in 50ml)
"Blank"	0	0	0	0	0

Table 6.4: *The concentration range of the ICP standards. High, mid, low and lowest are equivalent to the same labels in Table 6.3. For example, Calcium in the "40" standard would have a concentration of 40 mg/L, whereas Copper in the "40 mg/L" standard would have a concentration of 2 mg/L. 'Vol from stock' refers to the amount taken from the bulk stock solution and placed into the 50 ml centrifuge tube for dilution to 40 ml volume.*

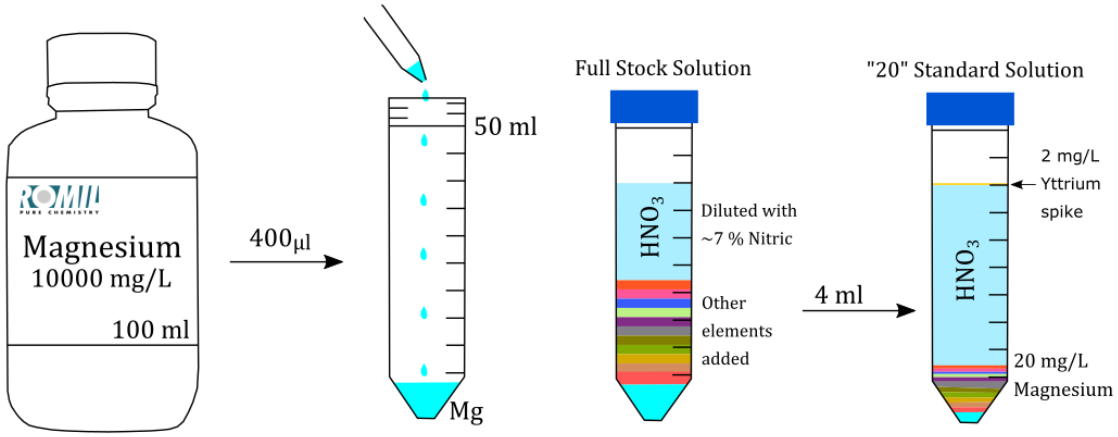

Figure 6.2: *Stock and standard preparation diagram, using Magnesium as an example fluid. To produce the stock solution, 40 ml (or 400 µl) of 10,000 mg/L stock Magnesium are added into the 50 ml centrifuge tube. The remaining analytes are added in their respective quantities and then the fluid is diluted to 40 ml with 7 % nitric acid, this is the stock solution.*

Using magnesium as an example, the production of a standard from stock to standard is shown in Figure 6.2. From the 10000 mg/L stock of magnesium, 400 µl was added to a 50 ml centrifuge tube. Other analytes were then added in their respective amounts and the fluid is then brought to 40 ml with the addition of HNO_3. No yttrium was added to the bulk stock solution. The stock was then diluted down, and as per the example in Figure 6.2, 4 ml of bulk stock solution was added to 36 ml of HNO_3 to produce the standard solution named "20" in

Table 6.4. The example fluid in Table 6.4 contains 20 mg/L of Ca, K, Mg and Na; 5 mg/L of Al, Fe and Si; 1 mg/L of Cu, Mn, Pb and Zn and; 0.2 mg/L of Cd.

6.4.3. Sample Preparation

For all samples that were to be analysed on the ICP-OES, 1 ml of flow-back sample, stored from the adsorption experiments, was pipetted into a 15 ml polypropylene centrifuge tube. This 1 ml sample was then diluted with 10 ml of ~7 % HNO_3 to produce an 11-fold dilution of every fluid sample. The 11-fold dilution was used to dilute out potential signal suppression that may have derived from the fluids with the higher PAM concentrations, due to the saturation of carbon from the PAM and the viscosity of the material. The use of the 11-fold dilution was also small enough as to not dilute out the analysis of analytes that would return in very small quantities, such as Cd. All samples were then spiked with 2 mg/L of yttrium used as an internal standard. In a fluid 'sample' of 11 ml, only 22 µl of a 1000 mg/L yttrium stock was needed for this spike in the samples, but in a standard of 40 ml, 40 µl of yttrium stock is needed for the same 2 mg/L concentration. Once all fluids and analytes were added, sample must be sealed and shaken well before analysis.

In addition to the samples of flow-back fluid from the relevant experiments in Chapters 3 and 4, eight tap waters from multiple locations around the UK were analysed for their compositions. Alongside the tap water, a simple 1000 mg/L PAM slick-water fluid is also analysed, identical to the fluids used in the experiments. Testing the tap water and slick-water fluids helps understand the variation in different mains tap waters around the country that are likely to be used by operators in shale exploitation.

The same dilution procedure is used in Chapter 7 of this thesis, when analysing fluids from the colloid experiments.

6.4.4. Yttrium Spike

To ensure that the ICP-OES was working correctly for all samples, and so that sample suppression could be accounted for, yttrium was used as a spike in all standards and samples. Yttrium is a lithophile trace element and in very rare abundance on Earth, therefore making contamination in detectable quantities both within rock and fluid samples highly unlikely. yttrium never occurs in nature as a free element, but is found in almost all rare earth minerals and uranium ores (Lenntech., 2017). Multiple literature sources using an ICP-OES analysis technique cite the use of yttrium as an internal standard (eg. Marucco et al., 1999; Zachariadis and Vogiatzis, 2010). In this study the equivalent measurement for 2 mg/L of yttrium was

pipetted into each sample and standard after the preparation. No yttrium spike is added to the stock solution.

In the results, yttrium was measured with a wavelength of 3710 nm displayed as Y3710. The intensity of all analytes, including yttrium, is measured in counts per second (ct/s). When analysis is in progress, checks on results every so often will help you know if the internal standard is working or not. A working internal standard means that all samples have the correct and same amount of yttrium in and that you have correctly pipetted and mixed the samples. If correct, yttrium will generally have very similar ct/s across all standards and samples. If not, yttrium counts will vary. Standards were run every so often in between the samples to ensure the machine is consistently working and no major measurement drift has occurred. For example, if a standard was measured at the start of the analysis with 250,000 cts of yttrium and then measured again in the middle of the sample run, the yttrium should still return approximately 250,000 cts.

6.4.5. Sample Run Order

Samples were run in batches of ~60 – 80 samples per batch as the machine could not be run overnight. Each run consisted of one set of ICP standards containing all analytes (ICP STDs) and one set of adsorption standards (PAM STDs) related to each adsorption experiment run. If two adsorption runs managed to be run in one ICP batch, the corresponding two sets of PAM standards would be run too, samples and some procedural standards (Procedural/P STDs).

ROOM TEMPERATURE		HPHT	
RUN No.	Samples	RUN No.	Samples
1	Tests	1	0 mg/L - 62.5 mg/L PAM
2	Tests		
3	Tests	2	125 mg/L - 1000 mg/L PAM
4	BH 5 OC 3 OC 1		
5	BH 4 BH 1		
6	BH 6 Rock sample tests		
7	BH 2 BH 3		
8	Tests		
9	OC 5 OC 6		
10	OC 8 OC 2 OC 4 OC 7		

Table 6.5: *Table showing the run order for all the flow-back fluids from both the RT and HPHT adsorption experiments. Multiple tests were run to test and analyse suppression from a PAM rich fluid. Run #4 for RT adsorption failed due to an ICP machine failure.*

Multiple tests were run at the start of the study to obtain the right dilution for the PAM fluid, and thus an 11 fold dilution was settled on. A flow-back fluid sample of 1 ml was diluted with 10 ml of ~7 % analytical grade HNO_3. Results were then corrected for at the end of the analysis process. Sample run #4, highlighted in red in Table 6.5, failed on the ICP.

All samples were tested for the 12 analytes displayed in Table 6.3. Of these analytes, multiple wavelengths were analysed to ensure no analytes were using the same or similar wavelengths for analysis (Table 6.6).

ANALYTE	WL 1	WL 2	WL 3	WL 4	WL 5	WL 6
Al	1670	2204	3961			
Ca	3158	3179	3736	3933		
Cd	2144	2265	2288			
Cu	2135	2199	3247			
Fe	2343	2382	2395	2599	2730	
K	4044	7664				
Mg	2025	2790	2795	2802	2852	
Mn	2576	2605	2939	3482	4030	4033
Na	3302	5688	5889	8183		
Pb	2169	2203	2833			
Si	1988	2124	2506	2516		
Zn	2062	2138	3302			
Y	3242	3710				

Table 6.6: *Analytes selected for measurements on the ICP and their respective wavelengths.*

6.4.6. Results Analysis and Quality Control

Immediately after analysis, each yttrium signal was checked for suppression. Samples that exhibited major problems were investigated. Final output results were then subtracted from their respective PAM experiment standards in two ways. This subtraction was used to understand two things:

1) What is the composition of the whole fluid that would be returning to surface, inclusive of metal additions made by adding the PAM?
    - Metal additions were processed by subtracting the 0 mg/L PAM standard from every sample processed, thus giving a result indicative of the whole fluid that is returned.
2) What have the rock samples added to the composition of the flow-back fluid, i.e. minus the original frack fluid concentration?
    - The addition from the samples is processed by subtracting the relevant PAM standard concentration from the sample with the same concentration. This would give a result indicative of contaminants that may have been added (or in some cases been subtracted) from the bulk fluid by the sample. For example, the results for the 62.5 mg/L OC 7 (2) sample would have the 62.5

mg/L PAM standard of that adsorption run subtracted from it to observe increases of decreases per analyte.

Negative values in this process are useful. Negative values represent uptake of these contaminants by the shale as there will be less in solution than at the beginning of the experiment.

Once all data has been processed, accounting for '1' and '2' above, all values were multiplied by 11 to account for the sample dilution. This final result is the observed concentration of the analyte from each 40 ml experiment detailed in both Chapters 3 and 4.

Ratios of the losses and gains of certain metals are then calculated using concentration range and comparing it to the original standard fluid. These values were compared to 1, where > 1 is a gain (increase into the original fluid) and < 1 is a loss (decrease from the original fluid). For this analysis, PAM concentration ranges were amalgamated and results based purely on sample type. A paired sample t-test was conducted on all results from the loss or gain ratio data based upon factors of metal type, experiment type, and sample type.

Line graphs were plotted by analyte type and concentration range for each sample. These graphs aided analysis into how PAM concentration could affect the composition of the flow-back fluid, both in total returned fluid concentration range, and the concentration range of anything 'added' by the rock type.

Tap water (or mains water), as the predominant carrier fluid in hydraulic fracturing fluids, is also analysed as part of this study. Mains water will vary in concentrations of certain metals (albeit below regulatory values) and this will depend on factors such as aquifers, piping, sampling sites and infrastructure. The mains water used in this study as the carrier fluid comes from the Department of Earth Sciences Environmental Laboratory taps. An analysis of Durham University tap water is compared to various tap waters across the country, and both United Utilities water composition (as used in Preese Hall (Broderick et al., 2011)) and Northumbrian Water sample testing (the water from Durham but at the point of sample for NWL) were included.

A three factor ANOVA was undertaken to assess the difference between the overall values. The three factor ANOVA would assess if there was a significant difference between the losses and gains, to the ratio of 1, of the RT and HPHT datasets. The three factors included were;

1) Experiment: Either RT or HPHT.
2) Sample: Samples BH 6, OC 5 and OC 7 were used in this analysis. A comparison between BH 5 RT and BH 5 HPHT was not possible as fluid data from BH 5 RT was unavailable due to machine failure (Figure 6.4).
3) Metal: Ratio values for each individual metal were available for all data.

6.5. Suppression associated with PAM in the matrix

If the internal standard was suppressed, then analytes in the sample could also be suppressed. With a matrix fluid that was rich in PAM and sodium, in quantities between 20 and 100 mg/L, signal suppression becomes an issue. With the addition of PAM to the matrix, the fluid is more viscous or 'stickier', the full analyte is not being homogeneously distributed either in the fluid mixture or in the machine components.

The main problem of the PAM-rich fluids used in this study is the viscosity of these fluids. The viscosity of these PAM-rich fluids is highly dependent on the concentration of the solution, shear rate and temperature (Jung et al., 2016). Higher concentration PAM fluids are more viscous than fresh or DI water. When samples were analysed in the ICP-OES, no fluids were heated until they reached the plasma torch. All fluids were initially sampled at room temperature (15 – 20 ^{o}C) after either RT or HPHT experimentation. Heating may have caused subtle changes to the viscosity of the fluid which may have varied amongst runs.

6.5.1. Suppression on Room Temperature Flow-back Samples

Yttrium was consistently measured in all samples and sample runs at the same 2 mg/L concentration. Data from this can be plotted to observe drift or suppression that may be present in each sample. The following plots (Figure 6.3 through Figure 6.9) demonstrate this for the flow-back fluids from the room temperature adsorption experiments. Each plot is one run on the machine, and the different samples analysed per respective run are colour coded, as per the legend. In summary, the legend refers to:

- ICP STDs: *Analyte standards run to calibrate machine*
- PAM STDs: *Standards used in the respective adsorption experiment*
- P STDs: Procedural Standards. *These are 'ICP STDs' placed in the sample run for second or third measurement if a different results is provided from the first, there is an issue.*

All plots display the same y axis to show variability in machine sensitivity between different sets of runs. All samples here have been diluted 11-fold, so the actual ICP-OES measured concentration range of PAM is between 1.42 mg/L and 90.9 mg/L.

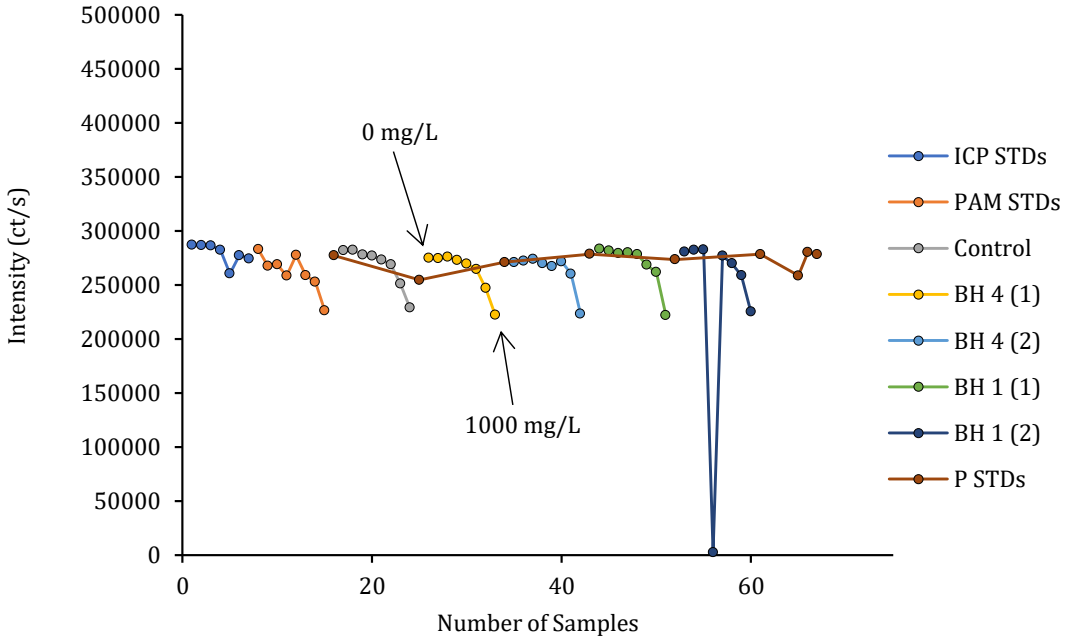

Figure 6.3: *Intensities of Yttrium 3710 for the 4th run of room temperature flow-back fluids. Note the consistent curve of each sample when the sample concentration of PAM increases.*

An example of how PAM concentration supresses the yttrium 3710 intensity is shown in Figure 6.3. At the top left of each coloured curve, annotated in Figure 6.3, is the 0 mg/L and 15.625 mg/L (14.42 mg/L PAM after dilution) with the base of each coloured curve (bottom right) having the greatest concentration of PAM (1000 mg/L).

Procedural standards, re-runs of the ICP standards that are used to calibrate the machine, are run throughout each sample run on the ICP. These procedural standards should exhibit the same results as the ICP STDs tested at the beginning of the run. If the procedural standards (P STDs) do not match the ICP-STDs then the sample run must be paused whilst issues are rectified. As shown in both Figure 6.3 and Figure 6.4, procedural standards (P STDs) exhibit very similar intensities to the 'ICP STDs'. Results were plotted to show similarities, or differences, between standards, samples and procedural standards.

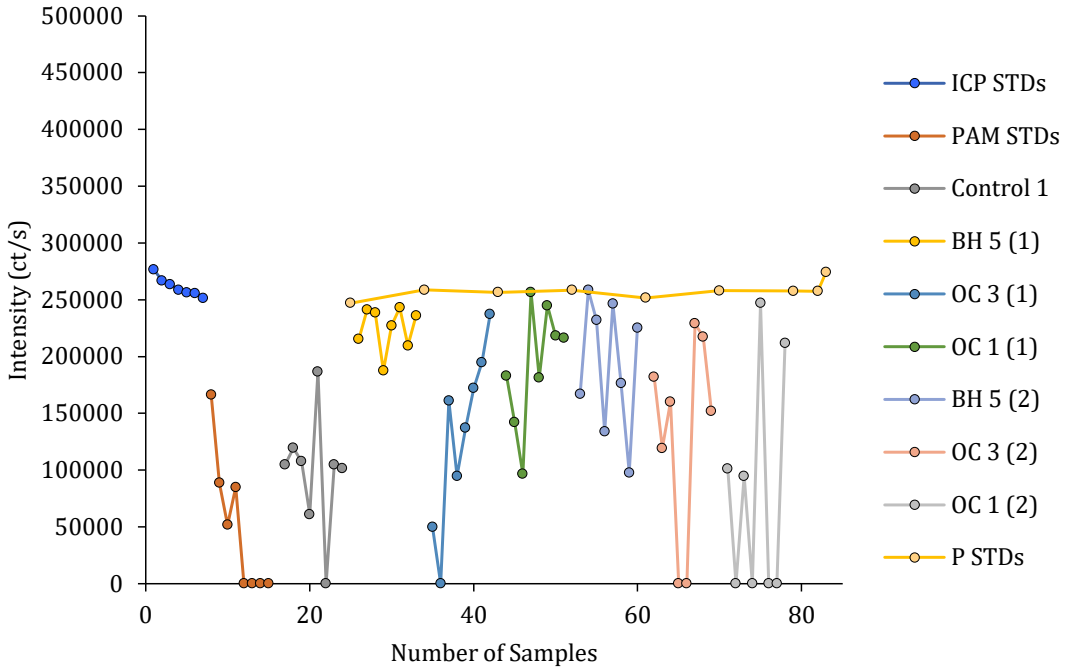

Figure 6.4: *Intensities of Yttrium 3710 for the 5th run of room temperature adsorption flowback fluids. As seen above, the suppression observed here is a lot more random in comparison to that shown in Figure 6.3.*

The samples shown in Figure 6.4 (ICP 5th run) were rendered unusable due to the scattering of suppression. This scattering was not consistent with the typical curve pattern of yttrium for the PAM concentration ranges (Figure 6.3). The starting intensity of Y3710 (ICP STDs) (Figure 6.4) is similar to that seen in the 4th run (Figure 6.3). Counts range between 250,000 and 270,000 ct/s.

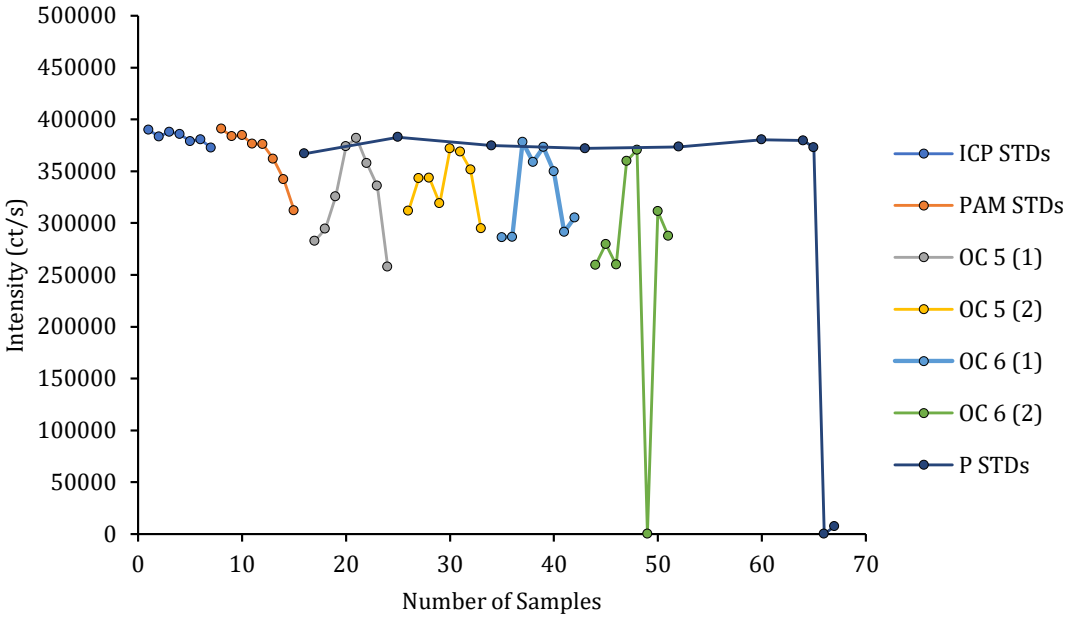

Figure 6.5: *Intensities of Yttrium 3710 for the 9th run of room temperature adsorption flow-back fluids. As seen above the suppression is less random than those observed in Figure 6.4 but a lot more random than those observed in Figure 6.3.*

Comparing run #5 against run #9, a more consistent pattern of suppression is observed in run #9 (Figure 6.5), however the patterns of suppression are still not as uniform or consistent as the suppression pattern seen in Figure 6.3 (run #4). The signal intensities observed in Figure 6.5 are in the region of 350,000 ct/s to 400,000 ct/s, higher than those in both Figure 6.3 and Figure 6.4. Procedural standards in Figure 6.5 still follow a pattern consistent with the respective initial ICP standards.

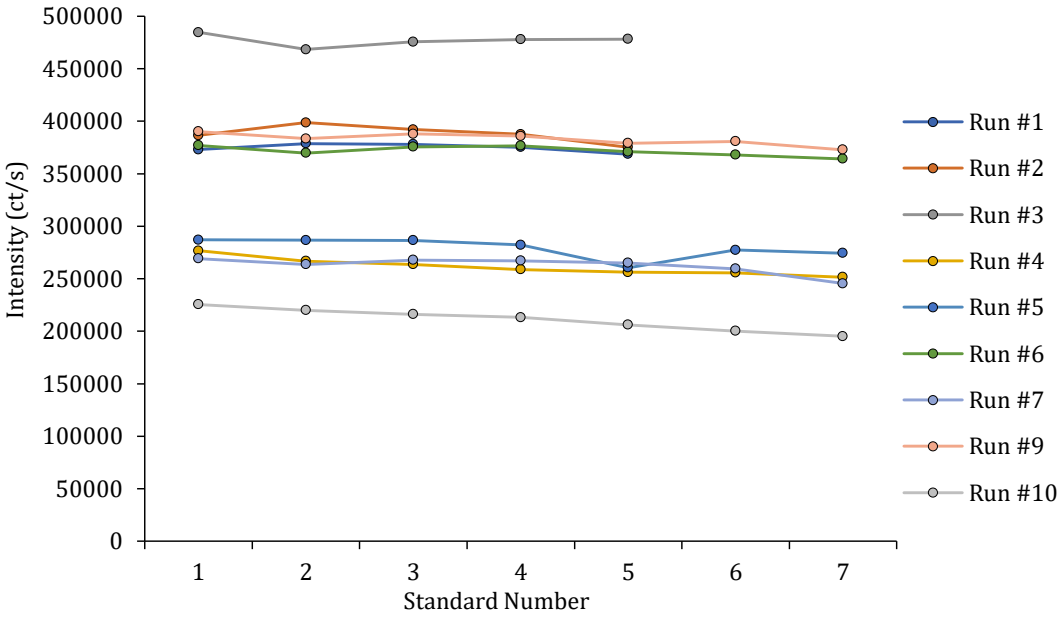

Figure 6.6: *Standard intensities summarised for all room temperature adsorption flow-back sample runs and sample tests. This depiction shows the intensity variation per operational run of the machine, independent of sample or sample type.*

The variability in machine sensitivity across all runs for flow-back fluids taken from the RT adsorption experiments can be viewed in Figure 6.6. Sensitivity (signal intensity measured in ct/s) varies amongst all runs, despite containing the same concentration and amount of yttrium in each run. Run #1 (478,210 ct/s) exhibits over twice the ct/s for yttrium 3710 than run #10 (195,240 ct/s) despite all containing the same 2 mg/L.

6.5.2. Suppression on HPHT Flow-Back Samples

Only two sample runs on the ICP were needed for the full suite of HPHT flow-back fluids. Due to the nature of how the HPHT experiment was undertaken, ordered by PAM concentration rather than ordered by sample as per the RT experiments, runs on the ICP machine were based upon this premise. Run #1 would account for PAM concentrations between 0 and 62.5 mg/L PAM, and run #2 would account for the remaining 125 to 1000 mg/L PAM concentrations.

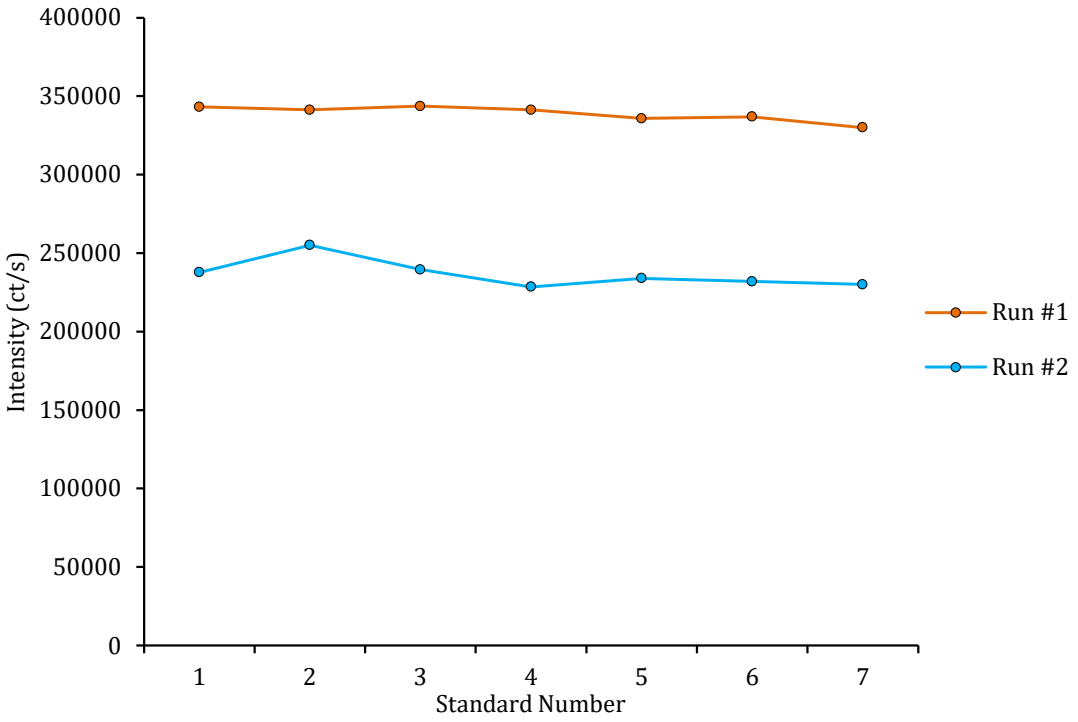

Figure 6.7: *Intensities of standards for all HPHT adsorption flow-back sample runs.*

Yttrium intensities of the standards in both runs #1 and #2 varied but stable, as shown in Figure 6.7. No notable deviations from either line were observed. Intensities shown in Figure 6.7 replicate the intensities of the samples seen in Figure 6.8 for run #1 and Figure 6.9 for run #2. Sample values for HPHT run #1 sat at intensity values of ~ 350,000, as do the standards. Only higher PAM concentrations from the 'PAM STD's' show deviation from the value of 350,000 ct/s (Figure 6.8). More deviation was observed in HPHT run #2 (Figure 6.9) with the higher PAM concentrations.

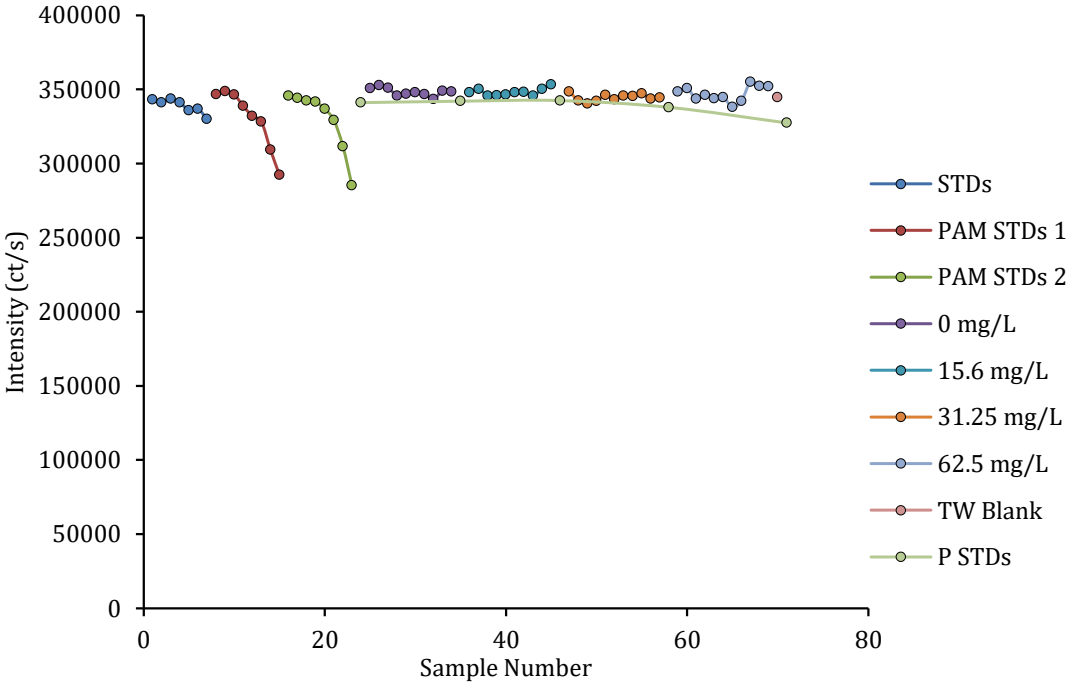

Figure 6.8: *Intensities of Yttrium 3710 for run #1 of HPHT adsorption flow-back fluids. Due to the nature of the HPHT adsorption experiments, same concentration but different samples per batch, sample runs were based on PAM concentration rather than samples.*

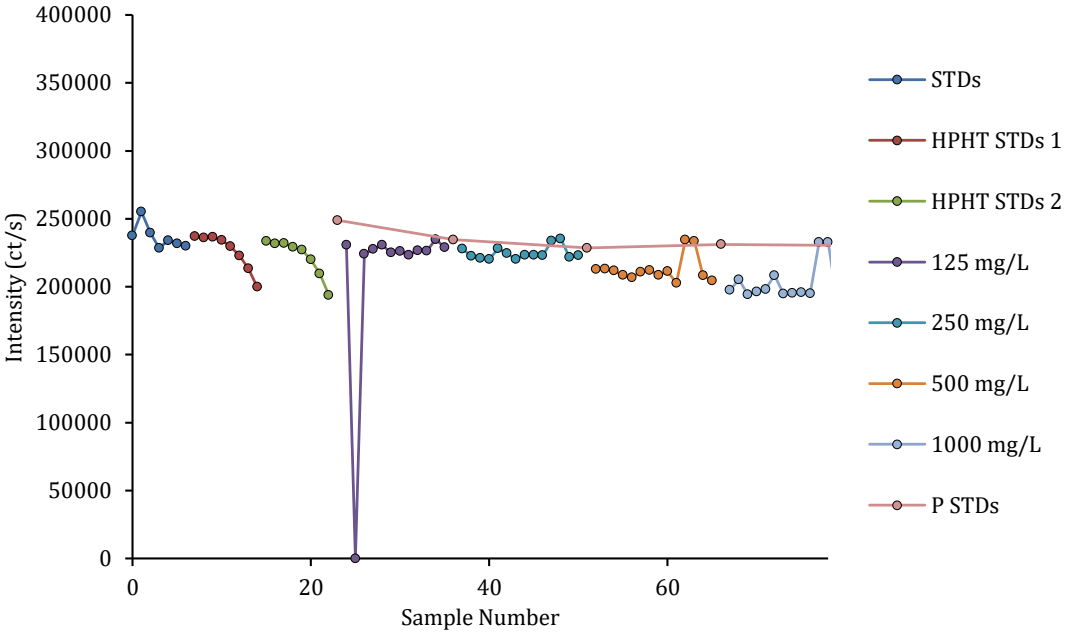

Figure 6.9: *Intensities of Yttrium 3710 for run #2 of HPHT adsorption flow-back fluids.*

Throughout both ICP runs for the HPHT flow-back fluids, there were no obvious problematic suppression issues caused by the PAM. Only one sample in run #2 appears to have

been failed by the internal standard. Procedural blanks in both runs maintained consistent ct/s with the ICP STDs and the samples.

Suppression, when necessary, could be multiplied out to produce corrected values. This could not be undertaken on sample run #5 where values were unsystematic.

6.6. Fluid Analysis Results

This section of the study is divided into three sub-sections. The first sub-section analyses the typical compositions of tap water, used as a base fluid in fracking operations and a 1000 mg/L PAM slick-water fluid. The second sub-section exhibits the results for the flow-back fluid from the room temperature adsorption experiments. The final and third sub-section exhibits the results of the flow-back fluids for the HPHT adsorption experiments.

6.6.1. Tap Water and Slick-Water Standards

Mains tap water is predominantly used as the main carrier fluid in hydraulic fracturing operations. It is the base carrier fluid that contains all other additives and proppant. Slick-water fracking fluids usually range between 90-99 % water (EPA, 2015; Gregory et al., 2011; Hammond et al., 2015) with the remaining as additives and proppant. Mains tap water compositions could vary hugely due to multiple reasons including piping, storage, and aquifer location. Here, a range of mains tap waters from around the UK have been sampled to examine this difference (Figure 6.10).

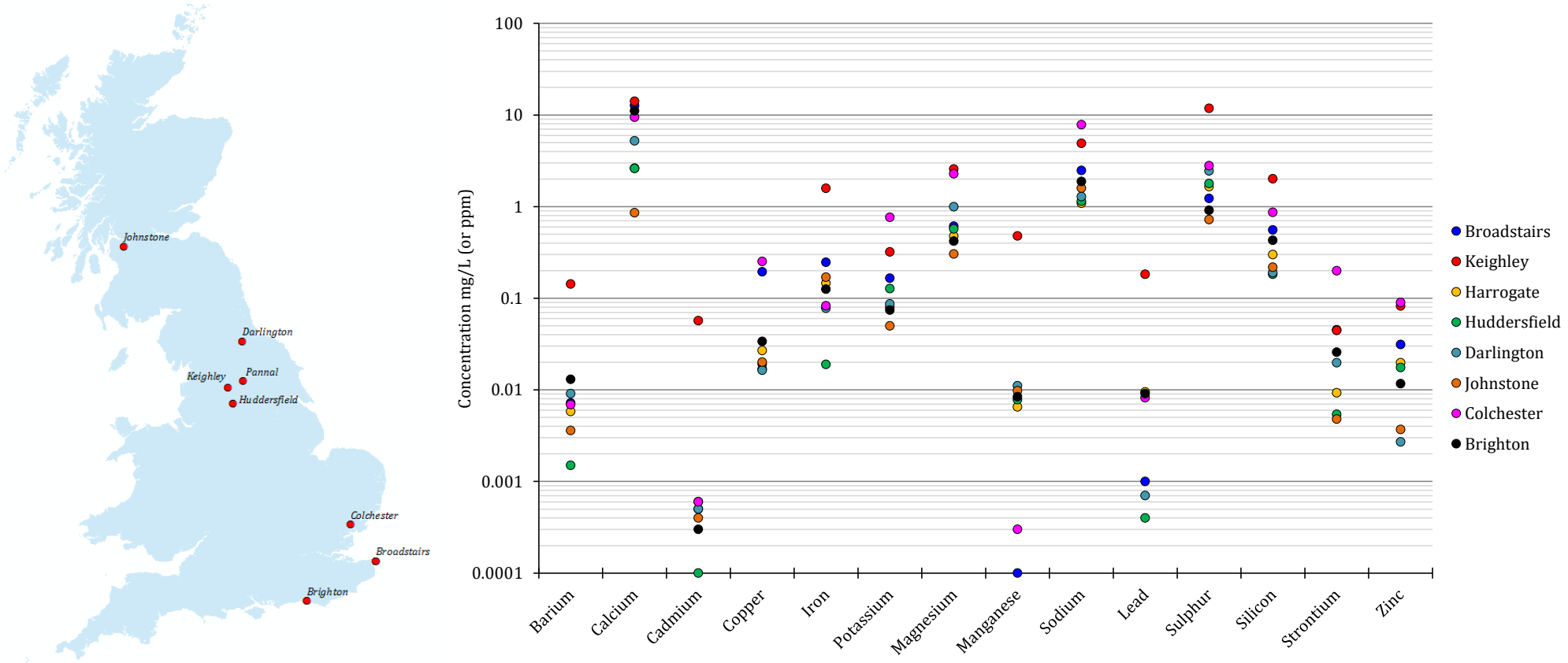

Figure 6.10: *The variation in tap water compositions from various locations in the UK. Note the logarithmic scale.*

A compositional analysis of the mains tap water used in the aforementioned experiments (Durham university tap water) is displayed alongside the typical composition of the relevant Northumbrian Water sampling site (Northumbrian Water Ltd, 2017) (Table 6.7 and Figure 6.11). Results of the compositional analysis of the 1000 mg/L PAM solution are displayed in Figure 6.12.

	DURHAM UNIVERSITY			NORTHUMBRIAN WATER		
	Max	Min	Avg	Max	Min	Avg
Al	0.829	0.003	0.126	0.24	0.018	0.036
Ca	24.277	15.521	18.688			
Cd	0.001	0.001	0.001	0.000017	0.000009	0.0000128
Cu	0.301	0.022	0.119	0.069	0.002	0.020
Fe	0.167	0.003	0.028	0.150	0.002	0.014
K	1.192	0.985	1.083			
Mg	4.616	2.555	3.389			
Mn	0.036	0.001	0.006	0.01	0.00022	0.0008338
Na	8.818	1.059	6.685	8.8	7.6	8.238
Pb	0.186	0.013	0.051	0.002	0.000033	0.0003133
Si	1.301	0.261	0.735			
Zn	0.768	0.032	0.450			

Table 6.7: *Composition of tap water at Durham University and from the Northumbrian water sampling site. Concentrations are displayed in mg/L. Gaps denote where no data was available. A tap water blank was measured with each sample blank, results above are the averaged results for all data.*

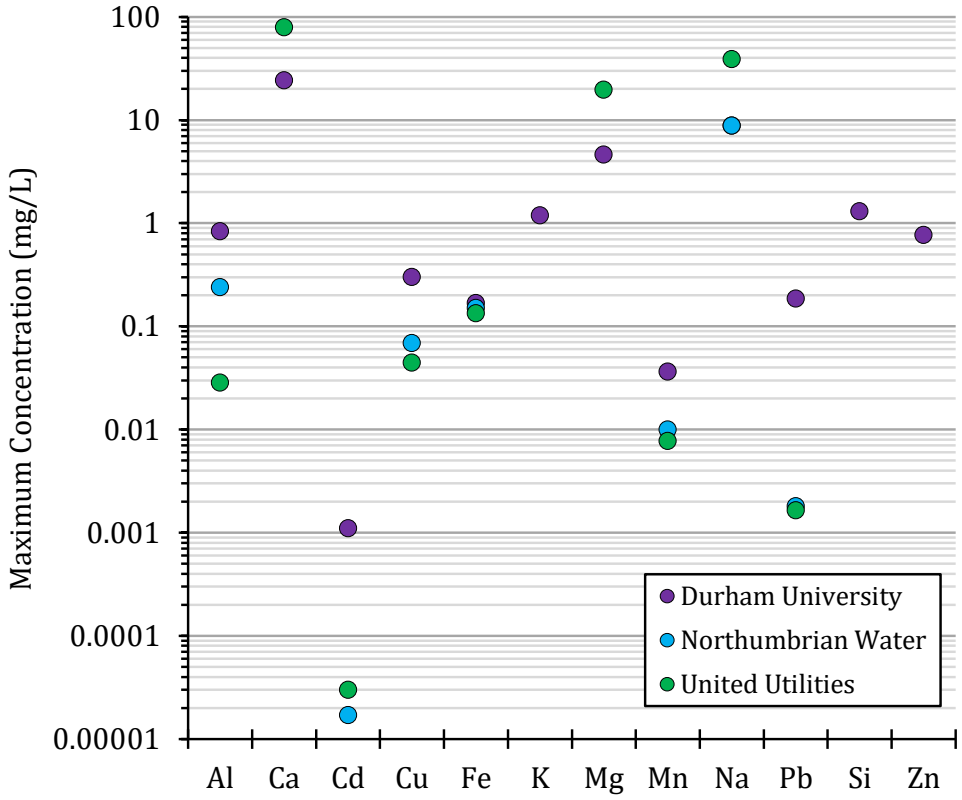

Figure 6.11: *Scatter plot of data exhibited in Table 6.7. Additionally, approximate maximum values for United Utilities mains water (the supplier for Preese Hall 1A) are also plotted for reference. Note logarithmic scale. Some data are missing due to limited datasets of differing water company sampling procedures.*

The mains tap water used in all of the experiments in this study is typical of the type of carrier fluid used in fracks, particularly in the UK. Values between Durham tap water and the NWL (Northumbrian Water) sampling site do vary (Table 6.7), Data in Table 6.7 shows the variation between the water used in this study (Durham University), the water used at Preese Hall (United Utilities) and the closest to sampled water for Durham University, independent of infrastructure influences (Northumbrian Water). Durham university tap water shows a greater range across max, min and average values and overall, maximum concentrations observed are higher with Durham University tap water. Copper is 4.3 times greater, cadmium 64.7 times and lead 103 times in Durham university tap water than at the NWL sampling site. This difference, or increase, may be due to piping and workings between sampling site and the point of source at Durham University.

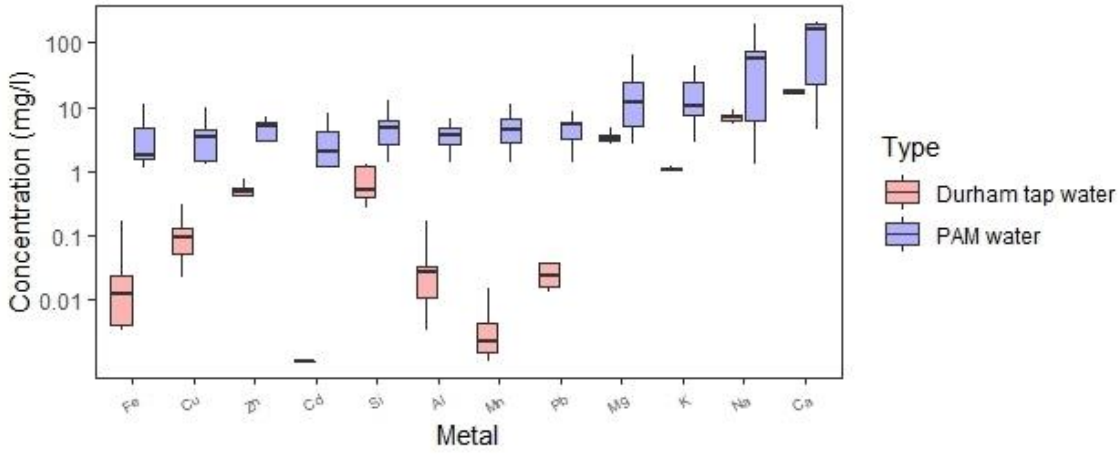

Figure 6.12: *Composition of a 1000 mg/L non-ionic PAM solution (the slickwater fluid used in all the aforementioned experiments) compared to the mains tap water at Durham University with no PAM added.*

When 1000 mg of non-ionic powdered PAM is added to 1 L of mains tap water, the composition changes (**Error! Reference source not found.**). The addition of the PAM to a freshwater fluid increases the pH to 7.16 from 6.61 and the conductivity from 211 μS/cm to 1369 μS/cm (calibrated to 1999.99 μS/cm). In total, 9 out of the 12 metals tested increase in concentration with only three decreasing (calcium, magnesium and silicon). The largest increase is that of cadmium, up by 392 times to 0.432 mg/L. Once the PAM solution is made the element with the highest concentration is now sodium, up 48 times to a maximum of 431 mg/L. Adding 1000 mg of PAM to 1 L of water produces a slightly saline fluid initially which will be pumped downhole.

6.6.2. Room Temperature Flow-back Results

In this section, results for 11 of the 14 room temperature adsorption samples are exhibited. The lack of data for the three remaining samples, OC 1, OC 3 and BH 5, was due to the ICP-OES failure for run #5, as discussed in Section 6.5.1 . Results in this section are divided into two main sections:

1) Bulk Flow-back Results: Testing the ratio of concentrations in flow-back to that of the original input water (increases to decreases from original composition) of the metals dependent on sample. Data in this section is depicted as a ratio of 1. Values > 1 depict an increase of that metal from the original quantity in the starting 1000 mg/L PAM solution, and values < 1 represent a decrease in solution concentration from the original 1000 mg/L PAM solution.

2) Individual Flow-back results: Analysing the results per sample and displaying the actual concentrations returned in flow-back fluids.

6.6.2.1. Bulk Flow-back Results

In this section, the whole fluid is analysed, irrespective of initial PAM concentrations. Here, data is expressed as the ratio of the observed concentration to that in respective sample of the PAM concentration standard. These results are then plotted to see the overall mean increases and decreases per sample (Figure 6.13).

Results show that across all samples, all but one metal showed an average increase into the flow-back fluid (Figure 6.14). Copper is the only exception where the concentration is consistently lower than the original fluid in all but one of the produced water samples (OC 8) (Figure 6.13).

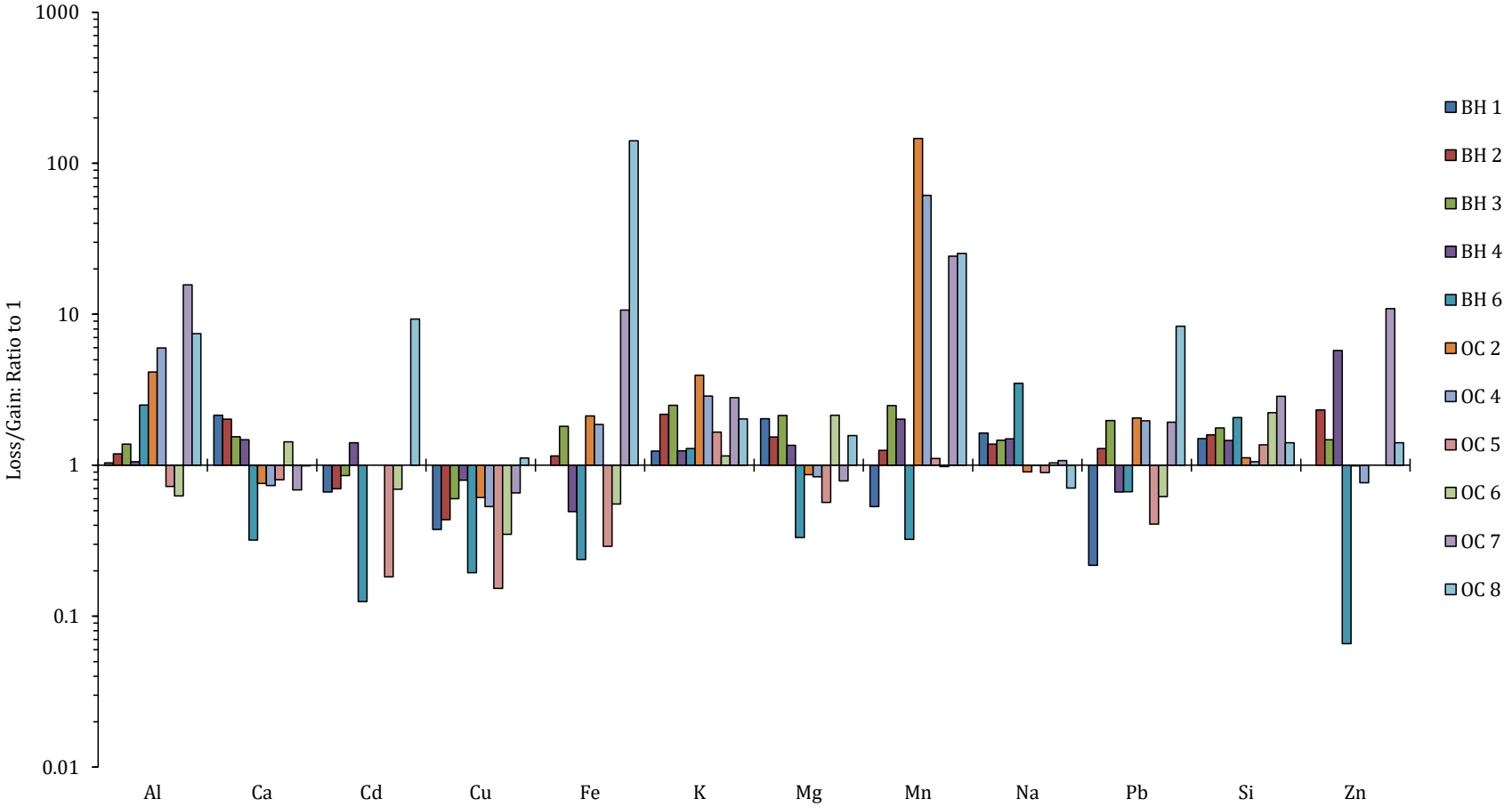

Figure 6.13: *The increase ratio of the various analytes coloured by sample name. Values > 1 represent an increase into the fluid, whilst < 1 represent a decrease. Data plotted here utilises all PAM concentrations to show a maximum total per sample.*

ANALYTE	RATIO Loss/Gain
Al	3.796
Ca	1.172
Cd	1.392
Cu	0.529
Fe	14.561
K	2.082
Mg	1.288
Mn	24.138
Na	1.371
Pb	1.829
Si	1.674
Zn	2.630

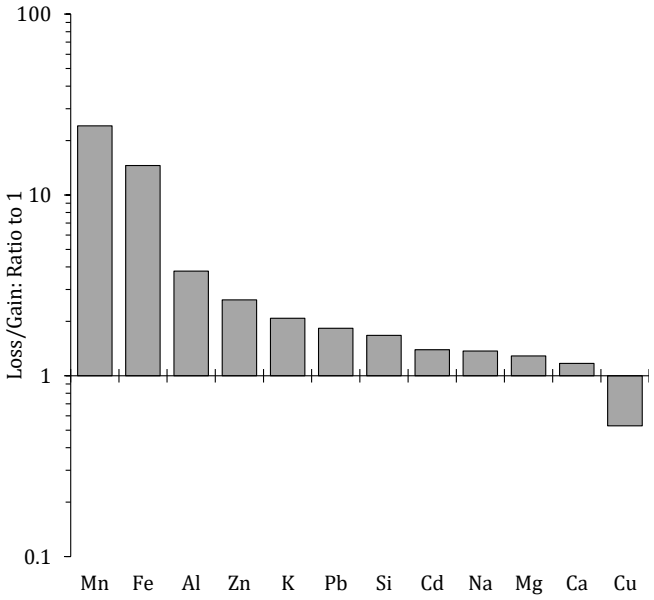

Figure 6.14: *Average increase ratio to 1 for all metals irrespective of PAM concentration or sample type.*

ANALYTE	RATIO Loss/Gain		
	Sh	Sst	Lst
Al	4.116	4.105	0.627
Ca	1.273	0.849	1.429
Cd	0.625	3.157	0.693
Cu	0.512	0.627	0.349
Fe	2.315	47.804	0.554
K	2.016	2.544	1.151
Mg	1.288	1.002	2.143
Mn	13.175	57.437	0.981
Na	1.649	0.835	1.036
Pb	1.245	3.596	0.619
Si	1.756	1.299	2.226
Zn	3.038	1.200	n/a

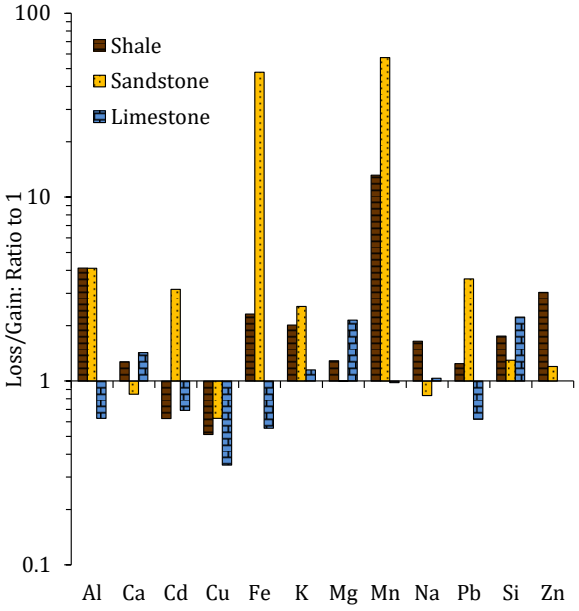

Figure 6.15: *Average increase ratio to 1 for all metals irrespective of PAM concentration but plotted by sample type; sandstone, shale or limestone.*

Manganese (Mn) had the highest average increase across the all the samples: up to 24 times the initial amount in the slick-water fluid (Figure 6.14). Iron (Fe) had the second largest increase with an average of 14 times the amount injected.

Dividing the samples by lithology, sandstone, shale and limestone (Figure 6.15), the large increases in the manganese and iron are from sandstone dominated lithologies. All sample types show decreases in copper and only limestone and shale showing decreases in

cadmium; albeit in concentrations that are so small they are negligible. Overall, shale samples show decreases in only two elements, cadmium and copper. Sandstone samples show decreases in solution with three elements (calcium, copper and sodium) and limestone samples show a decrease for six elements, aluminium, cadmium, copper, iron, manganese and lead. Whilst sandstone samples exhibit the greatest increases (57 times greater for manganese and 47 times greater for iron), shale samples produce the lowest number of decreases. Shale samples have the greatest influence on increases in concentrations of the metals analysed.

6.6.2.2. Metal Results per Sample

This section exhibits results for the room temperature adsorption experiments flow-back fluids using two approaches:

1) Accounting for all metal concentrations that have increased or decreased from the original pre-experiment fluid by the 'fracking of a rock' (Figure 6.16). This method subtracts the compositional concentrations of certain metals already in the fluid, before adsorption experimentation occurs.
2) Accounting for the total concentration of metals within the fluid (Figure 6.17). This method subtracts only the zero standards containing no PAM and accounts for the total amounts of all metals, irrespective of composition pre-experiment – essentially subtracting the concentration of tap water and being the final fluid that would be returned to surface.

The results of this are displayed on two A3 foldouts. Full tables of data can be found in Digital Appendix F.2.

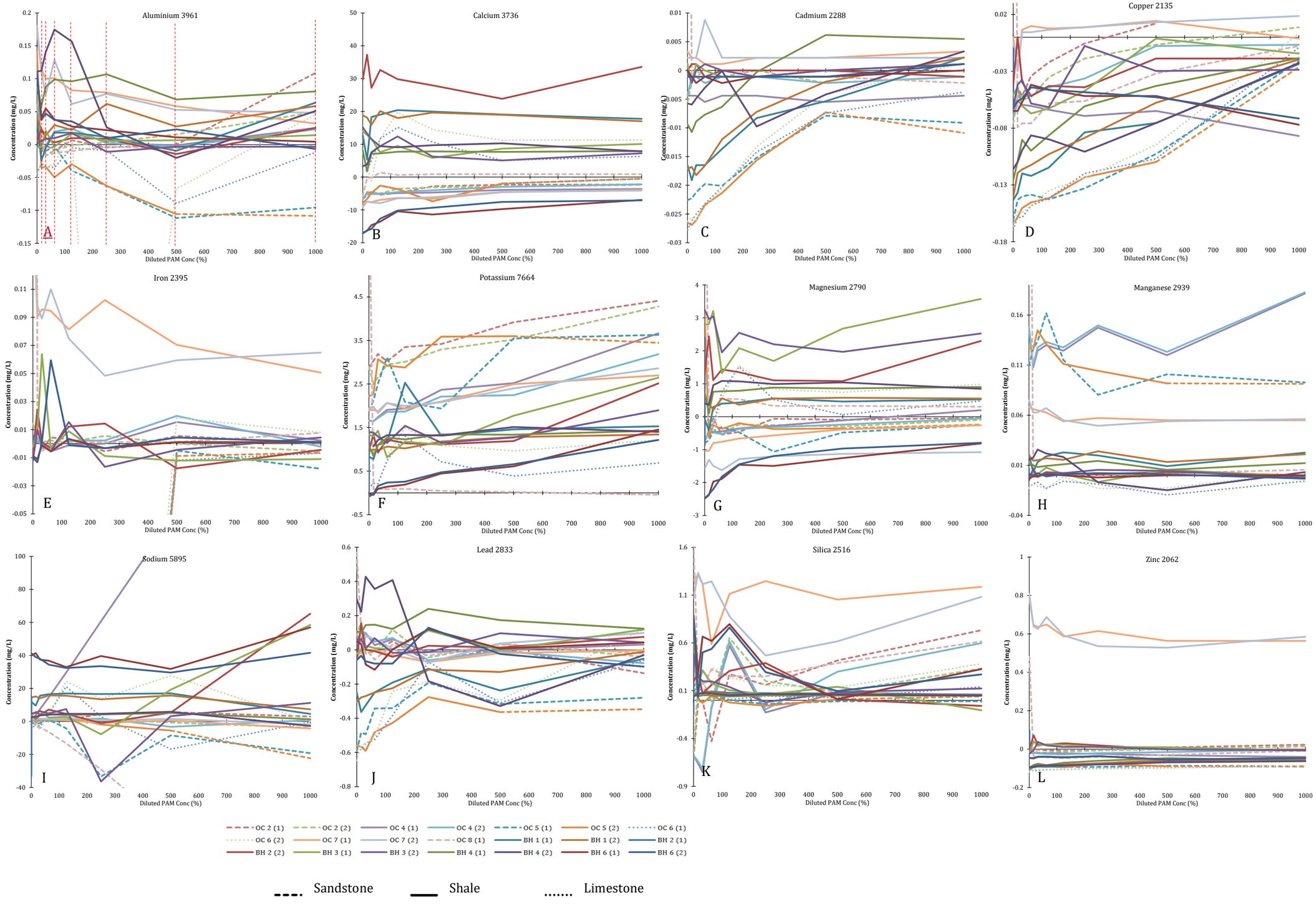

Figure 6.16: *All sample data plotted per analyte showing composition of increases in metals from the shale. Analysis here has subtracted metals within the initial concentrations of the PAM slick-water fluid. Data on all graphs is plotted for PAM concentrations of 15.625, 31.25, 62.5, 125, 250, 500 and 1000 mg/L PAM - denoted by the red vertical lines shown on aluminium (top left).*

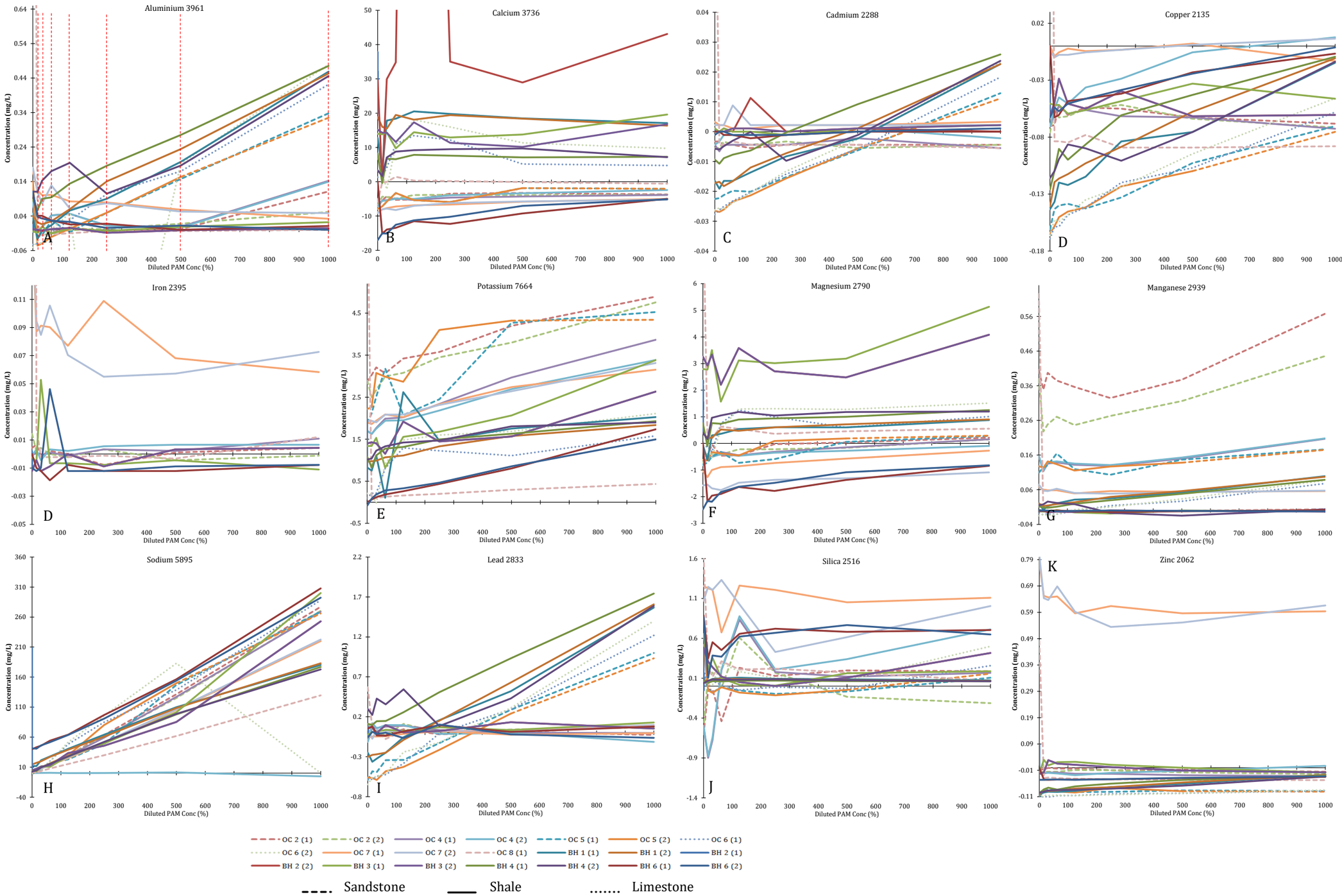

Figure 6.17: *All samples accounting for total concentration of flow-back fluid, inclusive of concentrations of metals in the initial slick-water fluid. Data on all graphs is plotted for PAM concentrations of 15.625, 31.25, 62.5, 125, 250, 500 and 1000 mg/L PAM: denoted by the red vertical lines shown on aluminium (top left).Sample BH 2 (2) displayed erroneous results at 125 mg/L PAM.*

Data displayed on the multiple plots of Figure 6.16 and Figure 6.17 show trends generally based upon PAM concentration, i.e.ata from both these sets of figures exhibits the trends associated with an increase in PAM concentration.

Aluminium

Ignoring the composition of the PAM slick-water fluid (Figure 6.16), there is a general increase in Al concentration amongst the majority of the samples. The maximum Al concentration observed was 0.17 mg/L with a concentration of 62.5 mg/L PAM for BH 4 (2). Al concentrations at 1000 mg/L PAM range between 0 and 0.08 mg/L. Four samples show decreases of Al, none of which are shale lithologies (OC 6 1 & 2 and OC 5 1 & 2). Analysing the whole fluid, inclusive of the dilutions of a 1000 mg/L PAM solution (Figure 6.17), there was a notable increase from 0 mg/L Al for samples BH 4, OC 6, BH 1 and OC 5. The samples that showed an increase had Al concentrations ranging from 0.47 mg/L to 0.32 mg/L at a PAM concentration of 1000 mg/L. The remaining samples showed more constant values of Al between 0 and 0.04 mg/L whilst PAM concentrations increased to 1000 mg/L. Sample OC 4 showed an increase up to 0.13 mg/L at 1000 mg/L PAM from 0.006 mg/L at 500 mg/L PAM.

Calcium

Calcium remains, in general, constant and unchanged with an increase in PAM concentration. Some samples clearly favour adsorbing calcium (BH 6, OC 4, OC 5, OC 7 and OC 8) whilst in the remaining samples the PAM favours binding released calcium. The highest concentration of calcium at 1000 mg/L was 33.6 mg/L with sample BH 2, unsurprisingly containing the second highest TIC and the second highest amount of Ca (Section 2.4.1). The lowest concentration of calcium at 1000 mg/L PAM was -7 mg/L with sample BH 6 (2), alongside BH 6 (1). Analysing the total fluid, the same trend was observed, concentrations ranged between 19.6 and -5.1 mg/L. No increase or decrease in calcium concentration appears to be related to an increase in PAM concentration.

Cadmium

Cadmium was present in nearly all samples in small concentrations, sometimes negligible and below the detection limit of this analysis. Results show that cadmium present is generally adsorbed to the sample rather than being bound in the PAM-rich fluid. A maximum concentration of 0.005 mg/L of cadmium was released into the fluid for BH 4 (1)

but the majority of samples show negligible release into the fluid, primarily adsorbing to the samples. Inclusive of the PAM slick-water, the total fluid, up to 0.02 mg/L was returned to the surface.

Copper

Copper exhibits very similar results to cadmium, based on an increasing PAM concentration. In all samples, copper concentrations were less than 0 mg/L. The maximum concentration of copper observed was 0.01 mg/L for sample OC 7 (2) at 1000 mg/L PAM, and the same sample (OC 7 (2)) exhibits a maximum concentration of 0.006 mg/L when the total fluid is accounted for. Between all samples, copper in solution ranges from -0.08 mg/L to 0.0066 mg/L in fluids returned to surface.

Iron

Returned iron concentrations were higher in sample OC 7 than the remaining samples. The highest concentrations observed are between 0.07 and 0.05 mg/L for sample OC 7. The remaining samples concentrations range between 0.0044 and -0.01 mg/L, increasing to 0.01 and -0.01 mg/L analysing the total fluid returning to surface. There was no obvious increase or decrease in iron concentrations across all samples that were associated with an increase in PAM concentration. Using the composition of all fluids returned from all samples, iron may be removed from solution or returned to surface. Removal is sample dependent, but concentrations would be generally considered low with 0.01 mg/L as a general high, excluding the 0.07 mg/L observed with sample OC 7.

Potassium

Potassium was the only metal that exhibits an increase across all samples both in the metals added to the fluid, and the total fluid analysis. A trend of increasing potassium in relation to an increase in PAM concentration was also observed for all samples. Sample OC 8 had the lowest potassium content observed, at 0.43 mg/L The remaining concentration in the remaining samples ranged from 0.68 to 4.41 mg/L, increasing to between 0.43 and 4.89 mg/L when analysing the total fluid returned. The highest values of potassium were linked to the sandstone based samples, OC 2 and OC 5, with values of 4.89 and 4.34 mg/L

respectively at a PAM concentration of 1000 mg/L. The increase in concentration as PAM concentration increases suggests that potassium is being bound by the aqueous PAM.

Magnesium

Magnesium remains relatively stable with an increase in PAM concentration, showing no particular increase or decrease in concentrations across all samples. Sample BH 4 exhibits the highest increase in magnesium concentration with a maximum of 5.13 mg/L in the total fluid. The remaining samples showed no increase alongside an increasing PAM concentration. Samples range from -1.07 mg/L to 0.9 mg/L, increasing from -1.09 mg/L to 1.5 mg/L when analysing the total fluid. An increase in magnesium concentration may be present when PAM concentration increases.

Manganese

Three samples, samples OC 4, OC 5 and OC 7, showed an increase in manganese concentrations when observing concentrations increased after adsorption. Between these three samples, concentrations at 1000 mg/L PAM ranged from 0.05 mg/L to 0.18 mg/L. The remaining samples were close to 0 mg/L with both additions to fluid and removal from fluid occurring. The three samples with the highest increases, OC 4, OC 5 and OC 7, show concentrations of 0.05 mg/L (OC 7), 0.09 mg/L (OC 5) and 0.18 mg/L (OC 4) respectively at PAM concentrations of 1000 mg/L. All other samples were between values of -0.005 mg/L and 0.02 mg/L.

Sodium

Sodium is the metal that is returned in the largest concentrations for all samples. The addition of 1000 mg of PAM powder to a tap water solution increases the sodium concentration from an average concentration of 6 mg/L to 114 mg/L, with the observed maximum concentration being 434 mg/L. This increase in sodium turns the water from a ‘freshwater’ to a low concentration ‘slightly saline’ fluid. Sodium again shows no relationship between the metals increased from the samples associated with an increase in PAM. Fluid concentrations range from -22 mg/L (OC 5) to 65 mg/L (BH 2), with some sodium being removed from the fluid. There is however a relationship between sodium concentration and an increase in PAM concentration when analysing the total returned

fluid. The relationship is one of an increasing sodium concentration alongside an increasing PAM concentration. The total composition of fluids returning to surface across all samples ranges from 129.5 mg/L (OC 8) to 307 mg/L (BH 6) sodium.

Lead

Lead, similar to manganese, magnesium, calcium and iron, showed both increases and decreases in concentration between the samples. Lead correlation did not increase with increased PAM concentration. Across all samples, concentrations of lead were more variable (higher or lower) in lower concentrations of PAM (sub 250 mg/L PAM). Concentrations that increase after adsorption, range from -0.34 mg/L (OC 5) to 0.12 mg/L (BH 4). As a total fluid, samples BH 1, BH 4, OC 6, and OC 5 exhibited an increase with PAM concentrations, ranging from 0.93 (OC 5) to 1.71 mg/L (BH 4) at 1000 mg/L PAM. The remaining samples that do not show increases at 1000 mg/L PAM return negligible amounts of lead in the simulated flow-back fluid.

Silicon

Silicon concentrations across all samples exhibit varying concentration ranges. The highest silica concentration returned was observed with sample OC 7 p, with maximums of 1.1 and 1.18 mg/L using respective sample duplicates in the total fluid returned. Silicon increases after adsorption ranged from 0.06 mg/L (BH 4) and 1.10 mg/L (OC 6). There was no observable relationship between increases or decreases of silicon and an increase in PAM concentration, however, as was the case with magnesium, there was larger variation in concentrations lost or gained with samples with lower PAM concentration (sub 250 mg/L).

Zinc

Zinc concentrations exhibited large variations across all samples. Observing the total fluid returned, zinc was both removed from and added to the flow-back fluid. Only four samples (OC 7, OC 2, BH 3 and BH 4) show increases of zinc into the fluid, and three of these are negligible, OC 2, BH 3 and BH 4 only exhibiting up to a 0.01 mg/L increase in concentration at 1000 mg/L PAM. Sample OC 7 exhibited the greatest quantities of zinc at a maximum of 0.5852 mg/L in a 1000 mg/L PAM solution. The majority of zinc however does

not return to the surface in the flow-back waters as the remaining samples show negative results.

6.6.3. HPHT Flow-back Results

In this section, four samples (OC 5, OC 7, BH 5 and BH 6) are analysed for flow-back returns of the metals analysed in Section 6.6.2. As seen in the room temperature flow-back analysis, concentration ranges of returned metals varied between analyte, with some differing by magnitudes. As per Section 6.6.2, results in this section are divided into two main sections:

1) Bulk Flow-back Results: Testing the ratio of increases and decreases of the metals dependent on sample
2) Individual Flow-back results: Analysing the results per sample and displaying the actual concentrations returned in flow-back fluids.

6.6.3.1. Bulk Flow-Back Results

As per Section 6.6.2.1, the 'bulk flow-back results' analyse the whole fluid, irrespective of PAM concentration. Data was calculated as a ratio by dividing the observed result of the respective sample by the standard of the same PAM concentration. Ratios for all concentrations are then combined and a mean calculated ratio (increase >1 and decrease < 1). General increases and decreases of the relevant metals can be determined.

Results show that across all samples, on average no metals decreased (Figure 6.19). Dividing the results up by sample (Table 6.8), six of the metals analysed showed increases for every sample; iron, potassium, magnesium, manganese, sodium and silicon. The remaining metals exhibited both increases and decreases. Cadmium exhibited the largest decrease in concentration within the flow-back fluid. Samples BH 5 and BH 6 showed the greatest average decrease in metal concentrations. BH 5 exhibited a decrease in aluminium, cadmium, copper and zinc whilst BH 6 exhibited decreases in cadmium, copper, lead and zinc.

ANALYTE	OC 7	OC 5	BH 5	BH 6
Al	13.25	15.05	0.587	4.25
Ca	0.812	1.349	5.617	2.097
Cd	8.143	0.143	0.571	0.286
Cu	1.88	7.36	0.32	0.434
Fe	93.2	5.04	2.79	5.55
K	4.47	10.06	5.668	6.764
Mg	1.101	2.413	2.608	3.499
Mn	52.68	442.0	12.65	79.8
Na	1.067	2.686	2.182	2.777
Pb	1.464	3.5	1.113	0.375
Si	3.669	10.8	6.286	4.937
Zn	49.01	4.08	0.702	0.671

Table 6.8: *Loss/gain ratio data for the flow-back fluids associated with the HPHT adsorption experiments. Data linked to Figure 6.18.*

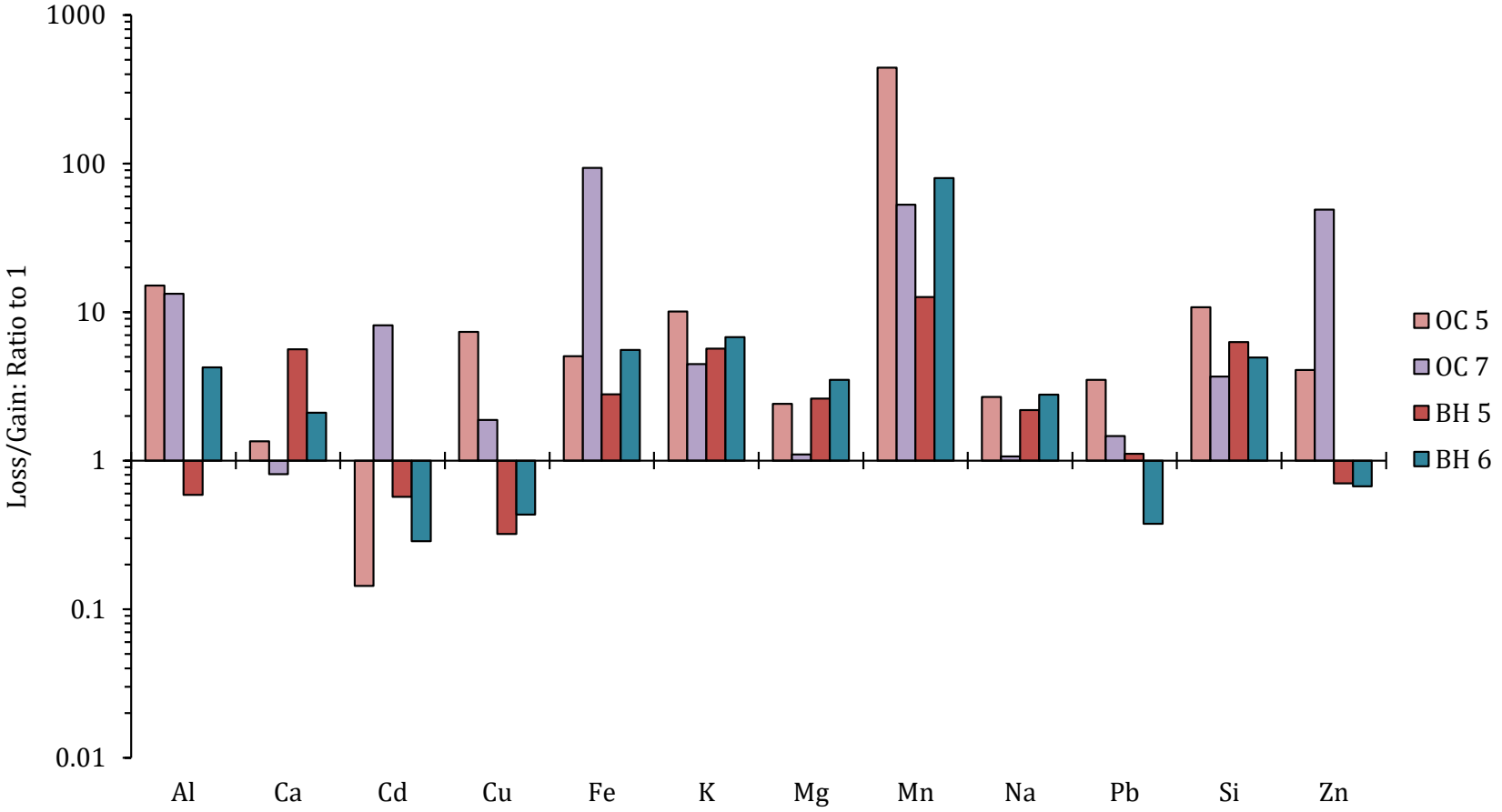

Figure 6.18: *The increase ratio of the various metals in the HPHT adsorption experiments. Data is coloured by sample name and displays maximums per sample.*

ANALYTE	RATIO Loss / Gain
Mn	146.783
Fe	26.645
Zn	13.616
Al	8.284
K	6.741
Si	6.423
Cu	2.499
Ca	2.469
Mg	2.405
Cd	2.286
Na	2.178
Pb	1.613

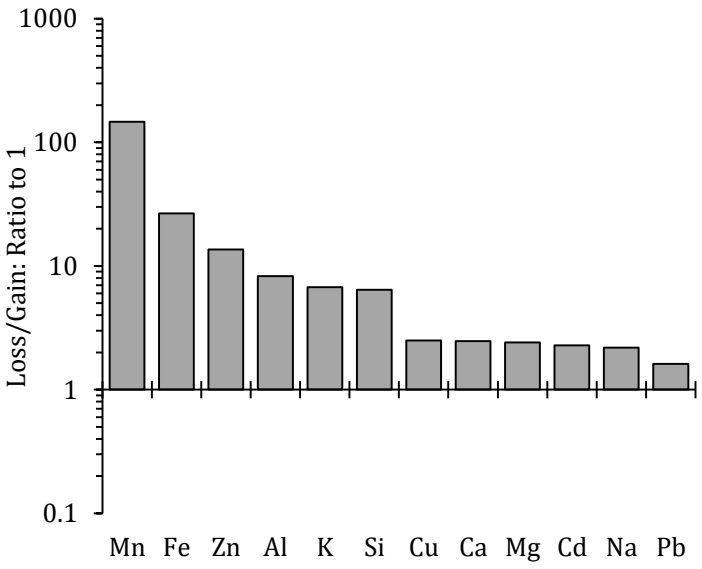

Figure 6.19: *Average increase ratio for all metals irrespective of PAM concentrations of sample type for all samples involved in the HPHT adsorption experiments.*

ANALYTE	RATIO Loss/Gain	
	Sh	Sst
Al	6.029	15.05
Ca	2.842	1.349
Cd	3.0	0.143
Cu	0.878	7.36
Fe	33.847	5.04
K	5.634	10.06
Mg	2.403	2.413
Mn	48.377	442.0
Na	2.009	2.686
Pb	0.984	3.5
Si	4.964	10.8
Zn	16.794	4.08

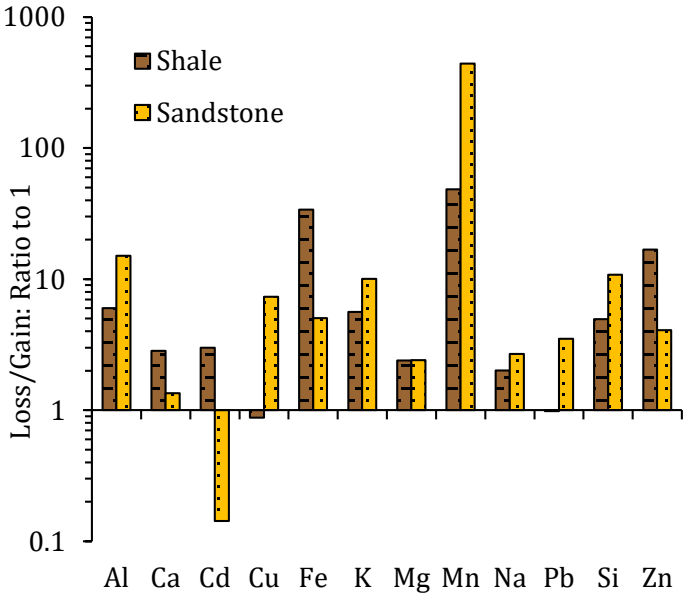

Figure 6.20: *Average increase ratio for all metals irrespective of PAM concentration for all the HPHT adsorption experiments. Data is plotted by sample type.*

By metal, Manganese showed the largest increase, amounts up to 146 times from the initial slick-water fluid (Figure 6.19). Iron showed the second largest increase at up to 26 times the initial amount, an identical result to the room temperature results (Figure 6.14). The majority of the samples, OC 5, BH5 and BH 6, exhibited a decrease in cadmium

content (Figure 6.18). Sample OC 7 exhibited considerable increases in cadmium and brought it to exhibit an average gain across all samples.

Dividing the samples into sample type (sandstone and shale) (Figure 6.20) there was no obvious relationship between sample type and concentration of metals that were increased or decreased. Shales showed an average increase across all metals apart from copper, whilst the one sandstone sample (OC 5) showed increases in concentration of all metals apart from cadmium. Dividing up by sample type, shale samples showed decreases for two metals, copper and lead, whereas the sandstone sample showed a decrease for only cadmium. Sample breadth was limited however, with only four samples tested, three of which are shales.

6.6.3.2. Metal Results per Sample

This section displays results from the HPHT adsorption experiments conducted at 65 ^{o}C and 30 bar (3 MPa). Like in Section 6.6.2.2, two sets of results are displayed:

1) Accounting for all metal concentrations increased into the bulk fluid by the 'fracking of a rock' (Figure 6.16). This method subtracts the compositional concentrations of certain metals already in the fluid, before adsorption experimentation occurs.
2) Accounting for the total concentration of metals within the fluid (Figure 6.17). This subtracts only the zero standard containing no PAM – essentially subtracting the concentration of tap water.

The results of this are displayed on two A3 foldouts. Full data tables can be found in Digital Appendix F.4.

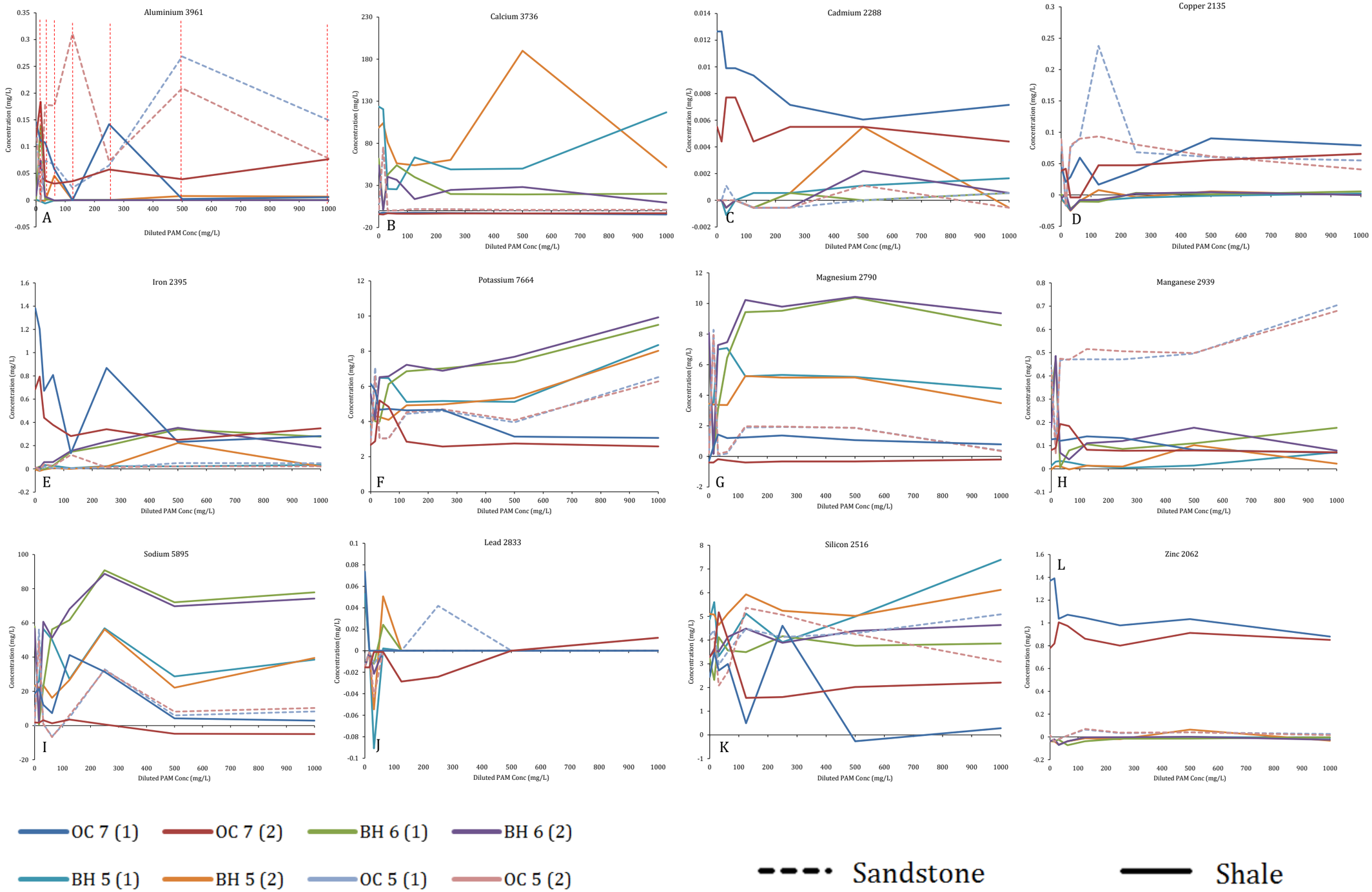

Figure 6.21: *All sample data plotted per analyte showing the composition of increased metal concentrations from the shale. Analysis here has subtracted concentrations within the initial PAM slick-water fluid. Data on all graphs is plotted for PAM concentrations of 15.625, 31.25, 62.5, 125, 250, 500 and 1000 mg/L PAM. This is denoted by the red vertical lines shown on aluminium (top left).*

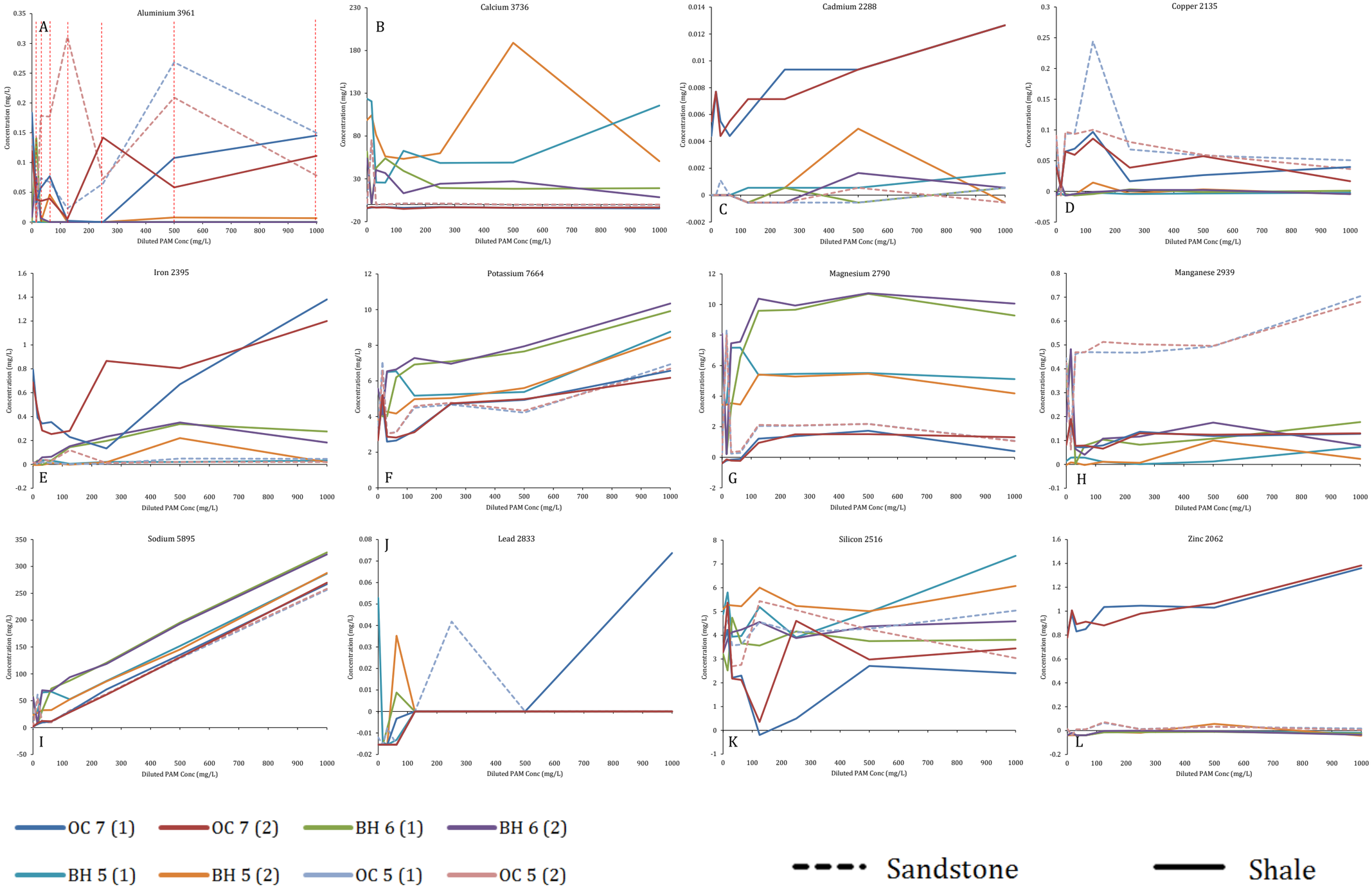

Figure 6.22: *All samples accounting for the total concentration of flow-back fluid, inclusive of concentrations of metals in the initial slick-water fluid.*

Data displayed on Figure 6.21 and Figure 6.22 show results associated with the PAM concentrations used (15.625, 31.25, 62.5, 125, 250, 500 and 1000 mg/L PAM).

Aluminium

Concentrations of aluminium varied between both samples and the PAM concentration. Sample OC 5 released the most aluminium into the flow-back fluid, with 0.31 mg/L at maximum, at a PAM concentration of 125 mg/L. At 1000 mg/L PAM, maximum concentrations of 0.14 and 0.07 mg/L were observed for the respective duplicates of sample OC 5. There was no observable link between increasing PAM concentrations and increasing, or decreasing, aluminium content across all samples. Sample OC 7 exhibited an increase with higher PAM concentrations to concentrations of 0.14 and 0.11 mg/L with respective sample duplicates in the whole fluid returned. Samples BH 5 and BH 6 exhibited negligible increases.

Calcium

Sample BH 5 exhibited the largest increase in calcium with 188 mg/L at a PAM concentration of 500 mg/L analysing the total fluid. Sample BH 6 exhibited the next highest increase of calcium within the fluid at a maximum of 53.9 mg/L at 62.5 mg/L PAM concentration. Samples OC 5 and OC 7 exhibited negligible increases or decreases of aluminium across all sample concentrations of PAM. Overall no relationship was observed between an increasing PAM concentration and increases or decreases in calcium concentration.

Cadmium

As per the room temperature flow-back fluids (Section 6.6.2), cadmium was present in very small quantities, up to 0.01 mg/L with sample OC 7. On some occasions a zero value was measured as the concentration was too low for the machine to properly calibrate. Analysing the total flow-back fluid there was an observable increase in cadmium concentration for sample OC 7 with an increase of overall PAM concentration of 0.012 mg/L. The remaining samples, OC 5, BH 5 and BH 6, showed minimal increases into the fluid, with a maximum concentration of 0.004 mg/L for sample BH 5 (2) at 500 mg/L PAM. At 1000 mg/L PAM sample BH 5 (1) exhibits a maximum cadmium value of 0.001 mg/L. Cadmium

observed at 1000 mg/L PAM lies in the range of -0.0005 mg/L and 0.001 mg/L for samples OC 5, BH 5 and BH 6, with only sample OC 7 showing even greater amounts between 0.004 mg/L and 0.007 mg/L at 1000 mg/L PAM.

Copper

Copper exhibited no relationship between concentrations lost or increasing with an increase in PAM concentration, across all samples. The largest increase in copper is observed with sample OC 7 at 0.242 mg/L at 125 mg/L PAM. Taking the total fluid returned, only samples OC5 and OC 7 showed consistent increases in copper content across all concentrations of PAM. Sample OC 7 concentrations ranged from 0.006 mg/L to 0.244 mg/L across all PAM concentrations. The remaining samples, BH 5 and BH 6 exhibited negligible increases of copper.

Iron

Iron concentrations fluctuated across all samples. All samples showed an increase in concentration, but this increase varied between samples. At 1000 mg/L PAM iron ranged from 0.022 mg/L (OC 5) to 0.35 mg/L (OC 7) as concentrations increased. Analysing the total concentration of fluid returned, iron increased to a maximum of 1.38 mg/L for sample OC 7 (1). Shale type lithologies, particularly OC 7 and BH 6, exhibited the largest increases of iron content, sandstone lithologies (OC 5) showed negligible increases. Only sample OC 7 exhibited a relationship between the concentrations of PAM, increasing steadily as the PAM concentration increased.

Potassium

Overall, much like in the RT metals analysis (Section 6.6.2), potassium showed an increase in concentration with an increase in PAM concentration, across all samples tested. Analysing the total fluid returned, 1000 mg/L sample concentrations ranged from 6.173 mg/L (OC 7) to 10.34 mg/L (BH 6). Results using the whole fluid that returned to surface show an increase in concentration alongside an increase in PAM concentration. Using sample OC 7 (1) as an example, a minimum increase of 2.59 mg/L was observed at a PAM concentration of 31.25 mg/L, increasing to 6.173 ,g/L at 1000 mg/L PAM. No decreases occurred with potassium and there was no distinct difference between shale and sandstone

type lithologies, apart from the fact the sandstone sample (OC 5) showed lower values of increases for the four samples, but similar to shale sample OC 7.

Magnesium

Magnesium across all samples showed increases into the flow-back fluids. Only one sample duplicate (OC 7 (2)) showed a decrease throughout, based upon the amount of magnesium released from the shale, not the total fluid composition. The largest increase in magnesium was from sample BH 6 with increases of up to 10.74 mg/L at 500 mg/L PAM and 10.06 mg/L at 1000 mg/L PAM. Between PAM concentrations of 125 and 1000 mg/L sample BH 6 ranged between 9.2 to 10.784 mg/L. Sample BH 5 exhibited the second largest increase of between 3.47 and 4.42mg/L at 1000 mg/L PAM whilst the sandstone lithology, sample OC 5, exhibited the smallest increase, between 0.35 and 0.78mg/L at 1000 mg/L PAM. Sample OC 5 showed maximum magnesium concentrations of 2.18 mg/L at 500 mg/L PAM. An increase in magnesium was observed with an increase in PAM concentration. This increase in magnesium with PAM concentration was only apparent with all samples showing vastly lesser concentrations when in a sample that had < 125 mg/L PAM.

Manganese

Sample OC 5 exhibited the largest increase in manganese, up to 0.70 mg/L at 1000 mg/L PAM. All other samples showed increases, but not of the nature of sample OC 5. The remaining samples were similar in trend, showing increases of between 0.02 (BH 5) and 0.17 mg/L (BH 6) at 1000 mg/L PAM. Incorporating the whole fluid shows that OC 5 has the largest increase at 0.70 mg/L while the remaining samples (OC 5, OC 7 and BH 6) exhibit concentrations between 0.02 and 0.17 mg/L. No relationship between PAM concentration and either concentration increases or decreases were observed across all samples.

Sodium

Sodium was increased in the majority of samples. The largest increase was from sample BH 6 exhibiting highs of 90.7 mg/L at 500 mg/L PAM and 77.8 mg/L at 1000 mg/L PAM. When accounting for the total fluid returned, sample BH 6 exhibited highs of 322 mg/L at 1000 mg/L PAM. The smallest increase was observed with sandstone sample OC 5, highs of 56.2 mg/L and 500 mg/L PAM and 39 mg/L at 1000 mg/L PAM. Analysing the total fluid, sodium increased for all samples with an increase in PAM concentration. Returned fluids

accounting for all fluid put downhole returned between 258 and 332 mg/L sodium using a 1000 mg/L PAM fluid, producing a slightly briny solution.

Lead

Lead was variable in both increases and decreases across all samples. Measurements were negligible. The largest increases in lead were seen at 62.5 mg/L PAM for sample BH 5 (0.05 mg/L). Lead was removed from solution in the lower concentrations of PAM fluid, up to -0.09 for BH 5 at 31.25 mg/L PAM. Utilising the total fluid, no relationship was observed between PAM concentration and lead concentration.

Silicon

Silicon showed varying increases across all samples, and all concentrations of PAM. Sample duplicate OC 7 (1) showed the least increase at 1000 mg/L PAM with only 0.28 mg/L present alongside a decrease in silicon at 500 mg/L PAM. Sample BH 5 exhibited the largest increase of silicon at 1000 mg/L PAM with 6.07 and 7.34 mg/L of the respective sample duplicates. No relationship between concentration increase or decrease was observed with an increase in PAM concentration.

Zinc

Much like in the room temperature flow-back fluids (Section 6.6.2), zinc showed negligible increases across all samples, apart from OC 7. Sample OC 7 showed the largest increase in zinc concentration, consistently between 0.8 mg/L at 0 mg/L PAM and 1.4 mg/L at 1000 mg/L PAM. The remaining samples (OC 5, BH 5 and BH 6) showed negligible fluctuations between increases and decreases throughout all concentrations of PAM. Only sample OC 7, when accounting for the total fluid concentrations, exhibited an increase in concentration of zinc with an increase in PAM concentration.

6.6.4. RT and HPHT Increase/Decrease Results Summary

Ultimately, with the wealth of data available from the RT and HPHT adsorption flow-back fluids, many different types of analyses can be undertaken, with multiple varied factors. Ratio values, used in this analysis, did not have a normal distribution (Figure 6.23),

and so ratio values for all the data were log base 10 transformed. Transforming the values produces a much more normal distribution (Figure 6.23).

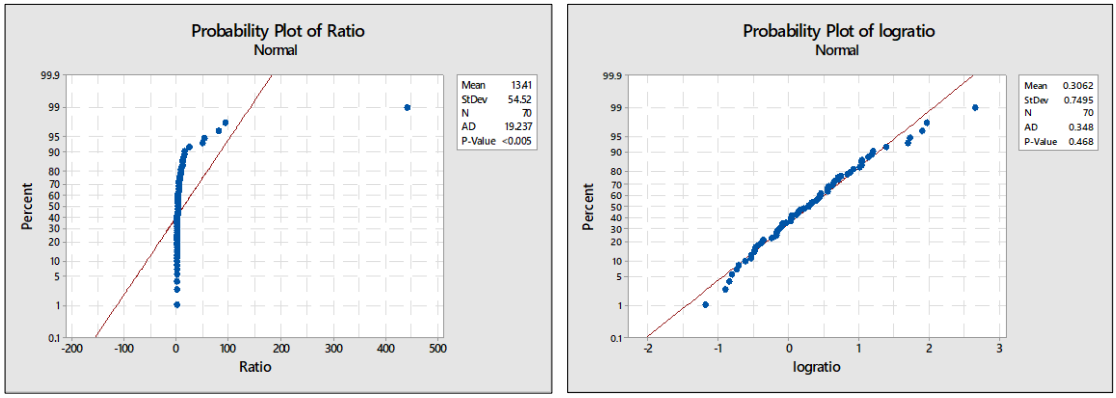

Figure 6.23: *Normality plots for all ratio data from both the RT and HPHT experiments. Normal data is located on the left, whilst logged data is shown on the right.*

MEANS	EXPERIMENT	FITTED MEAN (log10)	SE MEAN	FITTED MEAN (anti-log)
	HPHT	0.620	0.0538	4.172
	RT	-0.007	0.0583	0.985
Sample	BH 6	0.038	0.0659	1.091
	OC 5	0.220	0.0703	1.658
	OC 7	0.663	0.0703	4.604
Metals	Al	0.730	0.132	5.370
	Ca	-0.066	0.132	0.859
	Cd	-0.112	0.164	0.773
	Cu	-0.155	0.132	0.700
	Fe	0.547	0.132	3.524
	K	0.543	0.132	3.491
	Mg	0.023	0.132	1.054
	Mn	1.201	0.132	15.885
	Na	0.238	0.132	1.730
	Pb	0.000	0.132	
	Si	0.533	0.132	3.412
	Zn	0.198	0.164	1.578
Experiment x Sample	HPHT BH 6	0.384	0.0933	2.418
	HPHT OC 5	0.723	0.0933	5.288
	HPHT OC 7	0.754	0.0933	5.675
	RT BH 6	-0.308	0.0933	0.492
	RT OC 5	-0.284	0.105	0.520
	RT OC 7	0.572	0.105	3.733
Experiment x Metal	HPHT Al	0.976	0.187	9.462
	HPHT Ca	0.120	0.187	1.318
	HPHT Cd	-0.159	0.187	0.693
	HPHT Cu	0.260	0.187	1.820
	HPHT Fe	1.139	0.187	13.772
	HPHT K	0.828	0.187	6.730
	HPHT Mg	0.323	0.187	2.104
	HPHT Mn	2.090	0.187	123.027
	HPHT Na	0.300	0.187	1.995
	HPHT Pb	0.095	0.187	1.245
	HPHT Si	0.764	0.187	5.808
	HPHT Zn	0.709	0.187	5.117
	RT Al	0.484	0.187	3.048
	RT Ca	-0.252	0.187	0.560
	RT Cd	-0.064	0.27	0.863
	RT Cu	-0.570	0.187	0.269
	RT Fe	-0.045	0.187	0.902
	RT K	0.259	0.187	1.816
	RT Mg	-0.276	0.187	0.530
	RT Mn	0.313	0.187	2.056
	RT Na	0.175	0.187	1.496
	RT Pb	-0.094	0.187	0.805
	RT Si	0.302	0.187	2.004
	RT Zn	-0.312	0.27	0.488
Sample x Metal	BH 6 Al	0.513	0.228	3.258
	BH 6 Ca	-0.087	0.228	0.818
	BH 6 Cd	-0.723	0.228	0.189
	BH 6 Cu	-0.537	0.228	0.290
	BH 6 Fe	0.060	0.228	1.148
	BH 6 K	0.470	0.228	2.951
	BH 6 Mg	0.032	0.228	1.076
	BH 6 Mn	0.705	0.228	5.070
	BH 6 Na	0.493	0.228	3.112
	BH 6 Pb	-0.301	0.228	0.500
	BH 6 Si	0.505	0.228	3.199
	BH 6 Zn	-0.678	0.228	0.210
	OC 5 Al	0.519	0.228	3.304
	OC 5 Ca	0.017	0.228	1.040
	OC 5 Cd	-0.792	0.228	0.161
	OC 5 Cu	0.026	0.228	1.062
	OC 5 Fe	0.082	0.228	1.208
	OC 5 K	0.611	0.228	4.083
	OC 5 Mg	0.068	0.228	1.169
	OC 5 Mn	1.345	0.228	22.131
	OC 5 Na	0.190	0.228	1.549
	OC 5 Pb	0.077	0.228	1.194
	OC 5 Si	0.584	0.228	3.837
	OC 5 Zn	-0.090	0.371	0.813
	OC 7 Al	1.159	0.228	14.421
	OC 7 Ca	-0.127	0.228	0.746
	OC 7 Cd	1.181	0.371	15.171
	OC 7 Cu	0.045	0.228	1.109
	OC 7 Fe	1.499	0.228	31.550
	OC 7 K	0.549	0.228	3.540
	OC 7 Mg	-0.031	0.228	0.931
	OC 7 Mn	1.554	0.228	35.810
	OC 7 Na	0.030	0.228	1.072
	OC 7 Pb	0.226	0.228	1.683
	OC 7 Si	0.510	0.228	3.236
	OC 7 Zn	1.364	0.228	23.121

ANOVA	F-VALUE	P VALUE
Experiment	62.36	0
Sample	21.86	0
Metal	9.38	0
Experiment x Sample	8.74	0.002
Experiment x Metals	3.48	0.008
Sample x Metal	3.48	0.003

MODEL SUMMARY	
R^2	Adj R^2
94.62%	81.42%

Table 6.9: *ANOVA results for metal increase ratios between identical RT and HPHT samples*

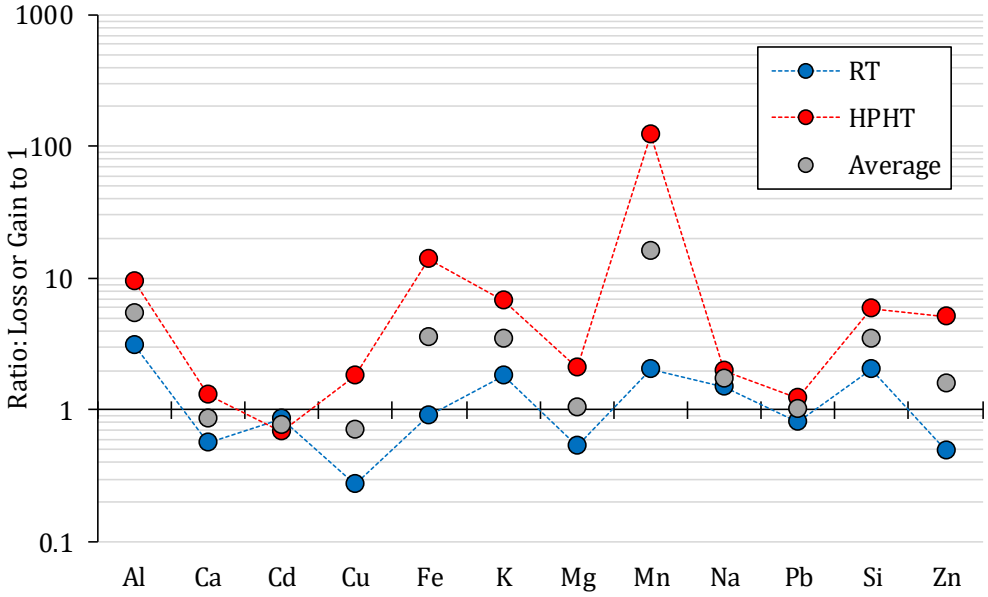

Figure 6.24: *ANOVA ratio fitted means for individual metals fromTable 6.10. Data is referenced from all samples per metal, not per sample. Overall, fluids tested in HPHT conditions show a higher increase ratio than those tested at RT.*

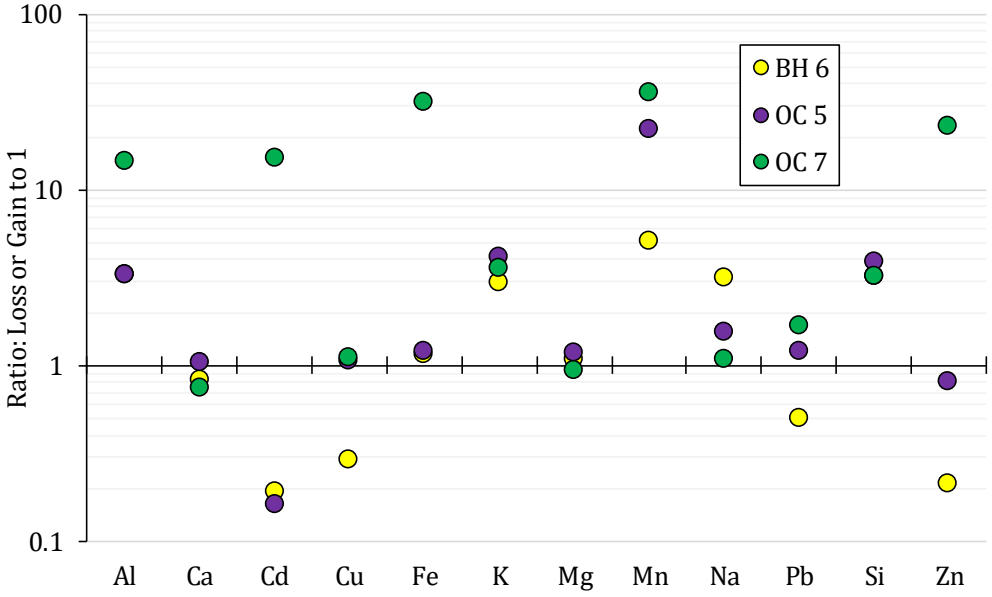

Figure 6.25: *ANOVA ratio of fitted means for individual metal per sample, and not based on experiment type.*

Using a three factor ANOVA test, the ratios of increases/decreases from the HPHT resultant fluids were significantly different from those flow-back fluids analysed from the RT experiments (Table 6.9). All three factors were shown significant to at least at a probability of 95%, being different from zero. Using the fitted means for the same ratio data, based on experiment type (RT or HPHT) and ignoring differences in sample type, means for

HPHT experiments are higher. These higher values showed greater increases of most of the metals in question into the fluid (Figure 6.24). In terms of samples (Figure 6.25), sample OC 7 exhibited the most amount of metal increases, with 10 of 12 showing this increase. Sample OC 7 also exhibited the most amount of metals that increased in quantities 10 + times greater than concentrations observed in the initial fluid. Sample BH 6 exhibited the most removal from the fluid, with 5 of 12 metals removed in some capacity. Under RT conditions, 9 metals (Ca, Cd, Cu, Fe, Mg, Pb and Zn) exhibited average decreases with the remaining (Al, K, Mn, Na and Si) exhibiting increases. Of the metals which showed decreases for the RT fluids, under HPHT conditions all but cadmium had increased to show an average increase.

6.7. Discussion

The majority of metals analysed showed an increase in concentration in both the RT and HPHT adsorption experiments, from the original non-reacted slick-water fluids to the flow-back fluids post experimentation (saturation with 1 g of rock sample). One of the most notable differences in the fluids in both types of experiment was the sodium content. Adding 1000 mg/L of PAM increased the sodium concentrations up to ~ 430 mg/L from the standard mains tap water sodium concentration of between 1 and 8 mg/L. The highest concentration of sodium observed in a flow-back fluid was 514 mg/L, in the RT experiment for sample OC 6 (Table 6.10). All samples analysed in the RT flow-back fluids exhibited higher than the EU regulation of 200 mg/L sodium (European Union, 1998). Three out of four samples in the HPHT flow-back fluids exhibited the same higher than regulation values (Table 6.10). Saline waters injected into rock for hydraulic fracturing purposes have the potential to mobilise salts and mineral ions bound within the connate waters of the rock itself (Boyle and Barron, 2014), potentially leading to increased concentrations of most metals within most flow-back fluids. Returned brackish, or saline fluids, would need intense treatment before reuse (O'Donnell et al., 2018). Lead is another metal where in all of the fluids analysed from the room temperature experiments, concentrations were above its EU regulation limit of 0.01 mg/L, whereas 3 out of 4 in the HPHT fluid exceeded 0.01 mg/L (Table 6.10). Manganese was also commonly present in tested flow-back waters at higher than the regulation guide of 0.05 mg/L with 8 out of 11 in the room temperature fluids and all fluids in the HPHT experiments (Table 6.10). For all fluids returned to the surface, specialist treatment is required for the removal of such contaminants before re-use or the safe disposal of the fluid. Often, as would be the case here, fluids will have to be treated in different ways for the removal of different contaminants (O'Donnell et al., 2018).

	ANALYTE	REGULATORY	TAP WATER		FLOWBACK		SLICK-WATER	SAMPLE (maximum concentration)											
		EU	NWL	Durham TW	PREESE HALL	USGS	1000 mg/L PAM	OC 2	OC 4	OC 5	OC 6	OC 7	OC 8	BH 1	BH 2	BH 3	BH 4	BH 5	BH 6
		mg/L	avg mg/L	avg mg/L	Max (mg/L)	Avg mg/L	mg/L	mg/L	mg/L	mg/L	mg/L	mg/L	mg/L	mg/L	mg/L	mg/L	mg/L	mg/L	mg/L
ROOM TEMP	Al	0.2	0.036	0.829	1.59	48.34	5.321	0.111	0.142	0.338	0.479	0.18	2.464	0.459	0.014	0.022	0.475		0.11
	Ca			24.28		5360	9.581	-3.278	-2.42	-1.856	18.075	-5.005	1.441	20.513	37.818	19.602	9.717		0
	Cd	0.005	0.0000128	0.001	0.00602	0.215	0.432	-0.003	0.001	0.013	0.023	0.009	0.107	0.023	0.002	0.002	0.026		0.001
	Cu	0.002	0.0196	0.301	0.036	0.554	0.900	-0.052	0.008	-0.07	-0.046	0.007	0.521	-0.011	-0.029	-0.029	-0.009		0
	Fe	0.2	0.014	0.167	137	-	3.284	0.014	0.011	-0.421	-0.48	0.191	3.05	-2.075	0.004	0.053	-2.073		0.046
	K			1.192	52.3	811.17	1.580	4.892	3.864	4.525	2.111	3.314	7.655	2.62	2.635	3.383	1.929		1.736
	Mg			4.616	1470	990.15	1.878	0.215	0.155	0.291	1.513	-0.272	9.544	0.9	4.083	5.133	1.253		0
	Mn	0.05	0.000834	0.036		6.809	2.215	0.568	0.208	0.176	0.087	0.075	0.625	0.099	0	0.001	0.089		0.001
	Na	200	8.238	8.818	28400	26953	431.47	277.12	268.87	269.16	514.67	222.51	277.12	326.41	255.90	301.55	331.87		307.76
	Pb	0.01	0.000313	0.186	0.6	29.59	1.279	0.111	0.121	0.998	1.399	0.097	0.569	1.608	0.132	0.132	1.743		0.102
	Si			1.301		54.87	0.817	0.608	0.877	0.518	0.499	1.332	1.637	0.107	0.485	0.653	0.085		0.889
	Zn			0.768	0.565	11.48	7.368	-0.001	0.007	-0.077	-0.085	0.81	0.481	-0.026	0.087	0.03	-0.03		0.000
HPHT	Al	0.2	0.036	0.829	1.59	48.34	5.321			0.311		0.184						0.046	0.141
	Ca			24.277		5360	9.581			75.70		-2.855						188.93	61.76
	Cd	0.005	0.0000128	0.001	0.00602	0.215	0.432			0.001		0.013						0.005	0.002
	Cu	0.002	0.0196	0.301	0.036	0.554	0.900			0.244		0.097						0.014	0.013
	Fe	0.2	0.014	0.167	137	-	3.284			0.119		1.381						0.22	0.351
	K			1.192	34800	811.17	1.580			7.107		6.569						8.763	9.926
	Mg			4.616	14770	990.15	1.878			8.324		1.74						7.18	10.742
	Mn	0.05	0.000834	0.036		6.809	2.215			0.704		0.19						0.1	0.482
	Na	200	8.238	8.818	92800	26953	431.47			129.39		266.86						286.55	325.93
	Pb	0.01	0.000313	0.186	0.6	29.59	1.279			0.042		0.074						0.053	0.009
	Si			1.301		54.87	0.817			5.437		5.374						7.343	4.739
	Zn			0.768	0.565	11.48	7.368			0.071		1.36						0.057	0

Table 6.10: *Table displaying the maximum concentrations of metals returning to surface for each sample compared to various literature including basic tap water compositions, flow-back waters and the EU regulatory legislation directives. Data taken from USGS produced waters database (Blondes et al., 2017), EU water regulatory directive (European Union, 1998), Northumbrian water sample site data (Northumbrian Water Ltd, 2017) and Preese Hall flow-back data (Broderick et al., 2011).*

In terms of overall increase and decrease, copper was predominantly removed in most fluids in the room temperature experiments (Figure 6.16 (D)). Data showed a loss ratio of 0.53 (Figure 6.14) potentially adsorbing to the shale over the experiment timescale, however crucially still returning in flow-back in quantities enough to be above regulation guidelines. In both experiment types (RT and HPHT), manganese was by far the metal with the greatest increases into the flow-back fluid (Figure 6.24 and Figure 6.25), with most samples by the end of experimentation reading above the regulation 0.05 mg/L. Manganese showed an increase of between 12 and 442 times in the HPHT experiments and increases between 1.1 and 145 times in the room temperature fluids, however it must be noted that decreases in manganese were observed in fluids from the RT experiments. Iron is another metal that is returned in increased concentrations considerably larger than those of other metals, from that of the initial slick-water fluid concentration. Between 2 and 93 times the amount of iron is returned in fluids from the HPHT experiments (Figure 6.19), and between 1 and 141 times in the room temperature experiments (Figure 6.15). Some decreases with iron were observed for some samples, but these were not significant enough to alter the average increase-decrease ratio for Fe.

Temperature

Higher temperatures are a controlling variable in metal release. Overall, fewer metals were removed from the fluids associated with the HPHT experiments. Fluids saw more of a rise in metal concentrations under HPHT conditions with only 20 % of results showing decreases in comparison water from the RT experiments where decreases are observed in 42 % of all samples tested. An ANOVA on the loss/gain ratios for all metals in both RT and HPHT experiments shows that there was a significant difference in values between the RT and HPHT datasets (Figure 6.24). The majority of these decreases occur with copper, cadmium, lead and iron. In the HPHT experiments, the majority of these decreases occur with cadmium and copper, with iron showing no loss. Using the loss/gain ratio data, manganese, a transition metal, increases in the largest quantities over both RT and HPHT experiments. The next three metals to increase in the largest quantities are iron, zinc and aluminium, good reducing agents. A hydraulic fracture, in a non-laboratory and experimental setting, is an oxidative environment by means of the addition of much larger quantities of oxygen to the subsurface through the means of oxygen rich carrier fluid, water. Transition metals such as copper and cadmium are mostly removed from all solutions, both in the RT and HPHT experiments.

	RT FLUIDS					
	Cu		Pb		Zn	
	XRF (ppm)	% leached	XRF (ppm)	% leached	XRF (ppm)	% leached
BH 1	46.5	0.52	12.9	12.46	93.6	*-0.03*
BH 2	10.4	0.35	2.3	6.76	28.7	0.34
BH 3	3.1	0.97	3.4	3.9	13.5	0.3
BH 4	5.5	4.78	3.3	52.59	20.7	*-0.14*
BH 5	32.8	NO DATA	11.2	NO DATA	58.5	NO DATA
BH 6	25.9	0	21.2	0.61	64.3	0
OC 1	<0.3	< LLD	4.1	NO DATA	4.2	NO DATA
OC 2	3.4	0.55	11.0	1.51	18.7	0.13
OC 3	16.2	0.05	45.1	0.27	580.2	0
OC 4	15.7	NO DATA	17.3	NO DATA	21.6	NO DATA
OC 5	<0.3	< LLD	8.2	12.16	5.9	108.18
OC 6	<0.7	< LLD	2.0	69.89	22.5	39.25
OC 7	16.3	0.11	72.3	0.01	341.3	0.25
OC 8	<0.3	< LLD	4.6	13.23	4.0	12.45
	HPHT FLUIDS					
	Cu		Pb		Zn	
	XRF (ppm)	% leached	XRF (ppm)	% leached	XRF (ppm)	% leached
BH 5	32.8	0.06	11.2	0.53	58.5	0.15
BH 6	25.9	0.09	21.2	0.21	64.3	0.05
OC 5	<0.3	< LLD	8.2	0.62	5.9	1.73
OC 7	16.3	0.62	72.3	0.06	341.3	0.41

Table 6.11: *Percentage increases observed in the RT and HPHT fluids using the concentrations of Cu, Pb and Zn from the XRF data (<LLD denotes values lower than the limit of detection).*

Percentage release of minerals was calculated by using the XRF data for Cu, Pb and Zn (Table 6.11 – data shown in ppm). These analytes were the only analytes that were measured in both the XRF and the ICP-OES analysis. Overall, the majority of mineral release is < 5 %, however some samples produce more than 50 % release. The Pb shows the overall largest release, with RT sample OC 6 releasing 69.89 % (equating to 1.39 ppm) and the next largest being RT sample BH 4 which released 52.59 % (equating to 1.73 ppm) (Table 6.10). Under HPHT conditions, for these particular metals, mineral release was less than the for the RT samples. For example, HPHT sample OC 5 showed only a 0.62 % release of Pb compared to the RT sample releasing 12.16 %. This substantial release of Pb within some samples agrees with literature citing the affinity of lead to PAM in solution, or grafted to materials such as attapulgite (Zhou et al., 2011) or tin (Shubha et al., 2001).

Acidity (pH)

The pH is a key factor in affecting the solubility of metals within fluids, and the subsurface (Chuan et al., 1996; Zhang et al., 2018). There is a considerable body of literature investigating pH effects on the impact of leaching of metals, particularly common ones of

interest to human, animal and environmental health such as Cd, Cu, Zn, Ni, Co and Pb. Different metals behave in different ways, but in general, under more acidic conditions (pH 5.5 or less), metals are more soluble. Metal cations are more soluble under low-pH conditions (McAlister et al., 2003). Studies of mine-waters and river sediments show that transition metals such as Zn, Cu and Mn are mobilised under acidic conditions (Bowell and Bruce, 1995; Johansson et al., 1995; Wingenfelder et al., 2005; Zhang et al., 2018). In this study, Cu and Cd are mostly removed from solution, suggesting no acidic environment. Other metals such as lead and cadmium remain largely unchanged when varying the acidity of waters (pH 1-6) (Wingenfelder et al., 2005) but may be linked more to the DOM content of certain fluids (Johansson et al., 1995). The pH of the fluids used and analysed in this study, inclusive of all RT and HPHT fluids, and their respective samples was in the range of pH 7.0 to 7.9, i.e. circum-neutral. Based upon this data, it is difficult to tell if acidification of these fluids would have had an impact upon the compositions of the fluids observed for all samples, both RT or HPHT. The addition of CO_2 saturation during the HPHT experiments within the pressure vessel in theory would have acidified the solution (to an unknown degree) (Turley et al., 2006), however negligible pH change was observed and no acidification took place with fluids remaining neutral (see Section 4.10). TGA and XRF analysis confirms that calcium carbonate is present in samples in quantities of 0.03 (OC 8) – 41.64 (OC 6) wt% (Section 2.4.1). The presence of carbonate within the samples would act as a buffer in the presence of any acidity (Andersson et al., 2003) that may be brought on by pipe conditions, contact with rock or additive addition during the hydraulic fracturing process. Conducting a very simple literature review on two studies, Preese Hall flow-back fluid data (Broderick et al., 2011) and all data observed in the USGS Produced Waters database (Blondes et al., 2017), the majority of data suggest circum-neutral flow-back waters (Figure 6.26). In the USGS Produced Waters database, 94 % of 86,623 wells that display data for pH are between pH 5 and pH 9, with 68 % of these between pH 6 and pH 8 (Figure 6.26). The mean pH is 7.12.

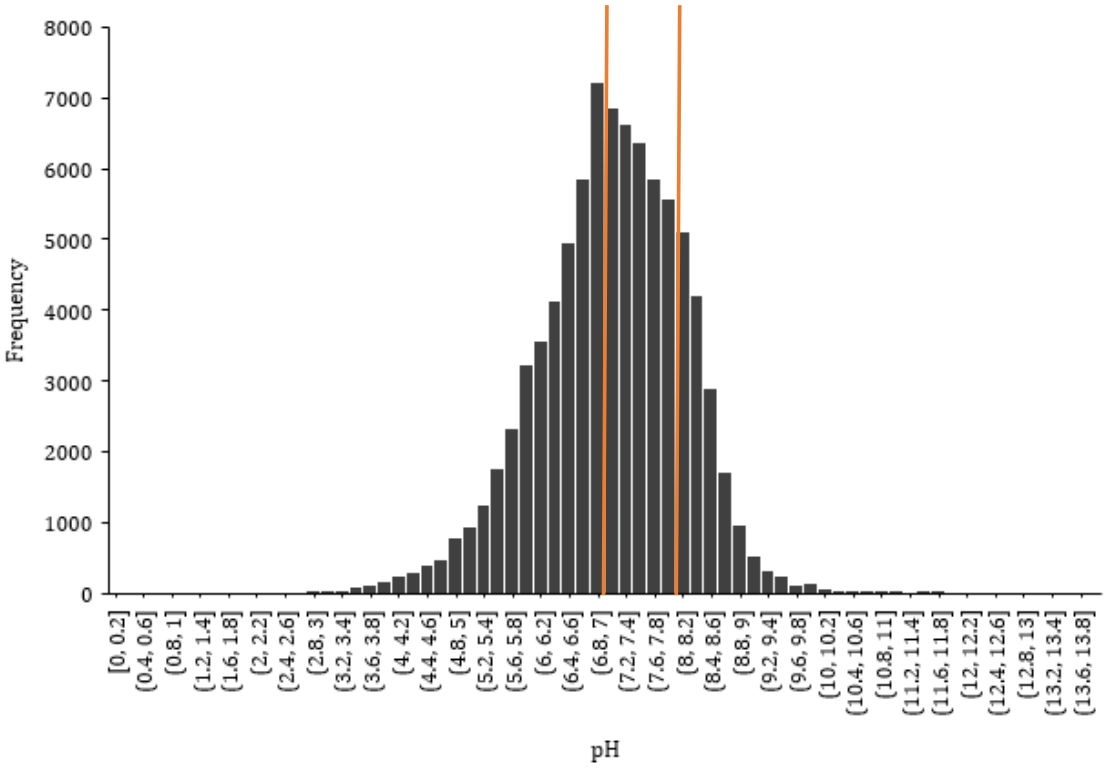

Figure 6.26: *Histogram depicting pH of flowback fluids from the USGS Produced Waters database (Blondes et al., 2017). Orange lines denote the neutral range of the fluids and samples used in this study, fitting within the majority of data reported in the USGS produced waters database.*

From data shown in Figure 6.26, it can be reasonably assumed that little acidification takes place within the subsurface from injected hydraulic fracturing fluids, unlikely mobilising large extra concentrations of Cu, Cd, Zn and Fe.

The use of multi-additives, i.e more than 3 additives, in a fracking fluid is not necessarily an issue for the UK based on previously used fluids (Preese Hall, Preston New Road, Grange Hill) containing 1-3 additives, however, historically many (> 3) additives have been added to fluids in countries such as the USA. If the addition of multiple additives results in an acidic solution, often a pH adjuster is added, such as sodium or potassium carbonate (FracFocus, 2018; Tasker et al., 2016). The pH adjusters are normally added to the fluid to "maintain the effectiveness of other additives" (FracFocus, 2018) but may have the unintentional effect of actually mobilising less minerals into flow-back fluids. Unfortunately, no data was available for the pH values of the hydraulic fracturing fluids pumped downhole, either for Preese Hall 1A or the subset of American wells used in Section 1.6.2.1 of this study. Acid washes may occur as part of the pre-frack preparations, for tubular and formation cleaning, dissolving scale, rust and other formation/pipe debris (American Petroleum Institute, 2014). These acid washes would typically use HCl of HF acids, usually in a weak form of < 10 wt%, and would be low in volume with pH values of 0-1 (strong acids). Acid washing with strong acids (pH 0-3), even in low volumes (3 m^3 per frack stage is an example of what would

be used in the UK Preston New Road site (Cuadrilla Resources, 2018a) would likely solubise metals initially. Any solubised metals may remain in aqueous form in residual fluid downhole until the main frack stage starts, and more fluid is pumped downhole and then returned to surface as flow-back. If the fluids used in this study were more acidic in nature, there would have been the potential of more zinc, copper, iron, cadmium and lead returning in solution. Acidic fracking fluids were not part of this study (Table 6.12 and Figure 6.26), utilising Preese Hall 1A as a proxy (Broderick et al., 2011) and observing results from the USGS flow-back database (Figure 6.26) (Blondes et al., 2017) and Preese Hall flow-back (Broderick et al., 2011).

	WATER TYPE	pH
SUPPLIERS (reported)	NWL	7.3 - 8.5
	United Utilities	7.14 - 7.91
RT SAMPLES	1000 mg/L PAM Tap Water	7.46
	1000 mg/L PAM DI Water	7.84
HPHT SAMPLES	0 mg/L PAM in vessel	7.74
		7.76
	250 mg/L PAM in vessel	7.56
		7.51
	0 mg/L Standard in vessel	7.65
		7.63
	250 mg/L Standard in vessel	7.54
		7.51
	0 mg/L Standard in vessel	7.61
		7.6
	250 mg/L standard NOT in vessel	7.42
		7.4
	Tap water (no PAM)	7.55
	DI Water (no PAM)	7.8
PREESE HALL FLOWBACK	18/05/2011	6.35
	14/06/2011	7.06
	01/08/2011	6.33
	United Utilities Mains Avg	7.54

Table 6.12: *Example pH values from fluids used throughout this study. 'Suppliers' are reported from Water Quality reports from Northumbrian Water (2019) and United Utilities (2019). 'RT Samples' refer to pH of a 1000 mg/L PAM tap water and DI water solutions. 'HPHT Samples' refer to blanks (0 mg/L) and PAM waters (250 mg/L) that were either pressurised and heated inside the vessel, or remained as controls outside of the vessel throughout the duration of a HPHT run (in vessel/NOT in vessel), observing no change with the addition of CO_2. 'Preese Hall Flowback' refers to reported pH values from (Broderick et al., 2011).*

Oxygen

Although pH is a primary control in the mobilisation of certain metals into a fluid (Chuan et al., 1996; Pinto et al., 2014), the addition of oxic waters to a predominantly anoxic subsurface environment by the injection of fracking fluids (Charlet et al., 2013) can also affect the mobilisation of many metals. Of the metals analysed within this study, the most commonly redox active are Fe, Mn and Pb. Within this study, no experiments, sample handling or storage were conducted under oxygen depleted conditions, therefore all experiments and samples are, or were in, constant contact with oxygen of some form. No information on the redox conditions of the fluids or shale were taken during these experiments. Oxidation is likely to be occurring between fluid and sample in the batch reactions in both the RT and HPHT experiments, simple by the addition of the simulated H_2O carrier fluid and the open air nature of sample preparation and storage. The HPHT experiments used CO_2 as a pressurising gas and so, temporarily, for the HPHT experiments, samples and fluids would have been exposed to less oxygen.

Large increases in manganese are observed in the RT experiments (Figure 6.13) and in the HPHT experiments, iron, and manganese are consistently increased in the flow-back fluid (Figure 6.18). In both the RT and HPHT experiments, Mn and Fe have the largest increases in solution. In the RT experiments, the majority of samples show increases in Fe and Mn (14 and 24 times increases, respectively), whereas in the HPHT experiments, all samples show increases of Fe and Mn (26 and 146 times increases respectively). Shale minerals, due to the reducing nature of formation, will contain reduced iron (Fe^{2+}), and the oxidation of this would form Fe^{3+}. However, Fe^{3+} is typically not very soluble, unless under specific conditions (Stumm and Morgan, 1996). In deep aquifers, or deep subsurface regions indicative of 2-5 km deep gas shales, dissolved oxygen is low and the decomposition of any organic matter depletes oxygen further – any iron would dissolve as Fe^{2+} (Oregon Health Authority, 2018) and is often accompanied by Mn. These oxic fluids that have been mixed with a sample that has undergone long alteration in a deep reducing environment, leading to increased efflux of Fe and Mn that are a lot more commonly mobile in reduced form. It is already observed that the fluids are not acidic in nature, and so any Fe^{3+} is unlikely to be aqueous (Lenntech, 2019; Stumm and Morgan, 1996), however no precipitates were observed at any stage of the experimentation. Under these mildly reducing conditions, it may be sensible to assume that the aqueous PAM within the fluid could be stabilising any aqueous Fe. Literature already states that PAM can be used to remove transition metals metals such as Pb, Cu, Cd, Co and Hg (Manju et al., 2002; Shubha et al., 2001; Zhou et al., 2011) from solution. The stabilisation/removal of metals from the fluid using PAM is discussed below, and is investigated using Cd in Chapter 7 of this study. In an operational fracking aspect, to prevent the build-up of any precipitates, citric acid is often used to counter this Fe precipitation (Batley and Kookana, 2012), and thus would be a reason why Fe and Mn are observed in flow-back fluids from various sources (Batley and Kookana, 2012;

Wood and Patterson, 2011), rather than as immobile precipitates. The precipitation of iron hydroxides may also lead to co-precipitation of other metals coincidentally limiting other dissolved metals in the solution if the pH increases from acid to neutral (Bowell and Bruce, 1995).

It is likely that the conditions of the experiments are, in part, indicative of concentrations that may be returned, when accounting for scaling up from a sample to full frack volumes. Moreover, during the initial stage of a hydraulic fracture, initial oxidisation would occur on the fracture surfaces within the shale. Redox reactions in this environment would be slow as there is a difference between surfaces immediately in contact with oxygen, and deeper layers of sediments (shales in this case) (Stumm and Morgan, 1996). Over a prolonged period of time, potential oxidation reactions would occur beyond the shale surface and so flow-back returning over longer periods, months for examples, may differ in composition.

So it is unlikely that it would be expected that the oxic fluids injected in to the reduced environment of these shale samples would lead to increased efflux from the samples of elements that are more commonly mobile in reduced form, in this case Fe and Mn. It should be noted that the use of the ratio of the increase between initial and final fluids could be misleading as it does not reflect the magnitude of the concentrations. The average concentration in Fe before and after were 0.77 mg/L and 0.494 mg/L respectively, i.e. these are close to the solubility of Fe expected in circum-neutral natural waters. Therefore, the increase is misleading for Fe and Mn and perhaps it is not necessary to invoke changes in pH or redox.

To fully understand certain metal mobility and solubility with regards to oxidation states, more would need to be understood regarding the microbial activity in the context of dissolution, transportation and precipitation as microorganisms could form soluble metal complexes that would have the ability to adsorb (McAlister et al., 2003).

Polyacrylamide

The concentration of PAM within the slick-water fluid does appear to have some effect on the increase or decrease of certain metals in solution, and PAM is used in the water treatment industry to remove certain heavy metals from solution by means of adsorption, in particular Pb, Hg, Co and Cd (Shubha et al., 2001; Zhou et al., 2011). Starting with room temperature flow-back fluids, notable increases in concentrations linking to an increase in PAM concentration up to 1000 mg/L are observed with potassium and manganese (Figure 6.17 (F & H)). Potassium shows increases of between 1 and 4 mg/L with a PAM concentration increase. Manganese shows increases of between 0.06 and 0.2 mg/L. Some samples exhibit increases in calcium content of up to 0.03 mg/L whilst other samples show no change. Sodium increases with an increase in PAM concentration amongst every sample tested, RT or HPHT

(Figure 6.16 (I) and Figure 6.22 (I)). Magnesium, silicon, iron and zinc remain largely unchanged by effects of an increasing PAM concentration. Copper and cadmium are removed from fluids, particularly in the lower concentrations of PAM, with decreases in concentrations becoming lesser when the PAM concentration increases. Sodium exhibits increases of up to 400 mg/L, likely due to residual sodium from the manufacturing process of PAM using sodium polyacrylate (Kalra and Gross, 2002). Iron, manganese, silicon, zinc and cadmium, in some samples also show a slight increase, although this is not the case for the whole sample suite. Magnesium, calcium, aluminium, copper and lead remain fairly consistent in increases across the PAM concentration range.

The adsorption, or removal by adsorption, of metals from solutions has been studied in the literature, predominantly for the heavy metals of Pb(II), Hg(II), Cd(II), Cu(II) and Co(II) (Ma et al., 2017; Manju et al., 2002; Shubha et al., 2001; Zhou et al., 2011) – some of which were not analysed in this study, however conclusions of which can still be drawn upon. Typically, PAM is used in this capacity by grafting it onto various gels or metal gels such as tin, iron oxide, chitosan/PAM hydrogel and PAM/attapulgite. Typically, pH is the driving factor in adsorption in this context (Manju et al., 2002; Rouquerol et al., 1999). Studies show that optimum adsorption is observed between pH values of 5 and 6 (Manju et al., 2002) or between 4 and 7 (Zhou et al., 2011), but this is metal dependent. An optimal average pH of 4.5 is suggested by Ma et al (2017) for Pb, Cu and Cd. Adsorption efficiency at lower pH's (specifically > 2.5) is reduced due to the large competition with H^+ ions in solution (Ma et al., 2017). The majority of literature suggests that lead has the highest bonding affinity, compared to other typical metals analysed such as Hg, Cd, Cu and Co. Of the metals suggested above, Cu, Cd and Pb are the metals analysed within this study. Based upon results, Pb, Cd and Cu display negligible to no increase in concentration in solution with regard to PAM concentrations used in this study (up to 1000 mg/L). To start to investigate the adsorbance, or affinity to any PAM in solution of any transition metals, Cd was further studied in Chapter 7 as a basis for future work.

Importantly however, results show that fewer metals decrease in concentration within these HPHT conditions than in the RT conditions (comparison between Figure 6.14 and Figure 6.19), ultimately suggesting that in more geologically realistic settings (i.e. not the room temperature settings) higher concentrations of metals are likely to return to surface. It is not known if there is a further link between even higher temperatures and pressure and even higher metal concentrations as this experiment was only conducted at one setting. It is impossible to tell of any acidification of fluids or rocks at particular points that may have aided the solubility of some metals within the solution, due to the neutral nature of all PAM fluids used within this study. Literature would indicate that, in general, oxidising environments that are acidic would mobilise the most amount of metals into flow-back solutions in a hydraulic fracturing setting. Geological conditions simulated in these experiments, particularly

temperature (Table 4.1) are reasonably low. Is an increase on both temperature and pressure likely to have an impact on concentrations and, will higher temperatures or changes in PAM concentration bind more metals in solution and return them to surface in even greater quantities?

6.8. Conclusions

The majority of metals analysed are present in the flow-back fluid in greater quantities than were originally 'injected' via the slick-water PAM fluid. Varying PAM concentrations occasionally impacted upon the hardware and affected measurement clarity. Adding 1000 mg of powdered non-ionic PAM to the mains water solution increased the sodium content to concentrations up to ~500 mg/L, producing a briny type fluid. The addition of PAM also increased levels of other trace metals, but in quantities far less than observed for sodium.

At room temperature, copper, cadmium and lead were removed from solution. The removal of copper and cadmium appears to decrease with an increase in PAM concentration. Metals such as aluminium, calcium, magnesium, lead and zinc do not exhibit large increases or decreases (unlike potassium or sodium for example) alongside increases in the PAM concentration.

Under HPHT conditions, the concentrations of the metals being added to the flow-back solution increases for the majority per sample. Consequently, based upon the overall increases in metal concentration, lower concentrations of all metals, across all samples, are being removed or adsorbed from the flow-back solution. The most decreases in solution were observed are with cadmium and copper, although not all samples exhibit decreases of these. PAM concentration does affect some metals, showing an increase in potassium, sodium and potentially iron with an increase in PAM concentration. Other metals, particularly potassium and sodium, show consistent increases in concentration alongside an increase in PAM concentration.

HPHT conditions inhibit the removal of certain metals to the sample in comparison to the RT conditions. It is not clear whether either temperature, pressure, or both are the primary factor for this behaviour– future work is needed to investigate this phenomenon (see Section 8.5.4). Due to the neutrality of the fluids used in the batch experiments, and the neutrality of the flow-back water from literature, it is unlikely that acidification is a major influence on the variance of metals returned in flow-back waters. More geologically indicative conditions, as simulated by the HPHT experiments, may favour increases in metals leaching from the sample and returning to the surface rather than the RT conditions. Based upon this, it would be expected that in a real-world situation, metals are more likely to return than be adsorbed based upon UK geothermal temperatures and fluid pH.

As discussed, literature suggests that PAM does have the capacity to adsorb or bind certain metals in certain conditions where pH is a major factor. Chapter 7, investigates the initial affects it has upon cadmium in a pH neutral environment, giving insight into how it would interact with a toxic metal of peak environmental importance.

Future work would be able to assess if pressure is another factor, and whether fluctuations in temperature can influence the concentrations of metals returning to surface in flow-back fluids. Future work would also assess the necessity for sequential extraction to analyse how the increase or decrease of certain metals will be affected over time, and potentially with the effects of pressure, temperature and pH running alongside this.

7. The Colloidal Behaviour of Polyacrylamide as a Hydraulic Fracturing Fluid Additive

7.1. Introduction

PAM is commonly used as a flocculent and coagulant in the water treatment and soil conditioning industries (Deng et al., 2006b). It is now fast becoming very popular in the fracking industry for its use as a friction reducer (Xiong et al., 2018b). As a colloid, the behaviour of PAM is of interest to the shale gas industry as it may have the ability to interact and bind aqueous metals released, or that were in equilibrium with the connate waters within the shale (Maguire-Boyle and Barron, 2014). To summarise, the presence of PAM in a fracking fluid may influence the composition of the flow-back waters, particularly with certain metals. The results of behaviour of this kind would be just as important as how much PAM could be removed from solution by means of adsorption. Does the PAM act as a colloid towards any of the metals released by the shale upon fracture, binding them and bringing them to surface in potentially dangerous and polluting concentrations? The opposite may also be true; certain metals may adsorb (chemically or physically) to the shale surface rather than remain in suspension within the fluid.

To test the hypothesis that PAM could influence certain metals within the flow-back fluid, two analytes were measured; cadmium and sodium. Cadmium was used as the primary tracer to see how either PAM or the shale would influence it in aqueous form. Cadmium is present in minor amounts in the natural world (Morrow, 2010) and in shales, often measured in parts per billion (1 mg/kg = 1000 ppb) (Gong et al., 1977). Cadmium is classified as a priority pollutant by the USEPA (Shubha et al., 2001) due to its toxicity, threat to human life and the environment, and the fact no effective treatment for over-exposure exists (Tucker, 2008). Examples of the threats cadmium poses include: effects on reproduction rates on humans and animals; renal damage in humans, decreased enzyme activity on plants; and nervous system mutations in both humans and animals (de Vries et al., 2007). With the danger and toxicity of cadmium high, EU regulatory limits set it at 0.005 mg/L (European Union, 1998). Sodium was measured as the second analyte for ease as PAM contains large quantities of residual sodium from its production process, utilising sodium polyacrylate, hence sodium values of ~ 500 mg/L observed in Chapter 6 of this study.

The results of this analysis ultimately let us understand if PAM has the potential to influence the composition of flow-back fluid with regard to cadmium and other heavy metals. Building upon the results of this test, similar slick-water fluids would have their role assessed

in relation to other analytes, potentially others that are likely present in greater quantities and more harmful to humans and the environment.

7.2. Aims and Objectives

This chapter assessed how non-ionic PAM behaves as a colloid within a fracking fluid. The behaviour of both PAM and metal transference in the presence and absence of shale will be analysed. Varying concentrations of PAM will be used to see if low or high concentrations show specific behaviours. This analysis was used to understand if the aqueous cadmium favours adsorption to the shale or the PAM, whether that PAM is behaving colliodally or not. Using a PAM-rich fluid contained within a semi-permeable membrane (dialysis tubing), that is submerged in a freshwater fluid containing the metal cadmium and sometimes shale, this favourability was tested. If the metal favours the PAM then more than expected cadmium will cross the semi-permeable membrane. If the metal favours the shale then more cadmium than expected will remain in the beaker with the shale.

Ultimately, the results of this chapter will allow us to understand how the use of PAM as an additive may influence the composition of flow-back waters. The PAM and the shale will compete to adsorb and bind metals in the fluid that were either present initially or have been released by the shale. The behaviour, and potential to bind metals in the aqueous fluid, may have important influence on certain trace elements returning to surface or being able to migrate through strata.

7.3. Colloid Experiment Method

For this experiment there are two main methodologies, each analysing a different outcome. The first methodology analyses aqueous PAM that may or may not have travelled through a semi-permeable membrane (dialysis tubing) into a higher volume matrix fluid. Aqueous PAM concentration was measured to see how much may have transferred across the membrane using the *N*-Bromination method previously mentioned (Section 3.3.5). The second methodology utilises ICP-OES (Inductively Coupled Plasma – Optical Emission Spectroscopy) to measure concentrations of cadmium (Cd) and sodium (Na) that may have transferred across the dialysis membrane due to competing adsorption between aqueous PAM and shale (Figure 7.1). The PAM manufacture uses large amounts of sodium polyacrylate in its manufacturing process and so sodium was measured as proxy for PAM.

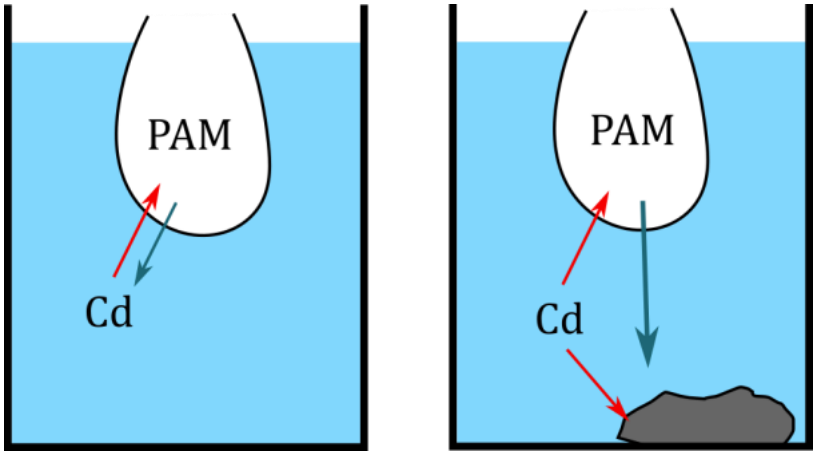

Figure 7.1: *Experiment setup for the colloid analysis. In order to understand the competition between PAM and the shale interface the same concentration of PAM and the same concentration of Cadmium will be measured against a beaker containing shale and one not containing shale.*

To statistically test the colloidal behaviour of PAM, and how this alters the behaviour of cadmium in the presence or absence of shale, there needed to be multiple concentrations of PAM and cadmium measured. Essentially, the experiment is multi factor:

1. The concentration of cadmium is measured in the bag at the end of the experiment to determine how much cadmium can transfer across the membrane with no shale present.
2. The concentration of cadmium is measured in the bag at the end of the experiment to determine how much cadmium can transfer across the membrane when there is shale present – does the cadmium favour PAM or the shale?
3. Differing concentrations of PAM and cadmium were used to see if either has an effect on the transference, in the presence or absence of shale.

Each specific cadmium concentration needed to be tested against the presence or absence of a shale competitor. The experiment breadth in terms of numbers of experiments run can be viewed in Table 7.1.

SHALE	PAM Conc (mg/L)	CADMIUM CONC (mg/L)				EXPERIMENT NUMBER
NO	0	1	5	10	20	#1
	15.625	1	5	10	20	#2
	62.5	1	5	10	20	#3
	500	1	5	10	20	#4
YES	0	1	5	10	20	#5
	15.625	1	5	10	20	#6
	62.5	1	5	10	20	#7
	500	1	5	10	20	#8

Table 7.1: *Experimental setup for the colloid experiment. There were four differing PAM concentrations that each contained a range of cadmium concentrations in the beaker. Of these four PAM ranges, one contained shale and the other no shale.*

Each experiment consisted of 4 dialysis bags containing 20 ml of identical PAM slick-water concentrations submerged in 4 glass beakers full of 400 ml of solution of differing cadmium concentrations. Each row in Table 7.1 represents one experiment run, and thus 8 experiment runs were completed. Four runs were completed with no shale in the cadmium matrix fluid and an identical four runs were completed with shale in the cadmium matrix fluid (Figure 7.2).

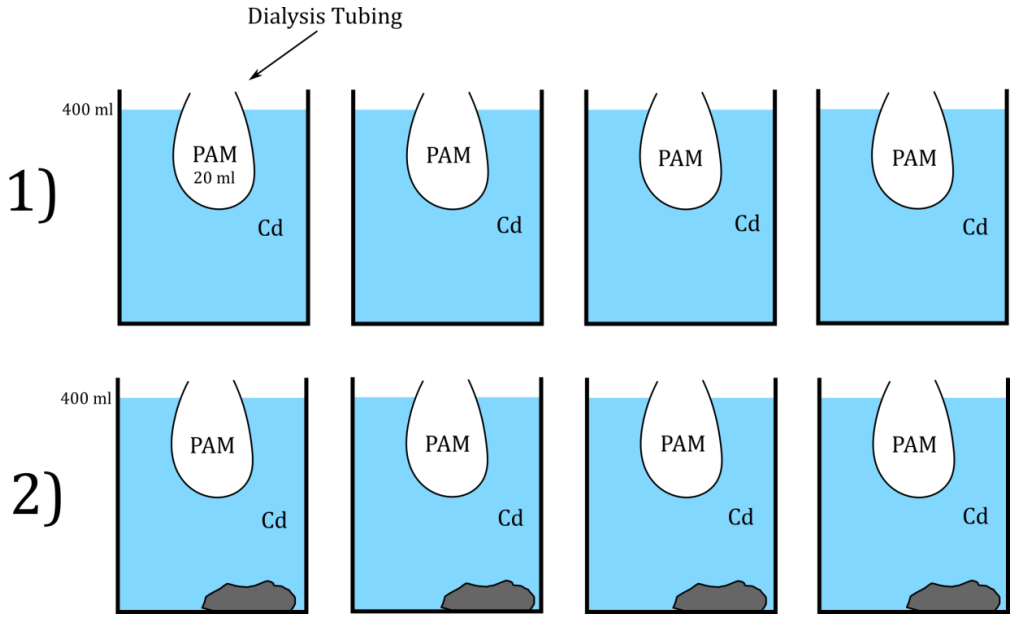

Figure 7.2: *Colloid setup runs in terms of cadmium concentrations spiked into the beakers. Row 1 represents the four beakers for a run of a certain concentration of PAM in the dialysis bag – in total there would have been four runs of these, each with a differing concentration of PAM. Row 2 represents the four beakers for a similar run, but this time with the addition of shale to the cadmium matrix fluid – in total four*

of these would have been run for the four different concentrations of PAM necessary. Shaded grey mass in line '2' refers to the presence of shale.

Overall, 32 experiments were run to test these ranges of both PAM and cadmium concentrations (Table 7.1). For each experiment, aqueous polyacrylamide concentration was measured both in the dialysis bag and the beaker at the start and end of the experiment. Fluid from the both the bag and beaker before and after the experiment was syphoned off for ICP analysis. ICP-OES analysis tested for cadmium and sodium to see the concentration transfer in the presence or absence of shale.

7.3.1. Sample Preparation

Only one shale sample was used for this experiment, OC 3 (Hazelhurst Fell, Upper Bowland Shale). Sample availability resulted in the use of this sample. Shale used in this experiment used the same powdered material as used in the RT and HPHT adsorption experiments (Sections 3.3 and 4.5). Sample OC 3 was chosen as a very 'typical' shale. The OC 3 shale contains mainly kaolinite and illite type clays, typical of the Bowland Shale (Gross et al., 2015), has very typical organic shale carbon and TOC values; 4.71 wt% and 3.33 wt% respectively, and contains reasonable clay content based on the Si/Al ratio (Table 2.11, Section 2.4.2).

7.3.2. Cadmium Solution Preparation

A 2000 mg/L cadmium solution was made by mixing 4.063 g of cadmium chloride with 1 L of DI water, thus producing a solution that could be diluted down into 400 ml volumes for the desired concentrations of 1, 5, 10 and 20 mg/L (Table 7.2).

2000 mg/L CADMIUM SOLUTION	
Desired mg/L	ml in 400 ml
20	4
10	2
5	1
1	0.2

Table 7.2: *Dilution calculations for diluting down the 2000 mg/L cadmium stock solution into workable concentrations within a 400 ml matrix fluid. For example, 4 ml of 2000 mg/L cadmium in 400 ml of water produces a 20 mg/L cadmium solution.*

Cadmium chloride was found to be the best compound for dissolution in the matrix water. It offered very little interference at a 570 nm wavelength on the spectrophotometer making it easier to analyse aqueous PAM using the *N*-Bromination method (Section 3.3.5). Other compounds initially tested for inclusion in this study were: magnesium sulphate, manganese sulphate and copper (II) chloride. All were tested and deemed unsuitable.

7.3.3. PAM Adsorbancy method overview

As detailed in the full *N*-Bromination method, Section 3.3.5, an aqueous sample thought to contain PAM was taken from both inside and outside the dialysis bag, before the experiment started, and after overnight completion. This aqueous PAM solution was diluted tenfold to bring aqueous PAM into an analytical range for the spectrophotometer. All samples were diluted, regardless of whether they contained a known negligible amount of PAM or not. Despite using only 3 concentrations containing PAM; 15.625 mg/L, 62.5 mg/L and 500 mg/L, the same full suite of calibration standards, between 0 and 1000 mg/L PAM, was used. Using the same calibration standards maintained consistency across all experiments which measured for aqueous PAM content.

7.3.4. ICP-OES Analysis setup overview

As is standard throughout this study for ICP-OES analysis, explained in more detail in Section 6.4.3, each 1 ml sample of fluid was diluted eleven fold with 10 ml of ~ 7 % ANALR grade Nitric Acid (HNO_3). This dilution ensured there was enough sample for the machine to use at least once, and potentially twice if necessary. The dilution also ensured that any suppression effects on the internal standard (Yttrium), because of the presence of PAM in the analyte, were at a minimum. Equally, dilutions had to minimised to avoid lowering concentrations of analyte below detection. This dilution procedure was adhered to on all ICP samples, whether or not they were suspected of containing aqueous PAM. The cadmium was measured using three wavelengths; 2144 nm, 2265 nm and 2288 nm. Sodium was measured on four different wavelengths; 3302 nm, 5688 nm, 5889 nm and 8183 nm. All wavelengths were used in the data analysis as none produced any erroneous results. All samples were spiked with 2 mg/L yttrium 3710 as an internal standard – this spiking would aid the discovery of signal suppression, where present.

7.3.5. Step by step method

A depiction of how the experiment works is given in Figure 7.3.

Day 1: A 1000 mg/L PAM solution was produced by adding 1 g of non-ionic PAM powder to 1 L of mains tap water. Four 500 ml glass beakers were filled with 400 ml of a tap

water matrix fluid. From here the relevant amount of tap water was removed as per Table 7.2, and the desired amount of 2000 mg/L cadmium solution was added to obtain the desired cadmium concentration. 1 ml of fluid was removed from the overall now cadmium rich matrix fluid and stored for ICP analysis. Alongside this, 10 cm of SnakeSkin ® 3.5 kDa MWCO (molecular weight cut-off) dialysis tubing (Thermo Scientific) was cut and sealed at one end. 20 ml of the relevant PAM fluid was pipetted into the dialysis bag and 1 ml removed for ICP analysis. The dialysis bag was then sealed. Shale sample was then added (if experiment required it) to the 400 ml matrix fluid in the beaker and thoroughly mixed. Once mixed the dialysis bag containing the 20 ml of PAM slick-water fluid was then fully submerged within the 400 ml matrix fluid in the beaker. The top of the beaker was then sealed with parafilm and left overnight for 16 hours to allow for any fluid transfer to take place.

Day 2: Parafilm was removed from the sealed beakers and the dialysis bags were removed from the matrix fluid. 1 ml of each fluid was syringed off from the respective vessels and stored frozen for ICP analysis. The remaining fluid was then tested for the presence of aqueous PAM using the *N*-Bromination method detailed in Section 3.3.5.

Fluid samples were taken from each vessel before and after the reaction had taken place: this was to measure the change in concentrations across the membrane.

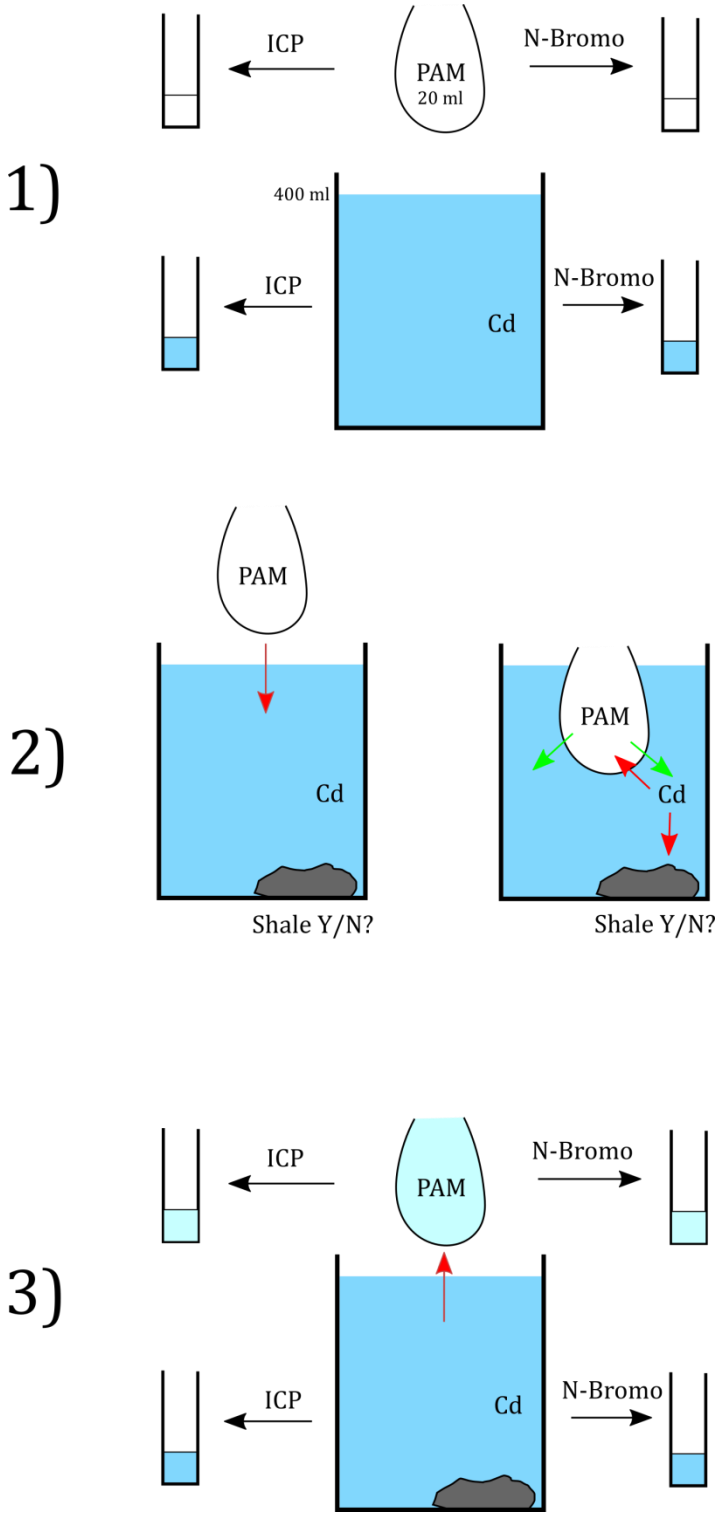

Figure 7.3: *Graphical depiction of the working of the colloid analysis. Stage 1) Before the experiment has started, fluids are syphoned away from both the PAM fluid within the dialysis bag, and the cadmium rich matrix fluid. Both fluids are tested for cadmium and Na content on the ICP, and aqueous PAM content on the spectrophotometer. Stage 2) The dialysis bag is sealed and placed into the 400 ml of cadmium rich matrix fluid. Dependent on experiment, shale may or may not have been added to the fluid. Sample is left to soak overnight and allow any transfer to occur. Stage 3) Dialysis bag is removed from the cadmium rich fluid. Samples of both fluids are tested for cadmium and sodium on the ICP, and aqueous PAM on the spectrophotometer, as per stage 1.*

7.3.6. Data Analysis Method

Raw data outputted from the ICP-OES was immediately checked for any erroneous data and erroneous suppression values (Figure 7.7). Once erroneous data was rectified or removed, all values were multiplied by 11 to correct for the dilution via the 10 ml addition of HNO_3 to each sample.

To measure the amount that will have migrated across the dialysis tubing's semi-permeable membrane, the level of fractionation needed to be calculated in terms of the dilution between the dialysis bag of 20 ml and the glass beaker of 400 ml. The fractionation value was determined by dividing the diluted value (the cadmium concentration with the additional 20 ml of PAM fluid to the 400 ml cadmium matrix) by the observed concentration of cadmium in the bag after submerging. This value was calculated from the control experiment, #1, where no PAM was present in the bag, and no shale present in the beaker. The cadmium here is not influenced by anything and the concentration remaining in the bag classed as the normal transference concentration based upon no additional factors.

The loss/gain ratios for sodium within the beaker were analysed using t-tests, based upon fractionation results and the measurement of aqueous PAM. A four factor ANOVA (analysis of variance) was performed on the final results to observe any relationships between the factors in the experiment. Factors were classed as the PAM concentration, the cadmium concentration, the presence or absence of shale and the wavelength of the cadmium tested. The responses were based on the calculated and observed results from the experiments. The responses were; observed cadmium concentration (mg/L); the colloid fraction (the difference between the observed and the expected concentration (based upon the colloid fraction)); the concentration on colloid (the difference between the expected concentration (based on the colloid fraction) and the observed concentration; and finally the K value (the result when dividing the concentration on colloid by the observed concentration). The K value for each experiment shows how the cadmium behaves. A lower K value, for this experiment, demonstrates that cadmium prefers the substance (rock type) in the beaker, and higher K values prefer the PAM contained within the dialysis bag.

7.4. PAM Colloid Results

For this study, it was not necessary to plot Freundlich or Langmuir isotherms to determine adsorbed and aqueous PAM. Aqueous PAM concentration was measured in both the bag and the beaker at the start and end of each experiment. The addition of cadmium chloride to the matrix fluid provided minimal effect upon the absorbance of light in the spectrophotometer, an average of 0.013 absorbance units which was subtracted from all

adsorption results to account for the aqueous PAM. Results for all both experiments, shale or no shale, can be seen in Table 7.3. Results showing the concentration of aqueous PAM can be seen in Figure 7.5 for no shale presence and Figure 7.6 where the shale was present.

	Cd	POLYACRYLAMIDE			
	CADMIUM (mg/L)	INITIAL BAG (mg/L)	PREDICTED (mg/L)	ACTUAL (mg/L)	RATIO (loss/gain)
NO SHALE	1	15.6	0.743	0	
	5	15.6	0.743	0	
	10	15.6	0.743	4.443	5.980
	20	15.6	0.743	1.008	1.356
	1	62.5	2.976	0	
	5	62.5	2.976	1.008	0.339
	10	62.5	2.976	0	
	20	62.5	2.976	0	
	1	500	23.810	0	
	5	500	23.810	0	
	10	500	23.810	1.580	0.066
	20	500	23.810	0	
SHALE	1	15.6	0.743	0	
	5	15.6	0.743	0	
	10	15.6	0.743	0	
	20	15.6	0.743	0	
	1	62.5	2.976	0	
	5	62.5	2.976	0	
	10	62.5	2.976	4.214	1.416
	20	62.5	2.976	0.664	0.223
	1	500	23.810	0	
	5	500	23.810	0	
	10	500	23.810	0	
	20	500	23.810	6.504	0.273

Table 7.3: *Results of the colloid experiment runs in terms of aqueous PAM. 'Initial Bag' refers to the PAM concentration inside the dialysis bag at the start. 'Predicted' refers to the detectable concentration range using the fractionation value. 'Actual' refers to the measured concentration of PAM detected in the beakers after fluid transfer has taken place.*

Multiple measurements from the beaker measured 0, showing that either zero PAM, or amounts of PAM that are so small they are undetectable by the method (Table 7.3). The detection limit, using the lowest PAM concentration of 15.625 mg/L was 0.74 mg/L. Out of all

8 results for the lowest concentration of PAM, aqueous PAM in the beaker after dissolution was so low it was undetectable in most samples. The highest concentration was at 4.4 mg/L. Knowing that the minimum detectable limit was 0.74 mg/L, results show that for the most part, aqueous PAM is present in a concentration lower than this, hence why zero values have been measured for 17 out of the 24 samples (Figure 7.4).

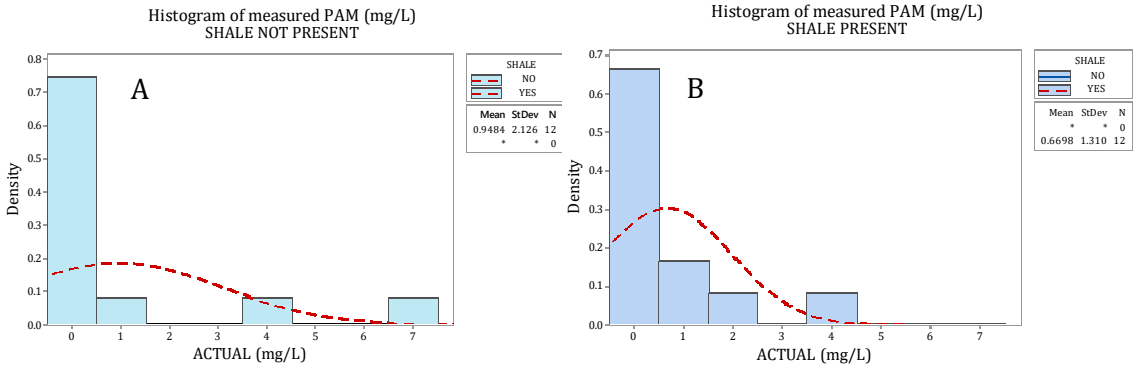

Figure 7.4: *Histograms displaying the distribution of the measured aqueous PAM in the 400 ml beaker full of cadmium matrix fluid after the experiment had finished. A) without shale, B) with shale.*

The majority of the ratios, for the loss or gain above or below the 'predicted' value (Table 7.3), are below 1 showing a lack of transference of PAM over the semi-permeable membrane, either with or without the presence of shale. Values that are greater than 1 are in the minority for each set of results, being either completely undetectable lower concentrations of aqueous PAM with the hypothetical full fluid dilution. These ratios that are > 1 may be erroneous results as only 2/24 exhibited values such as these.

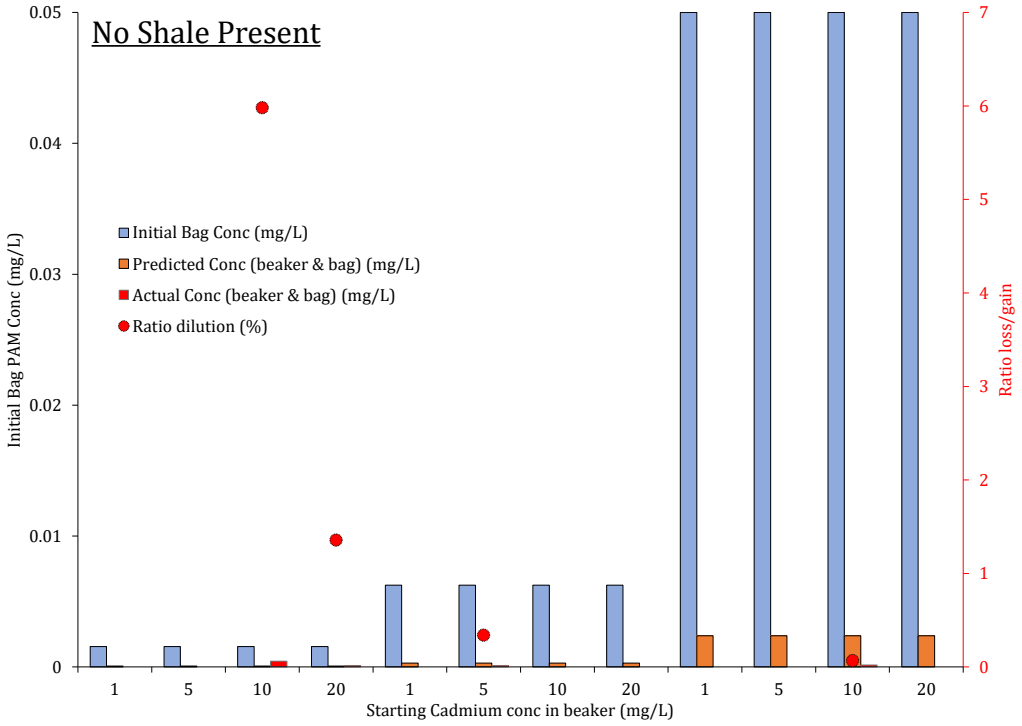

Figure 7.5: *PAM transference from dialysis bag to beaker over 12 hour period <u>without</u> shale present within the beaker. 'Predicted conc (beaker & bag)' refers to the concentration of PAM across the full volume of both bag and beaker if there was total equilibrium between the two (420 ml). 'Actual Conc (beaker & bag)' refers to the actual measured concentration of PAM in the 420 ml. 'Ratio dilution' refers to whether the conc of PAM measured in the beaker at the end of the experiment is greater or lesser than the expected concentration if the initial 20 ml of PAM is diluted with 400 ml of water.*

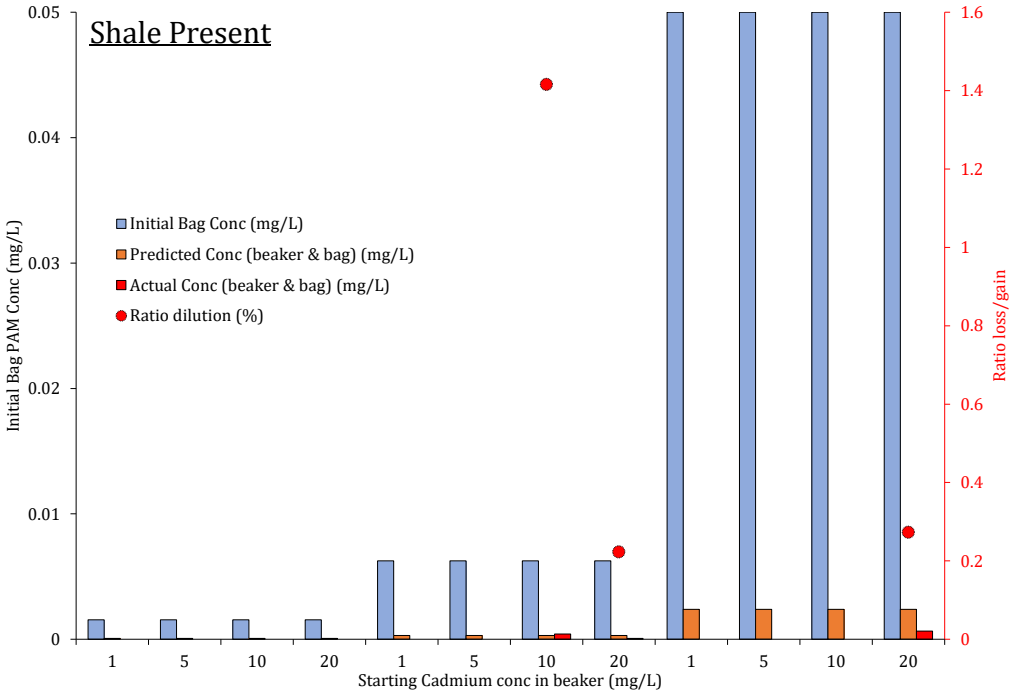

Figure 7.6: *PAM transference from dialysis bag to beaker over 12 hour period <u>with</u> shale present within the beaker. 'Predicted conc (beaker & bag)' refers to the concentration of PAM across the full volume of both bag and beaker if there was total equilibrium between the two (420 ml). 'Actual Conc (beaker & bag')' refers to the actual measured concentration of PAM in the 420 ml. 'Ratio dilution' refers to whether the*

conc of PAM measured in the beaker at the end of the experiment is greater or lesser than the expected concentration if the initial 20 ml of PAM is diluted with 400 ml of water.

Overall, results exhibited here show that PAM does not pass through the pores of the semi-permeable membrane of the dialysis tubing. This behaviour is unaffected by the presence or absence of shale. The presence of shale does not bring any PAM through the membrane.

7.5. Cadmium and Sodium Colloid Results

Cadmium was analysed as the primary cation for the transfer between the semi-permeable membranes. Sodium was initially measured as a proxy for the amount of aqueous PAM that may have also transferred across this membrane. Yttrium 3710 was run as an internal standard when measuring samples on the ICP-OES machine. This standard failed on one attempt, run #3, and so result set number 6 was not used due to erroneous measurement on the ICP (Figure 7.7). Set number 6 was the analysis of colloid at a PAM concentration of 15.625 mg/L in the presence of shale (Figure 7.1). The remaining runs (1, 2 and 4) analysed all remaining samples with no large errors on the internal standard.

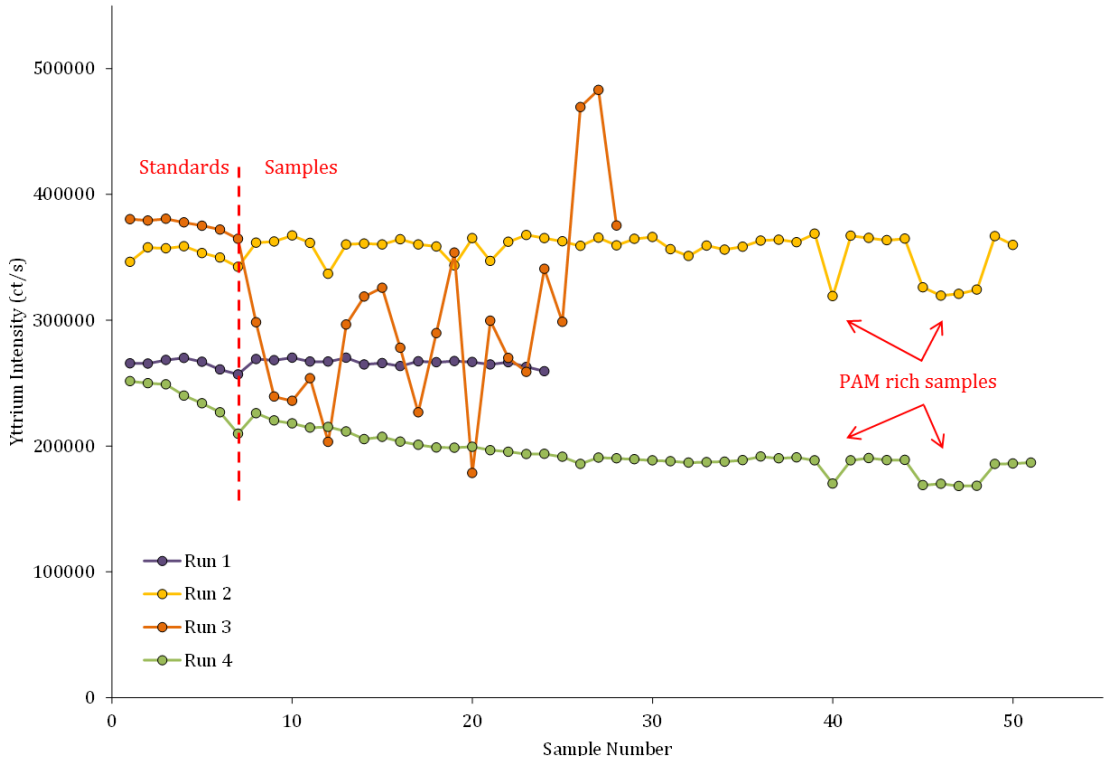

Figure 7.7: *The suppression of the Yttrium 3710 spike for the four runs that were needed to analyse all samples for cadmium and Na. Run 1 analysed experiment #1, run 2 analysed experiments 2, 3 and 4, run #3 analysed experiment #6 and run 4 analysed experiments 5, 7 and 8. The difference in intensity counts exhibits the sensitivity of the machine at different time periods. Run #3 completely failed to provide any results for experiment number 6.*

The differing intensity between the different runs is normal, so long as the samples follow a similar intensity pattern as the spike is the same. Run #4 (Figure 7.7) exhibits slight drift throughout the whole sequence. Experiment #4 starts the analysis at ~ 25,000 ct/s and ends on ~ 20,000 ct/s, but does level out as the sample number increases. Runs #1 and #2 exhibit the least amount of drift or suppression for the internal standard. PAM offers some level of suppression in the machine itself (full details of this suppression itself detailed in Section 6.5), with higher concentrations producing more suppression – this can be accounted for by using the internal standard. Runs #2 and #4 show the most amount of suppression due to the higher PAM concentration present (labelled on Figure 7.7). These ten points respectively represent an initial PAM concentration of 500 mg/L that has been diluted with 10 ml of ANALR HNO3. The value observed represents the Yttrium suppression for a 45.45 mg/L PAM solution. Experiment #5 failed to measure concentrations of cadmium for an unknown reason. Sodium readings were present for experiment #5 and were used in the sodium analysis, but not the cadmium analysis. Based on the results from other experiments, it is unlikely that the lack of cadmium is due to the cadmium being a) all adsorbed to the shale, or b) having precipitated out of solution. It is more likely to be due to instrument failure.

7.5.1. Sodium

Sodium was initially utilised in the ICP analysis as a proxy for PAM, however, as has already been mentioned, negligible amounts of PAM were transferred through the semi-permeable membrane (3.5 kDa MWCO). There is an increase in sodium concentration when the PAM concentration is increased (8). This transference of sodium across the semi-permeable is likely to just be residual sodium, not directly associated to the colloid behaviour itself.

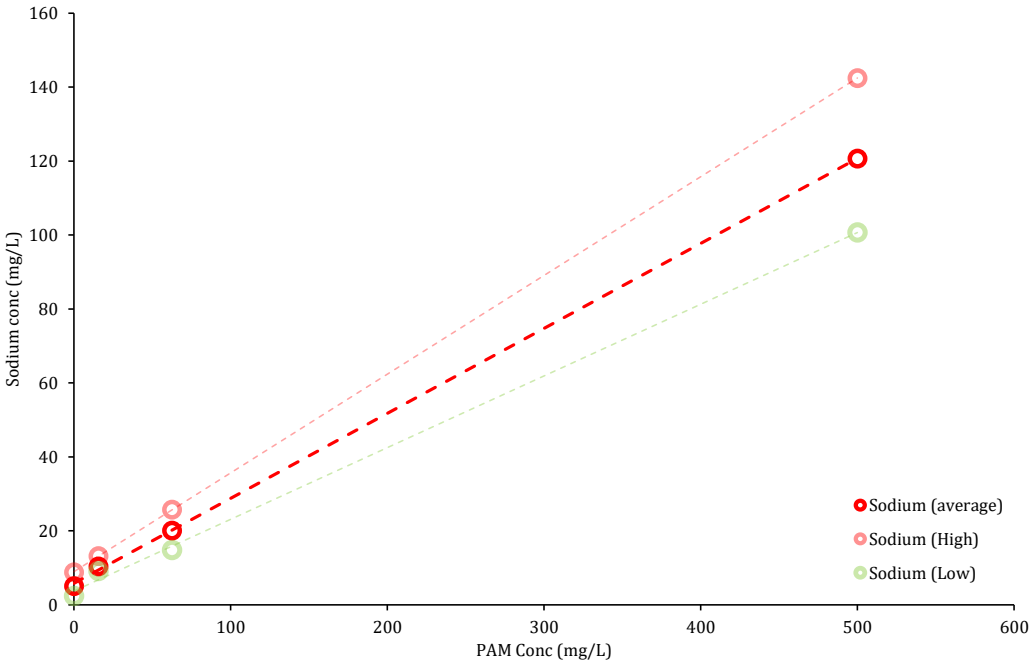

Figure 7.8: *Sodium concentrations shown for the four concentration of PAM fluids used in the dialysis bags before the bags had been submerged in the cadmium rich matrix fluid. Values are shown in terms of the highest and lowest sodium values observed for each concentration of PAM.*

Results show that this residual sodium related to PAM is able to pass through the semi-permeable membrane of the dialysis tubing. Sodium quantities for the PAM used were unavailable from the manufacturer. A full results table for all concentrations measured for Sodium can be viewed in Digital Appendix G.1. Dilution factors were calculated to obtain the concentration value of the sodium in the beaker if the original concentration of 20 ml is diluted with a further 400 ml of cadmium rich matrix fluid – if the sodium had equilibrated across the membrane.

$$\frac{(\mathbf{400} \times \boldsymbol{a} + \mathbf{20} \times \boldsymbol{b})}{\mathbf{420}} \qquad \textbf{Equation 7.1}$$

The dilution calculation used to calculate the dissolution concentration of the sodium in a 420 ml fluid (400 ml beaker and 20 ml dialysis bag) is shown in Equation 7.1. '*400*' refers to the original volume of the cadmium-rich fluid in the beaker containing no additional sodium from PAM; '*a*' is the concentration of sodium in the beaker before the addition of the PAM filled dialysis bag; '20' refers to the volume of PAM fluid in the dialysis bag; '*b*' is the concentration of sodium in the 20 ml dialysis bag before submersion and; '*420*' is the total volume of the beaker and the bag combined. A full set of results can be observed in Appendix G.1.

When the concentration is calculated, to confirm total transference over the membrane, this calculated concentration must be a very similar, if not the same value to the actual measured concentration. Ratios between the calculated and actual concentration were calculated, the t-test of these results are shown in Table 7.4.

PARAMETERS	95 % CI for μ	MEAN	T-VALUE	P-VALUE
All data	0.9746 - 1.0807	1.0276	1.03	0.303
Shale Present Any PAM	0.9589 - 1.0843	1.0216	0.7	0.49
No Shale Present Any PAM	0.9533 - 1.1095	1.0314	0.8	0.424
Shale Present No PAM	0.8531 - 1.2029	1.028	0.35	0.735
Shale Present Only PAM	0.9835 - 1.0522	1.0178	1.08	0.293
No shale Present No PAM	0.7168 - 1.0594	0.881	-1.42	0.18
No Shale Present Only PAM	0.9816 - 1.1534	1.0675	1.58	0.121

Table 7.4: *t-test results of the ratio results for all combinations of fluid and shale present. 'Only PAM' refers to all concentrations of PAM grouped together. 'No PAM' refers to ratios calculated from experiments that contained no concentration of PAM at any stage of the experiment.*

Overall, all the average ratios for the differing parameters are not significantly different from 1.0 for any parameter (Figure 7.4). The most deviation is seen in samples that contained no shale or PAM, the smallest dataset for the t-test ("No Shale Present, No PAM" in Figure 7.4), exhibiting a negative t-value. The P-value for all datasets is greater than the error margin used (0.05) showing that there is weak evidence against the null hypothesis (no significant difference between the populations) for all samples. The fact that there is no significant deviation from the mean of 1, and no significant difference in populations shows us that none of the three experiment factors; PAM concentration, cadmium concentration or the presence or absence of shale, have any influence on the sodium content in any part of the system.

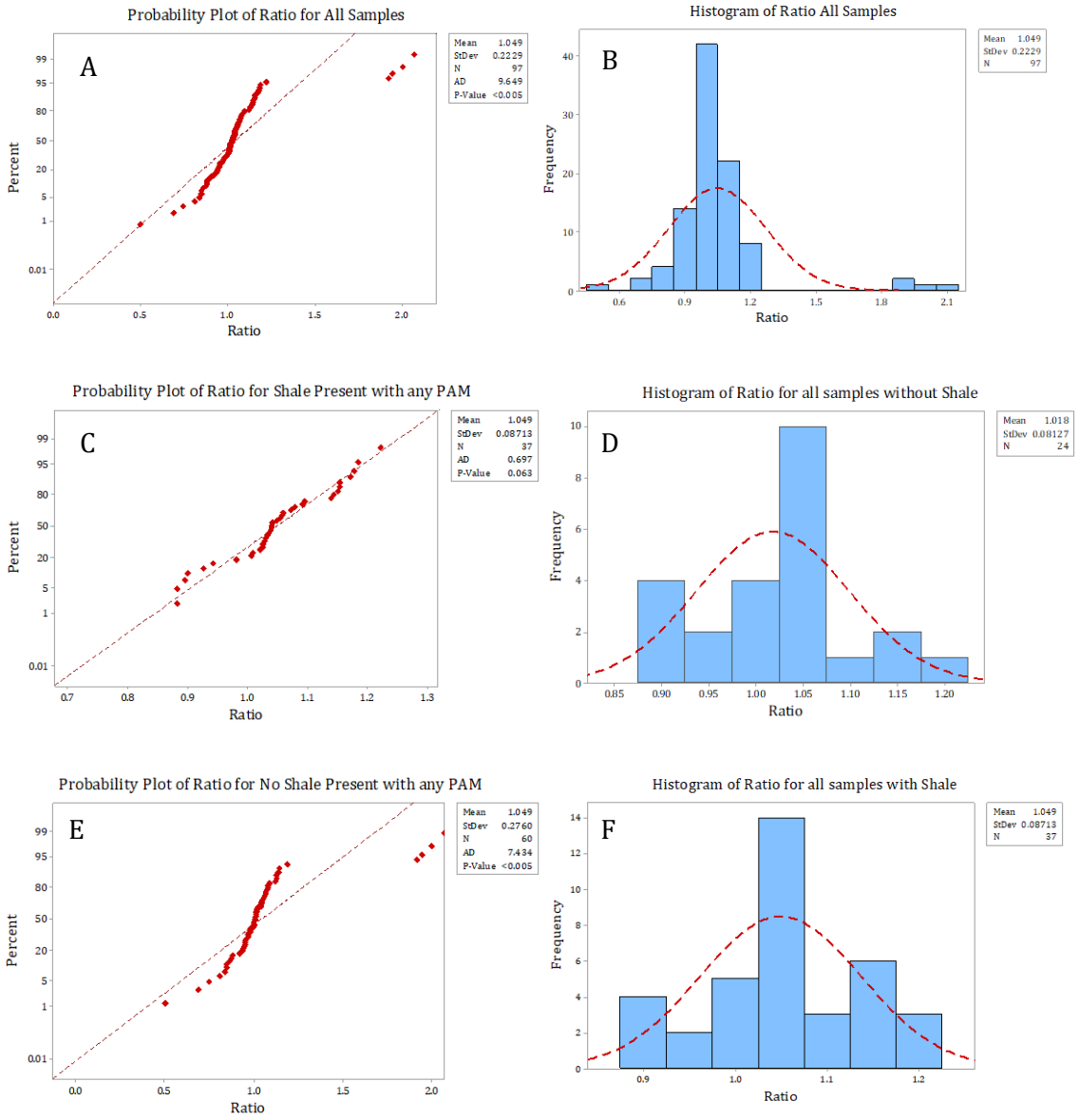

Figure 7.9: *Normality tests and histograms for the key parameters of the sodium tests. The majority of distributions stick to a ratio of approximately 1, showing minimal migration from the calculated diluted value and thus a general complete equal distribution in the finishing fluid of 420 ml.*

Histograms show that the majority of ratio results are between 1.0 and 1.1 (Figure 7.9). Results between 1.0 and 1.1 are true for all data tested together, and data tested with PAM and without PAM. Statistically there was no change in the sodium concentration across all parts of the system, even with differing experimental factor, i.e. sodium passes freely through the membrane and appears to be controlled by its source and by its solubility.

7.5.2. Cadmium

Due to the method of producing the 2000 mg/L cadmium chloride solution, slight inaccuracies were present in the exact initial starting concentrations for the experiment. These inaccuracies however, were not an issue as the starting concentrations in each beaker were known values. Percentage migration and colloid fraction can be calculated by the start and end values being both known concentrations. Planned concentrations (i.e. 20, 10, 5 and 1 mg/L) vs observed concentrations can be viewed in Figure 7.10.

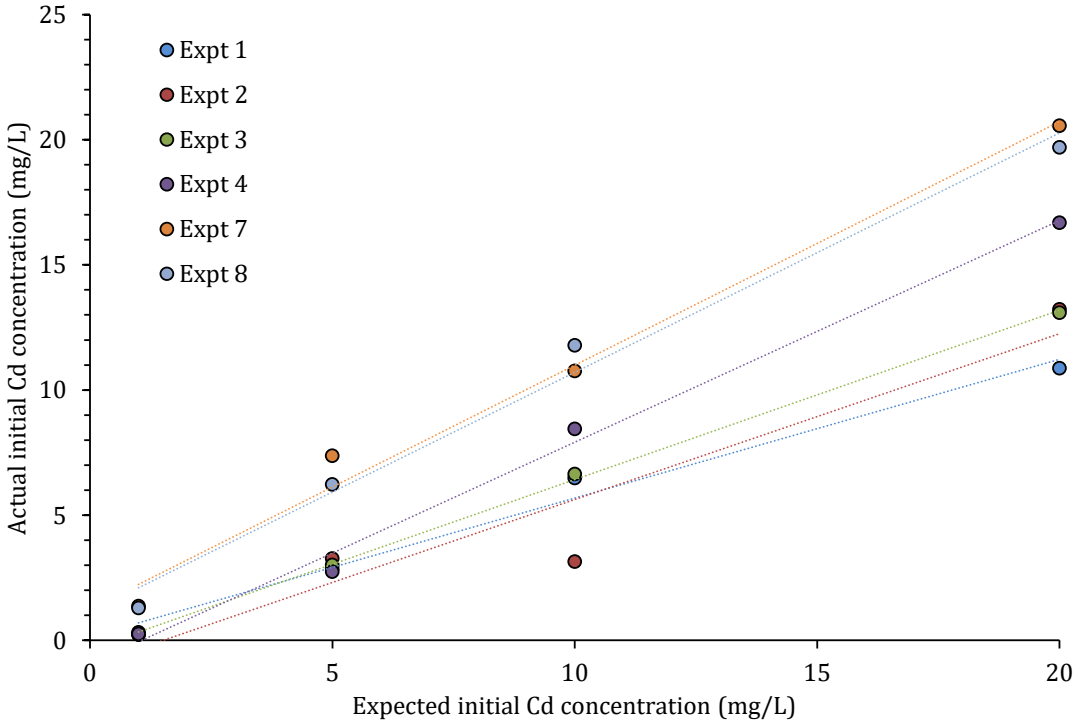

Figure 7.10: *Initial starting concentrations of cadmium for each 400 ml beaker before dialysis bags or shale were added, depending on the experiment being run. The four columns of data represent each of the four beakers used per experiment, from highest cadmium concentration to lowest. Experiment #5, shown as zeroes on the figure, measured no cadmium due to machine error.*

Despite the range observed in the starting concentrations of cadmium (Figure 7.10), all data was within the correct ratio for each individual experiment. All fits for all data seen in Table 7.5 are > 90 % r^2, showing consistent steps in concentration for each experiment run.

EXPT NO.	Cd STARTING R^2
1	0.9854
2	0.9139
3	0.9993
4	0.9941
5	N/A
6	N/A
7	0.9877
8	0.988

Table 7.5: *r^2 fits for all starting concentration ranges seen in Figure 7.10*

This confirmation of the fits for each cadmium concentration range ensured that the initial concentrations are correct and linear for each experiment. From this, the fractionation value could be estimated for each experiment.

	BLANK - NO PAM IN BAG				
Cd WAVELENGTH	INITIAL CONC (mg/L)	DILUTED CONC (mg/L)	OBSERVED CONC (mg/L)	FRACTIONATION	% GAIN
2144	10.860	10.342	13.079	1.265	26.45
2265	9.990	9.514	11.869	1.247	24.7
2288	10.253	9.764	12.375	1.267	26.7
Average	10.368	9.873	12.441	1.260	25.950

Table 7.6: *Table of results for a subset of experiment #1, the blank, containing no PAM in the dialysis bag and no shale sample in the beaker. 'Initial concentration' is the concentration of cadmium in the beaker before the experiment has begun; 'diluted concentration' is the concentration in the beaker if the 20 ml bag transfers at equilibrium producing a 420 ml solution; 'observed concentration' is the concentration measured in the bag after the experiment has finished and; 'fractionation' is the amount gained or lost over the semi permeable membrane.*

Results for the blank displayed in Figure 7.11 show that in the absence of PAM slick-water fluid or shale to influence substance transfer, an average of 25.9 % extra cadmium is observed within the bag, accounting for only the volume of the bag (20 ml) and not the whole 420 ml system inclusive of the bag and beaker. This fractionation figure, ranging from 1.247 to 1.267 is used as a calibration as the 'normal' behaviour, and all other results are calibrated from these values, respective to the wavelength measured.

Experiment #1 is treated as the overall blank having no shale or PAM present to influence the migration of the cadmium in either the dialysis bag or the beaker. The other experiments (#2 through to #8) all link to each other. For example, #2 to #6 without and with shale respectively, #1 to #5, #3 to #7 and #4 to #8. In this instance, experiments #5 and #6 failed on ICP analysis due to both hardware and internal standard issues. Useable data is present in #1, #2, #3, #4, #7 and #8. Direct comparisons between the presence and absence of shale can only be calculated in #3 and #7 and #4 and #8 respectively, measurements for 62.5 mg/L PAM and 500 mg/L PAM. Results for all samples using the fractionation value stated above can be seen in Table 7.7. A full table of results can be viewed in Digital Appendix G.1.

		NO SHALE PRESENT				SHALE PRESENT			
		BLANK							
	EXPT No.	#1	#2	#3	#4	#5	#6	#7	#8
	PAM Conc (mg/L)	0	15.625	62.5	500	0	15.625	62.5	500
	Cd Wavelength								
	2144	13.079	15.921	15.765	20.076			24.760	23.713
Expected Conc (mg/L)	2265	11.869	14.637	14.611	18.714			20.074	19.133
	2288	12.375	15.215	15.255	19.516			22.145	21.203
	2144	13.079	11.880	10.310	14.311			19.635	25.652
Observed (mg/L)	2265	11.869	11.132	9.678	13.442			16.082	20.658
	2288	12.375	11.396	9.933	13.684			17.501	22.462
	2144	0.000	0.254	0.346	0.287			0.207	0.000
Colloid Fraction	2265	0.000	0.239	0.338	0.282			0.199	0.000
	2288	0.000	0.251	0.349	0.299			0.210	0.000
	2144	0.000	4.041	5.455	5.765			5.125	0.000
Conc on Colloid	2265	0.000	3.505	4.933	5.272			3.992	0.000
	2288	0.000	3.819	5.322	5.832			4.644	0.000
	2144	0.000	0.340	0.529	0.403			0.261	0.000
K Value	2265	0.000	0.315	0.510	0.392			0.248	0.000
	2288	0.000	0.335	0.536	0.426			0.265	0.000
	2144	7.035	3.407	7.198	9.152			11.669	12.776
Expected Conc (mg/L)	2265	6.369	3.112	6.636	8.484			9.456	10.294
	2288	6.640	3.242	6.943	8.864			10.409	11.427
	2144	7.035	5.597	4.828	8.313			10.794	12.771
Observed (mg/L)	2265	6.369	5.240	4.523	7.810			8.857	10.282
	2288	6.640	5.363	4.643	7.951			9.624	11.187
	2144	0.000	0.000	0.329	0.092			0.075	0.000
Colloid Fraction	2265	0.000	0.000	0.318	0.079			0.063	0.001
	2288	0.000	0.000	0.331	0.103			0.075	0.021
	2144	0.000	0.000	2.370	0.839			0.875	0.005
Conc on Colloid	2265	0.000	0.000	2.113	0.674			0.599	0.012
	2288	0.000	0.000	2.300	0.913			0.785	0.240
	2144	0.000	0.000	0.491	0.101			0.081	0.000
K Value	2265	0.000	0.000	0.467	0.086			0.068	0.001
	2288	0.000	0.000	0.495	0.115			0.082	0.021
	2144	2.877	3.299	3.043	2.765			7.445	6.292
Expected Conc (mg/L)	2265	2.611	3.032	2.817	2.564			6.066	5.097
	2288	2.714	3.154	2.946	2.682			6.664	5.654
	2144	2.877	1.989	2.318	2.270			6.333	6.736
Observed (mg/L)	2265	2.611	1.854	2.170	2.130			5.196	5.437
	2288	2.714	1.898	2.226	2.167			5.652	5.907
	2144	0.000	0.397	0.238	0.179			0.149	0.000
Colloid Fraction	2265	0.000	0.389	0.230	0.170			0.143	0.000
	2288	0.000	0.398	0.244	0.192			0.152	0.000
	2144	0.000	1.310	0.725	0.495			1.112	0.000
Conc on Colloid	2265	0.000	1.179	0.647	0.435			0.869	0.000
	2288	0.000	1.256	0.719	0.515			1.013	0.000
	2144	0.000	0.659	0.313	0.218			0.176	0.000
K Value	2265	0.000	0.636	0.298	0.204			0.167	0.000
	2288	0.000	0.662	0.323	0.238			0.179	0.000
	2144	0.180	0.126	0.132	0.140			0.769	0.726
Expected Conc (mg/L)	2265	0.163	0.115	0.122	0.129			0.626	0.586
	2288	0.169	0.119	0.127	0.135			0.683	0.646
	2144	0.180	0.086	0.091	0.095			1.304	1.286
Observed (mg/L)	2265	0.163	0.079	0.085	0.089			1.069	1.035
	2288	0.169	0.081	0.088	0.091			1.161	1.122
	2144	0.000	0.319	0.309	0.322			0.000	0.000
Colloid Fraction	2265	0.000	0.310	0.306	0.308			0.000	0.000
	2288	0.000	0.315	0.307	0.323			0.000	0.000
	2144	0.000	0.040	0.041	0.045			0.000	0.000
Conc on Colloid	2265	0.000	0.036	0.037	0.040			0.000	0.000
	2288	0.000	0.037	0.039	0.044			0.000	0.000
	2144	0.000	0.469	0.448	0.476			0.000	0.000
K Value	2265	0.000	0.450	0.442	0.445			0.000	0.000
	2288	0.000	0.461	0.442	0.478			0.000	0.000

Table 7.7: *Full suite of results for cadmium transference across the semi permeable membrane at different concentrations of PAM present and the presence or absence of shale. Data is calculated using the colloid fraction values observed in Table 7.6.*

PARAMETER	Model R^2	SOURCE	P-VALUE	FITTED MEANS		
Observed Conc (mg/L)	99.65%	Cd (mg/L) x Cd WL (nm)	0.013	Shale	No	5.135
		Shale Presence x Cd WL (nm)	0.001		Yes	9.489
Colloid Fraction	94.58%	Cd (mg/L)	0.001	Shale	No	0.262
		PAM (mg/L) x Cd (mg/L)	0.001		Yes	0.054
Concentration on Colloid	91.50%	PAM (mg/L)	0.001	Shale	No	1.889
		PAM (mg/L) x Cd (mg/L)	0.029		Yes	0.803
		PAM (mg/L) x Shale Presence	0.014			
K	94.72%	PAM (mg/L) x Cd (mg/L)	0.001	Shale	No	0.3698
					Yes	0.0646

Table 7.8: *Analysis of variance (ANOVA) table for cadmium concentration using all the four parameters specified in Section 7.3.6. Data is shown for experiments #3 and #7, and #4 and #8 respectively.*

The ANOVA shows that the presence of a shale effects the behaviour of aqueous cadmium, regardless of the concentration of PAM within the dialysis bag (Table 7.8). 'Fitted means', present in Table 7.8, predict the mean response values, useful for observing responses that are caused by changes in levels of the same factor, rather than unbalanced scenarios. Fitted means in the presence of shale are consistently lower than when the shale is not present. The K value fitted mean sits at 0.06 when there is shale present in the sample, rather than 0.36 when there is no shale present. A difference of 0.3052 between the two factors shows a vastly reduced concentration on colloid. This reduced concentration on colloid shows that the presence of shale is affecting the ability of cadmium to cross the membrane of the dialysis tubing. Using the data for comparable samples (#3 and #7 for 62.5 mg/L PAM and #4 and #8 for 500 mg/L PAM) and calculating the fractionation constants between the samples with and without shales, linear isotherms can be produced by plotting the K value (details in 7.3.6) against the concentration of cadmium on the colloid.

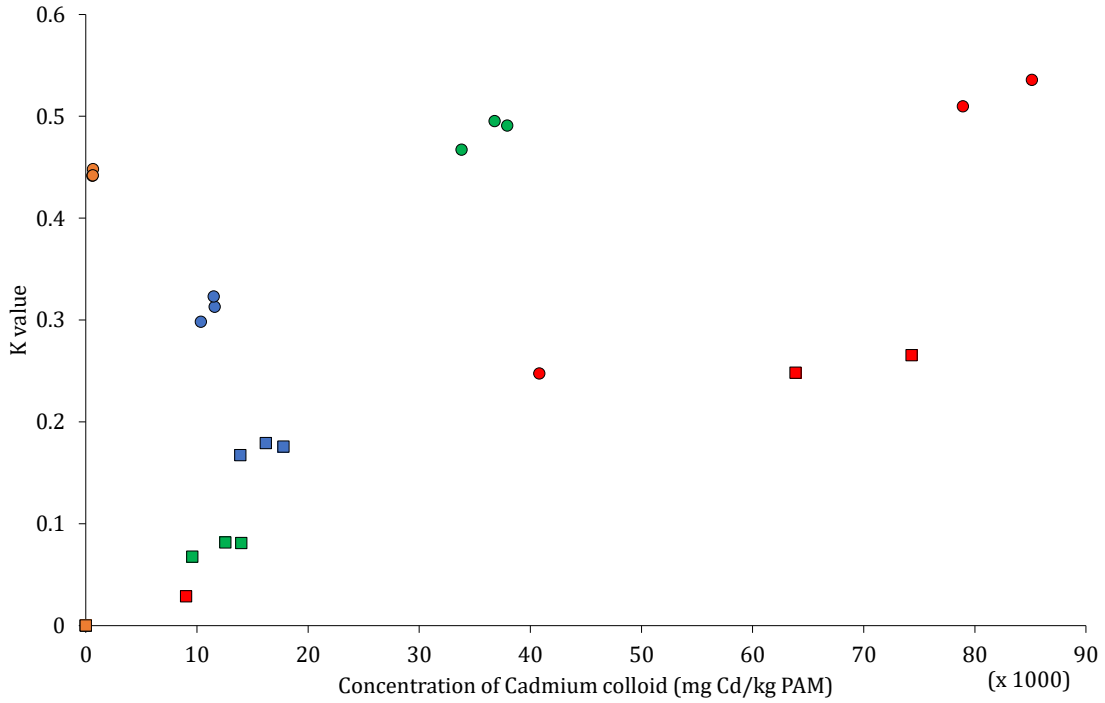

Figure 7.11: *Linear isotherm plotting the K value against the concentration of cadmium on colloid (mg/L) for a dialysis bag PAM concentration of 62.5 mg/L. Data is divided up between initial cadmium concentration and whether shale was present or absent within the beaker. The further to the right the data, the higher the initial starting cadmium concentration within the beaker.*

When a PAM concentration of 62.5 mg/L was used as the slick-water fluid within the bag, there is a clear difference between samples where there was a shale present, and samples where there was not. This presence or absence of the shale influences where the cadmium travels presence and absence of a shale influencing the cadmium (Figure 7.11). As observed, the K value reduces when a shale sample is involved rather than removed altogether. The K value is the calculated ratio between the observed concentration in the bag at the end of the experiment and the concentration on the colloid. The reduction observed here tells us that less cadmium than was predicted is present within the bag where there is shale present, particularly at PAM concentrations of 62.5 mg/L (Figure 7.11). Shale is significantly influencing the behaviour of cadmium more than the PAM is, providing the cadmium is freely available to travel across this semi-permeable membrane. Results shown here imply that due to this, cadmium is more likely to be adsorbed by the shale rather than bound by the aqueous PAM in fluid, and thus less likely to return to the surface in large quantities.

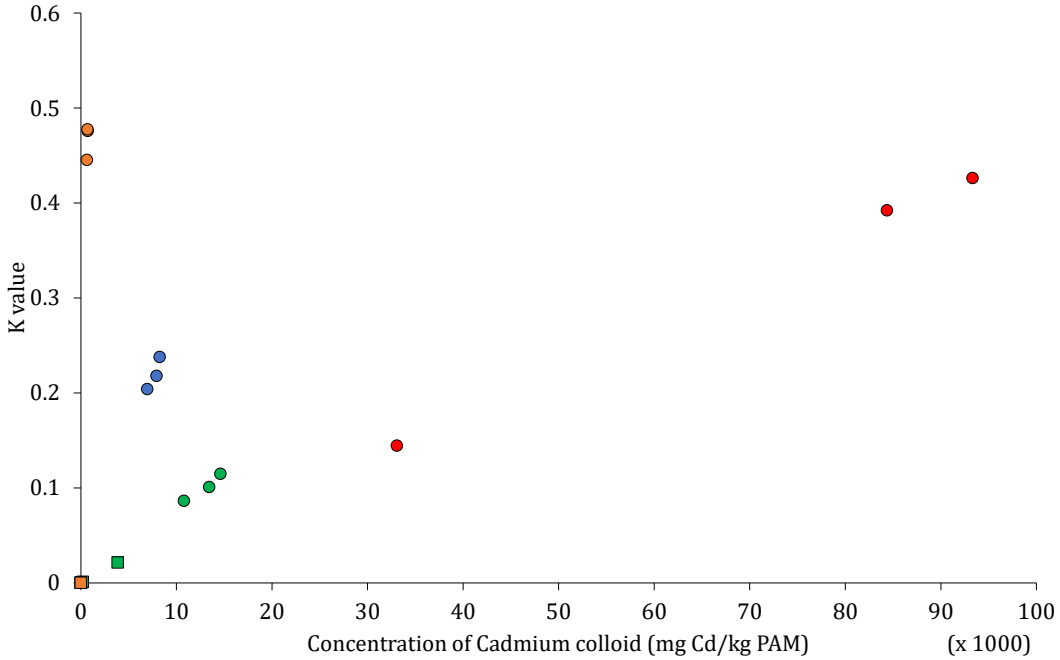

Figure 7.12: *Linear isotherm plotting the K value against the concentration of cadmium on colloid (mg/L) for a dialysis bag PAM concentration of 500 mg/L. Data is divided up between initial cadmium concentration and whether shale was present or absent within the beaker. The further to the right of the graph the data, the higher the initial starting cadmium concentration within the beaker. A high proportion of the K values seen within this data are zero, this is due to the overwhelming concentration of PAM that now seems to be out competing the shale for the cadmium.*

Using an initial PAM concentration of 500 mg/L in the dialysis bag, again another clear pattern is defined between the presence and absence of the shale in the beaker. The presence of shale, as denoted by squares in Figure 7.12, is having an overwhelming effect upon the adsorption of cadmium. K values of zero, shown in Table 7.7 and Figure 7.12, show that the shale has outcompeted the PAM significantly. In this scenario, cadmium is actively being drawn through the semi-permeable membrane of the dialysis tubing due to the influence of sample OC 3.

Experiments using a PAM concentration of 62.5 mg/L saw a reduction in K value when shale was added to the matrix fluid. This reduction in K value denotes that more cadmium is present in the beaker than the bag. Where the shale was present, Figure 7.11, all data sits at a lower K value than in the experiments where the shale was not present. Using an initial PAM concentration of 500 mg/L, the K values of the samples where shale was present were calculated at negative or zero values. These negative and zero values show that with an increase in PAM concentration, and with the shale present in the matrix fluid, the presence of shale outcompeted the colloid binding any cadmium present. Using a PAM concentration of 62.5 mg/L in Figure 7.11 shows that the shale still out competed the PAM. It would appear that increases in PAM concentration would promote the adsorption of cadmium to the shale, further intensifying the already strong forces binding cadmium and shale together, without the

need for PAM. ANOVA demonstrates this with consistently lower values for each parameter whenever there is shale present in the beaker (Table 7.8).

7.6. Discussion

It can be concluded from these experiments that PAM is acting as a colloid. Negligible amounts of PAM are able to transfer through the 3.5 kDa semi-permeable membrane of the dialysis tubing, with maximum concentrations of 4.4 mg/L and 6.5 mg/L present in the beaker after submersion of bags full of a 15.6 mg/L and 500 mg/L PAM fluid, respectively. Of the results where a PAM concentration was detected, 7/24 tests, three of the seven displayed greater amounts of PAM than predicted according to fractionation based upon the 20 ml bag diluted with a 400 ml beaker fluid. As learnt from Chapters 3, 4 and 5, PAM can readily adsorb onto shale (or other lithologies) and so if no barrier was present between the shale and the PAM-rich fluid, it is likely that adsorption would have occurred. However, due to the molecule size of the PAM within the fluid, this was unable to pass through the 3.5 kDa membrane and adsorb to the shale present, irrespective of concentration.

Cadmium, however, was able to successfully transfer across this membrane uninfluenced into the whole 420 ml fluid, as results from the blank (Expt #1 in Table 7.7) show. Based upon literature that cadmium adsorbs well to shales or treated materials (Shubha et al., (2001) investigating heavy metal removal using polyacrylamide grafted hydrous tin and Ma et al (2017) investigating the removal of heavy metal ions using a functionalised polyacrylamide hydrogel), it was expected that some cadmium would adsorb to the shale, but would the PAM be a competitor to the shale? From experiments, seen in Section 6.6, no cadmium is released from this particular shale sample, and negligible amounts from others.

If PAM had been a greater competitor to the shale then in this case, cadmium would have favoured adsorption to the colloid (PAM). Cadmium would have crossed the membrane leaving greater concentrations of cadmium in the PAM rich fluid than there would have been with just the 20 ml dilution from the addition of the bag to the beaker. In a more geologically realistic scenario, this may have meant that more cadmium would have been returned in flow-back waters, however evidence shown is that cadmium favours adsorption to the shale. Much of this cadmium may have been released by the shale. Expt #2 used a PAM concentration of 15.625 mg/L. Results show that using the fractionation value from the blank, between 12 and 15 mg/L was expected in the bag after dissolution, however only concentrations between 11.1 and 11.8 mg/L were observed, showing that more cadmium had remained in the matrix fluid within the beaker, than crossing the membrane. The cadmium concentrations that were dealt with here, up to 20 mg/L, are far higher than geologically likely to be contained or released

from shales. Cadmium content of shale ranges between 0.20 and 36 mg/kg, typically seen in black shales in China and Korea (Liu et al., 2017) and 04-46 mg/kg in Swedish shales (Lavergren et al., 2009). A study by Tuttle et al., (2003) for the Huron Shale, SW of the Marcellus in the USA states that cadmium concentrations ranges from 0.12 mg/kg to 26 mg/kg, with an average of 1.2 mg/kg. Flow back water data suggests that minimal amounts of cadmium will be returned to surface with cadmium being probed but not detected in flow-back data for the Marcellus, Eagle Ford and Barnett in (Maguire-Boyle and Barron, 2014). Flow-back events from Preese Hall 1A over a period of 4 months showed that the maximum cadmium measured was 6.02 μg/L, with a maximum of < 2 μg/L of filtered (full data can be seen in Table 6.2) (Broderick et al., 2011). The USGS flow-back database (Blondes et al., 2017) states that cadmium is returned in quantities ranging from 0.0001 mg/L to 24 mg/L, but with an average of 0.216 mg/L, across thousands of samples of flow-back fluid.

If cadmium is favouring adsorption to the selected shales in this study, it is unlikely it will become much of an issue in the contamination of groundwater and or drinking water. The EU limit for cadmium in drinking water is 5 μg/L (European Union, 1998) and this is followed by England and Wales ("The Water Supply (Water Quality) Regulations 2016," 2016). Cadmium released by the rock, according to literature, is generally very low. This is further investigated in relation to this study in Chapter 6 by analysing flow-back style waters from the adsorption experiments in Chapter 3 and Chapter 4 of this study.

On the other hand, the other analyte measured was sodium, initially to be a proxy for PAM content, however as very little to no PAM makes it across the semi-permeable membrane, the sodium is present as residual sodium and not PAM. Results show that sodium did not favour either shale or the PAM, and just equilibrated across a 420 ml solution when the 20 ml bag was added to the 400 ml of matrix solution.

A 500 mg/L PAM solution contains up to 138 mg/L of sodium, drastically increasing the salinity of the water from that of regular tap water (tap water compositions used in all experiments in this study are viewable in Digital Appendix F.3) with a mean value of 8.2375 mg/L (Northumbrian Water Ltd, 2017). Fluids being put downhole are already saline and these fluids are entering deep shales that are likely situated in saline or brackish style environments. This addition of saline waters, with multiple other additives is likely to mobilise salts and other mineral ions within the connate waters of the rock (Maguire-Boyle and Barron, 2014). This behaviour would potentially mean that fluids returning to the surface are very saline, leading to them having to be treated by means such as distillation or reverse osmosis (O'Donnell et al., 2018). Flow-back fluids for the Marcellus, Eagle Ford and Barnett Shales as shown in (Maguire-Boyle and Barron, 2014) show that Na in produced waters ranges from 45.9 mg/L to 5548.9 mg/L, a huge range. The USGS flow-back water database states that sodium is returned in ranges from 0.1 to 434403 mg/L, with an average of 26953 mg/L.

7.7. Conclusions

Using only two elements, cadmium and sodium, it has been shown that PAM and shale have an effect on cadmium. Cadmium that will have entered the system, either through the fracking fluid or by being released from the shale during fracturing, is likely to be adsorbed by the shale. Using a blank containing no PAM in the bag and no shale in the matrix fluid, approximately 25 % extra cadmium makes it into the bag. When a competitor is added, i.e. the PAM or the shale, significantly more cadmium is retained within the matrix fluid, with or without PAM.

Sodium, being the residual in the PAM fluid, on the other hand seemed to favour neither the shale or the colloid. Calculating the dilution factor when 20 ml of Na rich fluid is added to 400 ml of non Na rich fluid gave results of an average ratio of 1 showing that no more sodium was present either in the matrix fluid or the bag after dissolution. The results of t-tests results showed that there was no significant deviation from a ratio of 1, showing that no significant transference of sodium across the membrane.

The main implications of this show how either the shale or the PAM as an additive may be able to slightly influence the composition of the flow-back water dependent on the nature of the sample. A limited range of PAM concentrations were used, only one type of sample was used, and only two analytes measured. Future work would principally consider a larger array of analytes released by the shales using a range of differing PAM concentrations.

8. Conclusions

8.1. Introduction

The additives in hydraulic fracturing fluids and the potential environmental effects of these fluids are of critical importance. Due to safety legislation and potential environmental harm, numerous nations and individual US states have banned the practice of hydraulic fracturing. With global energy demand increasing, and green alternatives not matching this trend, understanding how to make existing non-renewable sources safer and cleaner is paramount to guarantee energy demands in the near future. Hydraulically fractured natural gas is one such way. With hydraulic fracturing in the UK having not yet started on a large scale, the scientific community is at a critical point in being able to understand these effects in a context that is relevant to the UK, before and after.

PAM has already been suggested as a key additive to fracking fluids. It has already been used multiple times in the USA (Blondes et al., 2017; King, 2012), with data seen in Section 1.6.2.1 and Digital Appendix A.1, and in the proxy for this study, Preese Hall 1A (Broderick et al., 2011). It is seen to be a key future additive, especially for any onshore UK operations. Because of the concentrations ranges of PAM in cited fluids (Aften and Watson, 2009; Stringfellow et al., 2014), a range of PAM concentrations were tested for adsorption, ranging from 15.625 mg/L to 1000 mg/L (Chapters 3 and 4).

8.2. Thesis Objectives

The objectives of this study were:

1. To characterise the samples chosen for this study, predominantly the Bowland Shale but also the overlying Pendle Grit and underlying Hodderense Limestone.
2. To assess if any PAM would likely be removed from the slick-water fluid and adsorb to the samples present (UK relevant samples such as the Bowland Shale and Pendle Grit).
3. If the PAM does adsorb, does it desorb easily? For example, during the flushing stages of a frack.
4. What is the likely composition of flow-back fluid associated with a simple slick-water based fluid, and the relevant associated shales?

5. Does PAM behave like a colloid? Is the addition of PAM into a fluid able to influence certain metals in solution, or would the shale and/or PAM act as competitors?

8.2.1. Chapter 2: Sample Collection and Characterisation

Chapter 2 focussed on the collection and characterisation of the UK relevant lithology types, focussing on objective 1. Samples were characterised to ascertain carbon content (TOC, TIC and TC) (Section 2.4.1) and mineralogy through the means of TGA (Section 2.4.1), XRF (Section 2.4.2) and XRD (Section 2.4.3). The samples analysed, both borehole and outcrop samples, were taken from the Bowland Shale (Upper and Lower), the Pendle Grit and the Hodderense Limestone. Results from this chapter were used, where possible, in statistical analyses in the adsorption chapters (Chapters 3, 4 and 5) to assess if the compositions had any influence on the adsorptive properties of the samples.

8.2.2. Chapter 3: The Adsorption of Polyacrylamide at Room Temperature

Chapter 3 assessed how this simple PAM rich slick-water fluid (based upon typical slick-water fluids and the Preese Hall 1A proxy) would interact with the samples used in this study. It focussed in particular on objective 2, how much PAM would be removed from the slick-water fluid by means of adsorption to the shale surface? Samples of 1 g were submerged in varying concentrations of a PAM rich fluid overnight. Equilibrium aqueous PAM was measured, and adsorbed amounts calculated. Three isotherm types were considered (Section 3.4) and results were statistically analysed against the characterisation data to see if there were any mineralogical or carbon based controls on amounts of adsorption. Using Langmuir isotherms, it was shown that up to 15,365 mg/kg of PAM could be adsorbed (Table 3.5), and up to 98 % of aqueous PAM removed from solution by means of adsorption (Figure 3.10).

8.2.3. Chapter 4: The Adsorption of Polyacrylamide in High Pressure High Temperature Environments

Chapter 4 considered a subset of the samples from Chapter 3. It stuck with objective 2, but this time samples were tested in a different environment; a closed system at 65 °C and 30 bar (3 MPa) to closer replicate sub surface (geologically realistic) conditions. These more realistic conditions were run at temperatures close to those observed between 3-5 km in the Bowland and Cleveland Basins (Table 4.1). Again, data was plotted on three main isotherms and results were statistically analysed alongside the sample characterisation data. Using the Langmuir isotherm, it was shown that a higher amount is adsorbed compared to the RT samples, up to 22,972 mg/kg adsorbed (Table 4.4). Percentage removals were also shown to be high, at up to 95 % of aqueous PAM removed from solution (Figure 4.9). Results for objective

2 were higher here in Chapter 4 (the largest concentrations at maximum coverage reaching 22,972 mg/kg), than in Chapter 3 (largest concentrations at maximum coverage reaching 15,365 mg/kg).

8.2.4. Chapter 5: The Desorption Properties of Adsorbed Polyacrylamide

Chapter 5 investigated desorption, and objective number 3. Results obtained in Chapters 3 and 4, for objective number 2 showed that PAM was highly adsorbative. But, would this PAM remain? To investigate this, PAM was adsorbed to 1 cm cubed shale samples and then flushed with fresh water (Figure 5.2). This flushing simulated the 'flushing' stages towards the end of a frack, designed to remove any remaining additives and proppant. Results showed that very small amounts of adsorbed PAM did desorb back into solution. A maximum of 0.919 mg/L (from 65.02 mg of adsorbed PAM) was desorbed, equating to a 1.4 % desorption (Table 5.6).

8.2.5. Chapter 6: Metals Analysis of Flow-back Fluids

This chapter combined the fluids taken from the RT and HPHT adsorption experiments and analysed the concentrations based on a set of metals for objective 4. Results were compared to literature and real-world examples (Table 6.11). Results also gave insight into what some flow-back fluid may be comprised of. The two main objectives of this chapter were objectives 4 and 5. It was concluded that the use of PAM slick-water fluids has an influence on the concentration of particular metals in the flow-back fluid, and that higher pressure and temperatures did inhibit the adsorption to the rock of the majority of the metals analysed (Figure 6.18). It is likely that the elevated temperatures and pressures help increase concentrations.

8.2.6. Chapter 7: The Colloidal Behaviour of Polyacrylamide as a Hydraulic Fracturing Additive

PAM is commonly used in the agricultural and water treatment industries as flocculent, binding together solids within the fluid. Chapter 6 investigated objective number 5, whether this behaviour can be attributed to shale and metals, interacting with the shales and/or any contaminants released (Figure 7.1). It was established that cadmium favoured being adsorbed to any shale present rather than being bound in the PAM rich fluids (Table 7.3). PAM could not pass through the semi-permeable membrane of the dialysis tubing, even with the presence of shale as an adsorbant on the opposite side of the dialysis membrane.

8.3. Principal Findings and Conclusions

Based upon the project aims, specified in Section 1.10 and above, the principle findings can be summarised below.

- At room temperature and pressure, all rock samples were highly adsorptive of the aqueous PAM in solution. Using maximum coverages calculated from the Langmuir isotherm, up to 15,365 mg PAM can be adsorbed per kilogram of rock available (Table 3.5). Simple calculations show that, with a 430 mg/L PAM fluid released into a shale with a 4000 mg/kg maximum coverage (or adsorption capacity), only ~903,000 kg of shale is required to remove all from solution at equilibrium (Figure 3.13). This amount of shale is a vastly small amount compared to the volumes involved in a typical fracture. Statistical analysis shows that concentrations at maximum coverage seem to be controlled by Al_2O_3, MgO, Na_2O and losses between 300 and 650 ˚C (Table 3.6). With respect to fracking in the UK, it is evident that PAM is highly likely to adsorb to the Upper or Lower Bowland Shales in large quantities.
- Under more geologically reasonable conditions, in-particular temperature, simulated in the HPHT batch reactor vessel, it was observed that PAM remains highly adsorptive to the rock samples. Here, the quantities have increased and, using the Langmuir isotherm, maximum coverages can be up to 10 times higher than in the RT adsorption experiments (Table 4.4). With temperatures of 65 ˚C and pressures of 30 bar (3 MPa) the greatest concentration at maximum coverage observed was 22,972 mg/kg (Table 4.4). Using this value in a similar calculation used in the RT discussion (Equation 3.9) above, only 157,216 kg of rock surface would be needed to remove all PAM at equilibrium.
- Percentage removal by adsorption, in both RT and HPHT adsorption experiments, decreased while PAM concentration increased (Figure 3.10 and Figure 4.9). In the RT adsorption, up to 98 % was removed at the lowest PAM concentration of 15.625 mg/L, whilst 95 % was removed from the same PAM concentration in under HPHT conditions. Increasing the PAM concentration to 1000 mg/L showed a reduction to an average of 11 % in RT, and 16 % in HPHT. This decrease suggests monolayer adsorption is the principle adsorption type occurring.
- Very little desorption occurs when samples adsorbed with large quantities of PAM are flushed with a freshwater solution. A maximum of 1.4 % of adsorbed PAM was desorbed back into solution, but the majority of results read zero

values, implying no PAM present after flushing (Table 5.6 and Figure 5.8). Any PAM that remains downhole has the potential to degrade, depolymerise or migrate over time. A study of this type, assessing the degradation over certain realistic weeks to months flow-back time periods (Brownlow et al., 2018; Harrison et al., 2017), may be the focus of some key future work.

- The room temperature samples showed variation between losses and gains for some metals (Figure 6.13). Copper and cadmium showed the greatest loss from fluid and favoured adsorption to the sample. Manganese and iron were returned in quantities up to 24 times (0.625 mg/L) the original slick-water concentration. Further analyses of fluids from the HPHT adsorption experiments showed overall less reduction across all samples than those in the RT experiments (Figure 6.18). An overall decrease was only observed for cadmium in the HPHT fluids and a higher gain ratio was observed in HPHT fluids for all metals apart from cadmium. Calcium, copper, iron, magnesium, lead and zinc all exhibited an average gain under HPHT conditions, when under RT conditions they exhibited an average loss. Under HPHT conditions, again manganese and iron are returned in the highest quantities, up to 146 times the original slick-water concentration (0.704 mg/L). Metals that have returned are largely in quantities above the regulation data, and thus will need special types of treatment after flow-back events (O'Donnell et al., 2018).
- Using the ratios from the increases and decreases in metal concentrations, there is significant difference between the RT and HPHT flow-back fluids. Data from the two subsets of experiment type reject the null hypothesis (Table 6.10 and Figure 6.24). Mean increase values for HPHT are higher than those observed in the RT fluids. Samples under higher pressure and higher temperature conditions release more metals into solution, or at least far fewer metals seem to favour adsorbing to the shale but rather be bound into the PAM fluid matrix and returned to surface.
- Fluids used in the RT and HPHT experiments, and those commonly used in hydraulic fracturing activities are near pH neutral, as are those returning to surface (Blondes et al., 2017; Broderick et al., 2011) and so it is unlikely any metal solubility is promoted by the acidification of the fluids. Carbonates present within lithologies may act as buffers for any acidification.
- The initial PAM concentration does appear to influence the uptake of certain metals. In particular, metals such as potassium, sodium and iron exhibit increases. Cadmium and copper show the largest decreases, but with decreases reducing with an increase in PAM concentration.

- PAM slick-water fluids, in the concentrations used in this study, were of a freshwater to briny composition, showing up to 500 mg/L sodium (Figure 6.12). Saline fluids are more likely to mobilise potential salts and minerals. Fluids, dependent on rock type exploited, may also return to surface highly saline and require specialist cleaning.
- Experiments with colloids undertaken in Chapter 7 of this study, show that PAM has an effect on cadmium. Any cadmium that enters the subsurface fluid system through fracking fluid, or the release from rock, will likely be adsorbed by the present of PAM in the fluid. When a competitor is added to a freshwater and cadmium system (i.e. shale or PAM), significantly more cadmium is retained within the matrix fluid (Table 7.7 and Table 7.8). Future work in this area would look more closely at multiple analytes and how they may or may not influence the metals within the flow-back fluid.

Based upon the premise that any hydraulic fracturing fluids in the UK are likely to be very simple (JAGDAG, 2018), predominantly slick-water based fluids, environmental impact is likely to be low. Polyacrylamide does adsorb to samples in vast quantities and is very unlikely to desorb throughout the fracking process. The lack of desorption leads to questions about how a non-hazardous PAM may depolymerise or degrade over large timescale (up to decade long time-scales) in the subsurface, somewhat already assessed by literature such as Nyyssölä and Ahlgren (2019) and Xiong et al (2018). The amount of adsorption does increase under the HPHT conditions used in this study (Section 4.5) and thus more PAM is likely to be adsorbed in the subsurface, especially at typical subsurface basin temperatures of the onshore UK linked to this study (Table 4.1). Future work would assess how crucial a role either temperature and pressure influence this that could be applied to other basins globally. PAM fluids produced are briny in solution and can contain up to 300 mg/L more sodium than the EU regulation (Table 6.11), having the potential for flow-back fluids to be > ~500 mg/L, dependent on the lithology exploited. Certain metals, examples being Al, Cd, Cu, Fe, Mn, Na and Pb, do return to the subsurface in quantities greater than the EU regulations (sample dependent), and PAM concentration does impact upon some of these increases. Further work on PAM concentrations would investigate how compositions of flow-back fluid could have the ability to be manipulated, thus reducing environmental harm and the necessity for specialist water treatment.

The results from this study would likely aid the Environment Agency, and other regulatory bodies or investigative consultancies, understand and regulate (if necessary) the usage of PAM in the deep subsurface. Because large quantities of PAM do not desorb over short timescales easily with a 'flush' of freshwater, simulated in Chapter 5 of this study, they are likely

to stay in the subsurface longer term. Over the longer term in the subsurface, they may have the chance to depolymerise or degrade, and even migrate over larger distances over much longer timescales, if it is proven to desorb over longer time periods. The results of simulated flow-back fluids, and the metals they contain, give an insight into how companies that would use PAM slick-water fluids may have to think about safe disposal of returned, slightly saline fluids and how the different relative lithologies in the UK may influence the fluids in different ways. Furthermore, this study could aid the geothermal industry. Over time, shale gas basins may be subsequently used for geothermal activities and certain fluid information will be useful in determining the compositions or presence of any degraded PAM contaminants that may be encountered, or returned to surface in geothermal waters.

8.4. Data Limitations

The following is a summary of limitations that have affected data and analysis across this study.

- Sample type was limited. Samples from the BGS Corestore in Keyworth were strictly limited for sampling, especially from wells of scientific and media interest (i.e. Preese Hall 1A and Becconsall 1Z). This limitation meant that samples had to be carefully used and may not have been used for all analyses where it was preferred. Outcrop samples, whilst almost unlimited, did have potential problems attributed to weathering. The issues of weathering were mitigated as best as possible with the removal of all weathered surfaces before any preparation or analysis (Section 2.2.5).
- Analysing adsorption at 'geologically realistic' temperatures and pressures was limited by the pressures the hardware could achieve. Whilst typical UK subsurface temperatures were achievable, the batch reactor used in the experiments could only reach pressures of 10.9 MPa (109 bar or 1580 psi). These pressures are lower than the typical pressures at depths of 3-5 km in the onshore UK basins. Typical lithostatic pressures here would be between 34 MPa and 55 MPa.
- The presence of PAM in the typical slick-water fluid produced for this study, in concentrations up to 1000 mg/L, meant that in some cases there was suppression of analyte signals when analysed using ICP-OES. The problem was mitigated as best possible with the 11-fold dilution of fluids with 7 % nitric acid. Further dilution may have diluted out the analyte, but less dilution may have increased the chance of suppression issues.

- The sample size throughout the whole study is small, 14 samples and their duplicates as a maximum. This small sample size significantly inhibits rigorous statistical analysis, and increases the chance of random or unusual data influencing the outcome.

8.5. Future Work

Future work has been discussed in the individual chapters. This Section will focus on a summary of future work that has the potential to be funded, over the wider context of the whole thesis.

8.5.1. RT and HPHT Adsorption Future Work

One of the key conclusions of this project is the fact that nearly all aqueous PAM, up to 98 % (Figure 3.10 and Figure 4.9), can be removed from the fluid by means of adsorption. This adsorption increases, as concentrations at maximum coverage show, when the pressure and temperatures are brought to more geologically realistic conditions. The conditions tested in this thesis are however only one pressure and temperature setting, and this pressure setting at a low geological pressure. It is unknown whether pressure or temperature is the principle factor in increasing the adsorption capacity (or concentration at maximum coverage). To establish this further, more of the same experiments would be needed to be run varying both temperature and pressure parameters. In addition, the use of machinery that could reach more geologically reasonable pressures (> 550 bar) would be required to fully simulate these conditions.

8.5.2. Ads-Des Future Work

This study was conducted at room temperature, just to understand the initial desorption behaviour of any adsorbed PAM. Ideally, future work would look at:

- Increasing the temperature of the Ads-Des experiments to temperatures more in line with subsurface temperatures seen in the Bowland Basin (60-110 ˚C) (Table 4.1). This increase in temperature would mimic work conducted by Guo et al., 2018 but in a more relevant setting to the UK shale gas basins and industry.
- Test desorption over time. Realistically, flow-back and flushing events occur over days and weeks, rather than hours - as tested here. Under agitated conditions, fluids could be sampled every 24 hours over much longer timescales to see if desorption increases, and at what point does any increase in desorption or change, take place.

- Based on the fact that desorption of PAM is very minimal (Section 5.9), certain additives could be added, such as urea (Yang et al., 2018) to the flushing stages to see if desorption could be promoted if required.

8.5.3. Colloid Future Work

- As noted in Chapter 7, cadmium was the only metal tested for, and in this case, shale out competed the PAM for the adsorption of cadmium. The logical progression from using only cadmium is to test different analytes to see if PAM or shale favours certain metals differently. One next step would be to test the metals based on the results observed in Chapter 6, and focus on the most environmentally relevant, eg. lead.
- A further step would be to test the full range of PAM concentrations ranging from 15.625 mg/L to 1000 mg/L and potentially further.
- Testing different samples would establish if certain mineral constituents or organic content promoted adsorption to the sample, or binding to the colloid.

The main output of future work would be tailoring this experiment to understanding the contaminant output of the differing shales and dependent of the additives involved. Lots of fine tuning could help develop fluid types that specifically promote or inhibit the binding of metals to different colloidal additives.

8.5.4. Metals Flow-Back Future Work

There is lots of future scope for an experiment of this type based upon methods used here.

- As this work was conducted at only one pressure and temperature setting, change in either variable could not be measured. The next stages here would be to keep one variable the same, either pressure or temperature, while changing the other (30 bar and > 65 ˚C or 65 ˚C and > 30 bar). A factorial designed experiment like this would help understand if pressure or temperature is the key component in either metal release or removal on these relatively pH neutral fluids.
- Pressures and temperatures could be changed to simulate other geological settings, not just related to the UK. Further future work would look more in depth at the fluid additive. Is PAM in quantities greater than 1000 mg/L helping to bind more metals into the fluid, or promote adsorption of these metals to the

shale surface? As discussed, PAM can be used in quantities that range between 30 and 2140 mg/L in slick-water fluids, globally (Aften and Watson, 2009; Stringfellow et al., 2014).

- Linking to the above, flow-back fluid would also be sampled off from extra HPHT experiments in the same way. As specified in chapter 6, there were fewer metals lost from solution in the HPHT experiment resultant fluids compared to the RT resultant fluids. More geologically reasonable settings promote the release of a higher proportion of metals into the flow-back fluid, but is it pressure or temperature that is the primary factor? Conducting at least two more experiments, one increasing temperature and one increasing pressure, conclusions could be drawn. Further experimentation could fine tune pressures and temperatures to test the geological settings of differing basins worldwide, in countries where fracking is possible such as Poland, Argentina, Australia, USA and Russia. In terms of rates or mechanisms of loss or gain of certain metals, sample fluids would benefit from a sequential extraction technique to better understand over time which metals are first to be released. The variables in this could be temperature and pressure, as well as taking it further and altering the additive composition.
- Testing the composition of flow-back waters could be further investigated by changing the additives within the fracking fluid, or by making a more complex style fracking fluid with more than one additive, unlike this study. Do other additives, that are used to perform other jobs, affect compositions in different ways?

To conclude, the key findings of this study are the fact that 1; PAM will adsorb in large quantities to rock surfaces, particularly shales, and 2; once adsorbed, PAM does not desorb readily in typical freshwater flushes used in post-frack operations. The conclusion that PAM adsorbs in large quantities and does not desorb readily poses the critical question of PAM degradation over time. Future work and funding should target and focus on the degradation of adsorbed PAM, particularly under subsurface conditions of higher temperatures and pressures. An assessment of how PAM degrades over time, particularly in time-scales observed in flow-back operations (weeks to months), would help inform regulatory bodies of the risks that adsorbed non-toxic PAM may pose if it degrades to more toxic substances. In addition, the use of other additives to promote desorption could be investigated alongside the degradation. Finally, flow-back fluids will likely return contaminants in quantities that are above regulation for multiple metals, and this is unavoidable. PAM may be able to help

manipulate, to a degree, concentrations of certain metals such as cadmium, iron, manganese and lead, more work in this area is needed to confirm any facts.

Appendices

Appendices are provided as both printed and digitally accessed, provided on the CD supplied with this study. A brief outline of each Appendix is supplied below.

Appendix A

Supplied in digital form providing the analysis for the 200 US wells, analysed in Section 1.6.2.1, for their use of PAM and friction reducers.

Appendix B

Supplied both in digital and printed format displaying all results relating to the shale characterisation data from Chapter 2. TOC literature overview for Figure 2.10 is supplied in digital appendix B.1. Full TGA data from Section 2.3.1.2 is supplied in Digital Appendix B.2. Full XRF numerical data for Section 2.4.2 is supplied in Digital Appendix B.3. Full XRD numerical data and curves for Section 2.4.3 are supplied in Digital Appendix B.4 and diffractograms are printed in Appendix B.

Appendix C

Supplied in digital format for all RT adsorption results, isotherms and calculations (C.1). Langmuir isotherm confidence intervals and calculations are supplied in Appendices C.2 (0-250 mg/L calibration) and C.3 (0-1000 mg/L calibrations).

Appendix D

Supplied in digital format for all HPHT adsorption results, isotherms and calculations (D.1). Langmuir isotherm confidence intervals and calculations are supplied in Appendices D.2 (0-250 mg/L calibration) and D.3 (0-1000 mg/L calibrations).

Appendix E

Supplied in digital format for all Ads-Des experiments, Chapter 5. Calculations and isotherms are observed in digital Appendix E.1. Appendix E.2 supplies results for ANOVA on percentage removal from Table 5.5. Appendix E.3 supplies results for ANOVA on adsorbed concentrations from Table 5.4. 220

Appendix F

Supplied in digital format for all ICP metals results. Digital Appendix F.1 refers to all tap water data used in Section 6.6.1. Digital Appendix F.2 displays all data for RT fluids and samples measured in 6.6.2. Digital Appendix F.3 refers to all tap water data displayed in Section 6.6.1. Digital Appendix F.4 displays all data for HPHT fluids and samples measured in 6.6.3.

Appendix G

Supplied in digital format for all colloid results and calculations for Chapter 7(G.1)

Appendix B – Non digital

Thermogravimetric Analysis Curves (TGA) – Section 2.4.1.2

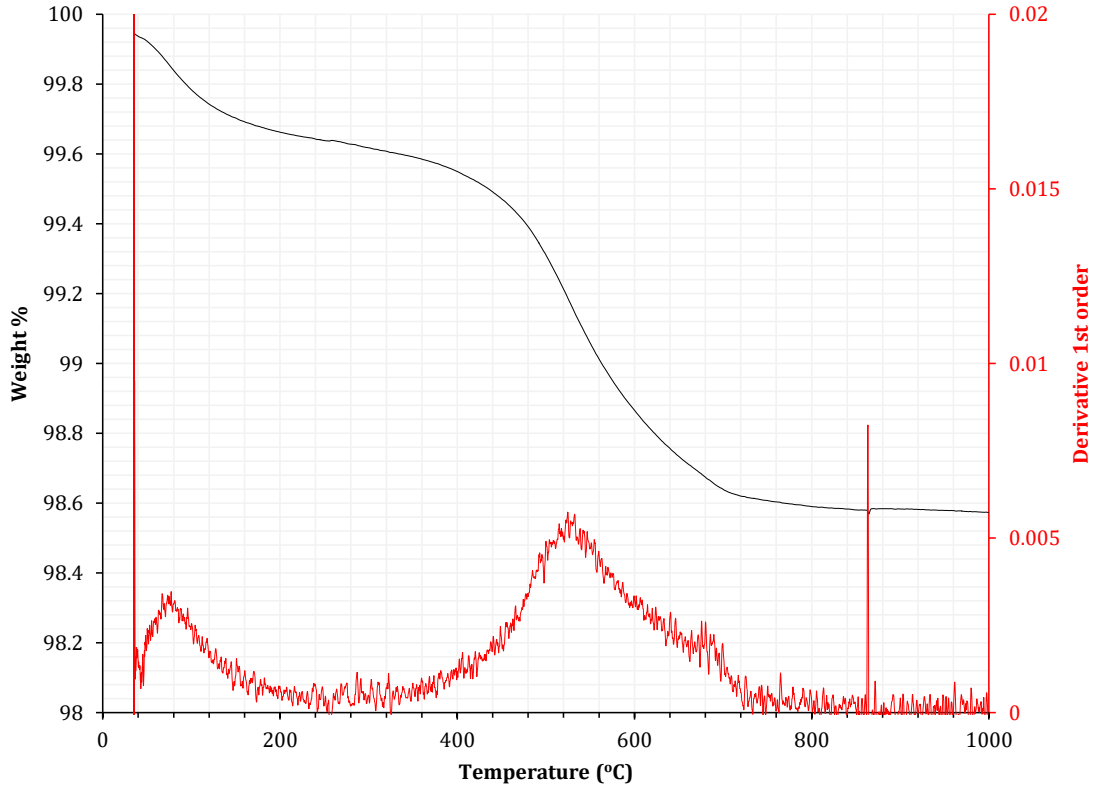

Figure 0.1: *TGA curve for OC 1 (Hazelhurst Fell Pendle Grit)*

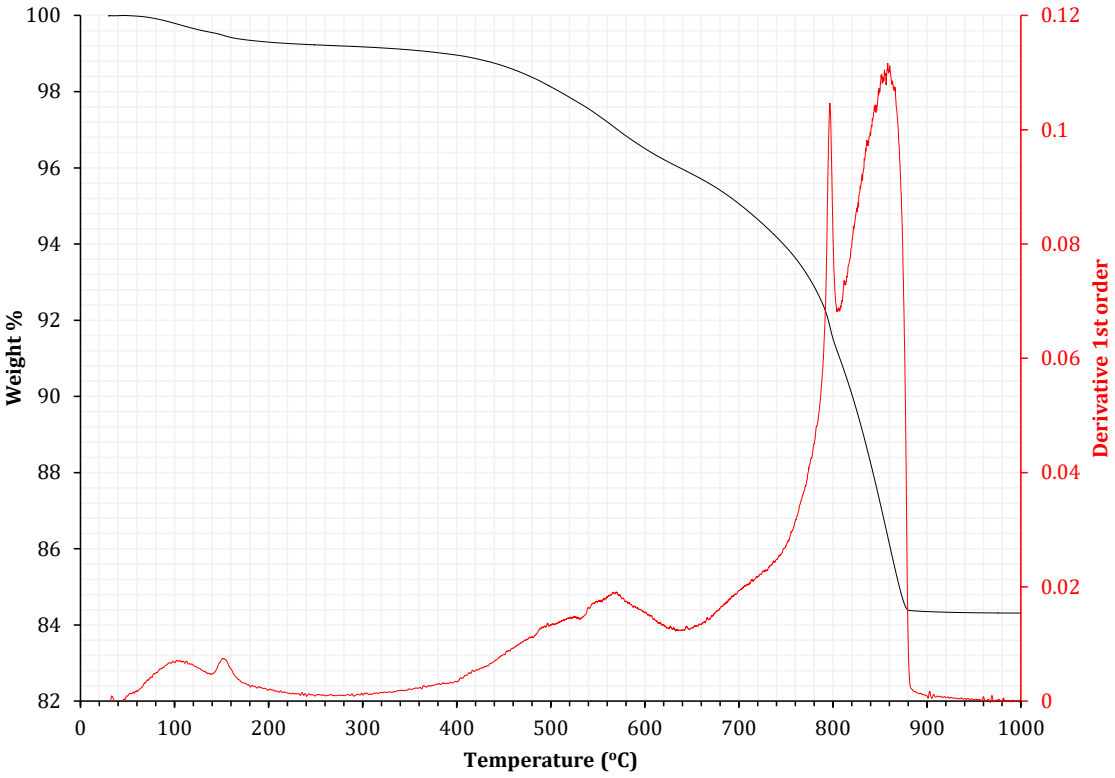

Figure B.2: *TGA curve for OC 3 (Hazelhurst Fell, Upper Bowland Shale)*

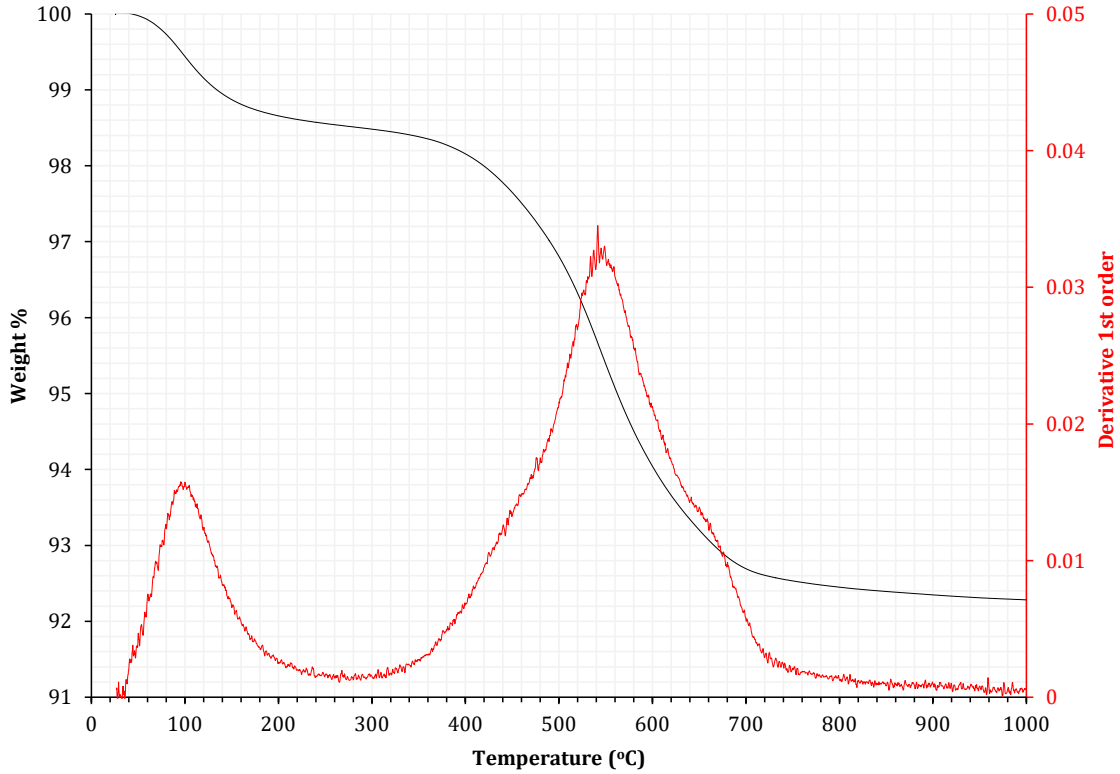

Figure B.3: *TGA curve for OC 4 (Hazelhurst Fell, Upper Bowland Shale, Sandy)*

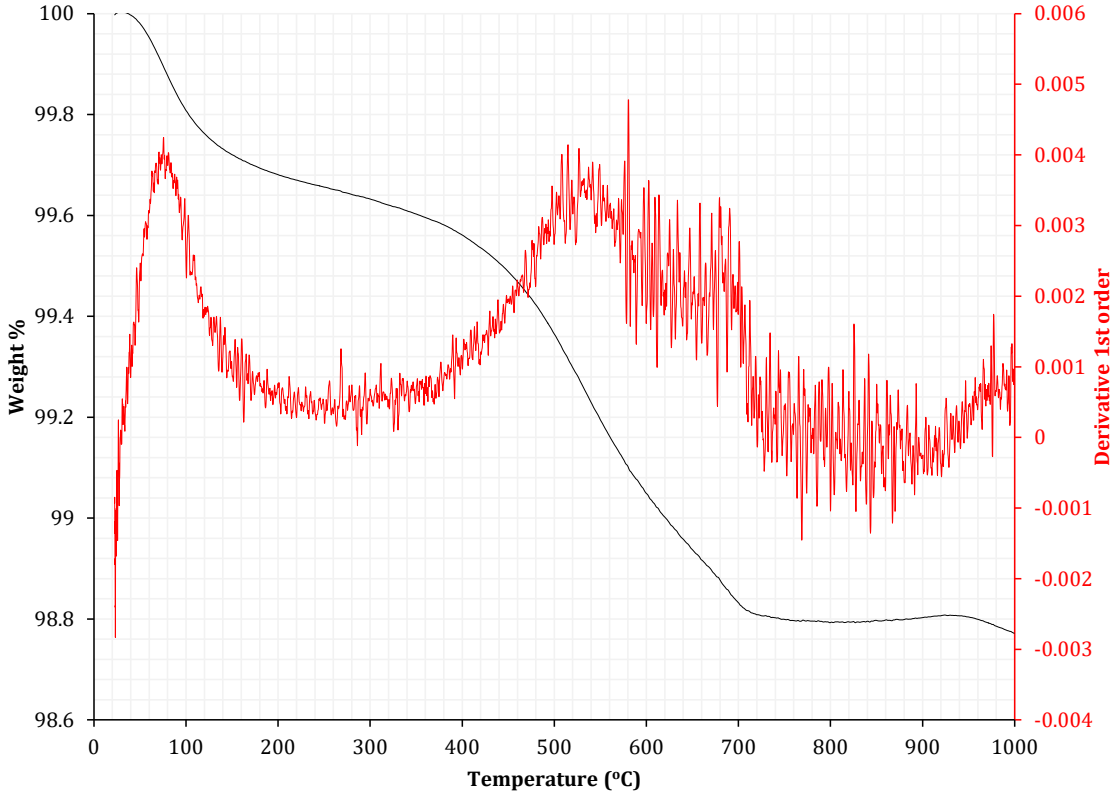

Figure B.4: *TGA curve for OC 5 (Sabden, Nick O'Pendle, Pendle Grit)*

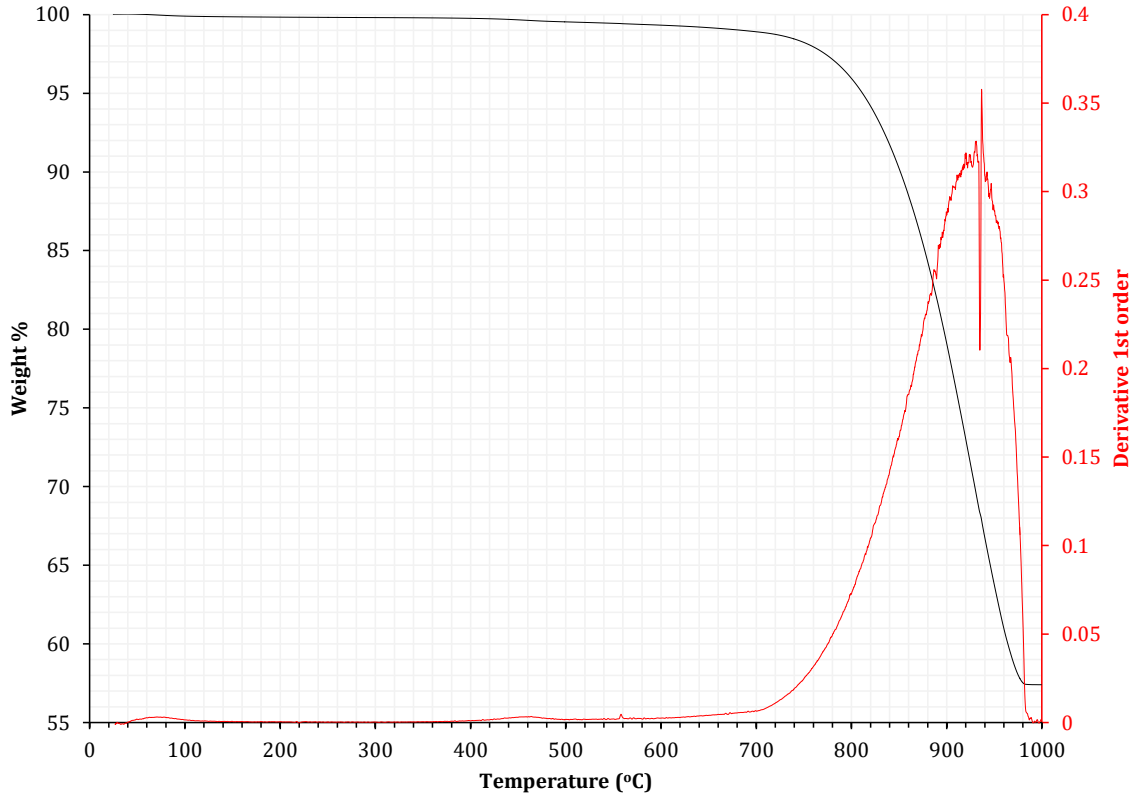

Figure B.5: *TGA curve for OC 6 (Sykes Quarry, Limestone based shale)*

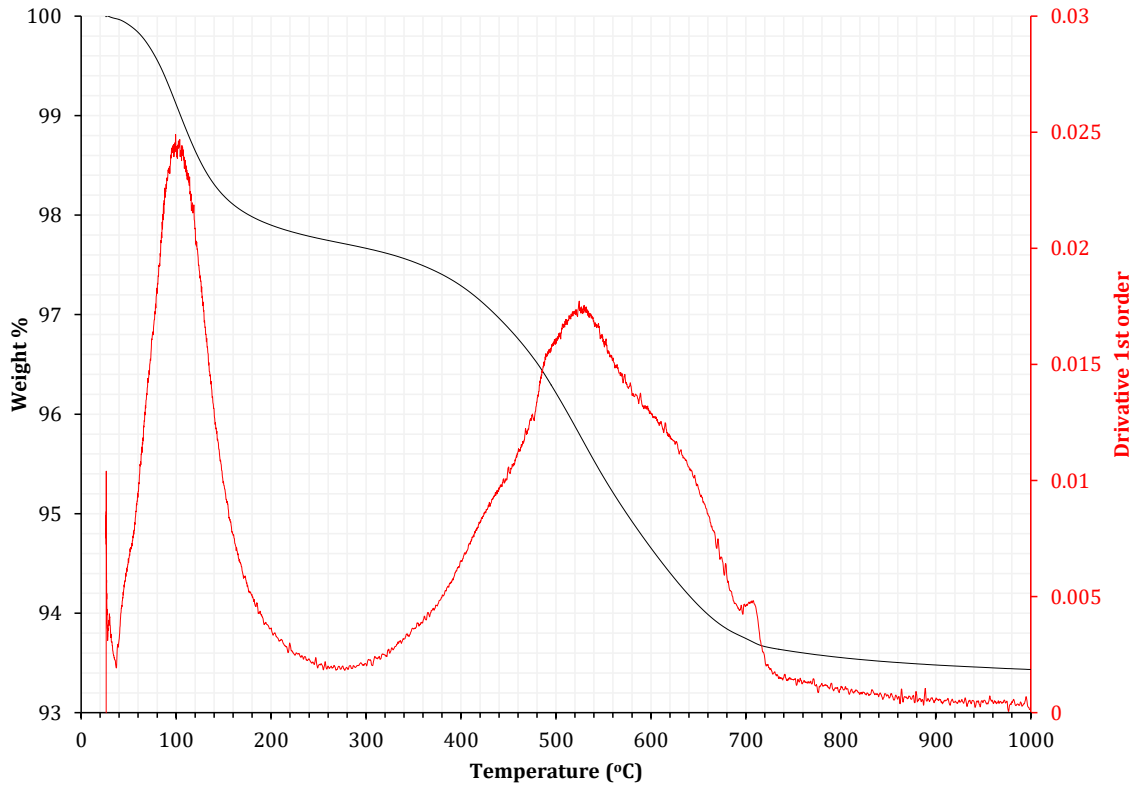

Figure B.6: *TGA curve for OC 7 (Wolf Fell, Upper Bowland Shale*)

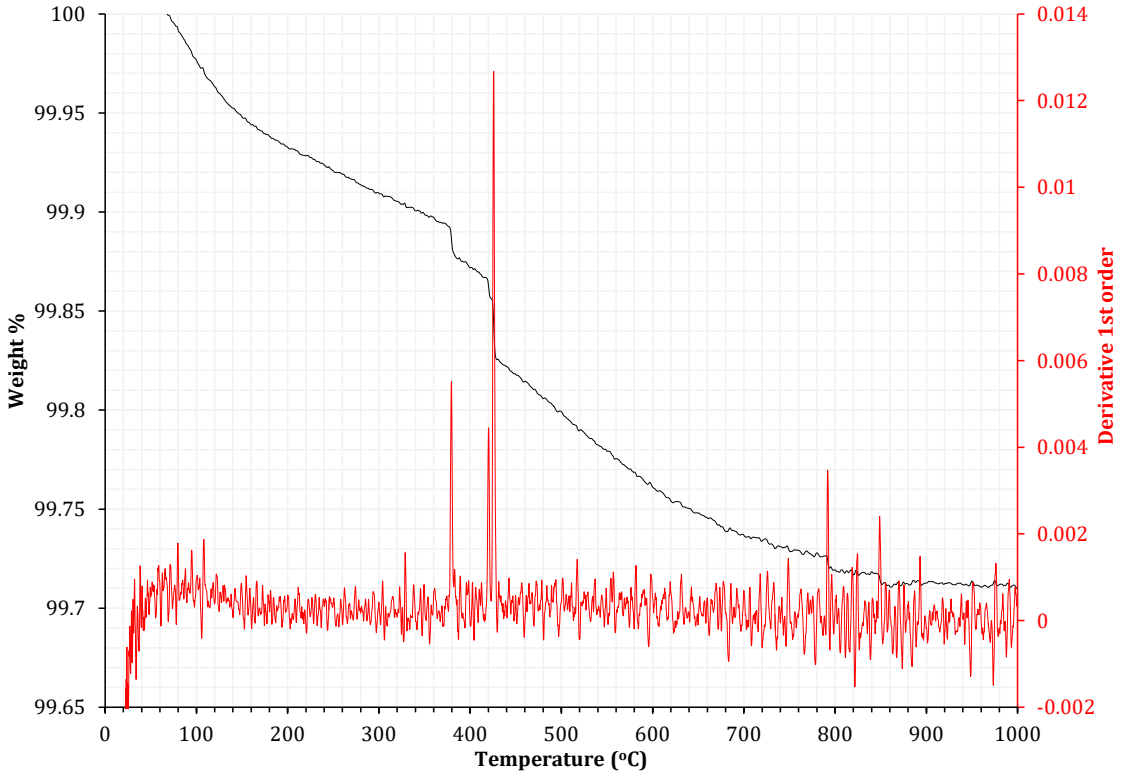

Figure B.7: *TGA curve for OC 8 (Congleton Sand, Proppant)*

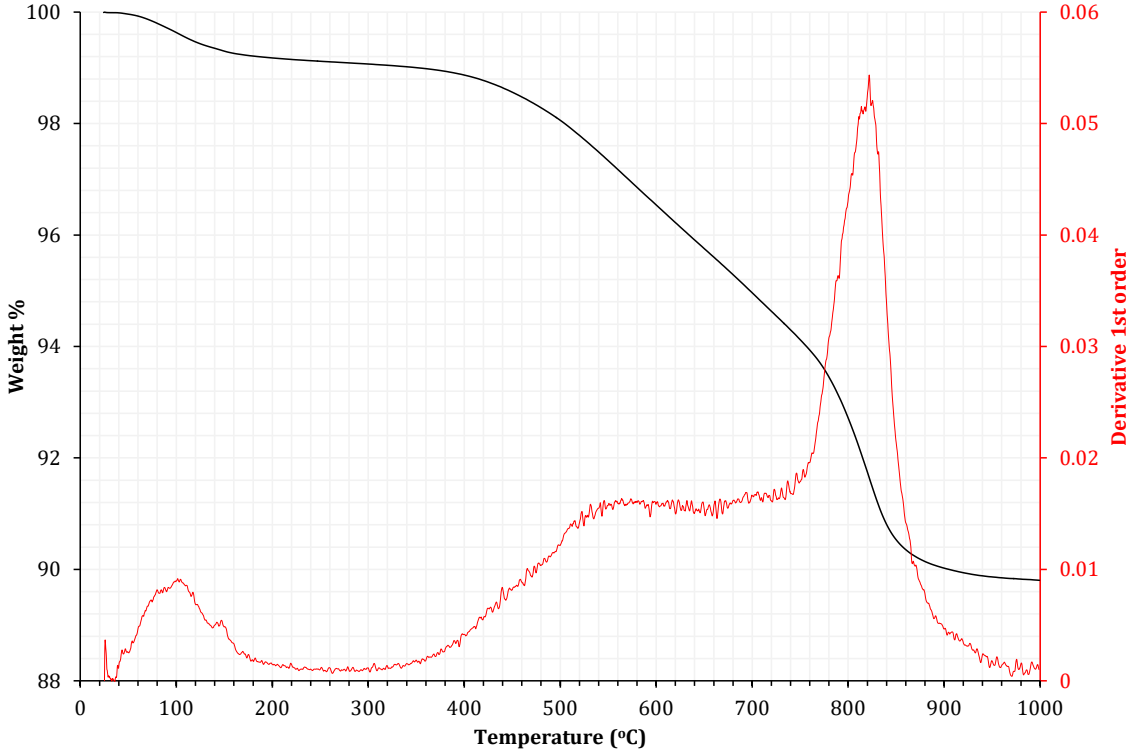

Figure B.8: *TGA curve for BH 1 (Becconsall 1Z, 7030 ft, Upper Bowland Shale)*

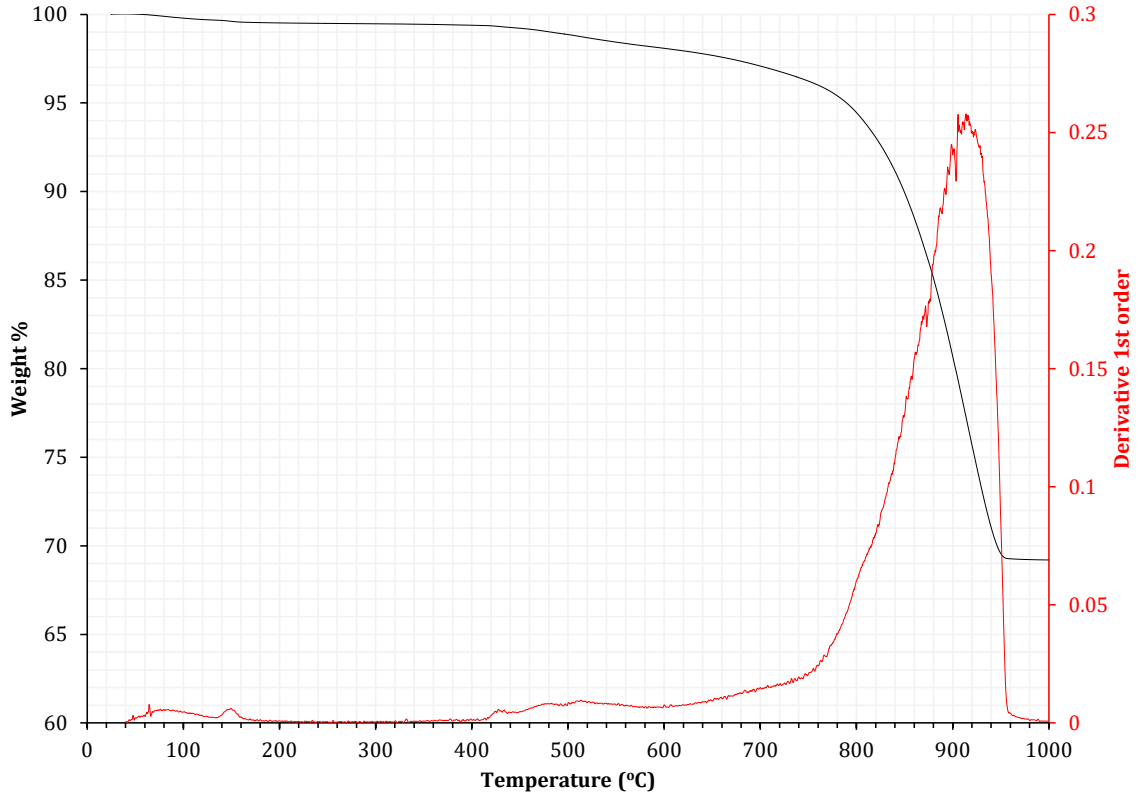

Figure B.9: *TGA curve for BH 2 (Becconsall 1Z, 7420 ft, Lower Bowland Shale)*

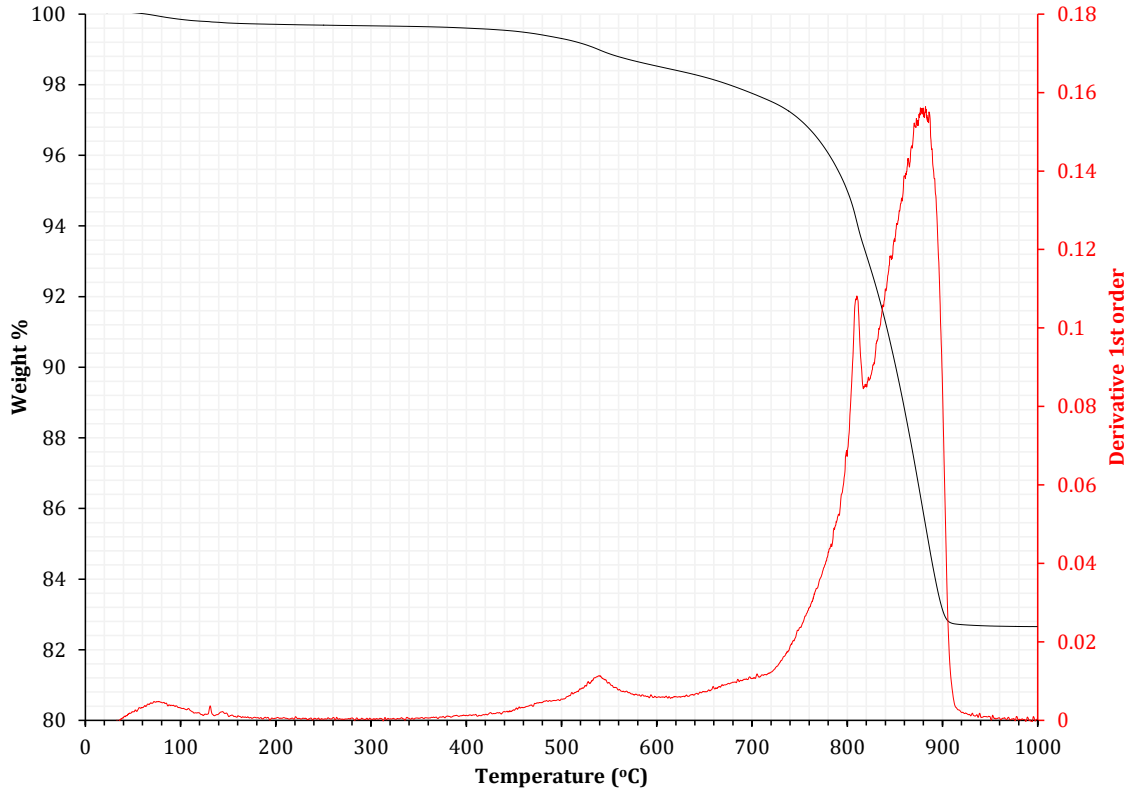

Figure B.10: *TGA curve for BH 3 (Grange Hill 1, 7026 ft, Upper Bowland Shale)*

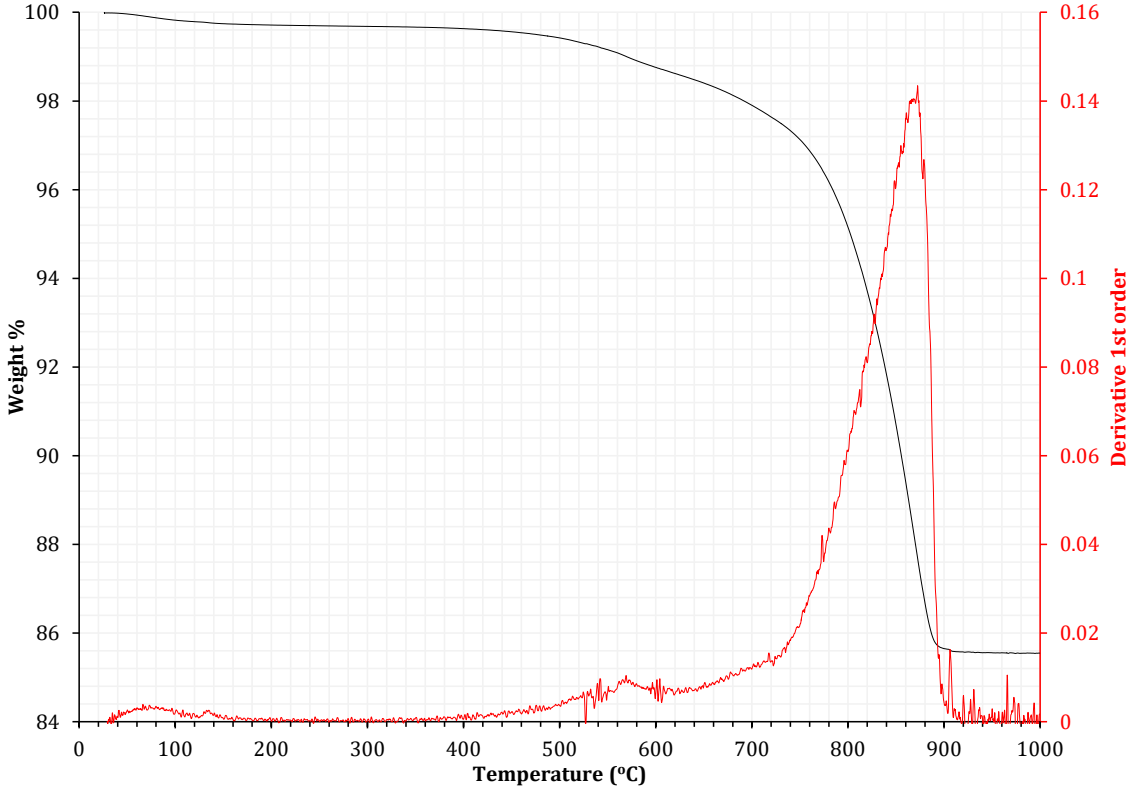

Figure B.11: *TGA curve for BH 4 (Grange Hill 1, 8134 ft, Upper Bowland Shale)*

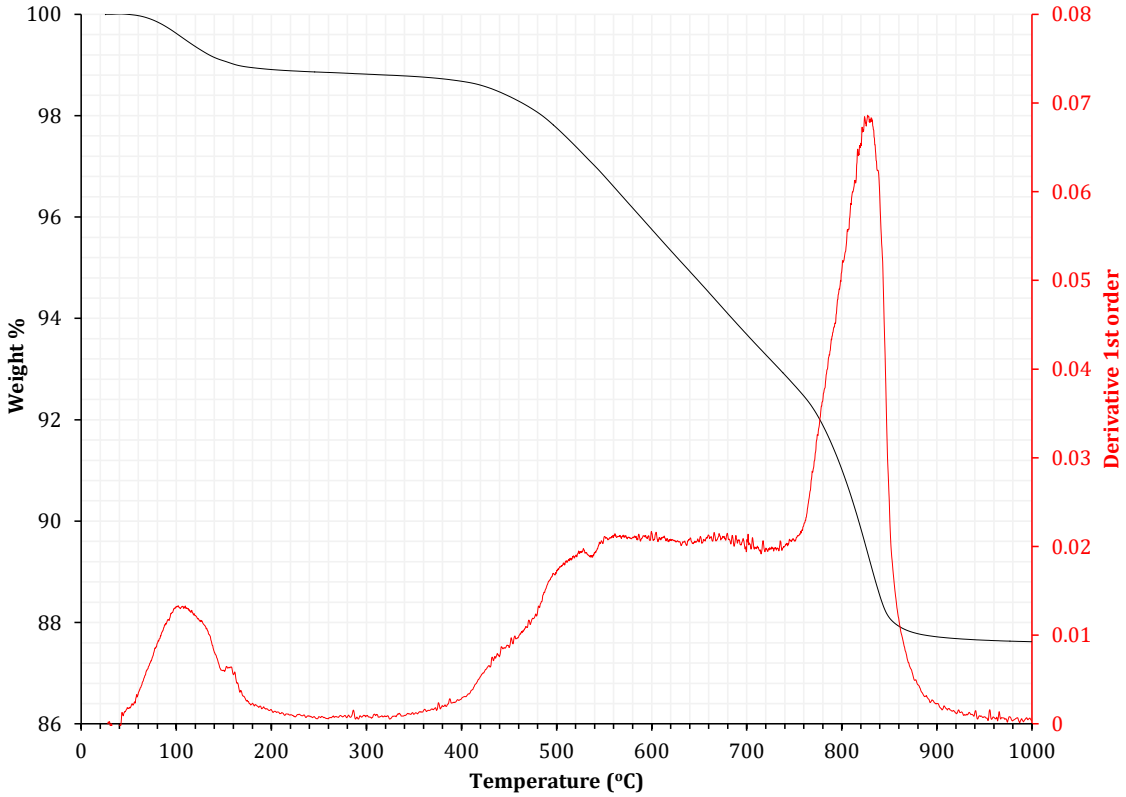

Figure B.12: *TGA curve for BH 5 (Preese Hall 1A, 8885 ft, Lower Bowland Shale)*

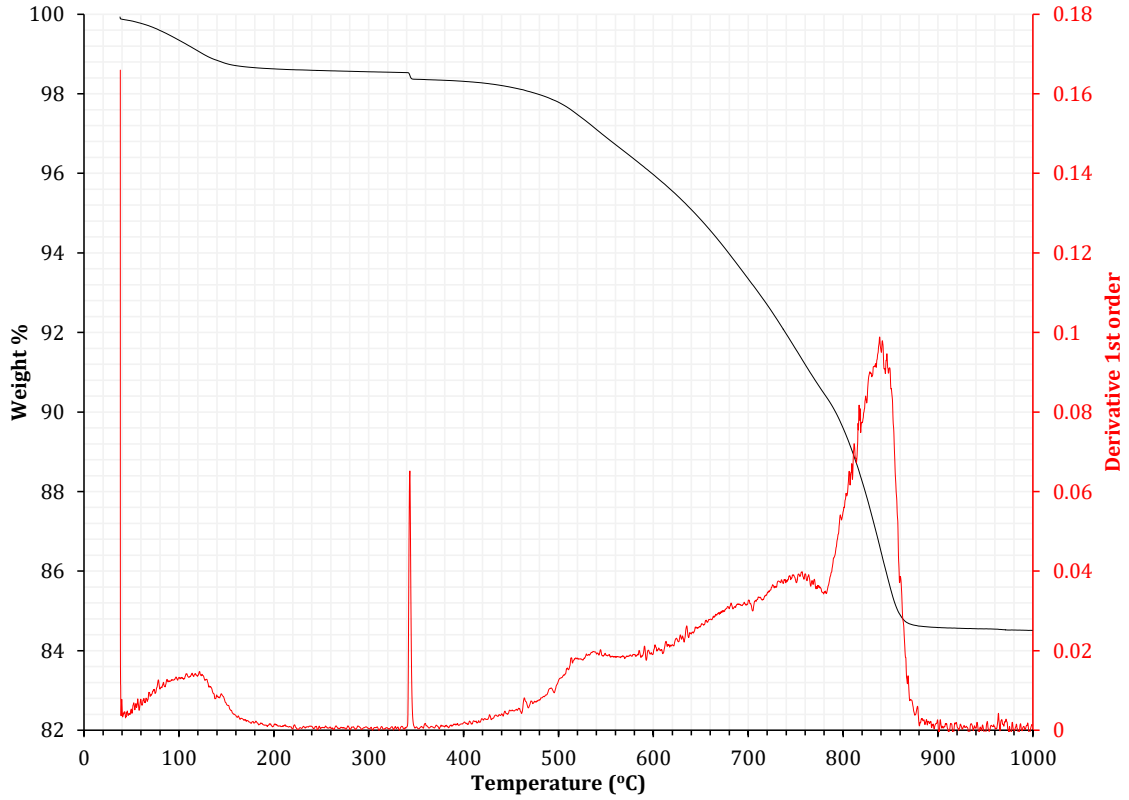

Figure B.13: *TGA curve for BH 6 (Lockton 3, 7049 ft, Carboniferous Shale)*

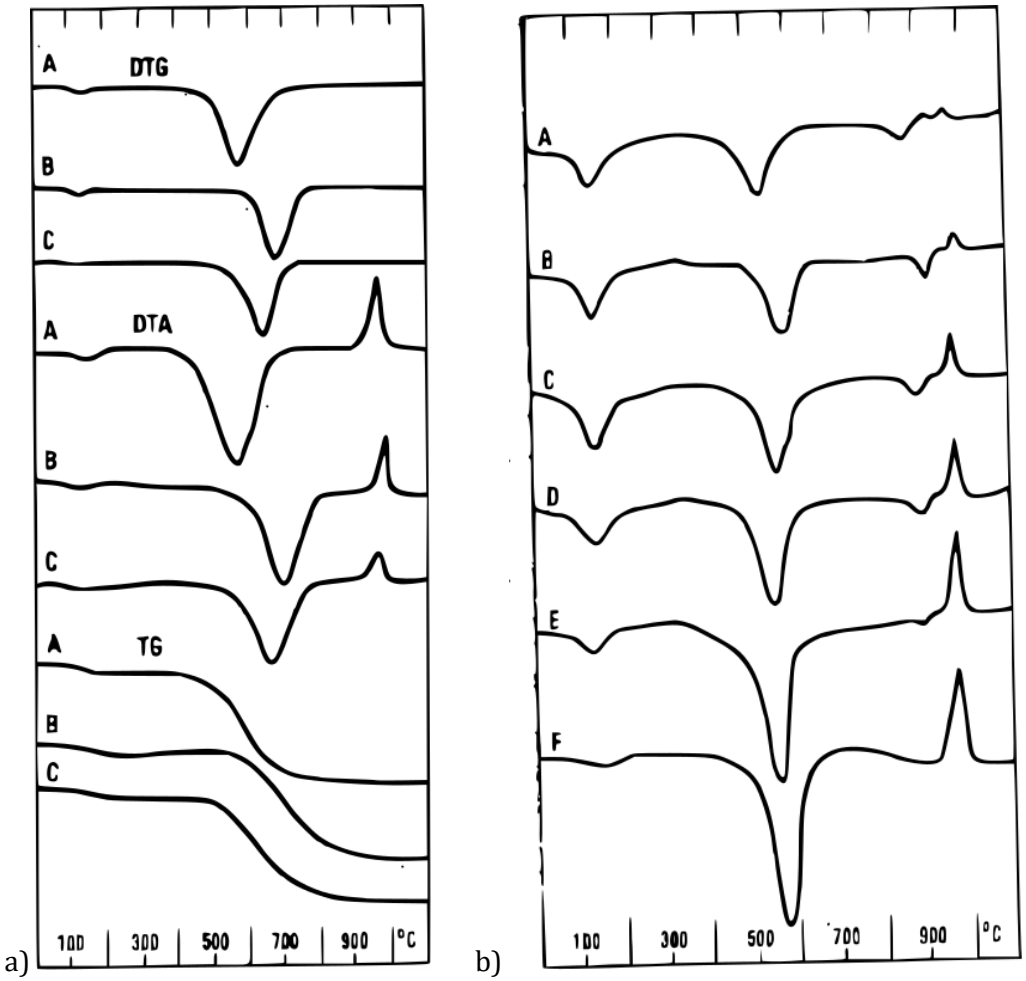

Figure B.14: *"a" –thermal curves of A: kaolinite, B: dickite and, C: nickrite. "b" – derivative curves for varying illite and kaolinite mixtures; A: 95 % illite, B: 90 % illite, C: 75 % illite, D: 50 % illite, E: 25 % illite, F: 10 % illite. Adapted from (Todor, 1976).*

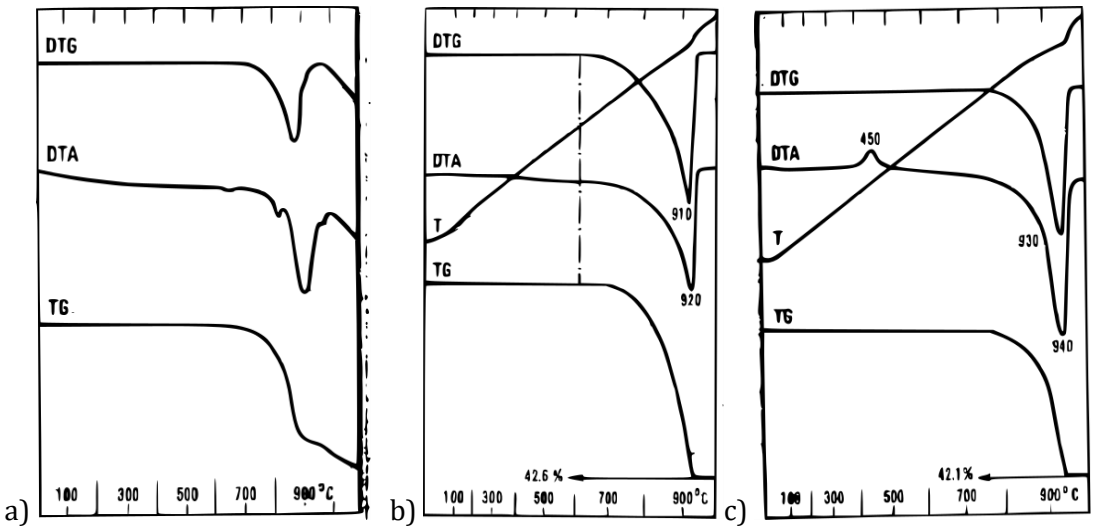

Figure B.15: *"a" – thermal curves for a natural mixture of $CaCO_3$ + $SrCO_3$ + $BaCO_3$. "b" – thermal curves of a typical calcite lattice. "c" – thermal curves for calcite containing finely dispersed sulphides. Adapted from (Todor, 1976).*

XRF Tables – Section 2.4.2

SAMPLE	SiO_2	TiO_2	Al_2O_3	Fe_2O_3	MnO	wt % MgO	CaO	Na_2O	K_2O	P_2O_5	SO_3
BH 1	67.18	0.28	7.85	3.27	0.04	1.08	7.12	0.36	1.470	0.084	2.281
BH 2	22.80	0.12	3.02	2.01	0.02	1.12	36.85	0.13	0.393	0.066	3.819
BH 3	54.75	0.17	3.11	2.52	0.03	2.55	17.20	0.42	0.421	0.073	0.880
BH 4	60.50	0.22	2.88	2.02	0.02	1.12	15.97	0.48	0.450	0.085	1.360
BH 5	59.46	0.42	8.75	2.64	0.01	0.77	10.72	0.60	1.452	0.995	2.827
BH 6	46.41	0.75	17.42	16.15	0.19	2.01	1.00	0.73	1.566	0.253	0.138
OC 1	90.79	0.14	4.90	0.55	0.00	0.08	0.01	0.17	1.307	0.023	0.005
OC 2	87.11	0.31	7.52	0.46	0.08	0.18	0.02	0.41	1.501	0.072	0.008
OC 3	56.69	0.31	5.70	2.72	0.08	2.59	13.04	0.17	1.073	0.136	2.632
OC 4	70.38	0.90	17.25	0.84	0.01	0.56	0.03	0.31	2.733	0.099	0.008
OC 5	89.76	0.28	5.19	0.99	0.01	0.13	0.02	0.63	1.083	0.023	0.004
OC 6	2.65	0.01	0.27	0.17	0.02	1.03	52.87	<0.004	0.019	0.004	0.289
OC 7	78.95	0.41	9.36	3.92	0.01	0.45	0.02	0.21	1.373	0.126	0.010
OC 8	98.72	0.04	1.41	0.21	<0.001	0.07	0.08	0.16	0.670	0.012	0.005

Table B.0.15: *XRF majors and trace mineralogy for all samples*

	As	Ba	Ce	Co	Cr	Cs	Cu	Ga	La	Mo
BH 1	22.0	214.2	37.2	11.4	63.8	6.7	46.5	8.0	24.7	19.1
BH 2	18.1	73.5	30.9	3.9	9.3	1.2	10.4	4.6	12.8	10.5
BH 3	3.1	97.4	16.6	2.1	16.6	<1.9	3.1	3.3	12.5	2.4
BH 4	5.4	328.9	24.6	2.4	25.9	<1.9	5.5	3.7	14.2	3.5
BH 5	14.0	161.9	38.5	9.0	309.2	7.1	32.8	10.2	30.8	16.2
BH 6	7.3	376.6	104.3	22.7	178.4	5.2	25.9	23.7	48.0	1.9
OC 1	0.3	353.3	28.1	<1.0	43.2	<1.5	<0.3	4.4	16.3	1.8
OC 2	3.8	305.6	46.3	11.9	53.6	0.5	3.4	7.6	22.3	1.4
OC 3	9.1	1207.5	37.3	7.0	42.5	3.7	16.2	7.0	22.1	10.2
OC 4	3.6	445.6	117.9	3.3	339.2	9.2	15.7	20.6	57.7	2.0
OC 5	<0.4	265.9	46.9	1.4	58.5	<1.5	<0.3	5.1	24.0	1.4
OC 6	2.7	104.9	9.3	<1.6	-5.4	<3.0	<0.7	1.6	5.5	2.6
OC 7	41.1	155.7	40.9	5.1	51.7	8.8	16.3	10.8	24.6	15.0
OC 8	<0.4	146.4	4.3	<1.0	19.5	<1.4	<0.3	1.4	3.5	0.4

Table B.16: *Trace elements As – Mo (units in mg/L)*

	Nb	Nd	Ni	Pb	Rb	Sb	Sc	Se	Sn	Sr
BH 1	6.3	21.1	79.2	12.9	55.5	2.8	12.5	16.6	<0.9	179.0
BH 2	3.6	15.2	20.8	2.3	16.8	5.9	38.6	4.2	<1.0	1058.2
BH 3	3.1	12.1	5.2	3.4	17.1	1.1	14.5	<0.6	<0.9	516.8
BH 4	3.6	17.0	7.8	3.3	18.5	1.1	13.5	0.7	<0.9	630.8
BH 5	7.8	23.0	78.2	11.2	77.9	6.2	16.0	25.5	<0.9	486.2
BH 6	13.7	43.7	51.4	21.2	83.5	<1.1	16.9	0.8	2.1	145.3
OC 1	1.0	14.2	0.7	4.1	32.7	<0.8	3.7	<0.5	<0.7	54.5
OC 2	4.5	21.5	25.5	11.0	46.8	<0.8	8.1	<0.5	<0.7	40.6
OC 3	6.0	21.6	35.9	45.1	50.2	1.8	14.6	6.6	<0.9	286.6
OC 4	13.2	58.7	20.3	17.3	90.0	<0.8	15.1	<0.5	2.4	83.9
OC 5	3.3	21.2	3.6	8.2	30.6	1.5	4.0	<0.5	<0.7	48.5
OC 6	0.6	9.4	2.5	2.0	2.9	<1.2	65.7	0.5	<1.1	443.3
OC 7	7.7	18.6	31.1	72.3	70.6	3.2	7.9	1.3	<0.8	104.3
OC 8	0.9	5.1	0.4	4.6	27.2	<0.8	1.2	<0.4	<0.7	22.5

Table B.17: *Trace elements Nb – Sr (units in mg/L)*

	Th	U	V	W	Y	Zn	Zr
BH 1	3.7	7.9	378.8	<1.0	19.6	93.6	60.7
BH 2	0.8	3.7	55.3	<1.2	11.7	28.7	40.1
BH 3	1.9	1.9	25.0	<1.0	11.3	13.5	127.7
BH 4	2.0	1.4	27.5	<1.0	18.7	20.7	204.8
BH 5	4.7	6.8	561.3	<1.0	30.2	58.5	91.1
BH 6	11.8	3.0	103.5	<1.4	34.0	64.3	176.3
OC 1	1.7	0.9	18.8	<0.8	3.0	4.2	532.3
OC 2	3.6	1.2	37.9	<0.8	11.2	18.7	308.7
OC 3	3.8	4.8	94.7	<1.0	24.0	580.2	119.4
OC 4	9.9	2.9	109.9	<0.8	23.1	21.6	395.7
OC 5	5.2	0.9	26.1	<0.8	5.3	5.9	480.8
OC 6	<0.6	1.4	13.1	<1.3	8.1	22.5	8.1
OC 7	6.6	5.2	73.3	<0.9	17.3	341.3	99.5
OC 8	<0.4	0.7	4.5	<0.7	3.3	4.0	48.1

Table B.18: *Trace elements Th – Zr (units in mg/L)*

XRD Diffractograms – Section 2.4.3

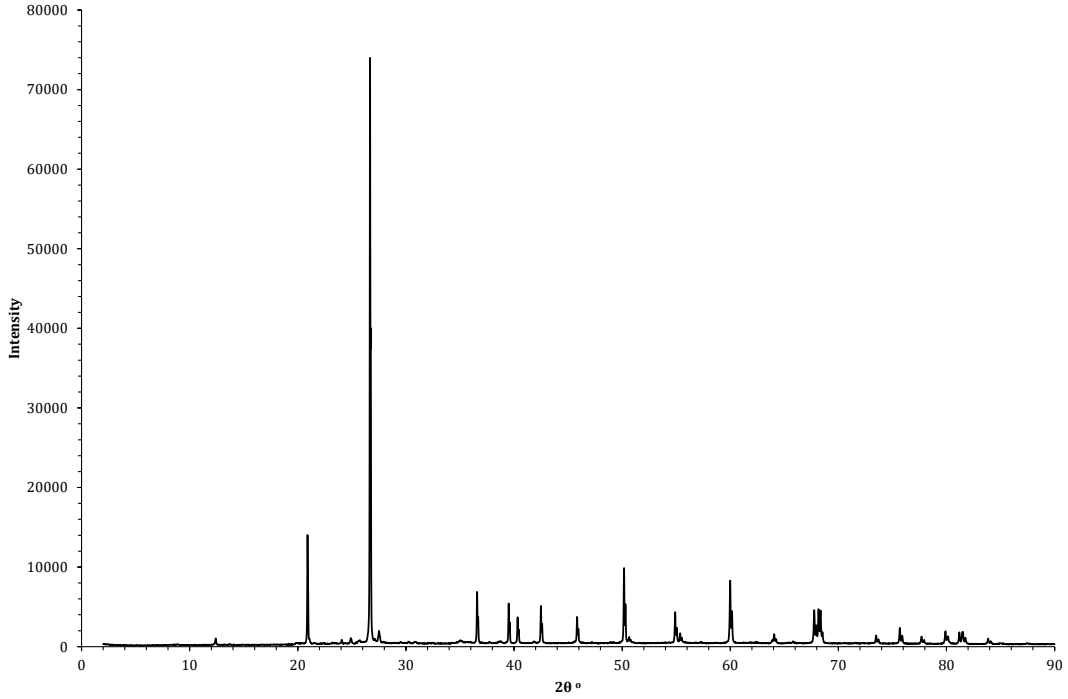

Figure B.19: *XRD pattern for OC 1 (Hazelhurst Fell, Pendle Grit)*

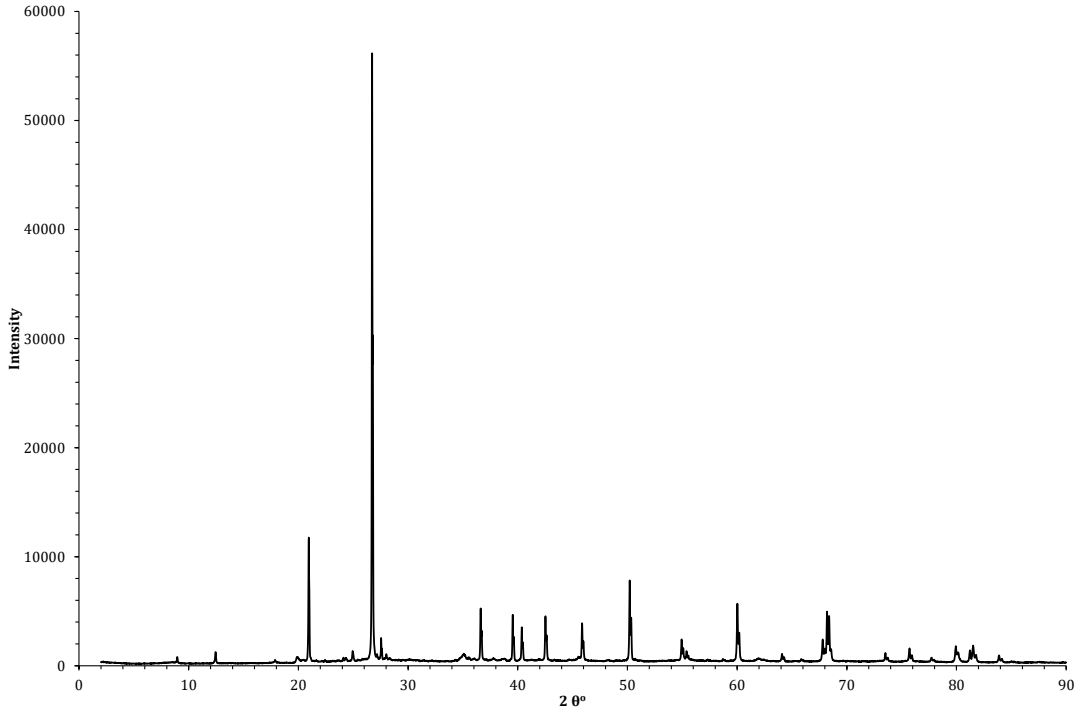

Figure B.20: *XRD pattern for OC 2 (Hazelhurst Fell, Pendle Grit, Silty)*

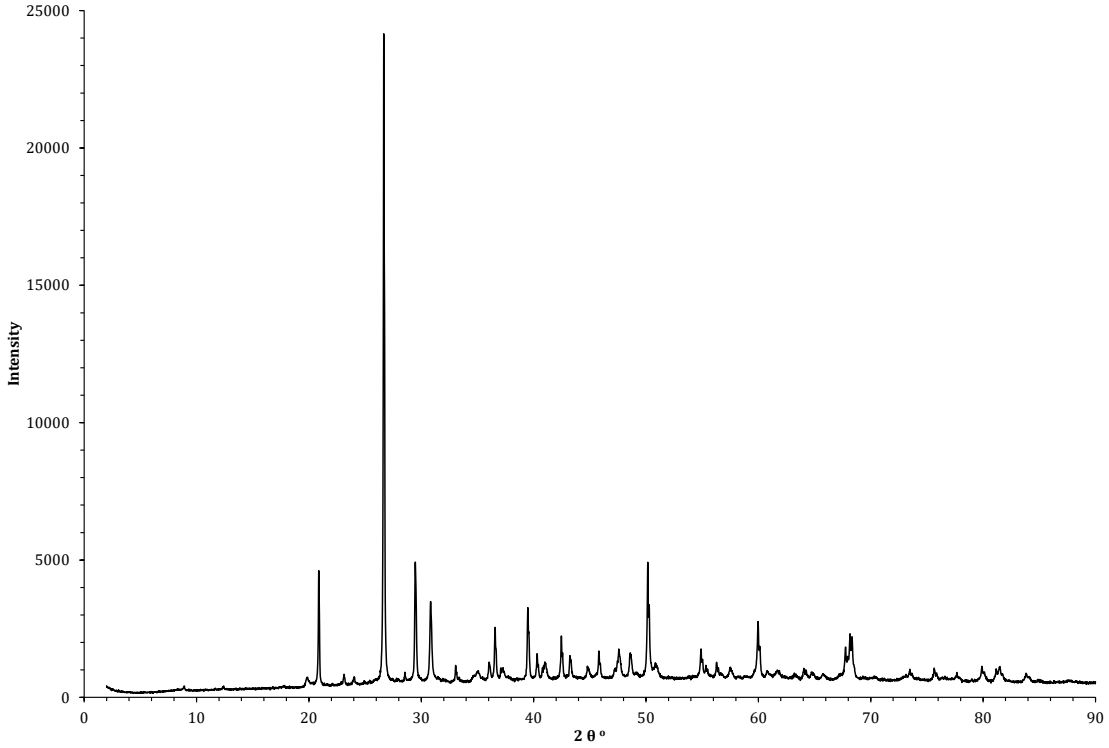

Figure B.21: *XRD pattern for OC 3 (Hazelhurst Fell, Upper Bowland Shale)*

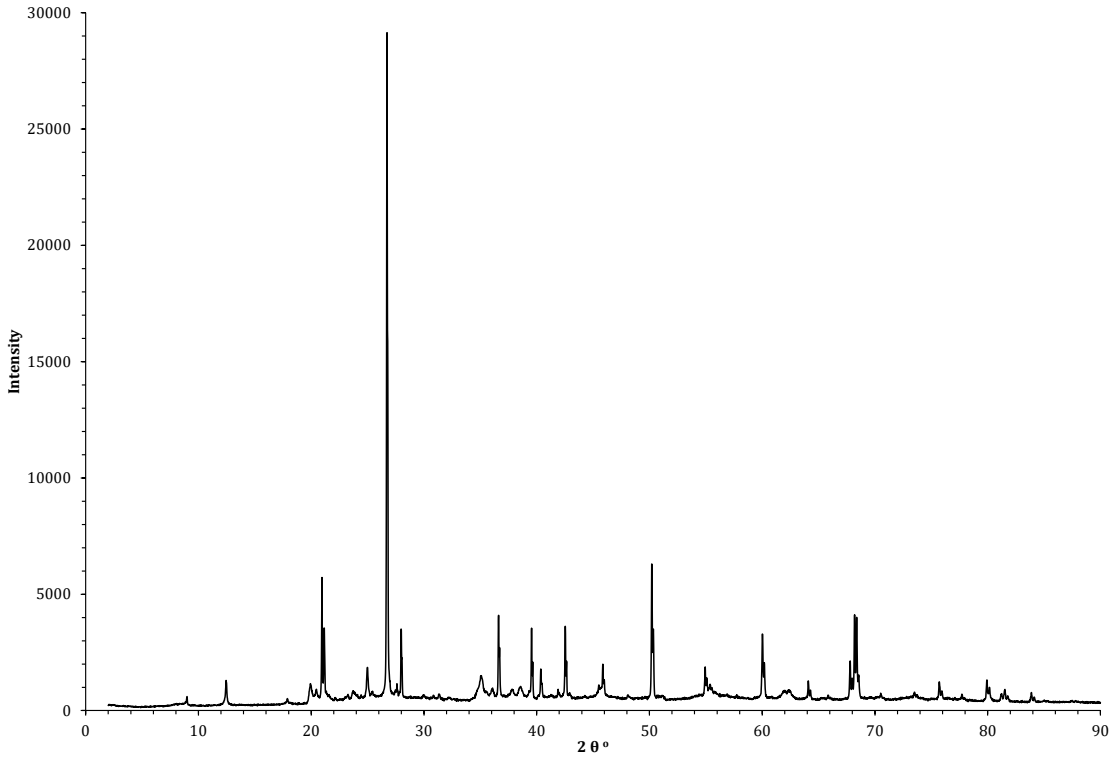

Figure B.22: *XRD pattern for OC 4 (Hazelhurst Fell, Upper Bowland Shale, Sandy)*

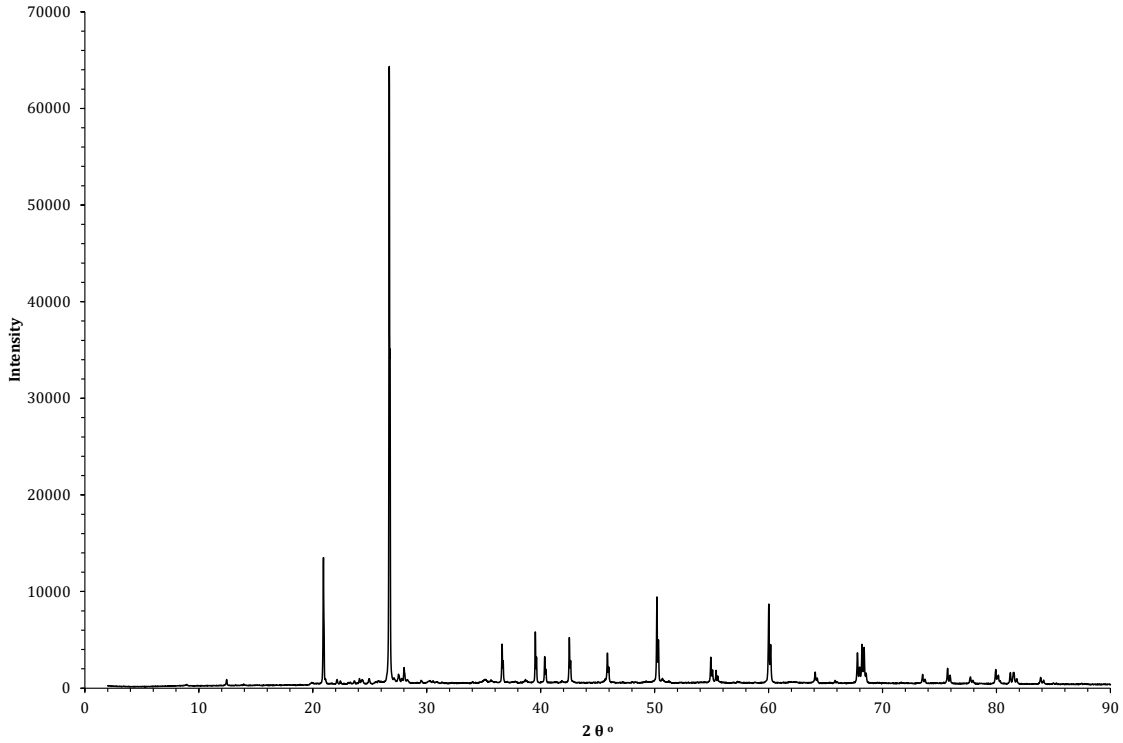

Figure B.23: *XRD pattern for OC 5 (Sabden, Nick O'Pendle, Pendle Grit)*

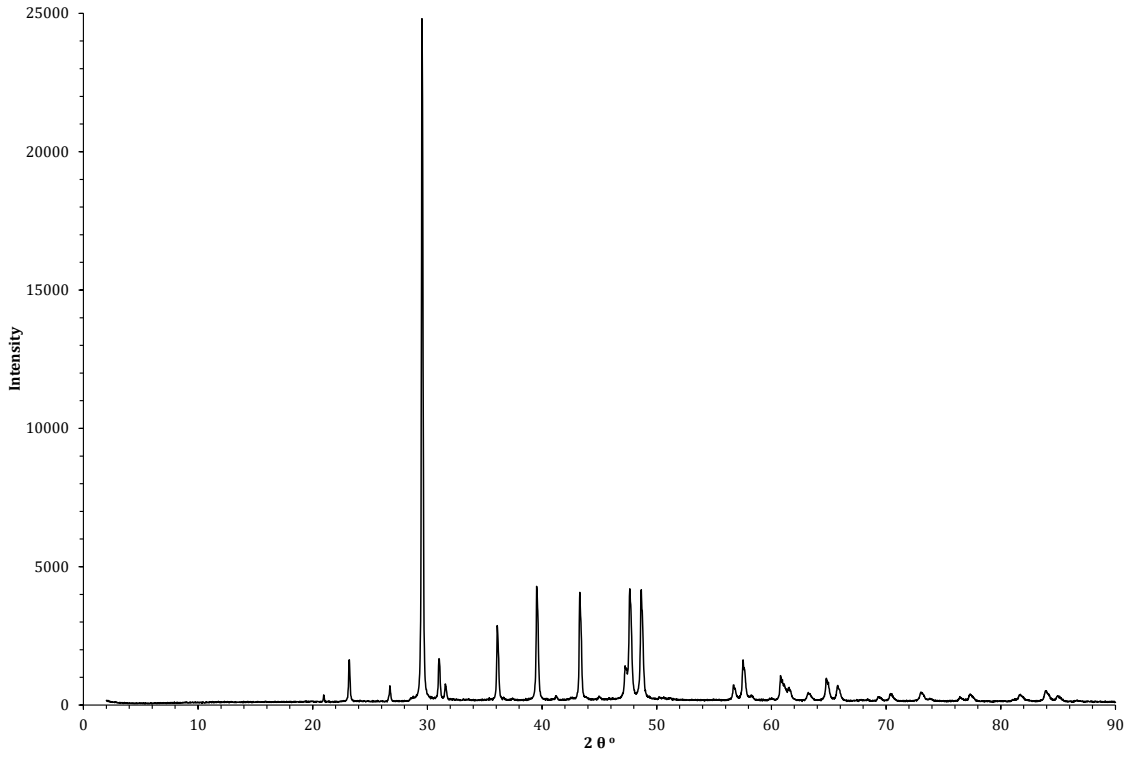

Figure B.24: *XRD pattern of OC 6 (Sykes Quarry Limestone based shale)*

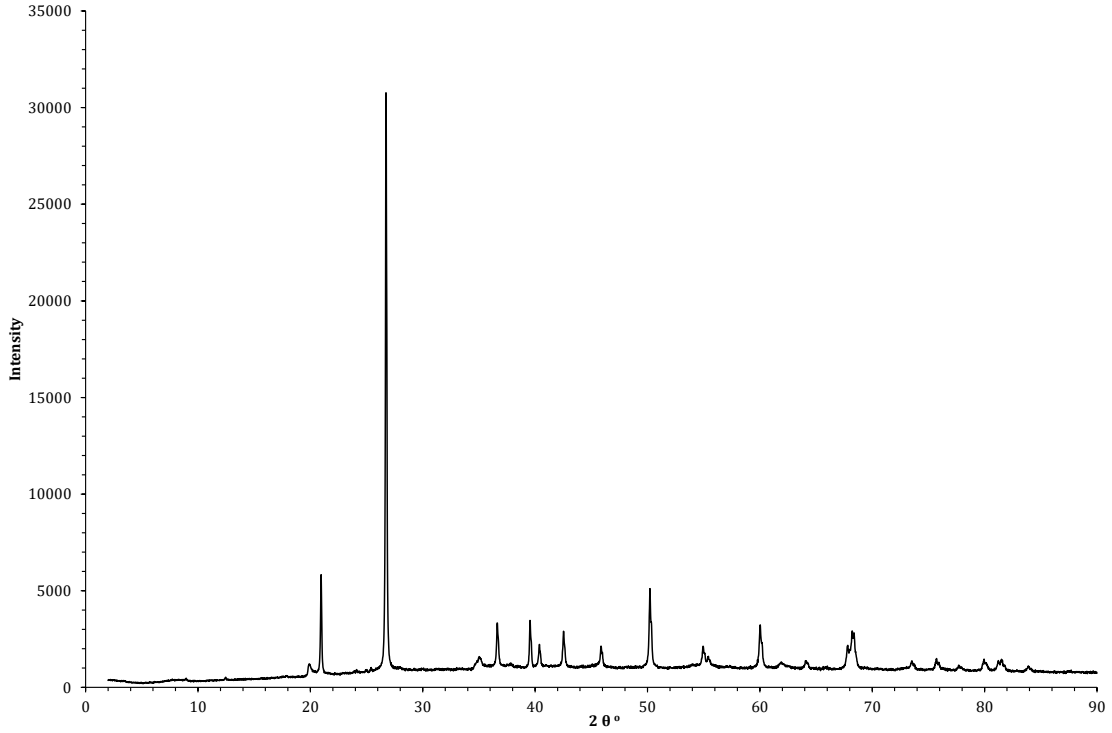

Figure B.25: *XRD Pattern for OC 7 (Wolf Fell, Upper Bowland Shale)*

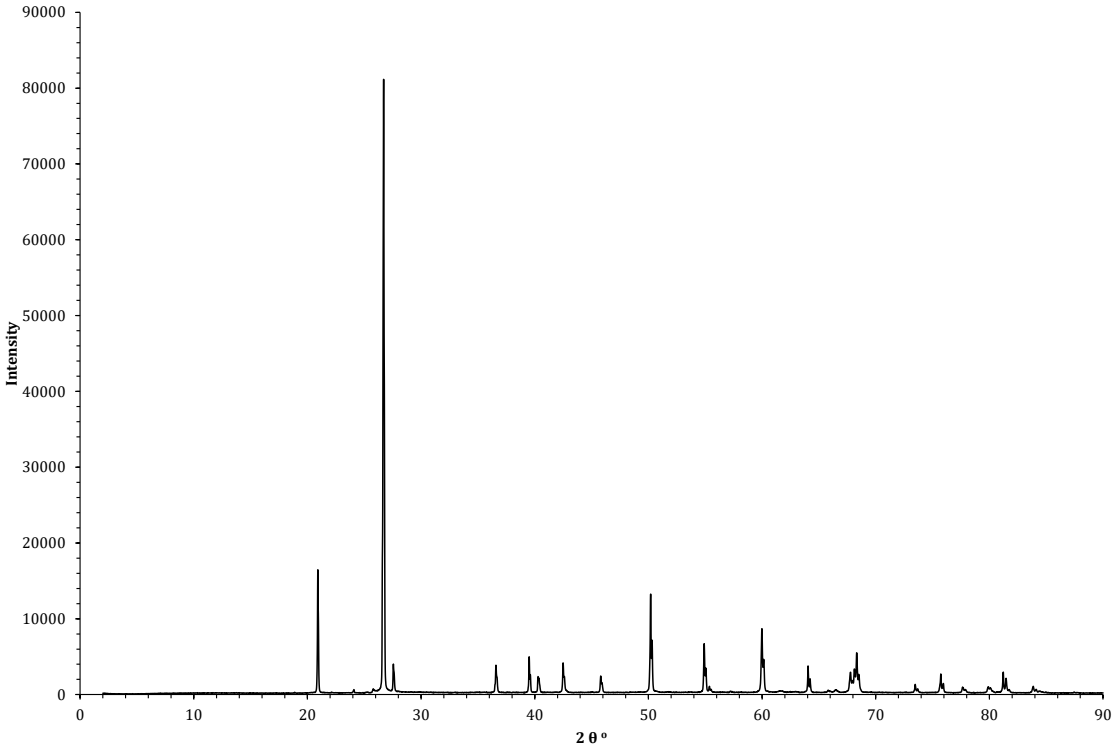

Figure B.26: *XRD pattern for OC 8 (Congleton Sand, Proppant)*

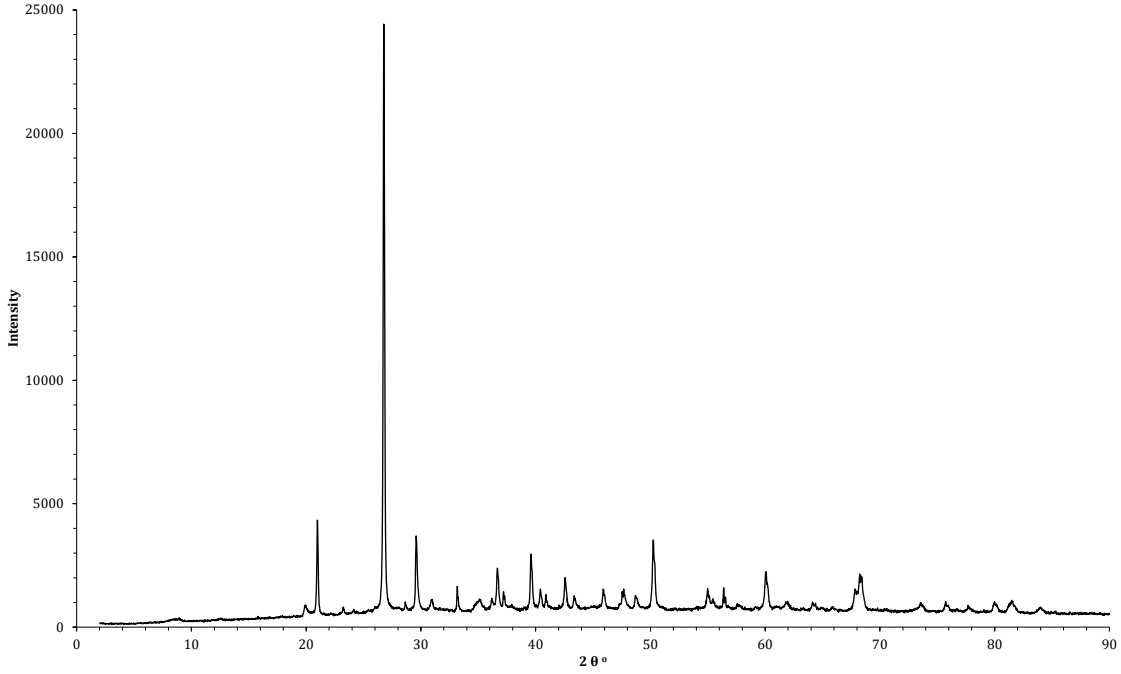

Figure B.27: *XRD pattern for BH 1 (Becconsall 1Z, 7030 ft, Upper Bowland Shale)*

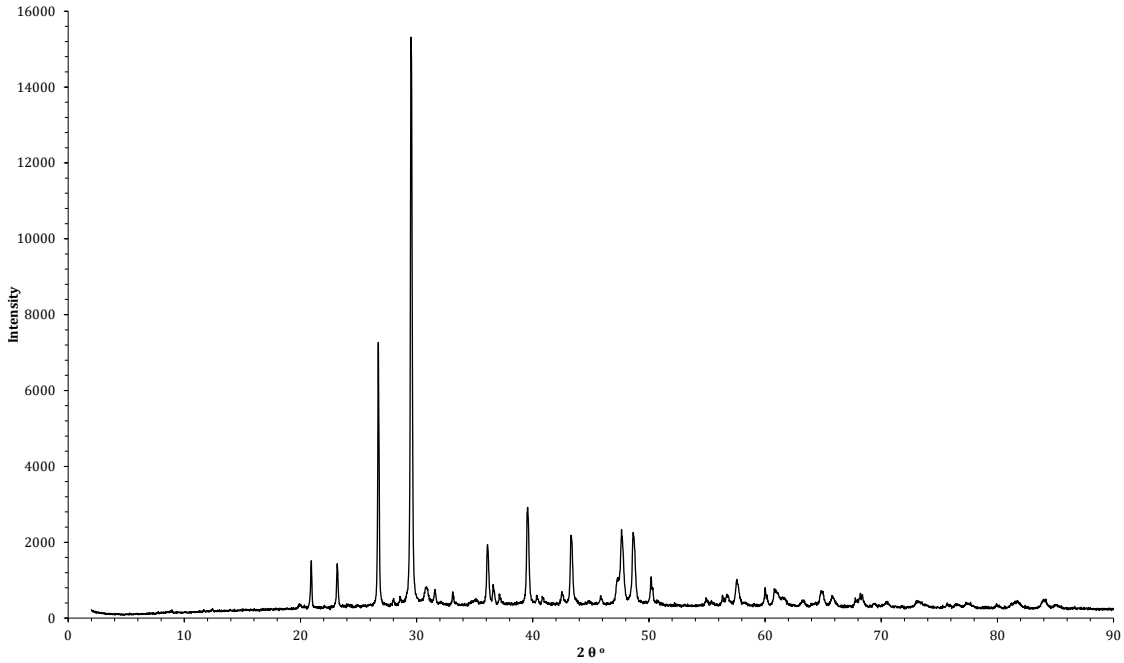

Figure B.28: *XRD pattern for BH 2 (Becconsall 1Z, 7420 ft, Lower Bowland Shale)*

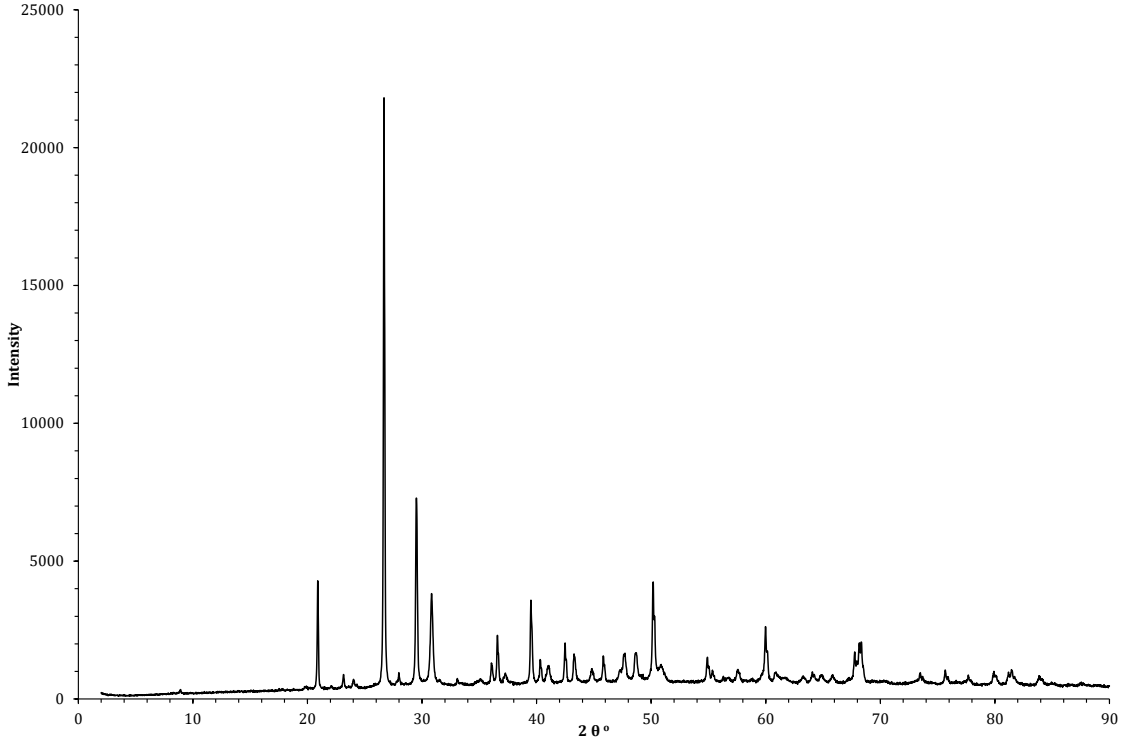

Figure B.29: *XRD pattern for BH 3 (Grange Hill 1Z, 7026 ft, Upper Bowland Shale)*

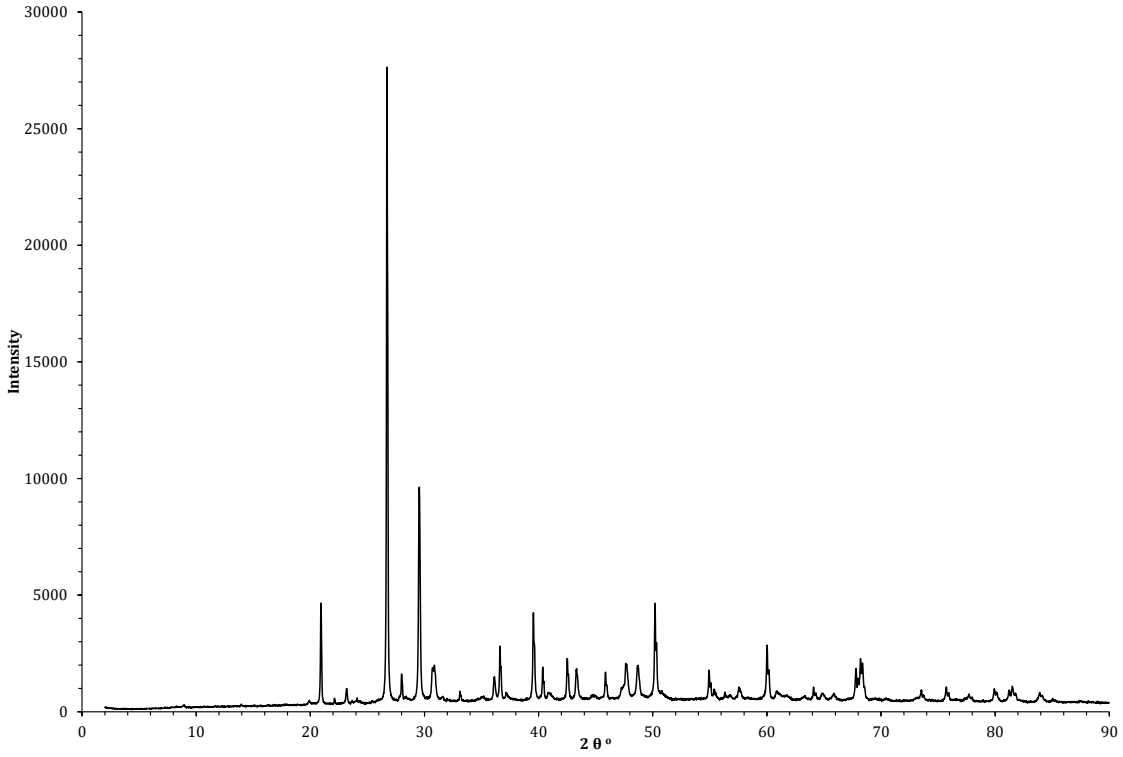

Figure B.30: *XRD pattern for BH 4 (Grange Hill 1Z, 8134 ft, Upper Bowland Shale)*

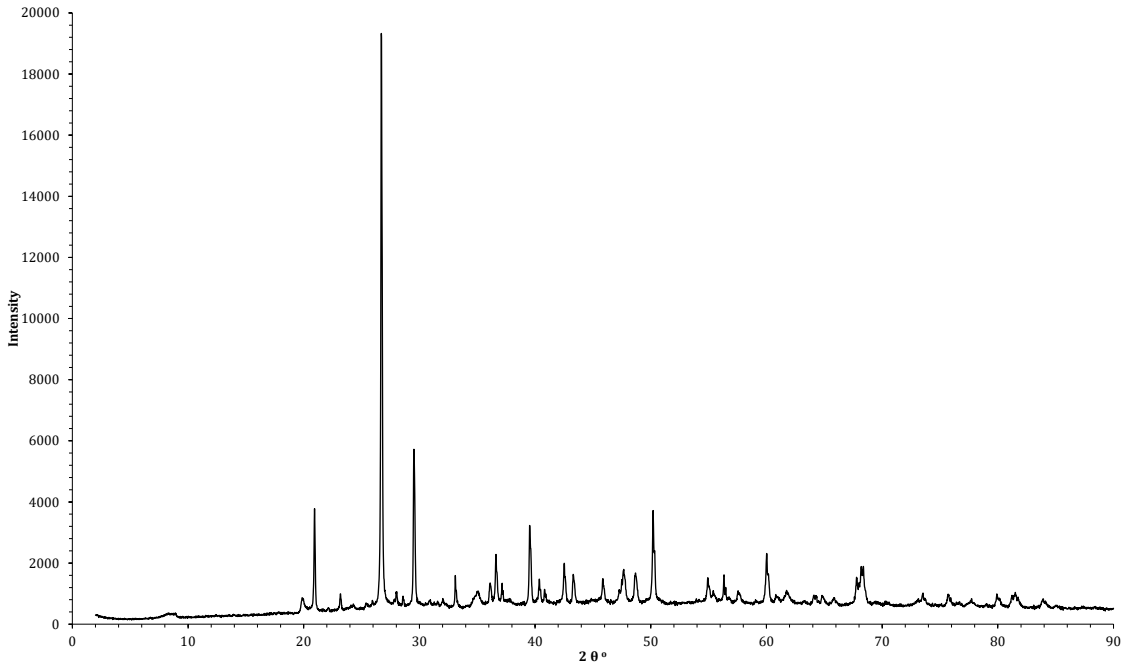

Figure B.31: *XRD pattern for BH 5 (Preese Hall 1A, 8885 ft, Lower Bowland Shale)*

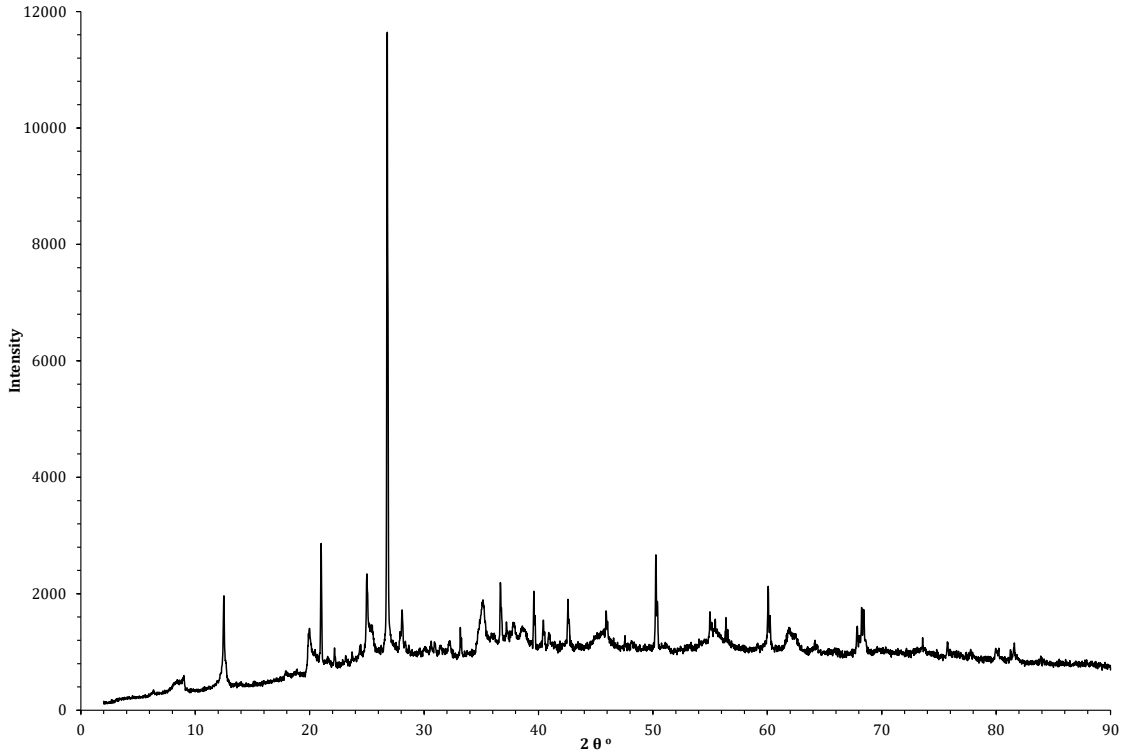

Figure B.32: *XRD pattern for BH 6 (Lockton 3, 7049 ft, Carboniferous Shale)*

References

Acros Organics, 2009. Polyacrylamide: Safety Data Sheet.

Aften, C., Watson, W.P., 2009. Improved Friction Reducer for Hydraulic Fracturing. Presented at the SPE Hydraulic Fracturing Technology Conference, Society of Petroleum Engineers. https://doi.org/10.2118/118747-MS

Ahmaruzzaman, Md., 2008. Adsorption of phenolic compounds on low-cost adsorbents: A review. Advances in Colloid and Interface Science 143, 48–67. https://doi.org/10.1016/j.cis.2008.07.002

Aitkenhead, N., Bridge, D., Riley, N., Kimbell, S., Evans, D., Humphreys, B., BGS, 1992. Geology of the country around Garstang.

Allen, S.J., Gan, Q., Matthews, R., Johnson, P.A., 2003. Comparison of optimised isotherm models for basic dye adsorption by kudzu. Bioresource Technology 88, 143–152. https://doi.org/10.1016/S0960-8524(02)00281-X

Alloway, B., Ayres, D.C., 1997. Chemical Principles of Environmental Pollution, Second Edition. CRC Press.

Almond, S., Clancy, S.A., Davies, R.J., Worrall, F., 2014. The flux of radionuclides in flowback fluid from shale gas exploitation. Environ Sci Pollut Res 21, 12316–12324. https://doi.org/10.1007/s11356-014-3118-y

Al-Tailji, W.H., Northington, N., Conway, M.T., Davidson, B.M., 2014. Minimizing Over-Flush Volumes at the End of Fracture-Stimulation Stages - An Eagle Ford Case Study. Presented at the SPE Annual Technical Conference and Exhibition, Society of Petroleum Engineers. https://doi.org/10.2118/170743-MS

American Petroleum Institute, 2014. Acidizing - Treatment in Oil and Gas Operators (Briefing No. DM2014-113). American Petroluem Institute (API).

Anderson, D.M., Nobakht, M., Moghadam, S., Mattar, L., 2010. Analysis of Production Data from Fractured Shale Gas Wells. Presented at the SPE Unconventional Gas Conference, Society of Petroleum Engineers. https://doi.org/10.2118/131787-MS

Andersson, A.J., Mackenzie, F.T., Ver, L.M., 2003. Solution of shallow-water carbonates: An insignificant buffer against rising atmospheric CO2. Geology 31, 513–516. https://doi.org/10.1130/0091-7613(2003)031<0513:SOSCAI>2.0.CO;2

Andrews, I., J., 2014. The Jurassic Shale of the Weald Basin: Geology and Shale Oil and Shale Gas resource estimation. British Geological Survey for Department of Energy and Climate Change, London, UK.

Andrews, I., J., 2013. The Carboniferous Bowland Shale Gas Study: Geology and Resource Estimation. British Geological Survey for Department of Energy and Climate Change, London, UK.

Anglian Water, 2018. Drinking Water Quality Report of the Colchester South Public Water Supply Zone ES41 (No. ES41). Anglian Water.

Armstrong, J.P., Smith, J., D'Elia, V.A.A., Trueblood, S.P., 1997. The occurrence and correlation of oils and Namurian source rocks in the Liverpool Bay-North Wales area. Geological Society, London, Special Publications 124, 195–211. https://doi.org/10.1144/GSL.SP.1997.124.01.12

Bailey, L., Keall, M., Audibert, A., Lecourtier, J., 1994. Effect of Clay/Polymer Interactions on Shale Stabilization during Drilling. Langmuir 10, 1544–1549.

Batley, G.E., Kookana, R.S., 2012. Environmental issues associated with coal seam gas recovery: managing the fracking boom. Environ. Chem. 9, 425–428. https://doi.org/10.1071/EN12136

BBC, 2018. What is fracking?

Berner, R.A., 1984. Sedimentary pyrite formation: An update. Geochimica et Cosmochimica Acta 48, 605–615. https://doi.org/10.1016/0016-7037(84)90089-9

BGS, 2011. Earthquakes induced by Hydraulic Fracturing Operations near Blackpool, UK [WWW Document]. URL

http://earthquakes.bgs.ac.uk/research/BlackpoolEarthquakes.html (accessed 10.29.18).
BGS, NERC, Dept of Communities and Local Government, 2009. Silica Sand, Mineral Planning Factsheet.
Blondes, M.S., Gans, K.D., Engle, M.A., Kharaka, Y.K., Reidy, M.E., Thordsen, J.J., Rowan, E.L., Morrissey, E.A., 2017. U.S. Geological Survey National Produced Waters Geochemical Database v2.3 (PROVISIONAL) (No. USGSPWDBv2.3n). USGS.
Bloomfield, C., 1981. The Chemistry of Soil Processes. John Wiley & Sons, Chichester.
Bommer, J.J., Dost, B., Edwards, B., Stafford, P.J., Elk, J. van, Doornhof, D., Ntinalexis, M., 2016. Developing an Application-Specific Ground-Motion Model for Induced SeismicityDeveloping an Application-Specific Ground-Motion Model for Induced Seismicity. Bulletin of the Seismological Society of America 106, 158–173. https://doi.org/10.1785/0120150184
Bowell, R.J., Bruce, I., 1995. Geochemistry of iron ochres and mine waters from Levant Mine, Cornwall. Applied Geochemistry 10, 237–250. https://doi.org/10.1016/0883-2927(94)00036-6
BP Petroleum Development LTD, 1967. Lockton No 3 Completion Log (Completion Log). BR Petroleum.
Brindley, G., Brown, G., 1984. Crystal Structures of clay minerals and their x-ray identification. Mineralogical Society.
British Geological Survey, 1991. Garstang. England and Wales Sheet 67. Solid and Drift Edition.
Broderick, J., Anderson, K., Wood, R., Gilbert, P., Sharmina, M., Footit, A., Glynn, S., Nicholls, F., 2011. Shale Gas: An Updated Assessment of Environmental and Climate Change Impacts.
Brownlow, J.W., James, S.C., Yelderman Jr., J.C., 2018. Influence of Hydraulic Fracturing on Overlying Aquifers in the Presence of Leaky Abandoned Wells. Groundwater 781–792. https://doi.org/10.1111/gwat.12431@10.1111/(ISSN)1745-6584.TopAltmetricPaperGWandGWMR
Burton, G.A., Basu, N., Ellis, B.R., Kapo, K.E., Entrekin, S., Nadelhoffer, K., 2014. Hydraulic "Fracking": Are surface water impacts an ecological concern? Environmental Toxicology and Chemistry 33, 1679–1689. https://doi.org/10.1002/etc.2619
Busby, J., 2010. Geothermal prospects in the United Kingdom. Presented at the World Geothermal Congress 2010, Bali, Indonesia.
Caruso, F., Mantellato, S., Palacios, M., Flatt, R.J., 2017. ICP-OES method for the characterization of cement pore solutions and their modification by polycarboxylate-based superplasticizers. Cement and Concrete Research 91, 52–60. https://doi.org/10.1016/j.cemconres.2016.10.007
Caulfield, M.J., Hao, X., Qiao, G.G., Solomon, D.H., 2003. Degradation on polyacrylamides. Part I. Linear polyacrylamide. Polymer 44, 1331–1337. https://doi.org/10.1016/S0032-3861(03)00003-X
Caulfield, M.J., Qiao, G.G., Solomon, D.H., 2002. Some Aspects of the Properties and Degradation of Polyacrylamides. Chemical Reviews 102, 3067–3083.
Cesur, R., Tekin, E., Ulker, A., 2017. Air Pollution and Infant Mortality: Evidence from the Expansion of Natural Gas Infrastructure. Econ J 127, 330–362. https://doi.org/10.1111/ecoj.12285
Chapman, E.C., Capo, R.C., Stewart, B.W., Kirby, C.S., Hammack, R.W., Schroeder, K.T., Edenborn, H.M., 2012. Geochemical and Strontium Isotope Characterization of Produced Waters from Marcellus Shale Natural Gas Extraction. Environ. Sci. Technol. 46, 3545–3553. https://doi.org/10.1021/es204005g
Charlet, L., Markelova, E., Parsons, C., Couture, R.-M., Madé, B., 2013. Redox Oscillation Impact on Natural and Engineered Biogeochemical Systems: Chemical Resilience and Implications for Contaminant Mobility. Procedia Earth and Planetary Science, Proceedings of the Fourteenth International Symposium on Water-Rock Interaction, WRI 14 7, 135–138. https://doi.org/10.1016/j.proeps.2013.03.048

Charpentier, R., Cook, T., 2011. Assessment of Undiscovered Oil and Gas Resources of the Devonian Marcellus Shale of the Appalachian Basin Province, 2011 [WWW Document]. URL https://pubs.usgs.gov/fs/2011/3092/ (accessed 10.23.18).
Chermak, J.A., Schreiber, M.E., 2014. Mineralogy and trace element geochemistry of gas shales in the United States: Environmental implications. International Journal of Coal Geology, Environmental geology and the unconventional gas revolution 126, 32–44. https://doi.org/10.1016/j.coal.2013.12.005
Chew Kenneth J., 2014. The future of oil: unconventional fossil fuels. Philosophical Transactions of the Royal Society A: Mathematical, Physical and Engineering Sciences 372, 20120324. https://doi.org/10.1098/rsta.2012.0324
Chris Blandford Associates, Lancashire County Council, 2009. Forest of Bowland Area of Natural Beauty. Landscape Character Assessment.
Chuan, M.C., Shu, G.Y., Liu, J.C., 1996. Solubility of heavy metals in a contaminated soil: Effects of redox potential and pH. Water Air Soil Pollut 90, 543–556. https://doi.org/10.1007/BF00282668
Clancy, S.A., Worrall, F., Davies, R.J., Gluyas, J.G., 2017. An assessment of the footprint and carrying capacity of oil and gas well sites: The implications for limiting hydrocarbon reserves. Science of The Total Environment. https://doi.org/10.1016/j.scitotenv.2017.02.160
Cox, D.M., Temples, T., Young, M., 2013. Hydraulic Fracturing and Potential Environmental Impacts.
Cuadrilla Resources, 2018a. Hydraulic Fracture Plan PNR 1/1Z.
Cuadrilla Resources, 2018b. Preston New Road 1Z Hydraulic Fracture Plan.
Davies, R.J., Mathias, S.A., Moss, J., Hustoft, S., Newport, L., 2012. Hydraulic fractures: How far can they go? Marine and Petroleum Geology 37, 1–6. https://doi.org/10.1016/j.marpetgeo.2012.04.001
De Pater, C., J., Baisch, S., 2011. Geomechanical Study of the Bowland Shale Seismicity (Synthesis Report). StrataGen & Q-con.
de Vries, W., Lofts, S., Tipping, E., Meili, M., Groenenberg, J.E., Schütze, G., 2007. Impact of Soil Properties on Critical Concentrations of Cadmium, Lead, Copper, Zinc, and Mercury in Soil and Soil Solution in View of Ecotoxicological Effects, in: Reviews of Environmental Contamination and Toxicology, Reviews of Environmental Contamination and Toxicology. Springer, New York, NY, pp. 47–89. https://doi.org/10.1007/978-0-387-69163-3_3
Deng, Y., Dixon, J.B., White, G.N., 2006a. Adsorption of Polyacrylamide on Smectite, Illite, and Kaolinite. Soil Science Society of America Journal 70, 297–304. https://doi.org/10.2136/sssaj2005.0200
Deng, Y., Dixon, J.B., White, G.N., Loeppert, R.H., Juo, A.S.R., 2006b. Bonding between polyacrylamide and smectite. Colloids and Surfaces A: Physicochemical and Engineering Aspects 281, 82–91. https://doi.org/10.1016/j.colsurfa.2006.02.030
Dowell, Schlumberger, 1966. Lockton No.3 Well Report (Formation Test Report).
Downing, R., A., Gray, D., A., 1986. Geothermal Energy - The Potential in the United Kingdom. HMSO, London.
Drollette, B., D., 2014a. Organic Compounds Associated with Hydraulic Fracturing: Groundwater Composition and Natural Attenuation Potential. Duke University.
Drollette, B., D., 2014b. Organic Compounds Associated with Hydraulic Fracturing: Groundwater Composition and Natural Attenuation Potential. Duke University.
Earp, J., Magraw, D., Poole, E., Land, D., Whiteman, A., 1961. Geology of the Country around Clitheroe and Nelson. Her Majesty's Stationary Office.
Enomoto, C., B., Coleman, J., Swezey, C., S., Niemeyer, P., W., Dulong, F., T., 2015. Geochemical and Mineralogical Sampling of the Devonian Shales in the Broadtop Synclinorium, Appalachian Basin, in Virginia, West Virginia, Maryland, and Pennsylvania (No. 2015–1061). USGS, Virginia.
Environment Agency, 2011. Shale Gas: North West - Monitoring of Flowback Water.

EPA, 2015. Analysis of Hydraulic Fracturing Fluid Data from the FracFocus Chemical Dsiclosure Registry 1.0 (No. EPA/601/R-14/003). United States Environmental Protection Agency.
EPA, 2007. Framework for Metals Risk Assessment (Archive Document No. 120/R–07/001). Office of the Science Advisor.
EPA, 1974. Safe Drinking Water Act (No. 42 U.S.C 330f et seq. (1974)). United States Environmental Protection Agency.
Eriksson, J.E., 1989. The influence of pH, soil type and time on adsorbtion and uptake by plants of Cd added to the soil. Water Air Soil Pollut 48, 317–335. https://doi.org/10.1007/BF00283334
European Union, 1998. Council Directive 98/83/EC on the quality of water intended for human consumption. Official Journal of European Communities.
Evans, L.J., 1989. Chemistry of metal retention by soils. Environ. Sci. Technol. 23, 1046–1056. https://doi.org/10.1021/es00067a001
Ferrer, I., Thurman, E.M., 2015. Chemical constituents and analytical approaches for hydraulic fracturing waters. Trends in Environmental Analytical Chemistry 5, 18–25. https://doi.org/10.1016/j.teac.2015.01.003
Fisher, M.K., Warpinski, N.R., 2012. Hydraulic-Fracture-Height Growth: Real Data. SPE Production & Operations 27, 8–19. https://doi.org/10.2118/145949-PA
Fontenot, B.E., Hunt, L.R., Hildenbrand, Z.L., Carlton Jr., D.D., Oka, H., Walton, J.L., Hopkins, D., Osorio, A., Bjorndal, B., Hu, Q.H., Schug, K.A., 2013. An Evaluation of Water Quality in Private Drinking Water Wells Near Natural Gas Extraction Sites in the Barnett Shale Formation. Environ. Sci. Technol. 47, 10032–10040. https://doi.org/10.1021/es4011724
Foo, K.Y., Hameed, B.H., 2010. Insights into the modeling of adsorption isotherm systems. Chemical Engineering Journal 156, 2–10. https://doi.org/10.1016/j.cej.2009.09.013
FracFocus, 2018. Hydraulic Fracturing: The Process | FracFocus Chemical Disclosure Registry [WWW Document]. URL http://fracfocus.ca/hydraulic-fracturing-how-it-works/hydraulic-fracturing-process (accessed 2.22.19).
Freundlich, H., 1906. Adsorption in Solution. Phys. Chemie. 57, 384–410.
Gandossi, L., Von Estorff, U., 2015. An overview of hydraulic fracturing and other formation stimulation technologies for shale gas production (No. Report EUR 26347 EN). European Commission Joint Research Centre.
Gibbons, S., Heblich, S., Lho, E., Timmins, C., 2016. Fear of Fracking? The Impact of the Shale Gas Exploration on House Prices in Britain (Working Paper No. 22859). National Bureau of Economic Research. https://doi.org/10.3386/w22859
Gilbert, J., 2012. Cuadrilla Resources Preese Hall #1 Stage 2 Fracture Height Growth. Barree & Associates.
Gilman, J., Robinson, C., 2011. View PDF.
Gong, H., Rose, A.W., Suhr, N., 1977. The geochemistry of cadmium in some sedimentary rocks. Geochemica et Cosmochimica Acta 41, 1687–1692.
Goodman, P.S., Galatioto, F., Thorpe, N., Namdeo, A.K., Davies, R.J., Bird, R.N., 2016. Investigating the traffic-related environmental impacts of hydraulic-fracturing (fracking) operations. Environment International 89–90, 248–260. https://doi.org/10.1016/j.envint.2016.02.002
Green, C., A., Styles, P., Baptie, B., J., 2012. Preese Hall Shale Gas Fracturing: Review and Recommendations for induced seismic mitigation. Report for DECC. DECC.
Green, S., Stott, D., E., 2001. Polyacrylamide: A review of the Use, Effectiveness, and Cost of a Soil Erosion Control Amendment. Selected papers from the 10th International Soil Conservation Organization Meeting, May 24th-29th, 1999 384–389.
Gregory, K.B., Vidic, R.D., Dzombak, D.A., 2011. Water Management Challenges Associated with the Production of Shale Gas by Hydraulic Fracturing. Elements 7, 181–186. https://doi.org/10.2113/gselements.7.3.181
Gross, D., Sachsenhofer, R.F., Bechtel, A., Pytlak, L., Rupprecht, B., Wegerer, E., 2015. Organic geochemistry of Mississippian shales (Bowland Shale Formation) in central Britain:

Implications for depositional environment, source rock and gas shale potential. Marine and Petroleum Geology 59, 1–21. https://doi.org/10.1016/j.marpetgeo.2014.07.022
Guezennec, A.G., Michel, C., Bru, K., Touze, S., Desroche, N., Mnif, I., Motelica-Heino, M., 2015. Transfer and degradation of polyacrylamide-based flocculants in hydrosystems: a review. Environ Sci Pollut Res 22, 6390–6406. https://doi.org/10.1007/s11356-014-3556-6
Guo, H., Aziz, N.I., Schmidt, L.C., 1993. Rock fracture-toughness determination by the Brazilian test. Engineering Geology 33, 177–188. https://doi.org/10.1016/0013-7952(93)90056-I
Guo, J., Li, Y., Wang, S., 2018. Adsorption damage and control measures of slick-water fracturing fluid in shale reservoirs. Petroleum Exploration and Development 45, 336–342. https://doi.org/10.1016/S1876-3804(18)30037-5
Hammond, G., P., O'Grady, A., Packham, D., E., 2015. Energy Technology Assessment of Shale Gas "Fracking" - A UK Perspective. Energy Procedia 75, 2764–2771.
Harrison, A.L., Jew, A.D., Dustin, M.K., Thomas, D.L., Joe-Wong, C.M., Bargar, J.R., Johnson, N., Brown, G.E., Maher, K., 2017. Element release and reaction-induced porosity alteration during shale-hydraulic fracturing fluid interactions. Applied Geochemistry 82, 47–62. https://doi.org/10.1016/j.apgeochem.2017.05.001
Harvey, T., Gray, J., 2010. The Unconventional Hydrocarbon Resources of Britains Onshore Basins - Shale Gas. Department of Energy and Climate Change.
He, Q., Li, X., Miao, Z., Huang, S., Wan, K., 2019. The relevance between water release behavior and pore evolution of hard lignite during the thermal-drying process. Journal of the Energy Institute. https://doi.org/10.1016/j.joei.2019.01.005
Heybob, K., Mouser, P., 2015. Biodegradability of Organic Additives in hydraulic Fracturing Activities. Ohio State University.
Hird, C., Clarke, H., Turner, P., 2012a. Preese Hall 1A End of Well Report. LJ/06-5 (End of Well Report). Cuadrilla Resources.
Hird, C., Clarke, H., Wood, T., 2012b. Grange Hill 1Z End of Well Report. LJ/01-1Z (End of Well Report). Cuadrilla Resources.
Hird, C., Clarke, H., Wood, T., 2011. Becconsall-1 End of Well Report. LJ/06-6Z (End of Well Report). Cuadrilla Resources.
Ho, Y.S., Porter, J.F., McKay, G., 2002. Equilibrium Isotherm Studies for the Sorption of Divalent Metal Ions onto Peat: Copper, Nickel and Lead Single Component Systems. Water, Air, & Soil Pollution 141, 1–33. https://doi.org/10.1023/A:1021304828010
Holloway, M.D., Rudd, O., 2013. Fracking: The Operations and Environmental Consequences of Hydraulic Fracturing. John Wiley & Sons.
Jackson, R.B., Vengosh, A., Carey, J.W., Davies, R.J., Darrah, T.H., O'Sullivan, F., Pétron, G., 2014. The Environmental Costs and Benefits of Fracking. Annual Review of Environment and Resources 39, 327–362. https://doi.org/10.1146/annurev-environ-031113-144051
Jacobsen, O.S., Johnsen, A.R., Gravesen, P., Schovsbo, N.H., 2015. Measuring, monitoring, mitigating and managing the environmental impacts of shale gas (No. D8.1). Geological Survey of Denmark and Greenland & M4 Shale Gas.
JAGDAG, UK Technical Advisory Group on the Water Framework Directive, 2018. Technical report on Groundwater Hazardous Substances (No. 11b(iii) v12). Water Framework Directive UK TAG.
Jarosławski, J., Pawlak, I., 2018. Analysis of impact of the shale gas exploration and exploitation activities on the quality of ambient air – case study of Wysin, Poland. Presented at the EGU General Assembly Conference Abstracts, p. 7619.
Jarvie, D., M., 2012. Shale resource systems for oil and gas: Part 1 - Shale Gas Resource Systems. AAPG Memoir, Shale Reservoirs - Giant Resources for the 21st Century 97, 69–87. https://doi.org/10.1306/13321446M973489

Johansson, K., Bringmark, E., Lindevall, L., Wilander, A., 1995. Effects of acidification on the concentrations of heavy metals in running waters in Sweden. Water Air Soil Pollut 85, 779–784. https://doi.org/10.1007/BF00476924
Jung, J., Jang, J., Ahn, J., 2016. Characterization of a Polyacrylamide Solution Used for Remediation of Petroleum Contaminated Soils. Materials 9, 16. https://doi.org/10.3390/ma9010016
Kalra, B., Gross, R., 2002. HRP-mediated polymerizations of acrylamide and sodium acrylate. Green Chemistry 4, 174–178. https://doi.org/10.1039/B106735B
Kane, I.A., McCaffrey, W.D., Martinsen, O.J., 2009. Allogenic vs. Autogenic Controls on Megaflute Formation. Journal of Sedimentary Research 79, 643–651. https://doi.org/10.2110/jsr.2009.072
Kaufman, P.B., Penny, G.S., Paktinat, J., 2008. Critical Evaluation of Additives Used in Shale Slickwater Fracs. Presented at the SPE Shale Gas Production Conference, Society of Petroleum Engineers. https://doi.org/10.2118/119900-MS
Kekacs, D., Drollette, B.D., Brooker, M., Plata, D.L., Mouser, P.J., 2015. Aerobic biodegradation of organic compounds in hydraulic fracturing fluids. Biodegradation 26, 271–287. https://doi.org/10.1007/s10532-015-9733-6
Kenomore, M., Hassan, M., Dhakal, H., Shah, A., 2017. Total organic carbon evaluation of the Bowland Shale Formation in the Upper Bowland of the Widmerpool Gulf. Journal of Petroleum Science and Engineering 150, 137–145. https://doi.org/10.1016/j.petrol.2016.11.040
Keshavarzi, R., Mohammadi, S., Bayesteh, H., 2012. Hydraulic Fracture Propagation In Unconventional Reservoirs: The Role of Natural Fractures. Presented at the 46th U.S. Rock Mechanics/Geomechanics Symposium, American Rock Mechanics Association.
King, G., E., 2010. Thirty Years of Gas Shale Fracturing: What have we learned? SPE Annual Technical Conference.
King, G.E., 2012. Hydraulic Fracturing 101: What Every Representative, Environmentalist, Regulator, Reporter, Investor, University Researcher, Neighbor, and Engineer Should Know About Hydraulic Fracturing Risk. Journal of Petroleum Technology 64, 34–42. https://doi.org/10.2118/0412-0034-JPT
Kinniburgh, D.G., 1986. General purpose adsorption isotherms. Environ. Sci. Technol. 20, 895–904. https://doi.org/10.1021/es00151a008
Konitzer, S., F., Davies, S., J., Stephenson, M., H., Leng, M., J., Gabbott, S., E., Angiolini, L., Macquaker, J., H, S., Vane, C., H., Millward, D., Kane, I., A., 2015. Primary Controls on Organic Carbon Content in UK Upper Mississippian Gas Shales.
Kovats, S., Depledge, M., Haines, A., Fleming, L.E., Wilkinson, P., Shonkoff, S.B., Scovronick, N., 2014. The health implications of fracking. The Lancet 383, 757–758. https://doi.org/10.1016/S0140-6736(13)62700-2
Kozlowski, L.P., 2017. Proteome-pI: proteome isoelectric point database. Nucleic Acids Res 45, D1112–D1116. https://doi.org/10.1093/nar/gkw978
Kresse, T.M., Warner, N.R., Hays, P.D., Down, A., Vengosh, A., Jackson, R.B., 2012. Shallow Groundwater Quality and Geochemistry in the Fayetteville Shale Gas-Produced Area, North Central Arkansas, 2011 (No. 2012–5273). U.S. Department of the Interior. U.S. Geological Survey.
Kundu, S., Gupta, A.K., 2006. Arsenic adsorption onto iron oxide-coated cement (IOCC): Regression analysis of equilibrium data with several isotherm models and their optimization. Chemical Engineering Journal 122, 93–106. https://doi.org/10.1016/j.cej.2006.06.002
Lancashire County Council, 2015. The Geology of the Forest of Bowland | Forest of Bowland AONB [WWW Document]. URL https://forestofbowland.com/Geology-Forest-Bowland (accessed 5.9.18).
Lang, A., 2014. Fracking in Austria and the UK: a comparative study. ResAGorA: Governance framework for Responsible Research and Innovation.
Langenhoff, A., 2011. Shale Gas and Groundwater Quality: A Literature Review on Fate and Effect of Added Chemicals (No. 1202141– 008). Deltares.

Langmuir, I., 1917. The constitution and fundamental properties of solids and liquids. Journal of the Franklin Institute 183, 102–105. https://doi.org/10.1016/S0016-0032(17)90938-X
Lavergren, U., Åström, M.E., Bergbäck, B., Holmström, H., 2009. Mobility of trace elements in black shale assessed by leaching tests and sequential chemical extraction. Geochemistry: Exploration, Environment, Analysis 9, 71–79. https://doi.org/10.1144/1467-7873/08-188
Lee, J.-J., Fuller, G.G., 1985. Adsorption and desorption of flexible polymer chains in flowing systems. Journal of Colloid and Interface Science 103, 569–577. https://doi.org/10.1016/0021-9797(85)90132-8
Lee, L.T., Rahbari, R., Lecourtier, J., Chauveteau, G., 1991. Adsorption of polyacrylamides on the different faces of kaolinites. Journal of Colloid and Interface Science 147, 351–357. https://doi.org/10.1016/0021-9797(91)90167-7
Lenntech, 2019. Iron (Fe) and water [WWW Document]. Lenntech Water Treatment Solutions. URL https://www.lenntech.com/periodic/water/iron/iron-and-water.htm (accessed 11.28.19).
Li, Y., Wang, S., Guo, J., Gou, X., Jiang, Z., Pan, B., 2018. Reduced adsorption of polyacrylamide-based fracturing fluid on shale rock using urea. Energy Science & Engineering 0. https://doi.org/10.1002/ese3.249
Liu, Y., Xiao, T., Perkins, R.B., Zhu, J., Zhu, Z., Xiong, Y., Ning, Z., 2017. Geogenic cadmium pollution and potential health risks, with emphasis on black shale. Journal of Geochemical Exploration, Potentially Toxic Metals in the Environment 176, 42–49. https://doi.org/10.1016/j.gexplo.2016.04.004
López-Comino, J.A., Cesca, S., Heimann, S., Grigoli, F., Milkereit, C., Dahm, T., Zang, A., 2017. Characterization of Hydraulic Fractures Growth During the Äspö Hard Rock Laboratory Experiment (Sweden). Rock Mech Rock Eng 50, 2985–3001. https://doi.org/10.1007/s00603-017-1285-0
Lu, J.H., Wu, L., 2001. Spectrophotometric Determination of Polyacrylamide in Waters Containing Dissolved Organic Matter. J. Agric. Food Chem. 49, 4177–4182. https://doi.org/10.1021/jf010430o
Ma, J., Zhou, G., Chu, L., Liu, Y., Liu, C., Luo, S., Wei, Y., 2017. Efficient Removal of Heavy Metal Ions with An EDTA Functionalized Chitosan/Polyacrylamide Double Network Hydrogel. ACS Sustainable Chem. Eng. 5, 843–851. https://doi.org/10.1021/acssuschemeng.6b02181
Maguire-Boyle, S., Barron, A., 2014. Organic compounds in produced waters from shale gas wells. Environmental Science: Processes & Impacts 16, 2237–2248. https://doi.org/10.1039/C4EM00376D
Mair, R., Bickle, M., Goodman, D., Roberts, J., Selley, R., Shipton, Z., 2012. Shale Gas extraction in the UK: a review of hydraulic fracturing.
Malik, M., Letey, J., 1991. Adsorption of Polyacrylamide and Polysaccharide Polymers on Soil Materials. Soil Science Society of America Journal 55, 380–383. https://doi.org/10.2136/sssaj1991.03615995005500020014x
Manju, G.N., Anoop Krishnan, K., Vinod, V.P., Anirudhan, T.S., 2002. An investigation into the sorption of heavy metals from wastewaters by polyacrylamide-grafted iron(III) oxide. Journal of Hazardous Materials 91, 221–238. https://doi.org/10.1016/S0304-3894(01)00392-2
Marucco, A., Marcolli, C., Magarini, R., 1999. ICP-OES Analysis of Gold Alloys using Yttrium or Indium as Internal Standard. Atomic Spectroscopy 20.
Maxwell, S.C., Urbancic, T.I., Steinsberger, N., Zinno, R., 2002. Microseismic Imaging of Hydraulic Fracture Complexity in the Barnett Shale. Presented at the SPE Annual Technical Conference and Exhibition, Society of Petroleum Engineers. https://doi.org/10.2118/77440-MS
Maynard, J., R., Wignall, P., B., Varker, W., J., 1991. A “hot” new shale facies from the Upper Carboniferous of Northern England. Journal of the Geological Society 148, 805–808.

McAlister, J.J., Smith, B.J., Curran, J.A., 2003. The use of sequential extraction to examine iron and trace metal mobilisation and the case-hardening of building sandstone: a preliminary investigation. Microchemical Journal 74, 5–18. https://doi.org/10.1016/S0026-265X(02)00043-7
McGuire, M.J., Addai-Mensah, J., Bremmell, K.E., 2006. Spectroscopic investigation of the adsorption mechanisms of polyacrylamide polymers onto iron oxide particles. Journal of Colloid and Interface Science 299, 547–555. https://doi.org/10.1016/j.jcis.2006.03.015
Mitchell, C.J., 2015. UK Frac Sand Resources. Proceedings of the 18th Extractive Industry Geology Conferences, EIG Conferences Ltd.
Molofsky, L.J., Connor, J.A., Wylie, A.S., Wagner, T., Farhat, S.K., 2018. Evaluation of Methane Sources in Groundwater in Northeastern Pennsylvania. Groundwater 333–349. https://doi.org/10.1111/gwat.12056@10.1111/(ISSN)1745-6584.TopAltmetricPaperGWandGWMR
Monaghan, A., 2014. The Carboniferous shales of the Midland Valley of Scotland: geology and resource estimation. British Geological Survey for Department of Energy and Climate Change, London, UK.
Montcoudiol, N., Isherwood, C., Gunning, A., Kelly, T., Younger, P., 2017. Shale gas impacts on groundwater resources: insights from monitoring a fracking site in Poland. Presented at the EGU General Assembly Conference Abstracts, p. 7694.
Montgomery, C., 2013. Effective and Sustainable Hydraulic Fracturing | IntechOpen.
Montgomery, C.T., Smith, M.B., 2010. Hydraulic Fracturing: History Of An Enduring Technology. Journal of Petroleum Technology 62, 26–40. https://doi.org/10.2118/1210-0026-JPT
Moore, D.M., Reynolds Jr, R.C., 1997. X-Ray Diffraction and the Identification and Analysis of Clay Minerals, 2nd ed. New York University Press.
Morrow, H., 2010. Cadmium and Cadmium Alloys - Morrow - - Major Reference Works - Wiley Online Library [WWW Document]. URL https://onlinelibrary.wiley.com/doi/full/10.1002/0471238961.0301041303011818.a01.pub3 (accessed 3.6.19).
Morton, M.Q., 2013. Unlocking the Earth: A Short History of Hydraulic Fracturing.
Mouser, P.J., Liu, S., Cluff, M.A., McHugh, M., Lenhart, J.J., MacRae, J.D., 2016. Redox Conditions Alter Biodegradation Rates and Microbial Community Dynamics of Hydraulic Fracturing Fluid Organic Additives in Soil–Groundwater Microcosms. Environmental Engineering Science 33, 827–838. https://doi.org/10.1089/ees.2016.0031
Mullins, N.R., Daugulis, A.J., 2018. Characterization of transport through polymers for fracking fluid treatment and organic acid concentration in extractive membrane bioreactors. Journal of Chemical Technology & Biotechnology 0. https://doi.org/10.1002/jctb.5872
Nadler, A., Malik, M., Letey, J., 1992. Desorption of polyacrylamide and polysaccharide polymers from soil materials. Soil Technology 5, 91–95. https://doi.org/10.1016/0933-3630(92)90010-X
Newport, L.P., Aplin, A.C., Gluyas, J.G., Greenwell, H.C., Gröcke, D.R., 2016. Geochemical and lithological controls on a potential shale reservoir: Carboniferous Holywell Shale, Wales. Marine and Petroleum Geology 71, 198–210. https://doi.org/10.1016/j.marpetgeo.2015.11.026
Nguyen, Q.D., Boger, D.V., 1998. Application of rheology to solving tailings disposal problems. International Journal of Mineral Processing 54, 217–233. https://doi.org/10.1016/S0301-7516(98)00011-8
Northumbrian Water Ltd, 2017. Water Quality Summary Report W206 - Supply Zone Derwent Trunk Main South and Durham Zone 76130 (Water Quality Summary Report No. Z0021669). Northumbrian Water Ltd.
Nyyssölä, A., Ahlgren, J., 2019. Microbial degradation of polyacrylamide and the deamination product polyacrylate. International Biodeterioration & Biodegradation 139, 24–33. https://doi.org/10.1016/j.ibiod.2019.02.005

O'Donnell, M.C., Gilfillan, S.M.V., Edlmann, K., McDermott, C.I., 2018. Wastewater from hydraulic fracturing in the UK: assessing the viability and cost of management. Environ. Sci.: Water Res. Technol. 4, 325–335. https://doi.org/10.1039/C7EW00474E
Olesik, J., W., 1991. Elemental Analysis Using ICP-OES and ICP/MS: An Evaluation and Assessment of Remaining Problems. Analytical Chemistry 63.
Oregon Health Authority, 2018. Iron (Fe) and Manganese (Mn) in Groundwater, Drinking Water. Environmental Public Health.
Palisch, T.T., Vincent, M., Handren, P.J., 2010. Slickwater Fracturing: Food for Thought. SPE Production & Operations 25, 327–344. https://doi.org/10.2118/115766-PA
Pappas, R.S., 2012. Sample Preparation Problem Solving for Inductively Coupled Plasma-Mass Spectrometry with Liquid Introduction Systems I. Solubility, Chelation, and Memory Effects. Spectroscopy (Springf) 27, 20–31.
Parnell, J., Brolly, C., Spinks, S., Bowden, S., 2016. Selenium enrichment in Carboniferous Shales, Britain and Ireland: Problem or opportunity for shale gas extraction? Applied Geochemistry 66, 82–87. https://doi.org/10.1016/j.apgeochem.2015.12.008
Phan, T.T., Capo, R.C., Stewart, B.W., Graney, J.R., Johnson, J.D., Sharma, S., Toro, J., 2015. Trace metal distribution and mobility in drill cuttings and produced waters from Marcellus Shale gas extraction: Uranium, arsenic, barium. Applied Geochemistry, Geochemistry of Unconventional Shale Gas from Formation to Extraction: Petrogenesis, Hydraulic Fracturing, and Environmental Impacts 60, 89–103. https://doi.org/10.1016/j.apgeochem.2015.01.013
Pinto, P.X., Al-Abed, S.R., Holder, C., Reisman, D.J., 2014. Evaluation of metal partitioning and mobility in a sulfidic mine tailing pile under oxic and anoxic conditions. Journal of Environmental Management 140, 135–144. https://doi.org/10.1016/j.jenvman.2014.03.004
Poppe, L., J., Paskevich, J., C., Hathaway, J., C., Blackwood, D., S., 2002. A Laboratory Manual for X-Ray Powder Diffraction (No. 01–041). USGS.
Reap, E., 2015. The risk of hydraulic fracturing on public health in the UK and the UK's fracking legislation. Environ Sci Eur 27, 27. https://doi.org/10.1186/s12302-015-0059-0
ReFINE, 2018. ReFINE - Newcastle University [WWW Document]. What is Fracking? URL http://www.refine.org.uk/research/whatisfracking/ (accessed 10.31.18).
Rho, T., Park, J., Kim, C., Yoon, H.-K., Suh, H.-S., 1996. Degradation of polyacrylamide in dilute solution. Polymer Degradation and Stability 51, 287–293. https://doi.org/10.1016/0141-3910(95)00182-4
Rieuwerts, J.S., Thornton, I., Farago, M.E., Ashmore, M.R., 1998. Factors influencing metal bioavailability in soils: preliminary investigations for the development of a critical loads approach for metals. Chemical Speciation & Bioavailability 10, 61–75. https://doi.org/10.3184/095422998782775835
RigZone, 2019. How Does Well Fracturing Work to Stimulate Production? [WWW Document]. URL https://www.rigzone.com/training/insight.asp?insight_id=319&c_id= (accessed 2.22.19).
Ross, D.J.K., Bustin, M., R., 2009. The importance of shale composition and pore structure upon gas storage potential of shale gas reservoirs. Marine and Petroleum Geology 26, 916–927. https://doi.org/10.1016/j.marpetgeo.2008.06.004
Rouquerol, F., Rouquerol, J., Sing, K., 1999. Adsorption by powders and porous solids. Principles, methodology and applications. Academic Press.
Ruthven, D., M., 1984. Principles of Adsorption and Adsorption Processes. John Wiley & Sons, University of New Brunswick, Frederictin.
Scoggins, M.W., Miller, J.W., 1979. Determination of Water-Soluble Polymers Containing Primary Amide Groups Using the Starch-Triiodide Method. Society of Petroleum Engineers Journal 19, 151–154. https://doi.org/10.2118/7664-PA
Selley, R.C., 2012. UK shale-gas resources. Petroleum Geology Conference series 6, 707–714. https://doi.org/10.1144/0060707

Shawar, L., Halevy, I., Said-Ahmad, W., Feinstein, S., Boyko, V., Kamyshny, A., Amrani, A., 2018. Dynamics of pyrite formation and organic matter sulfurization in organic-rich carbonate sediments. Geochimica et Cosmochimica Acta 241, 219–239. https://doi.org/10.1016/j.gca.2018.08.048

Sher, C., Wu, C., 2018. Fracking in China: Community Impacts and Public Support of Shale Gas Development. Journal of Contemporary China 27, 626–641. https://doi.org/10.1080/10670564.2018.1433591

Shih, J.-S., Saiers, J.E., Anisfeld, S.C., Chu, Z., Muehlenbachs, L.A., Olmstead, S.M., 2015. Characterization and Analysis of Liquid Waste from Marcellus Shale Gas Development. Environ. Sci. Technol. 49, 9557–9565. https://doi.org/10.1021/acs.est.5b01780

Shubha, K.P., Raji, C., Anirudhan, T.S., 2001. Immobilization of heavy metals from aqueous solutions using polyacrylamide grafted hydrous tin (IV) oxide gel having carboxylate functional groups. Water Research 35, 300–310. https://doi.org/10.1016/S0043-1354(00)00234-7

Smith, E.A., Prues, S.L., Oehme, F.W., 1997. Environmental Degradation of Polyacrylamides. Ecotoxicology and Environmental Safety 37, 76–91. https://doi.org/10.1006/eesa.1997.1527

Smith, N., Turner, P., Williams, G., 2010. UK data and analysis for shale gas prospectivity. Petroleum Geology Conference series 7, 1087–1098. https://doi.org/10.1144/0071087

SNF FLOEGER, n.d. Preparation of Organic Polymers.

Sojka, R.E., Bjornberg, D., L., Entry, J.A., Lentz, R.D., Orts, W., J., 2007. Polyacrylamide in Agriculture and Environmental Land Management - ScienceDirect [WWW Document]. URL https://www.sciencedirect.com/science/article/pii/S0065211304920020 (accessed 10.8.19).

Sojka, R.E., Entry, J.A., 2000. Influence of polyacrylamide application to soil on movement of microorganisms in runoff water☆☆Mention of trade names or commercial products in this paper does not constitute endorsement or recommendation of use. Environmental Pollution 108, 405–412. https://doi.org/10.1016/S0269-7491(99)00194-3

Spears, D.A., Amin, M.A., 1981. Geochemistry and mineralogy of marine and non-marine Namurian black shales from the Tansley Borehole, Derbyshire. Sedimentology 28, 407–417. https://doi.org/10.1111/j.1365-3091.1981.tb01689.x

Speight, J.G., 2016. Handbook of Hydraulic Fracturing. John Wiley & Sons.

Srivastava, N.C., Eames, I.W., 1998. A review of adsorbents and adsorbates in solid–vapour adsorption heat pump systems. Applied Thermal Engineering 18, 707–714. https://doi.org/10.1016/S1359-4311(97)00106-3

Stringfellow, W.T., Domen, J.K., Camarillo, M.K., Sandelin, W.L., Borglin, S., 2014. Physical, chemical, and biological characteristics of compounds used in hydraulic fracturing. Journal of Hazardous Materials 275, 37–54. https://doi.org/10.1016/j.jhazmat.2014.04.040

Stuart, M., 2012. Potential Groundwater Impact from Exploitation of Shale Gas in the UK (No. OR/12/001), Groundwater Science Programme. British Geological Survey.

Stuart, M.A.C., Scheutjens, J.M.H.M., Fleer, G.J., 1980. Polydispersity effects and the interpretation of polymer adsorption isotherms. Journal of Polymer Science: Polymer Physics Edition 18, 559–573. https://doi.org/10.1002/pol.1980.180180315

Stumm, W., Morgan, J., J., 1996. Aquatic Chemistry - Chemistry Equilibria and Rates in Natural Waters, 3rd ed. John Wiley & Sons, USA.

Sutcu, H., 2007. Pyrolysis by thermogravimetric analysis of blends of peat with coals of different characteristics and biomass. Journal of the Chinese Institute of Chemical Engineers 38, 245–249. https://doi.org/10.1016/j.jcice.2007.03.002

Tasker, T.L., Piotrowski, P.K., Dorman, F.L., Burgos, W.D., 2016. Metal Associations in Marcellus Shale and Fate of Synthetic Hydraulic Fracturing Fluids Reacted at High

Pressure and Temperature. Environmental Engineering Science. https://doi.org/10.1089/ees.2015.0605
Taylor, K.C., 1993. Spectrophotometric Determination of Acrylamide Polymers by Flow Injection Analysis. SPE Advanced Technology Series 1, 130–133. https://doi.org/10.2118/21007-PA
Taylor, K.C., Burke, R.A., Nasr-El-Din, H.A., Schramm, L.L., 1998. Development of a flow injection analysis method for the determination of acrylamide copolymers in brines. Journal of Petroleum Science and Engineering 21, 129–139. https://doi.org/10.1016/S0920-4105(98)00042-4
Tekin, N., Demirbaş, Ö., Alkan, M., 2005. Adsorption of cationic polyacrylamide onto kaolinite. Microporous and Mesoporous Materials 85, 340–350. https://doi.org/10.1016/j.micromeso.2005.07.004
The Water Supply (Water Quality) Regulations 2016 [WWW Document], 2016. URL http://www.legislation.gov.uk/uksi/2016/614 (accessed 3.5.19).
Thompson, J., 2019. The Fracking Debate: The Risks, Benefits, and Uncertainties of the Shale Revolution, by. The European Legacy 0, 1–3. https://doi.org/10.1080/10848770.2019.1575076
Todor, D., N., 1976. Thermal Analysis of Minerals. Abacus Press, Romania.
Tucker, P., G., 2008. Cadmium Toxicity (Safety Course Documentation No. WB 1096), Case Studies in Environmental Medicine. Agency for Toxic Substances and Disease Registry.
Turley, C., Blackford, J., Widdicombe, S., Lowe, D., Nightingale, P., Rees, A., 2006. Reviewing the Impact of Increased Atmospheric CO2 on Oceanic pH and the Marine Ecosystem, Avoiding Dangerous Climate Change. Cambridge University Press, Downing Street, London.
Tuttle, L.W., Breit, G.N., Goldhaber, M.B., 2003. geochemical Data from New Albany Shale, Kentucky: A Study in Metal Mobility During Weathering of Black Shales (No. 03–207). USGS, Denver.
Tyler, G., 1995. ICP-OES, ICP-MS and AAS Techniques Compared.
U.S. Energy Information Administration, 2015. Technically Recoverable SHale Oil and Shale Gas Resources: United Kingdom.
Vengosh, A., Warner, N., Jackson, R., Darrah, T., 2013. The Effects of Shale Gas Exploration and Hydraulic Fracturing on the Quality of Water Resources in the United States. Procedia Earth and Planetary Science, Proceedings of the Fourteenth International Symposium on Water-Rock Interaction, WRI 14 7, 863–866. https://doi.org/10.1016/j.proeps.2013.03.213
Volpert, E., Selb, J., Candau, F., Green, N., Argillier, J.F., Audibert, A., 1998. Adsorption of Hydrophobically Associating Polyacrylamides on Clay. Langmuir 14, 1870–1879. https://doi.org/10.1021/la970358h
Wang, D.-M., Xu, Y.-M., He, D.-M., Guan, J., Zhang, O.-M., 2009. Investigation of mineral composition of oil shale. Asia-Pacific Journal of Chemical Engineering 4, 691–697. https://doi.org/10.1002/apj.319
Wang, J., Huang, C.P., Allen, H.E., Poesponegoro, I., Poesponegoro, H., Takiyama, L.R., 1999. Effects of Dissolved Organic Matter and pH on Heavy Metal Uptake by Sludge Particulates Exemplified by Copper(II) and Nickel(II): Three-Variable Model. Water Environment Research 71, 139–147.
Warner, N.R., Christie, C.A., Jackson, R.B., Vengosh, A., 2013. Impacts of Shale Gas Wastewater Disposal on Water Quality in Western Pennsylvania. Environ. Sci. Technol. 47, 11849–11857. https://doi.org/10.1021/es402165b
Warner, N.R., Jackson, R.B., Darrah, T.H., Osborn, S.G., Down, A., Zhao, K., White, A., Vengosh, A., 2012. Geochemical evidence for possible natural migration of Marcellus Formation brine to shallow aquifers in Pennsylvania. PNAS 109, 11961–11966. https://doi.org/10.1073/pnas.1121181109
Waters, C., N., Davies, S., J., 2006. Carboniferous: extentsional basins, advancing deltas and coal swamps.

Waters, C., N., Jones, N., S., Collinson, J., D., Cleal, C., J., 2013. Craven Basin and Southern Pennines, in: A Revised Correlation of the Carboniferous Rocks in the British Isles. The Geological Society, pp. 74–82.
Weinhold, B., 2012. The Future of Fracking: New Rules Target Air Emissions for Cleaner Natural Gas Production. Environ Health Perspect 120, a272–a279. https://doi.org/10.1289/ehp.120-a272
Wingenfelder, U., Hansen, C., Furrer, G., Schulin, R., 2005. Removal of Heavy Metals from Mine Waters by Natural Zeolites. Environ. Sci. Technol. 39, 4606–4613. https://doi.org/10.1021/es048482s
Wiśniewska, M., 2012. The temperature effect on the adsorption mechanism of polyacrylamide on the silica surface and its stability. Applied Surface Science 258, 3094–3101. https://doi.org/10.1016/j.apsusc.2011.11.044
Wiśniewska, M., Chibowski, S., Urban, T., 2016. Adsorption properties of the nanozirconia/anionic polyacrylamide system—Effects of surfactant presence, solution pH and polymer carboxyl groups content. Applied Surface Science 370, 351–356. https://doi.org/10.1016/j.apsusc.2016.02.188
Wood, S., Patterson, O., 2011. Health and environmental risk assessment of hydraulic fracturing.
Worrall, F., Burt, T.P., 2007. Trends in DOC concentration in Great Britain. Journal of Hydrology 346, 81–92. https://doi.org/10.1016/j.jhydrol.2007.08.021
Xiong, B., Loss, R.D., Shields, D., Pawlik, T., Hochreiter, R., Zydney, A.L., Kumar, M., 2018a. Polyacrylamide degradation and its implications in environmental systems. npj Clean Water 1, 17. https://doi.org/10.1038/s41545-018-0016-8
Xiong, B., Miller, Z., Roman-White, S., Tasker, T., Farina, B., Piechowicz, B., Burgos, W.D., Joshi, P., Zhu, L., Gorski, C.A., Zydney, A.L., Kumar, M., 2018b. Chemical Degradation of Polyacrylamide during Hydraulic Fracturing. Environ. Sci. Technol. 52, 327–336. https://doi.org/10.1021/acs.est.7b00792
Yang, L., Wang, S., Guo, J., Gou, X., Jiang, Z., Pan, B., 2018. Reduced adsorption of polyacrylamide-based fracturing fluid on shale rock using urea. Energy Science & Engineering 1–11. https://doi.org/10.1002/ese3.249
Yang, M.-H., 1998. The Two-Stages Thermal Degradation of Polyacrylamide. Polymer Testing 17, 191–198. https://doi.org/10.1016/S0142-9418(97)00036-6
Yang, Z.L., Gao, B.Y., Li, C.X., Yue, Q.Y., Liu, B., 2010. Synthesis and characterization of hydrophobically associating cationic polyacrylamide. Chemical Engineering Journal 161, 27–33. https://doi.org/10.1016/j.cej.2010.04.015
Zachariadis, G.A., Vogiatzis, C., 2010. An Overview of the Use of Yttrium for Internal Standardization in Inductively Coupled Plasma–Atomic Emission Spectrometry. Applied Spectroscopy Reviews 45, 220–239. https://doi.org/10.1080/05704921003719122
Zhang, Y., Zhang, H., Zhang, Z., Liu, C., Sun, C., Zhang, W., Marhaba, T., 2018. pH Effect on Heavy Metal Release from a Polluted Sediment [WWW Document]. Journal of Chemistry. https://doi.org/10.1155/2018/7597640
Zhou, S., Xue, A., Zhao, Y., Wang, Q., Chen, Y., Li, M., Xing, W., 2011. Competitive adsorption of Hg2+, Pb2+ and Co2+ ions on polyacrylamide/attapulgite. Desalination 270, 269–274. https://doi.org/10.1016/j.desal.2010.11.055
Zoback, M., Kitasei, S., Copithorne, B., 2010. Addressing the Environmental Risks from Shale Gas Development (No. Briefing Paper 1). Worldwatch Institute.